AN INVESTIGATION OF THE ROLE OF THE MDM2-NME INTERACTION IN CANCER CELLS

Thesis submitted in accordance with the requirements

of the University of Liverpool for the degree

of Doctor of Philosophy

by

Shie Hong Chang

April 2014

Acknowledgements

I would like to take this opportunity to express my warmest gratitude to all those who have supported me throughout my PhD studies. First of all, I would like to thank my supervisors Prof Mark Boyd and Dr Nikolina Vlatković for giving me the opportunity to be part of their research group, and for the valuable guidance and support throughout my research studies and thesis writing process. I would like to express my appreciation to Mersey Kidney First (formerly Mersey Kidney Research) for funding my PhD studentship. I would also like to thank Dr Carlos Rubbi for his generous support and help, especially with the live cell imaging system. I am also extremely grateful to all the past and present members of the Boyd lab, especially to Dr Kerryanne Crawford, Dr Radoslaw Polański, Dr Arpita Ray-Sinha, Dr Anna Behrendt and Mr Amro Ebbiary, for their friendship and willingness to help and to share their knowledge and experiences with me. A big thank you to Dr Kerryanne Crawford from whom I learnt a lot, and who supported me throughout the ups and downs of my time in Liverpool. I would also like to thank my dearest friend, Dr Despina Soteriou, for always giving me great care and support, and treating me like one of her family. Finally, I would like to express my deepest gratitude to my family, especially to my parents, Chang Kok Yok and Siew Kwai Kiew, for their undivided love and support and for always believing in their daughter.

Declaration of Originality

This thesis is a result of my own work performed during the course of studies in the Division of Surgery and Oncology, University of Liverpool, between May 2010 and April 2014. All work described was performed by me unless clearly indicated. The thesis was written wholly by me under the valued guidance of my supervisors Prof Mark Boyd and Dr Nikolina Vlatković.

S H Chang

April 2014

Abstract

MDM2 is a proto-oncogene well known for its role as a negative regulator of the p53 tumour suppressor. It has also been demonstrated that co-upregulation of MDM2 and wild-type p53 is linked with reduced disease specific survival in renal cell carcinoma (RCC). Moreover, MDM2 expression has been shown to promote cell motility and invasiveness in several cancer cell types including RCC cells in a p53- and RING-finger- independent manner, suggesting a role for protein-protein interactions in mediating this effect. The work presented in this thesis has aimed to study the role of MDM2 interaction with other proteins, in particular with members of the NME (Non-metastatic protein) family of metastasis suppressing genes, in order to decipher the mechanisms of action by which MDM2 may contribute to a more aggressive phenotype in cancer cells. To accomplish this we have used a range of methodologies including investigating the consequences of MDM2 expression using exon array analysis in an attempt to identify changes in gene expression induced by wild type MDM2 (Clone 9) and an MDM2 RING-mutant (RFM9) expressed stably in clonal derivatives of H1299 cells. In parallel studies in our research group, an interaction was identified between MDM2 and NME2. Since NME2 is a member of a family of genes that has been implicated in metastasis suppression, and since metastatic spread is a primary determinant of patient survival, we also focused on an analysis of this interaction. Thus the primary aim of this work became an examination of the mechanistic details and consequences of MDM2-NME interaction in cancer cells. The two most highly expressed forms of NME genes in most cell types are the highly related NME1 and NME2 genes which both encode nucleoside diphosphate kinase (NDPK) activity, essential for maintaining cellular pools of nucleoside triphosphates. They are also metastasis suppressor genes with an ability to suppress cellular motility. Since MDM2 possesses an E3 ubiquitin ligase activity, we have investigated whether MDM2 has an ability to modify NME proteins by ubiquitinating them and also whether MDM2 modulates the NDPK activity of NME proteins and/or their motility suppressing activity. Our results suggest that MDM2 may abrogate motility suppressive effects of NME2 through down-regulation of NME2 (and also of NME1) protein levels with potential consequences for suppression of NDPK activity. More interestingly, our studies have identified NM23-LV, which is

derived from a specific read-through transcription and alternative splicing event of the adjacent *NME1* and *NME2* genes, as an MDM2-interacting protein. In addition, we have identified NM23-LV as a novel substrate for MDM2-mediated ubiquitination that occurs in an MDM2 E3 ligase activity-dependent manner. Ubiquitination of NM23-LV by MDM2 seems to be highly specific, since neither NME1 nor NME2 are substrates for MDM2-mediated ubiquitination. Furthermore, our results have also shown that NM23-LV can substantially promote MDM2 stabilisation and enhance MDM2-dependent p53 inactivation, adding another layer of complexity to the interactions between MDM2 and NME family members. Functional studies of NM23-LV have suggested that NM23-LV plays a role in promoting cell motility, which contrasts with the canonical role of NME1 and NME2 as metastasis suppressors. Taken together, studies presented in this thesis have identified a novel relationship between MDM2 and NM23-LV, which could provide valuable insights into the underlying mechanisms leading to increased cell motility promoted by MDM2 and suggests that new studies examining how MDM2-NME interactions may regulate cell motility and cancer metastasis are needed. Given the role of MDM2 in promoting more aggressive RCCs, insights gained from these studies may ultimately identify opportunities for therapeutic interventions for RCC, as well as for other human cancers.

List of Abbreviations

Abbreviation	Definition
aa	Amino acid
ACTN4	Alpha-actinin-4
ADAMTS1	A disintegrin and metallopeptidase with thrombospondin type 1
AMP	Adenosine monophosphate
ARF	Alternate reading frame
ATM	Ataxia telangiestasia mutated
ATP	Adenosine triphosphate
AWD	Abnormal wing discs
BAX	B-cell-lymphoma-2-associated X protein
BER	Base-excision repair
BLAST	Basic local alignment search tool
bp	Base pair
Btl	Breathless
CBP	CREB-binding protein
ccRCC	Clear cell renal cell carcinoma
Cdc42	Cell division control protein 42
cfu	Colony forming units
Chk	Checkpoint kinase
chrRCC	Chromophobe renal cell carcinoma
CMV	Cytomegalovirus
COX-2	Cyclooxgenase-2
CREB	cAMP responsive element binding protein
DBD	DNA-binding domain
DHFR	Dihydrofolate reductase
DMEM	Dulbecco's modified eagle medium
DMSO	Dimethyl sulfoxide
DNA	Deoxyribonucleic acid
DUB	Deubiquitinating enzyme
ECFP	Enhanced cyan fluorescent protein
EDTA	Ethylenediaminetetra-acetic acid
EGFP	Enhanced green fluorescent protein

Abbreviation	**Definition**
EMT	Epithelial-mesenchymal transition
ER	Endoplasmic reticulum
ERE	Estrogen response element
ERK	Extracellular-signal-regulated-kinase
EYFP	Enhanced yellow fluorescent protein
FBS	Fetal bovine serum
FOXO4	Forkhead box O 4
FRET	Fluorescence resonance energy transfer
GADD45	Growth-arrest and DNA damage-inducible
GAP	GTPase-activating protein
GEF	Guanine nucleotide exchange factor
GFP	Green fluorescent protein
GR	Glucocorticoid receptor
GST	Glutathione S-transferase
GTP	Guanosine triphosphate
HA	Hemagglutinin
HAUSP	Herpesvirus-associated ubiquitin-specific protease
HCC	Hepatocellular carcinoma
HCT8/S11	Human colonic cancer cells
HEK	Human embryonic kidney
Hep2	Human epithelial type 2
HIF	Hypoxia-inducible factor
HPRT1	Homo sapiens hypoxanthine phosphoribosyltransferase 1
HRE	Hypoxia responsive elements
HSV	Herpes simplex virus
IB	Immunoblot
ICAP-1α	integrin cytoplasmic domain-associated protein-1a
IDC	Invasive ductal breast cancer
IGF-IR	Insulin-like growth factor 1 receptor
IP	Immunoprecipitation
K-pn	Killer of prune
KCa3.1	Ca^{2+} activated potassium ion channel
KSR	Kinase suppressor of RAS

Abbreviation	Definition
LAR II	Luciferase assay reagent II
Lbc	Lymphoid blast crisis oncogene
LOH	Loss of heterozygosity
LPA	Lysophosphatidic acid
MAPK	Mitogen-activated-protein-kinase
MDM2	Mouse double minute 2
MEF	Mouse embryonic fibroblast
MIF	Migration inhibitory factor
MMP-9	Matrix metallopeptidase-9
MMR	Mismatch repair
mRNA	Messenger RNA
MTBP	MDM2 binding protein
MTT	3-(4,5-dimethylthiazol- 2-yl)-2,5-diphenyltetrazolium bromide
NDP	Nucleoside diphosphate
NDPK	Nucleoside diphosphate kinase
NEDD	Neural precursor cell expressed, developmentally down-regulated
NER	Nucleotide-excision repair
NES	Nuclear export signal
NHE	Nuclease-hypersensitive element
Ni-NTA	Nickel-nitrilotriacetic acid
NLS	Nuclear localisation signal
NME	Non-metastatic protein
NoLS	Nucleolar localisation signal
NTP	Nucleoside triphosphate
p300/CBP	CREB-binding protein
PAGE	Polyacrylamide gel electrophoresis
PCDHB2	Protocadherin beta 2
PCI	Phenol:chloroform:isoamyl alcohol
PCNA	Proliferating cell nuclear antigen
PCR	Polymerase chain reaction
PDGF	Platelet-derived growth factor
PI	Propidium iodide
PI3	Phosphatidylinositol 3-OH

Abbreviation	Definition
PKB	Protein kinase B
pRB	Retinoblastoma protein
pRCC	Pappilary renal cell carcinoma
PUMA	p53 up-regulated modulator of apoptosis
qRT-PCR	Quantitative real-time PCR
RCC	Renal cell carcinoma
RFM	RING-finger mutant
RING	Really interesting new gene
RNA	Ribonucleic acid
RPS24	Ribosomal protein S24
rRNA	Ribosomal RNA
RT	Room temperature
SDS	Sodium dodecyl sulphate
Shi	Shibire
shRNA	short hairpin RNA
siRNA	small interference RNA
SNP	Single nucleotide polymorphism
STRAP	TGF-β-receptor-interacting protein
SV40	Simian virus 40
TAD	Transactivation domain
TAE	Tris-acetate-EDTA
TD	Tetramerisation domain
TGF	Transforming growth factor
TGF-β1	Transforming growth factor-beta 1
TP53	Tumour protein 53
TSP-1	Thrombospondin-1
TUBA1B	Tubulin, alpha 1b
Txl-2	Thioredoxin-like 2
Ub	Ubiquitin
UEV	Ubiquitin-conjugating enzyme variant
UV	Ultraviolet
VEGF	Vascular endothelial growth factor
VHL	Von Hippel-Lindau

Abbreviation	**Definition**
wt	Wild-type
XIAP	X-linked inhibitor of apoptosis
β-gal	Beta-galactosidase

Table of Content

List of Figures

Chapter 1

Chapter 2

Chapter 3.1

Chapter 3.2

Chapter 3.3

Chapter 3.4

Chapter 5

List of Tables

Chapter 1 **Page**

Chapter 2

Chapter 3.1

Chapter 3.4

List of Appendices

Chapter 1

Introduction

1. Introduction

1.1 Background on Cancer

Cancer is a broad group of diseases that share some common characteristics [1]. The main defining characteristic of cancer cells is that they divide and grow in an uncontrolled manner. Some tumours, if detected late or left untreated will become malignant, that is they are able to invade adjacent tissues and spread throughout the organism via the lymphatic system or blood stream. Cancer cells achieve these abnormal phenotypic traits largely by having defects in normal cellular programs that govern cell proliferation, migration, apoptosis and homeostasis [2, 3]. These regulatory defects are due to changes in the cell genome, leading to transformation of normal cells into malignant cancer cells. Therefore, broadly speaking, cancer is a genetic disease [2]. Changes in the genome can be caused by both internal factors, such as inherited mutations; and/or environmental or acquired factors, such as tobacco, diet, viruses, and UV radiation [4].

Different types of genetic alterations, such as subtle mutations at the nucleotide level, aberration in chromosome number (aneuploidy), chromosome translocations and gene amplifications [5] affecting growth, senescence and apoptosis have all been related to tumorigenesis [6]. Generally, genes altered in tumorigenesis can be grouped into three key types: oncogenes, tumour suppressor genes and genomic stability genes [7, 8]. Oncogenes are genes that typically promote cell growth and differentiation. Upon mutation, oncogenes become activated and can cause uncontrolled cell proliferation, which is fundamental for the development of cancer. On the other hand, tumour suppressors refer to genes that typically regulate cell division, promote apoptosis, and suppress metastasis. Inactivation of tumour suppressor function may lead to cancer by inhibiting normal cell death or cell cycle arrest [9, 10]. Tumour formation occurs when the regulatory balance between oncogene and tumour suppressor functions is lost. Typically, oncogenic mutations that occur in one allele of an oncogene are sufficient to drive selective cell growth advantage, and thus these are usually dominant [10]. Mutations in tumour suppressors, however, are typically considered to be recessive; which means two copies of a gene must be inactivated for a phenotypic effect to occur [10].

The third class of genes responsible for tumorigenesis are the genomic stability genes or housekeeping genes, which mainly function in detecting DNA damage and repairing errors made during DNA replication or induced by external mutagens [10]. The genomic stability genes, which include the mismatch repair (MMR), nucleotide-excision repair (NER) and base-excision repair (BER) genes, serve to keep genetic alterations to a minimum level [10]. Mutations that inactivate DNA repair genes can lead to the occurrence of multiple random mutations and propagation of genetic defects. This increase in genome instability allows for the outgrowth of abnormal cells which will then find it easier to acquire additional mutations, giving them a selective advantage over their normal counterparts [2].

Cancer is an intricate collection of specific genetic diseases acquiring a common set of hallmarks [2, 3, 11]. The foundation of the malignant process, as proposed by Hanahan and Weinberg include: self-sufficiency in growth signals, insensitivity to growth-inhibitory signals, evasion of apoptosis, limitless replicative potential, sustained angiogenesis, tissue invasion and metastasis, evading immune destruction, genome instability and mutation, tumour-promoting inflammation, and deregulating cellular energetics [2, 11]. These properties, shared by all types of human cancers, are acquired successively and the sequence in which they appear may vary in specific types of cancer or within the same type of cancer (Figure 1.1.1) [2, 11].

Cancer arises through a usually long, multistep, mutagenic process. Since most cancers are sporadic resulting from somatic mutations and that accumulation of genome alterations takes time, cancer is more likely to develop during later stages in life. However, when germline mutations are present, the time required to develop cancer is shortened by enabling the transfer of parental genetic defects from one generation to another. Therefore, people who are born with hereditary predisposition to cancer syndromes, such as Li Fraumeni (mutations in p53 gene) and von Hippel-Lindau (mutations in VHL gene), have higher chances of developing cancer at a younger age [10, 12, 13].

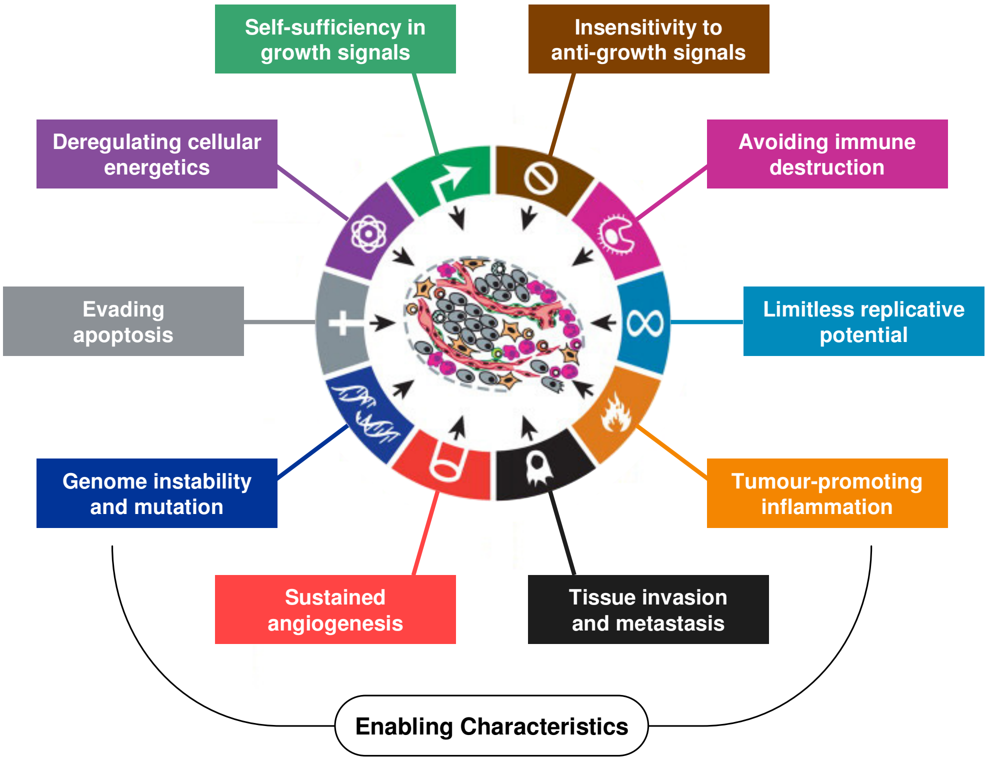

Figure 1.1.1: Hallmarks of cancer. Acquired functional capabilities common in all types of cancer cells, which establish the foundation of malignant process, together with enabling characteristics which are important to the acquisition of these hallmarks. Figure reproduced from references [11, 14].

1.2 Renal Cell Carcinoma (RCC)

Kidney cancer accounts for about 3% of all cancers. Cancer Research UK reported that around 9,600 people were diagnosed with kidney cancer and around 4,100 people have died of kidney cancer in 2010 in the UK (Table 1.2.1). The incidence rates for kidney cancer in Britain have more than doubled since the mid 1970s. Worldwide, it is estimated that more than 250,000 new cases of kidney cancers are diagnosed annually [15]. The majority of the kidney cancers (80-85%) are renal cell carcinomas (RCC) originating from the renal parenchyma [16].

Table 1.2.1: Kidney Cancer Statistic. Table reproduced from Cancer Research UK's Statistical Information Team [17].

Kidney Cancer Statistics	Males	Females	Persons	Country	Year[3]
Number of new cases per year	5,906	3,733	9,639	UK	2010
Incidence rate per 100,000 population[1]	15.7	8.4	11.8		
Number of deaths per year	2,451	1,611	4,062	UK	2010
Mortality rate per 100,000 population[1]	6.2	3.1	4.5		
One-year survival rate[2]	71.5%	71.4%	71.4%	England	2005-2009
Five-year survival rate[2]	53.3%	54.8%	53.9%	England	2005-2009
Ten-year survival rate[2]	43.0%	44.3%	43.5%	England & Wales	2007 (predicted)

[1] European age-standardised [2] Adults diagnosed [3] Latest statistics available

RCC is a heterogeneous disease. It comprises a group of tumours arising from the epithelium of the renal tubules, that not only display distinct histology and clinical behaviour, but are also caused by different genetic alterations [15, 16]. Recent reports show that different histological subtypes of RCC have different clinical outcomes and respond differently to therapy [18]. According to the 2004 (updated later in 2009) World Health Organisation classification, the three most common histological subtypes of RCC are: clear cell (ccRCC), papillary (pRCC), and chromophobe RCCs (chrRCC) [18, 19]. ccRCC is the commonest histologic subtypes and is believed to account for 75% of all RCCs. This is followed by pRCC, which accounts for 10% of RCC and is subclassified into type I and type

II, depending on the morphology of the cells covering the papillary lesions [20]. Both ccRCC and pRCC are thought to originate from cells in the proximal convoluted renal tubule (Figure 1.2.1) [21-23]. chrRCC is the third commonest subtype and accounts for 5% of the RCCs. chrRCC is believed to originate from type B intercalated cells of renal collecting ducts [22, 24].

Most cases of RCCs are sporadic and usually occur in the sixth decade of life. Only a small proportion of RCCs (2-4%) are heritable [25, 26]. Different inherited RCC syndromes, for example, von Hippel-Lindau disease, paraganglioma syndrome, hereditary leiomyomatosis, and Hogg-Dubé syndrome, have been classified based on their histopathological and genetic characteristics [27].

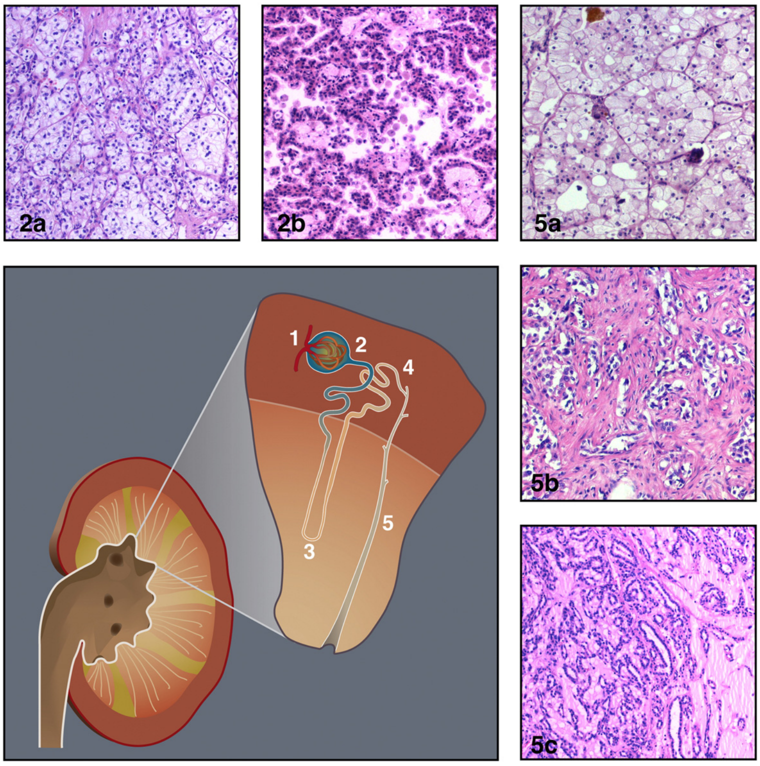

Figure 1.2.1: Classification of RCC subtypes. The nephron consists of the renal corpuscle (1) and renal tubule. The renal tubule is classified into four histo-physiological zones: proximal convoluted tubule (2), loop of Henle (3), distal convoluted tubule (4) and collecting tubule (5). The different RCC subtypes originate from different parts of the renal tubular system. For example, clear cell RCC (2a) and papillary RCC (2b) originate from the proximal convoluted tubule whereas chromophobe RCC (5a), collecting duct carcinoma (5b), and mucinous tubular and spindle cell carcinoma (5c) are believed to originate from the collecting tubule. Haematoxylin and eosin (H&E) staining shows that (2a) clear cell RCC consists of clear cytoplasm with an eosinophilic or granular appearance; (2b) papillary RCC is characterised by papillae covered by small cells with scanty cytoplasm, arranged in a single layer on the papillary basement membrane; (5a) chromophobe RCC is composed of large polygonal cells with a transparent slightly reticulated cytoplasm for numerous invaginated vesicles; (5b) collecting duct carcinoma is characterised by tubulopapillary architecture that consists of an admixture of dilated tubule and papillary structures commonly lined by a single layer of cuboidal cells; and (5c) mucinous tubular and spindle cell carcinoma is composed of tightly packed tubules separated by pale stroma and a spindle cell component with mucinous material [28]. Figure reproduced from [16].

1.3 Von Hippel-Lindau (VHL) disease

VHL disease is the most studied and commonest hereditary RCC syndrome [27]. RCCs that occur in people with heritable VHL syndrome are exclusively of the clear cell subtype [29-31]. VHL disease is an autosomal dominant inherited disorder. The disease is caused by germline mutations in the *VHL* tumour suppressor gene, accompanied by the inactivation or silencing of the second wild-type *VHL* allele in a susceptible cell, in accord with the Knudson Two-Hit Tumour Suppressor Model [21, 32-34]. The *VHL* gene product participates in the regulation of several cellular pathways, such as extracellular matrix assembly, cell-cycle control and oxygen sensing [21]. It has been suggested that one of the critical roles of VHL is its ability to interact with an E3 ubiquitin ligase complex and regulate the transcription of activator hypoxia-inducible factor 1α (HIF-1α) [35-38]. Under normoxic conditions, HIF-1α subunits become hydroxylated, and this allows binding and ubiquitination by VHL protein and subsequently degradation by the proteasome [37]. Under hypoxic conditions, however, HIF-1α subunits are non-hydroxylated and are able to heterodimerise with HIF-2β. The stabilised HIFα-β heterodimers are free to bind DNA at hypoxia responsive elements (HREs) and transcriptionally activate genes that are important in regulating angiogenesis, cell growth and apoptosis [31, 39]. Thus, in VHL-defective ccRCC, HIF-1α is constitutively stabilised and its accumulation leads to overexpression of proteins that are normally inducible with hypoxia, such as transforming growth factor α and β (TGF-α and -β, respectively), vascular endothelial growth factor-α (VEGF-α), and platelet-derived growth factor (PDGF) [40]. Over-expression of these proteins targets neighbouring vascular cells and promotes tumorigenesis [40].

Whilst heritable ccRCC is caused by a germline mutation of one allele and an acquired mutation of the remaining allele of VHL, sporadic ccRCCs are predominantly caused by biellelic *VHL* inactivation (Figure 1.3.1), which can be a consequence of somatic mutations, deletions, loss of heterozygosity (LOH) or epigenetic inactivation, such as promoter DNA methylation [16, 31, 41, 42]. Nevertheless, mutation of the *VHL* gene is an important event in the pathogenesis in both heritable and sporadic ccRCCs [43].

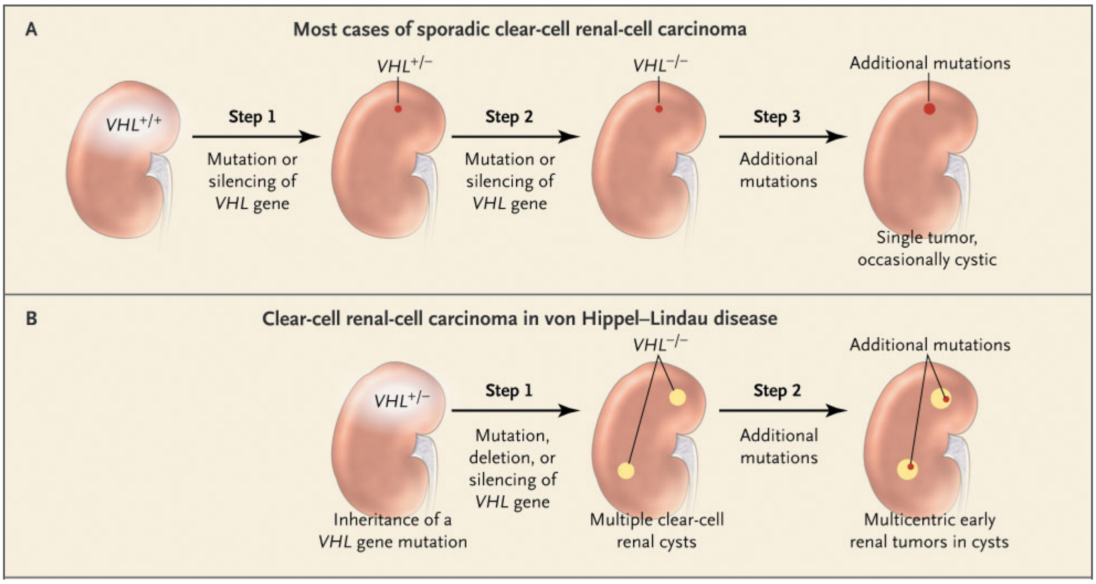

Figure 1.3.1: Development of clear cell RCC. (A) Sporadic RCC; (B) hereditary RCC (B). Figure adapted from [40].

1.4 An introduction to MDM2

The *MDM2 (Mouse Double Minute)* gene was initially identified on acentric double-minute chromosomes of spontaneously transformed mouse 3T3 fibroblasts [44]. These abnormal chromosomes were later discovered to contain more than 50-fold amplified genes that contribute to cellular proliferation and tumorigenesis [45]. It was found that amplification of the *MDM2* gene contributes to tumorigenicity as demonstrated in studies in which it was experimentally overexpressed in NIH3T3 cells and in Rat2 cells [45]. It was first thought that MDM2 primarily acted to inhibit the tumour suppressor p53-mediated transcriptional activation through direct interaction [46]. The ability of MDM2 to promote proteasomal degradation of p53 (as described Section 1.4.2.1) was not realised for a number of years [47, 48]. The importance of the interaction of MDM2 with p53 can be seen in gene targeting studies, which have demonstrated that mouse embryos lacking *Mdm2* die early after implantation, but this lethality can be completely rescued in a p53-null background, indicating that the embryo lethality was due to the lethal effects of unregulated *p53* [49, 50]. This has also demonstrated that Mdm2 is a major negative regulator of p53, at least during embryonic development.

A homolog of MDM2, called MDMX (also known as MDM4), also plays a critical role in the negative regulation of p53 during embryonic development [51, 52]. Similar to mice deficient in *MDM2*, *MDMX*-null mice also suffer p53-dependent embryonic lethality [53]. Whilst it was demonstrated that homozygous deletion of *MDM2* significantly elevates p53 protein levels in MEFs, homozygous deletion of MDMX in an MDM2 heterozygous background also resulted in an increase in p53 levels, but to a lesser extent [52]. Considering the fact that MDMX lacks the E3 ligase activity, it is widely accepted that MDM2 regulates p53 primarily through governing p53 protein stability, whereas MDMX does so through alternative mechanisms (see Section 1.4.4 for more details), for example, inhibiting p53 transcriptional activity via interaction with the p53 transactivation domain [51, 54-56].

1.4.1 MDM2 structure

Human MDM2 consists of 491 amino acids and of several major domains, including a p53-interacting domain, RING (Really Interesting New Gene) domain, nuclear localisation sequence (NLS), nuclear export sequence (NES), nucleolar localisation sequence (NoLS), and acidic domain (Figure 1.4.1.1) [57]. Located on the amino-terminus of MDM2, the p53-interacting domain, as suggested by its name, is able to interact with the transactivation domain of p53 [58]. This interaction permits MDM2 to inhibit p53 from binding to the basal transcriptional machinery, thus impeding p53-mediated transcriptional activation of its target genes [46, 59]. Additionally, through interaction with p53, MDM2 also facilitates nuclear export of p53 in a RING domain-dependent manner [60]. The evolutionary conserved carboxy-terminal RING domain of MDM2 is mainly responsible for its intrinsic E3 ligase activity. The RING domain contains a conserved cysteine-rich sequence motif, usually Cis_3-His-Cis_4, which forms two interleaved zinc-binding sites. The zinc-binding sites contain four pairs of cysteine and histidine residues in a 'cross-brace' configuration (Figure 1.4.1.2), which serve to coordinate two zinc ions for proper folding [61-64]. Mutations of these key cysteine or histidine residues have been shown to abolish the intrinsic E3 ubiquitin ligase activity of MDM2 [62, 65]. Apart from E3 ligase activity, the RING domain is also important for nucleotide and RNA binding, as well as protein-protein interaction, such as dimerisation between MDM2 and MDMX through their mutual RING domains [66-68]. Binding of ATP at the RING domain has also been reported to facilitate nucleolar localisation of MDM2 [68]. The nuclear localisation and nuclear export signals are responsible for nucleo-cytoplasmic shuttling of MDM2, providing another mechanism regulating p53 activity [69, 70]. MDM2 can export active p53 from the nucleus (where p53 can transactivate its target genes) to the cytoplasm, where p53 can no longer induce transcription but only exert other cytoplasmic functions [55, 71, 72]. MDM2 also contains a NoLS at its carboxy-terminal, which may be necessary for MDM2 to polyubiquitinate p53 [73]. The central acidic domain of MDM2 is required for interaction with the ribosomal protein L5 and p300/CBP (CREB-binding protein). Studies have found that an MDM2 mutant defective in p300-binding can promote ubiquitination but not degradation of p53 [74, 75]. This suggests the importance of p300 in regulation of MDM2-mediated p53 ubiquitination and proteolytic processes [76].

Another evolutionarily conserved domain of MDM2 is the zinc finger domain, which is believed to play a role in MDM2 interaction with ribosomal proteins and in MDM2-mediated degradation of p53 [77]. MDM2 zinc finger mutants are defective at mediating nuclear export and p53 degradation, but retain an ability to abrogate p53 transcriptional activity [77].

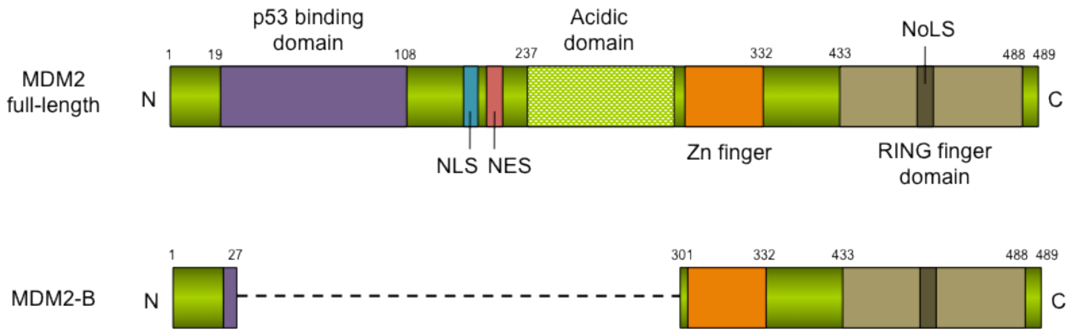

Figure 1.4.1.1: Schematic structure of full-length MDM2 protein and splice variant MDM2-B. NLS, nuclear localisation signal; NES, nuclear export signal; Zn-finger, Zinc-finger; NoLS, nucleolar localisation signal; N, amino-terminal; C, carboxyl-terminal. Figure adapted from [57, 78].

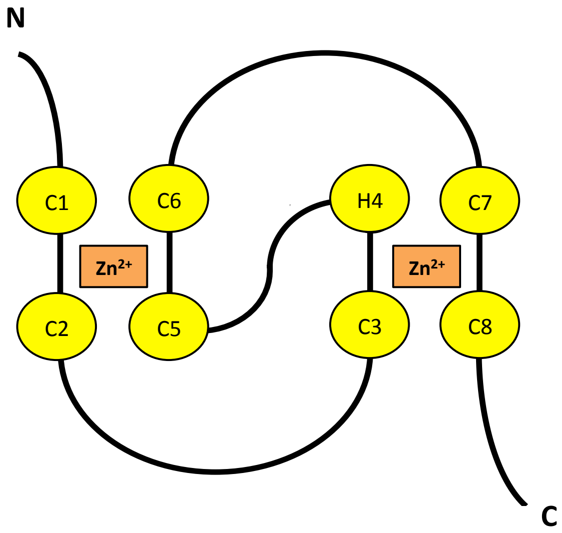

Figure 1.4.1.2: Zinc coordination topology for RING domain. The zinc-binding sites contain four pairs of cysteine (C) and histidine (H) residues in a 'cross-brace' configuration, which serve to coordinate two zinc ions (Zn^{2+}) for proper folding. The first pair of ligands (C1 and C2) together with the third pair (C5 and C6) coordinates one Zn^{2+}, and the second (C3 and H4) and fourth (C7 and C8) pairs bind the second Zn^{2+}. Figure adapted from [63].

1.4.2 MDM2 as an E3 ubiquitin ligase

One of the major roles of MDM2 is to act as a negative regulator of p53 by directly controlling p53 protein degradation rate (see Section 1.4.2.1 for more details) [48, 79-83]. As mentioned in Section 1.4.1, MDM2 possesses p53-specific E3 ubiquitin ligase activity within its carboxy-terminal RING-finger domain [62]. This E3 ligase activity allows MDM2 to transfer ubiquitin moieties onto other protein, in a process called ubiquitination. Similar to many other post-translational modifications, ubiquitination is an inducible and reversible process crucial for altering the properties of modified substrate [84, 85]. This inducible and reversible

process allows ubiquitination to modulate cellular homeostasis and signaling, including sub-cellular localisation, stability or enzymatic activity [84, 85].
Ubiquitination involves the covalent attachment of an 8.5 kDa polypeptide to lysine residues present on substrate protein [84]. It takes place according to a cascade of enzymatic reactions catalysed by three enzymes: ubiquitin-activating enzyme (E1), ubiquitin-conjugating enzyme (E2), and ubiquitin ligase (E3) (Figure 1.4.2.1) [86, 87]. E1 initiates the activation of ubiquitin in an ATP-dependent manner and forms a thioester bond between the carboxy-terminal carboxyl group of ubiquitin and the cysteine residue within the active site of E1 [88]. This generates a high-energy thiol ester intermediate and the ubiquitin molecule is subsequently transferred to the catalytic cysteine of E2, which also generates a thioester linkage [84, 88, 89]. The last step of ubiquitination involves an E3 ubiquitin ligase catalysing the attachment of the activated ubiquitin to its specific substrate, through forming an isopeptide between the lysine residue within the substrate and the carboxy-terminal carboxyl group of the ubiquitin [84, 88, 89].

Two main types of ubiquitination are mono-ubiquitination and poly-ubiquitination (Figure 1.4.2.2). Mono-ubiquitination involves the attachment of a single ubiquitin moiety on a lysine residue within a substrate, or of multiple single ubiquitin moieties on different lysine residues within the same substrate [84]. Mono-ubiquitination has been implicated in many fundamental non-proteolytic cellular processes, for example, sub-cellular localisation, DNA repair, endocytosis and histone regulation [84]. On the other hand, poly-ubiquitination is the formation of ubiquitin chain on a substrate protein. Ubiquitin itself has seven lysine residues that can serve as linking points for forming ubiquitin chains, of which Lysine (K) 48 and K63 are two of the best studied residues [90]. K48-linked ubiquitin chains usually serve as the primary targeting signals for proteolytic degradation by 26S proteasome [85, 91, 92]. K63-linked chains, however, do not support protein destruction, but are instead responsible for coordinating processes, such as DNA repair and protein sorting [85, 93]. Thus the type of ubiquitination has a huge influence on the fate of ubiquitinated substrates in signalling pathways.

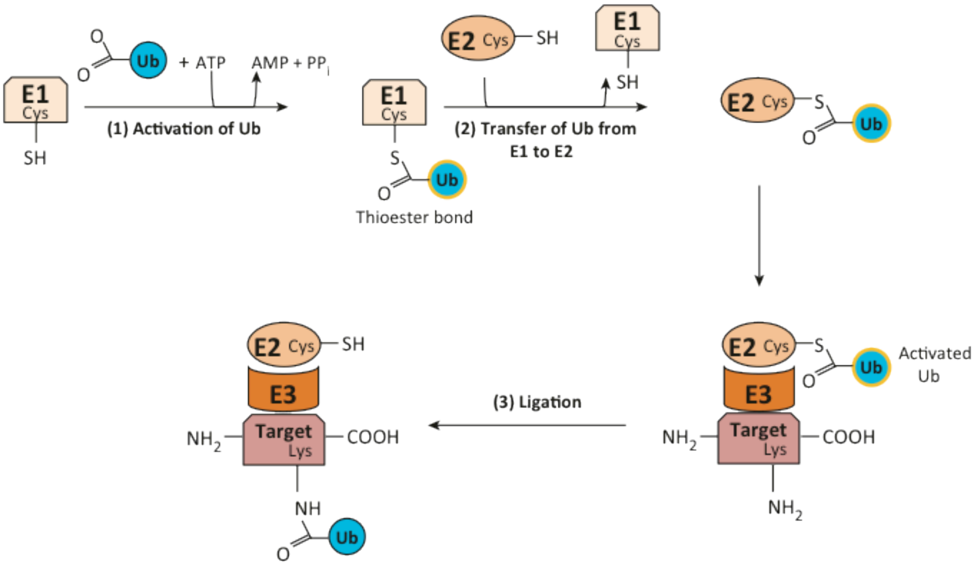

Figure 1.4.2.1: Ubiquitination cascade. Ubiquitination occurs according to a three-step catalytic cascade of three enzymes: ubiquitin-activating enzyme (E1), ubiquitin-conjugating enzyme (E2), and ubiquitin ligase (E3). Ubiquitin is coupled to the cysteine residue within the active site of E1 enzyme in an ATP-dependent manner to form a thioester. Secondly, ubiquitin is transferred to the catalytic cysteine of E2 enzyme, and again, forming a thioester. The third step is catalysed by E3 ubiquitin ligase and involves the covalent attachment of the activated ubiquitin to a lysine residue within the substrate. Figure reproduced from [88].

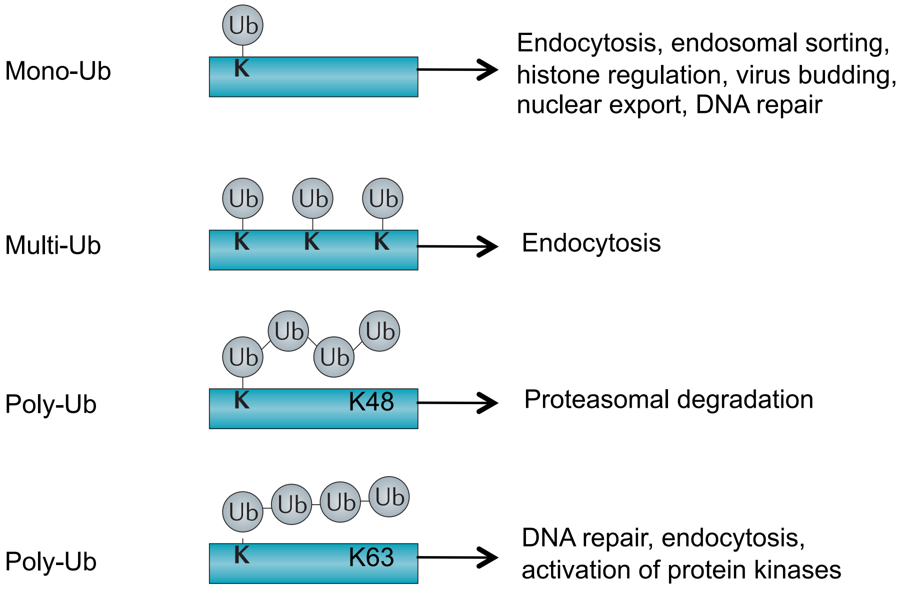

Figure 1.4.2.2: Types of ubiquitination and their cellular functions. Attachment of a single ubiquitin (Ub) moiety to a single lysine (K) residue results in protein mono-ubiquitination (mono-Ub). Addition of several single Ub molecules to different lysine residues is called multiple mono-ubiquitination (multi-Ub). These modifications are involved in a range of non-proteolytic cellular functions, including endocytosis, endosomal sorting, histone regulation and DNA repair. Poly-ubiquitination (poly-Ub) involves the addition of ubiquitin chain to one or more lysine residues. Ub chain forms via lysine 48 (K48) of Ub and usually represent a signal for proteasomal degradation of modified substrates. On the other hand, K63-linked ubiquitin chains are implicated in DNA repair and protein kinases activation. Figure adapted from [85, 94].

1.4.2.1 MDM2-mediated ubiquitination of p53 and other proteins

MDM2 can act as an E3 ubiquitin ligase for tumour suppressor p53. Mono-ubiquitination of p53 by MDM2 can cause changes in localisation of p53 through unmasking an intrinsic NES as a result of dissociation of p53 tetramers, whilst poly-ubiquitination of p53 by MDM2 leads to proteasomal degradation of p53 [47, 48, 80, 95]. Mono-ubiquitination of p53 by MDM2 plays an important role in facilitating nuclear export of p53 [96]. MDM2-mediated mono-ubiquitination of p53 has been shown to mediate cytoplasmic translocation of p53 in unstressed cells, which can inhibit p53 transcriptional activity in the nucleus [96, 97]. Furthermore, mono-ubiquitination of p53 can also result in localisation of p53 to mitochondria, where p53 can trigger a direct and transcription-independent apoptotic program [98].

It was initially thought that proteasomal degradation of p53 was exclusively cytoplasmic and thus MDM2-p53 nuclear export was indispensable for p53 degradation [69, 99]. However, it is increasingly evident that MDM2-mediated degradation of p53 can occur in either the nucleus or cytoplasm, omitting the need for nuclear export in p53 ubiquitination and degradation [100, 101]. Increased levels of ubiquitinated p53 have been observed in cells treated with the nuclear export inhibitor leptomycin B, suggesting that nuclear export is not required for p53 ubiquitination and that the ubiquitination process occurs in the nucleus [60]. In addition, Joseph *et al.* showed that during the down-regulation of a p53 response after multiple forms of DNA damage, degradation of endogenous p53 occurs in both nucleus and cytoplasm [100]. When DNA damage has been successfully repaired, an active p53 response is no longer required and could be deleterious to cell survival. Both nuclear and cytoplasmic proteasomes are recruited to efficiently degrade the elevated p53 proteins to restore normal homeostasis [100]. Recent studies have shown that MDM2-mediated degradation of p53 may also occur in the nucleolus, and that the transit of MDM2 through the nucleolus appears to be essential for p53 ubiquitination and export [102].

Apart from p53, MDM2 has various other ubiquitination substrates, including MDM2 itself (auto-ubiquitination), MDMX, retinoblastoma protein (pRB), dihydrofolate reductase (DHFR), E-cadherin, NUMB, Notch 1 receptor, Forkhead box O 4 (FOXO4), glucocorticoid receptor (GR), and insulin-like growth factor 1 receptor (IGF-IR) [65, 103-110]. Recent studies have shown that auto-ubiquitination of MDM2 facilitates stronger recruitment of E2 conjugating enzymes, thereby enhancing the efficiency of ubiquitination [111]. MDM2 was initially proposed to regulate its own stability via auto-ubiquitination [62, 112, 113]. However, the observation was later challenged by studies using mouse models lacking the E3 ligase function, which demonstrated that auto-ubiquitination is not necessary for degradation of MDM2 *in vivo* [79, 114]. Instead, MDM2 degradation may be regulated by other E3 ubiquitin ligases, such as $SCF^{\beta\text{-TRCP}}$ [115]. MDMX, can also be ubiquitinated by MDM2 leading to proteasomal destruction [116, 117]. Studies have demonstrated that upon DNA damage, MDM2 promotes ubiquitination and degradation of MDMX to ensure optimal p53 activation [116]. Additionally, MDM2 has also been reported to mono-ubiquitinate histones H2A and H2B, causing transcriptional repression of p53 target genes [118].

Like most post-translational modifications, the process of ubiquitination can be reversed, commonly by deubiquinating enzymes (DUBs). Deubiquitination allows for a binary switch between mono- and poly-ubiquitination or to switch off the ubiquitin signal completely [85, 86, 119]. For instance, deubiquinating enzyme, HAUSP (Herpesvirus-associated ubiquitin-specific protease), has been shown to deubiquitinate and stabilise the p53, MDM2 and MDMX proteins [120]. It has been demonstrated that ATM (ataxia telangiestasia mutated)-mediated phosphorylation of MDM2 and MDMX can lead to a disrupted interaction with HAUSP, resulting in stabilisation of MDM2 and MDMX upon DNA damage [121]. Since the interaction between HAUSP and p53 was not diminished upon DNA damage and that ATM-mediated phosphorylation activates the p53 protein, this allows proper p53 activation upon DNA damage [121].

1.4.3 MDM2 and human cancer

MDM2 was identified because it was oncogenic before it was known that it negatively regulates p53 [44, 46]. As an oncogene that is activated by increased expression, *MDM2* gene amplification has been observed in approximately one-third of human sarcomas [81]. In addition, the *MDM2* gene is also frequently overexpressed in various human cancers, notably in breast, renal, colon, prostate, and lung cancers, as well as in lymphomas and leukaemias [122-128]. Studies have shown that MDM2 overexpression is associated with tumours that have a higher degree of invasiveness, greater metastatic potential, poorer prognosis and are more resistant to chemotherapeutic agents and radiation [128]. In a recent study, it has been suggested that high levels of MDM2 are associated with poor prognosis in invasive ductal breast cancer (IDC) [129]. This observation may be due to MDM2 overexpression inducing matrix metallopeptidase-9 (MMP-9) expression, leading to a rise in extracellular breakdown and subsequently increased tumour invasiveness [129]. However, the mechanism by which MDM2 up-regulates MMP-9 remains unclear. In another study examining 100 samples of esophageal squamous cell carcinoma, MDM2 expression was identified as the most significant risk factor for distant metastasis [130]. These studies highlight the impact of MDM2 overexpression on metastasis, which is the main cause of cancer-associated deaths.

Metastasis is a highly complex multi-step process which involves the detachment of tumour cells from the primary tumour, invasion of stromal tissue, migration, intravasation into the circulation, survival in the vasculature, extravasation and colonisation of a secondary site [2, 131, 132]. Different mechanisms involving MDM2 have been reported to promote metastasis. For example, hypoxia has been demonstrated to up-regulate MDM2 in a p53-independent manner to promote metastatic efficiency in tumour cell [133]. In addition, this up-regulation of MDM2 leads to a reduction in p53 levels and inhibition of the p53-mediated transactivation of pro-apoptotic genes, hence rendering tumour cells less sensitive to stress-induced apoptosis [133]. Hypoxia is a crucial stimulator of new blood vessel formation during tumour angiogenesis and metastasis [134]. In cancer, an insufficiency of tissue oxygen within solid tumours often increases neovascularisation, in order to supply the metabolic needs of growing tumour tissue [134]. Hypoxia has also been found to mediate translocation of MDM2 from the nucleus to the cytoplasm, leading to increased expression of vascular endothelial growth factor (VEGF), a potent angiogenic factor that actively contributes to distant metastasis [135].

There is uncertainty as to how MDM2 exerts p53-independent oncogenic effects. Yang *et al* reported an inverse correlation between MDM2 and E-cadherin protein levels, accompanied by an increase in cell motility in breast carcinoma cells [103]. The same study also demonstrated that high expression of MDM2 is significantly correlated with E-cadherin suppression in primary tumours of breast cancer patients with lymph node metastases [103]. In another study, MDM2 overexpression was shown to confer transforming growth factor-beta 1 (TGF-β1) resistance by abolishing the TGF-β1-induced growth inhibitory activities in a p53-independent manner in cells in culture [136]. Consistent with this notion, elevated MDM2 expression has been associated with loss of TGF-β-sensitivity in human breast tumour cells, indicating a potential role of MDM2 overexpression in TGF-β-resistance in human tumours [136]. Overexpression of MDM2 has been shown to negatively regulate the cell cycle regulatory function of the retinoblastoma protein (pRB) in a p53-independent manner [137]. Down-regulation of pRB, a negative regulator of cell cycle progression from G1 to S phase, as a result of MDM2-mediated ubiquitination and degradation, has been implicated in carcinogenesis in human lung cancer [137].

Up-regulation of MDM2 regardless of p53 status also plays a major role in determining the outcome in various common cancers. In renal cell carcinomas, there is a strong positive correlation between MDM2 and p53 expression ($p<0.00004$), and this phenotype was associated with poor prognosis [138]. Consistent with this observation, a more recent study with higher numbers of RCC specimens supports the observation that there is an association between p53 and MDM2 expression and this is accompanied by a reduced disease specific survival ($p<0.001$) [139]. Interestingly, this study has also demonstrated that the up-regulated p53 is predominantly wild-type, a situation which is distinct from most other cancer types whereby *TP53* mutations are commonly found in up-regulated p53 [139, 140]. The wild-type status of p53 in RCC is likely to promote the observed MDM2 co-expression, which may explain the association between p53 and MDM2 expression [139]. Although the mechanisms leading to increased MDM2 and p53 expression in RCC are still largely unknown, there is a clear disease-specific feature in RCC, which makes combined up-regulation of wild-type p53 and MDM2 a promising prognostic biomarker [139].

1.4.4 p53-MDM2 interaction

The importance of p53 in cancer is supported by the fact that p53 is mutated in nearly 50% of all human cancers, and is functionally inactivated in most of the remaining cancers through alterations in p53-associated signalling pathways [141]. Patients with Li-Fraumeni syndrome, most commonly harbour p53 germline mutations and have increased susceptibility to cancer [142, 143]. Furthermore, p53 homozygous knockout mice are developmentally normal but susceptible to spontaneous tumours at a young age (all dead by 6 months) [144, 145].

During the past two decades, p53 has often been referred to as the ‘guardian of the genome’ owing to its indispensable function in maintaining cellular genetic stability. p53 plays a crucial role as a transcription factor for downstream target genes involved in many physiological processes [146]. Depending on the different stages in the cell cycle, cell type and the type and/or duration of stress or DNA damage, p53 can selectively activate cell cycle control (p21, WAF1/CIP1, cyclin G), apoptosis (BAX, NOXA, PUMA), DNA replication and repair (GADD45, PCNA) and angiogenesis regulatory proteins (TSP-1, BAI1), just to name a few [147-150]. Thus, the level of p53 in a cell must be very tightly regulated to ensure that a delicate balance of appropriate p53 activity is maintained [55].

Consisting of 393 amino acids, p53 protein contains three major functional domains (Figure 1.4.4.1). The acidic amino-terminal domain of p53 is responsible for translational activation. MDM2 binds to this transactivation domain to abrogate p53 transcriptional activity [151]. The central core DNA-binding domain of p53 is essential for the role of p53 as a sequence-specific transcription factor [152]. The carboxy-terminal end of p53 houses the tetramerisation domain, a nuclear export signal and nuclear localisation signals [95]. p53 oligomerisation has been suggested to be necessary for efficient binding to MDM2 and MDM2-mediated ubiquitination, whereby p53 mutants defective of oligomerisation ability have reduced affinity for MDM2 and DNA binding [153, 154]. p53 is also subjected to a wide and complex range of post-translational modifications, including phosphorylation, ubiquitination, acetylation, methylation, glycosylation and SUMOylation [155, 156]. These post-translational modifications, which usually occur at conserved residues of p53, are known to have significant regulatory potential, particularly in terms of stabilisation and activation of p53 [157].

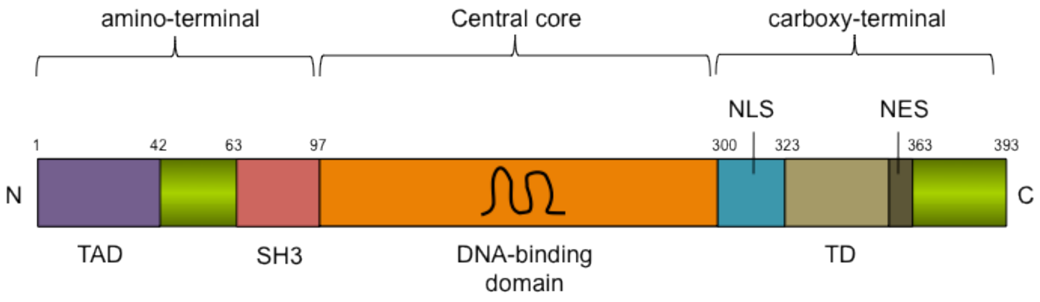

Figure 1.4.4.1: p53 protein structure. TAD, transactivation domain; SH3, SRC homology 3 domain; NLS, nuclear localisation signal; NES, nuclear export signal; TD, tetramerisation domain. Figure adapted from [156].

Since the consequences of uncontrolled p53 activity can be dire (deletion of *Mdm2* in mice leads to very early embryo lethality [49, 50]) it is imperative that the stability of p53 is tightly regulated. Indeed, in unstressed cells, p53 exhibits a very short half-life (typically ~6-30 minutes) as a result of efficient degradation [47, 158-160]. p53 protein is constantly being synthesised and continuously undergoes poly-ubiquitination leading to proteasomal degradation. However upon exposure to diverse stress signals, p53 levels rapidly accumulate as a result of p53 rescue from proteasomal degradation [156].

As a key negative regulator of p53, MDM2 employs several important mechanisms to effectively abrogate p53 functions that might otherwise lead to inappropriate cell cycle arrest or apoptosis. Apart from acting as an E3 ubiquitin ligase to regulate the localisation and degradation of p53 (as discussed in Section 1.4.2.1), MDM2 is also capable of binding to the transactivation domain of p53. This allows MDM2 to hinder p53 association with the general transcription machinery to exert p53 regulatory effects [46, 57, 161]. Another mechanism employed by MDM2 to regulate p53 activity is through a process analogous to ubiquitination, called NEDDylation. It has been demonstrated that MDM2 facilitates ubiquitin-like protein NEDD8 conjugation of p53 via its E3 ligase activity, resulting in inhibition of p53 transcriptional activity [162].

Interestingly, MDM2 is also a transcriptional target of p53. Wild-type p53 is capable of binding to the p53-responsive element of MDM2 to promote transcription of MDM2 [163]. When p53 levels increase, transcription of MDM2 is also induced. Hence, whilst MDM2 is a negative regulator of p53, it is itself being regulated by p53, establishing a negative auto-regulatory feedback loop [163]. In the absence of stress signals, p53 levels are kept low to allow normal cell proliferation and maintenance of cell viability. Upon cellular stress, p53 levels can rise through escaping the MDM2-mediated proteasomal degradation. Following DNA damage, protein kinases such as ATM and checkpoint kinase (Chk2), have been shown to stabilise p53 by phosphorylation [164, 165]. Phosphorylation of p53 interferes with MDM2 binding and thus prevents p53 ubiquitination and degradation [164, 165]. Once the stress is relieved, signals for p53 stabilisation are no longer required and MDM2 preferentially mediates p53 degradation to maintain p53 at low levels again [112].

Similarly to MDM2, MDMX is also an important negative regulator of p53. It has been reported that MDMX acts as an oncogene that becomes activated upon overexpression to promote tumour formation by inhibiting p53 activity [166]. In fact, MDMX is overexpressed in various types of cancers that retain wild-type p53, including breast, colon and lung cancers [166]. Despite having a RING domain, MDMX lacks the E3 ligase activity and is unable to directly poly-ubiquitinate p53 to promote proteasome-mediated proteolysis [67]. However, MDMX interacts with the p53 transactivation domain and thereby inhibits p53 transcriptional activity [51, 54]. It has been demonstrated that MDMX can inhibit p300/CBP-mediated p53 acetylation, which is likely to have a suppressive effect on p53 activity [167].

Despite high homology between them, MDMX and MDM2 seem to play non-redundant roles in inhibiting p53 [55]. Genetic studies show that, similarly to Mdm2, absence of *MdmX* expression in mice causes embryonic lethality that can be rescued by concomitant deletion of p53 [53]. Chavez-Reyes *et al.* demonstrated that the death in *Mdm2*-null mouse embryos due to apoptosis was partially rescued by the loss of *Bax*, a member of the *Bcl-2* gene family that positively regulates apoptosis [168, 169]. The same study has also shown that the absence of *p21*, a p53 target gene that initiates cell cycle arrest, in *MdmX*-null mouse switched the mechanism of cell death from cell cycle arrest to apoptosis [168]. The fact that *MdmX*-null mice seem to die because of loss of cell proliferation rather than because of uncontrolled apoptosis in the presence of *Mdm2* strongly argues that MDM2 and MDMX are non-overlapping regulators of p53 [53]. One possible explanation for this might be that whilst MDM2 is responsible for inhibition of the apoptotic activity of p53, MDMX may participate in the inhibition of p53-induced cell cycle arrest [53, 55]. For example, MDM2 and MDMX may bind different modified versions of p53 that could lead to the initiation of apoptosis and cell cycle arrest, respectively.

1.4.5 MDM2 interactions with other proteins

Despite its role as a major negative regulator of p53, MDM2 has p53-independent roles in tumorigenesis. Overexpression of MDM2 in tumours, accompanied by mutant or deficient p53, has been implicated in many cancers and has been associated with poor prognosis [131, 170, 171]. Analysis of a cohort of soft tissue sarcomas from adults has revealed that the tumours in which both MDM2 and p53 were overexpressed constitute 22 of the 207 screened (10.6%). Patients in this class also suffer the poorest prognosis and reduced survival ($p<0.05$) [124].

Studies using mouse models have addressed the *in vivo* effect of MDM2 overexpression in the absence of p53. Analysis of DNA content by Lungren *et al.* has shown that overexpression of MDM2 in epithelial cells of transgenic murine mammary gland led to polyploidy in 30-45% of the cells in both wild-type and p53-null mice [172]. This observation suggests a role for MDM2 in DNA replication that is independent of the ability of MDM2 to inhibit p53 activity [172]. In another study, the phenotype of *p53*-null mice was examined in the presence and absence of *Mdm2*. Intriguingly, tumour latency was prolonged in *p53*-null/*Mdm2* heterozygous mice, compared with *p53*/*Mdm2* double-null mice. In addition, the tumour spectrum also changed, in which the incidence of spontaneous sarcomas was higher in *p53*-null/*Mdm2* heterozygous mice than in *p53*-null or *p53*/*Mdm2* double-null mice [173]. The influence of MDM2 on the survival and tumour spectrum of *p53*-null mice supports the existence of additional roles for MDM2 other than inhibition of p53 function [173]. In addition, overexpression of an *MDM2* transgene in *p53*-null mice displays increased tumorigenesis, with higher rates of sarcomas in comparison to the incidence in *p53*-null mice without *MDM2* transgene expression, suggesting that MDM2 has fundamental p53-independent roles in tumorigenesis [174].

Furthermore, analysis of a variety of human tumours that overexpressed MDM2 has revealed more than 40 different splice variants of MDM2 [175]. Interestingly, the majority of these variants lack the p53-binding domain and are incapable of interacting with p53, suggesting that the tumour-isolated MDM2 variants may contribute to transformation in a p53-independent manner [175, 176]. One example is the MDM2-B variant, which lacks most of the p53-binding domain (as illustrated in Figure 1.4.1.1), has been shown to promote p53-independent cell growth and inhibit apoptosis [177]. Moreover, expression of MDM2-B also induces tumour formation in transgenic mice, implying that an alternate spliced form of MDM2 can contribute to tumorigenesis through a p53-independent manner [177].

It is not surprising that MDM2 exerts some of its p53-independent biological effects through interaction with a number of proteins. Most of these MDM2 interacting proteins have been identified using yeast two hybrid screening and immunoprecipitation methods and are involved in different cellular processes, such as cell cycle, differentiation, DNA synthesis, ribosome biosynthesis and transcription [57]. In particular, MDM2 interacts with major cell cycle regulators, including MDMX, alternate reading frame (ARF), E2F1/DP1 and retinoblastoma protein (pRB), as well as interacting proteins discovered in our laboratory, including MDM2 binding protein (MTBP), dihydrofolate reductase (DHFR), non-metastatic protein 2 (NME2) and DNA polymerase ε [66, 109, 178-184].

1.4.5.1 MDMX

MDMX is able to form heterodimers with MDM2 through their mutual RING finger domains [66]. Hetero-oligomers of MDM2 and MDMX have been found to be more stable than homo-oligomers of either protein [66]. MDMX was found to facilitate stabilisation of MDM2, since when full length MDMX was co-expressed with MDM2, degradation of MDM2 was significantly suppressed. Stabilisation of MDM2 has been shown to be dependent on the RING finger domain of MDMX, since mutants of MDMX that lack a RING domain do not interact with MDM2 and have no effect upon the half-life of MDM2 [66]. Hetero-dimerisation of MDMX and MDM2 has not only been shown to suppress auto-ubiquitination of MDM2 but promote p53 ubiquitination [67, 185-188]. Hence, the ability of MDMX to complex with MDM2 is important in regulating MDM2 and thus in determining p53 levels and keeping p53 activity low under physiological conditions [67, 186]. MDM2 and MDMX are functionally interdependent [189]. Whilst studies show that MDM2 E3 ligase activity is partially dependent on MDMX, MDMX function also depends on MDM2 [55]. Unlike MDM2, MDMX does not possess nuclear localisation and nuclear export signals, and is restricted to cytoplasmic localisation in the absence of MDM2 [190]. Thus, MDMX is dependent on MDM2 to enter the nucleus, where the MDM2/MDMX complex can form and inhibit p53 activity [189, 190].

1.4.5.2 Alternate Reading Frame (ARF)

ARF ($p14^{ARF}$ in humans and $p19^{ARF}$ in mice) was identified as an alternative reading frame in the *p16INK4a* tumour suppressor locus and is activated in response to oncogenic activity [180, 181]. ARF is a well-documented regulator of MDM2 and a potent activator of p53. Unlike MDM2, which mainly localises to the nucleoplasm, ARF is predominantly found in nucleoli [191]. Several mechanisms of ARF-mediated MDM2 inhibition have been documented. One proposed mechanism is that in response to oncogenic signals, ARF inhibits MDM2 E3 ligase activity towards p53, thus preventing MDM2 from promoting ubiquitination and subsequent degradation of p53, resulting in stabilisation and activation of p53 [192, 193]. It was initially thought that ARF binds to the RING finger domain of MDM2 and prevents nucleo-cytoplasmic shuttling of MDM2 through sequestering MDM2 in the nucleolus, and subsequently relieving nucleoplasmic p53 from MDM2-mediated degradation [99, 194-196]. However, these findings are debatable as later studies have suggested that nucleolar relocalisation of MDM2 is not essential during ARF-induced growth arrest and that redistribution of ARF into the nucleoplasm promotes its interaction with MDM2 and induces p53-dependent growth-suppressive activity [197, 198].

1.4.5.3 Retinoblastoma protein (pRB)

MDM2 has been identified to bind to pRB, a tumour suppressor that guards the advance of cell cycle through the restriction-point into late G1 phase [178]. In its unphosphorylated or hypophosphorylated state, pRB binds to the E2F transcription factor via a pocket domain. This interaction prevents E2F from acting as a transcription factor to stimulate transcription of S phase-specific genes [178]. Upon hyperphosphorylation of pRB, E2F is released to activate transcription of growth-promoting genes to promote cell cycle progression from G1 to S phase [178, 199, 200]. MDM2 can perturb pRB function through binding to a domain located in the carboxy-terminal of pRB which overlaps with a domain required for growth suppression function of pRB and for stable interaction with E2F [201]. In a manner similar to p53, MDM2 also regulates pRB function by targeting it for ubiquitin-dependent degradation as it has been demonstrated that pRB can be efficiently ubiquitinated by MDM2 and then degraded via the proteasome [110].

Down-regulation of MDM2 has been reported to stabilise endogenous pRB [110], supporting the role of MDM2 in pRB degradation. The MDM2-pRB interaction also plays an important role in regulating the stability and apoptotic function of p53 [202]. It has been suggested that MDM2 acts as a bridge that brings MDM2, pRB and p53 into a trimeric complex [203]. pRB prevents MDM2 from targeting p53 for degradation, thereby resulting in p53 stabilisation [202]. Although p53 in the trimeric complex is transcriptionally inactive, its apoptotic function remains intact [202]. Thus the trimeric complex allows pRB to selectively modulate the stability and function of p53 through counteracting the anti-apoptotic and degradation function of MDM2 [110, 202, 203].

1.4.5.4 E2F1

In addition to inhibition of pRB-E2F1 interaction by competition, MDM2 can also drive cells into S phase by direct interaction with E2F1 that leads to activation of E2F1/DP1-mediated transactivation [204]. The E2F1 transcription factor functions as a heterodimer with DP1 to activate genes required for S phase entry. MDM2 interacts with E2F1/DP1 and stimulates the transcriptional activity of the heterodimer and thus promotes cell proliferation [182]. On the other hand, it has been shown that *E2F1*$^{-/-}$ knockout mice lead to an increase in tumour formation [205]. Overexpression of E2F1 has also been shown to promote premature S phase entry and eventually lead to apoptosis [206]. These studies suggest that E2F1 also participates in growth-inhibitory and tumour suppressor activities [207]. It has been demonstrated in p53$^{-/-}$ cells that MDM2 promotes degradation of the E2F1/DP1 heterodimer, which leads to inhibition of the pro-apoptotic effect of E2F1/DP1 [208]. This indicates that MDM2 can prevent E2F1-dependent apoptosis in a fashion that is independent of p53 [208]. By blocking the apoptotic activity of E2F1, MDM2 turns the properties of E2F1 from a negative to a positive regulator of the cell cycle progression, parallels to the anti-apoptotic effect of MDM2 [208].

1.4.5.5 ATM (Ataxia Telangiectasia Mutated) and PI3 (Phosphatidylinositol 3-OH) kinase

Phosphorylation of MDM2 plays an important role in modulating its activity. Several kinases have been shown to interact with and phosphorylate MDM2, thereby affecting of MDM2 and p53 interaction [209]. One of these kinases is ATM encoded by *ATM* gene that is a frequently mutated in patients with a rare inherited disorder (Ataxia Telangiectasia) that makes them hypersensitive to radiation [210]. In response to cellular stresses such as ionising radiation and DNA damage, ATM kinase phosphorylates MDM2 and blocks its association with p53 [211, 212]. Meanwhile, ATM is also able to directly phosphorylate p53, protecting it from MDM2-mediated ubiquitination [213, 214]. As a result, phosphorylation of both MDM2 and p53 by ATM abrogates MDM2 ability to trigger nuclear export and proteasomal degradation of p53, causing an accumulation of p53 levels in the cell. Furthermore, PI3 kinase and its downstream target, Akt/PKB serine-threonine kinase, also appear to bind and phosphorylate MDM2, following mitogen-induced activation [215, 216]. Phosphorylation of MDM2 on serine 166 and serine 186 is required for translocation of MDM2 from the cytoplasm into the nucleus, where MDM2 ubiquitinates p53 and mediates its degradation [217, 218]. Ultimately, the effect of phosphorylation-induced elevation of MDM2 via the mitogenic signalling pathway leads to suppression of p53 protein levels.

1.4.5.6 MDM2 binding protein (MTBP)

MTBP was first identified as an MDM2-interacting protein using the yeast two-hybrid screen [179]. It has been demonstrated that MTBP is a growth regulator and its interaction with MDM2 may play both promoting and suppressive roles in tumorigenesis [131]. MTBP expression has been demonstrated to inhibit proliferation by inducing p53-independent G1 arrest, an effect which can be overcome by MDM2 [179]. On the contrary, there are also reports that suggest an oncogenic role of MTBP. Studies by Brady *et al.* demonstrated that overexpression of MTBP in tumour cell lines facilitates MDM2-mediated ubiquitination and degradation of p53, whilst reducing auto-ubiquitination and thus stabilising MDM2 [219]. Another study by Odvody *et al.* claimed that reduced MTBP expression decreased Myc-induced B-cell lymphomagenesis

[220]. The opposite roles of MTBP in cancer may indicate that MTBP's function is context-dependent. In fact, the expression levels of MTBP seem to be specific to the types of cancer. In B-cell lymphomas, an elevated MTBP expression is observed in comparison to normal human lymphoid tissue controls [220]. On the other hand, the loss of MTBP has been associated with a reduced survival in head and neck carcinoma patients, and serves as an independent prognostic factor when p53 is mutated in tumours [221].

To understand the physiological function of MTBP, mice with deletions of critical exons in the *Mtbp* gene were generated [222]. The loss of both alleles of *Mtbp* resulted in early embryonic lethality [222]. In contrast to *Mdm2* deletion, the lethality of homozygous *Mtbp* deletion could not be rescued by concomitant deletion of p53, indicating that this phenotype is p53-independent [222]. *Mtbp* heterozygous mice were viable and do not present with any obvious phenotype [222]. However, when these mice were predisposed to tumorigenesis in the $p53^{+/-}$ background, $Mtbp^{+/-}p53^{+/-}$ mice significantly increase invasiveness of osteosarcoma cells [222]. Moreover, overexpression of *Mtbp* in $Mtbp^{+/-}p53^{+/-}$ osteosarcoma cells inhibited invasiveness, suggesting the role of MTBP as a metastasis suppressor [222]. The mechanism by which MTBP inhibits cancer metastasis is not entirely clear. The same study also demonstrated that overexpression of MTBP in human osteosarcoma cell lines lacking wild-type p53 has no effect on primary tumour growth in mice, but significantly inhibits tumour metastases [222]. MTBP down-regulation significantly increased the migratory potential of $MDM2^{-/-}p53^{-/-}$ mouse embryonic fibroblasts, suggesting the MTBP suppresses cell migratory potential independently of MDM2 and p53 [223]. Using immunoprecipitation and mass spectrometry, alpha-actinin-4 (ACTN4) was identified as an MTBP-interacting protein [223]. ACTN4 plays important role in cytoskeleton organisation of the actin network and has been implicated in cancer cell migration and metastasis [224-226]. Co-expression of MTBP and ACTN4 has been shown to inhibit ACTN4-induced cell migration, suggesting that MTBP affects cell migratory potential, at least partly, through suppressing ACTN4 function [223].

1.4.5.7 p300/CBP

The transcriptional co-activator p300/CBP can both elevate p53 transactivation activity and promote MDM2-mediated degradation of p53. In particular, p300/CBP interacts with and acetylates p53 to facilitate p53-mediated transactivation [227]. On the other hand, p300/CBP promotes p53 degradation through interaction with the central acidic domain of MDM2 [76]. MDM2 lacking its p300/CBP-binding domain failed to destabilise p53 [75]. This suggests a dual role of p300/CBP in regulation of p53.

1.4.5.8 Dihydrofolate Reductase (DHFR)

DHFR plays an essential role in the synthesis of nucleic acids precursors. MDM2 interacts directly with DHFR and catalyses its mono-ubiquitination, in a RING finger-dependent manner [109]. Mono-ubiquitination of DHFR by MDM2 leads to a reduction in DHFR activity, and this effect is independent of p53 [109]. Nevertheless, it seems that MDM2 does not promote poly-ubiquitination of DHFR, which may explain why MDM2 has no effect on the stability of DHFR [109].

1.4.5.9 Non-metastatic protein 2 (NME2)

NME2 was identified as an MDM2-interacting protein using affinity chromatography and yeast two-hybrid screening, followed by validation by mass spectrometry [183]. The interaction between MDM2 and NME2 is highly specific, since NME1 which possesses high homology to NME2 does not seem to interact with MDM2. MDM2 and NME2 display opposing effects on motility since it has been demonstrated that NME2 contributes to motility suppression when MDM2 is expressed at normal physiological levels [183]. In addition, up-regulation of MDM2 in RCC cells abrogates the motility-suppressing effect of NME2 in a p53-independent manner [183]. This provides a potential mechanism for the ability of MDM2 to promote tumour cell motility and metastasis, potentially linking MDM2 expression with poor prognosis in RCC [183]. NME will be discussed in more details in the next few sections.

1.5 NME protein family

The *non-metastatic* (*NME*) (otherwise known as *NM23*, *NDPK* or *AWD*) gene family is a very ancient gene family found in all kingdoms of life, from bacteria *Escherichia coli* to *Homo sapiens*, showing a strong conservation throughout the course of evolution [228-231]. The NME protein family has been reported to be involved in a plethora of molecular processes, including tumour metastasis, cell proliferation, differentiation, development, motility, apoptosis, and DNA repair [183, 232-239].

Some of the members of the NME family exhibit a nucleoside diphosphate kinase (NDPK) activity, which corresponds to the phosphoryl transfer from a nucleoside triphosphate to a nucleoside diphosphate, as first described in pigeon breast muscle and yeast [231, 240, 241]. Sequences encoding proteins with validated NDPK activity and primary structures were later discovered in bacteria (*Myxoccus Xanthus*) and rat [242-244]. These proteins were originally named NDPK due to their NDPK activity [231, 243-245]. The NME was first identified as a cDNA clone that was down-regulated in highly metastatic murine melanoma cell lines, and hence was also named NM23 for ‘non-metastatic clone 23’ [246]. In Drosophila, the amino acid sequence of Abnormal Wing Discs (AWD) shares a high degree of conservation with the human NM23 [247]. AWD is in fact an NDPK kinase and the killer-of-prune mutation of AWD results in abnormalities in Drosophila cell morphology and differentiation [248]. For simplicity and to avoid confusion, as well as to follow the current official gene nomenclature, the term ‘NME’ will be used throughout this thesis [231, 245].

To date, there are over seventy cDNA sequences for NME obtained in a wide variety of organisms, displaying partial or complete NDPK domains [228, 231]. In humans, ten genes have been documented, and are typically classified into two distinct groups based on their sequence homology and NDPK activity [231]. Group I NME proteins, which comprised of NME1 to NME4 (NDPK-A to -D or NM23-H1 to -H4), share 58% to 88% sequence similarity with each other with no gap or insertion [228]. This group of NME proteins generally exhibit a highly conserved domain and possess the active sites for NDPK activity [228]. On the other hand, members of the Group II NME proteins are highly divergent and share only 25% to 45% of sequence similarity with the Group I proteins and between each other [228]. With the exception of *NME6*, all Group II genes (*NME5-10*) encode protein that are most found in ciliated structures such as primary cilia and sperm flagella [249]. Intriguingly, a read-through transcript for *NME1* and *NME2* genes that codes for a fusion protein has been reported [250]. This fusion protein, called NM23-LV (for long variant, also known as NME1-NME2), consists of part of NME1 fused to a complete NME2 [250, 251]. A summary of the characteristics and properties of various isoforms of the human NME family is represented in Table 1.5.1.

As mentioned in Section 1.4.5.9, MDM2 has been shown to interact with NME2 and has an antagonising effect on NME2 motility suppressive effect [183]. This finding has formed part of the basis for our project. Due to the high degree of homology between NME1 and NME2, their well known roles in cancer and for the purpose of my thesis, I will focus mainly on NME1, NME2 and the more recently discovered NM23-LV. We will first discuss the properties and functions of NME3 to NME10 proteins, followed by a more detailed discussion on NME1, NME2 and NM23-LV proteins in later sections.

1.5.1 NME3 to NME10 proteins

1.5.1.1 NME3

NME3 cDNA was identified through differential screening of a chronic myelogenous leukemia-blast crisis (CML-BC) cDNA library [233]. The NME3 protein has about 65% amino acid sequence similarity to the putative NME1 and NME2 proteins [233]. NME3 possesses an amino-terminal hydrophobic sequence, which is responsible for the anchorage of NME3 to membranes, in particular the mitochondrial outer membrane [252]. CML is a malignancy of the human hemapoietic stem cell that evolves in two clinically distinct stages: a chronic and a blast crisis phase. During the blast crisis transition of CML, NME3 mRNA was expressed at the early stages of myeloid differentiation [233]. When overexpressed by transfection, NME3 is able to inhibit granulocytic differentiation and induce apoptosis in myeloid precursor 32Dc13 cells [233]. These observations suggest a role for NME3 in hematopoiesis and CML blastic transformation [233].

1.5.1.2 NME4

NME4 was identified as a human NDPK that can target mitochondria via an amino-specific sequence, which is cleaved to reveal catalytic activity [253]. NME4 is ubiquitously expressed and active as a hexamer, like other NME isoforms from Group I [253-255]. Interestingly, NME4 naturally possesses the proline to serine substitution equivalent to the *K-pn* mutation (P97S) of *Drosophila* [256]. This point mutation of *awd* causes lethality in the genetic context of *prune* eye colour mutation, but has no effect on the catalytic activity of the enzyme [257]. The *K-pn* mutation is located in a loop, and thus named K-pn loop, which plays an important role in the stability of the hexamers [257, 258]. NME4 has been shown to be associated with the inner mitochondrial membranes, possibly for supplying NTP/NDP for nucleic acid and protein synthesis and respiration [253, 259]. Schlattner *et al.* (2013) demonstrated that NME4 interacts with the mitochondrial GTPase OPA1, which suggests that NME4 has a role in providing a local supply of GTP [260]. In addition, NME4 has also been shown to interact with anionic phospholipids, particularly cardiolipin, which leads to inhibition of the phospho-transfer activity but allows for the intermembrane lipid transfer function of NME4 and sensitises cells for apoptosis [260]. Thus, NME4 may act as a lipid-dependent mitochondrial switch with dual roles in phospho-transfer for delivering local GTP supply and in cardiolipin transfer for apoptotic signalling [260].

1.5.1.3 NME5

NME5 was first identified in spermatogonia and early spermatocytes in human testis [261]. NME5 encodes a 212 aa protein with 27-31% identity to other members of the NME family [261]. The biological roles of NME5 is not well documented. Studies have suggested that NME5 is involved in the differentiation of spermatozoa [262]. It has been shown that NME5 was down-regulated in several tumour types, including urothelial carcinoma and malignant breast cancer [263, 264].

1.5.1.4 NME6

The mRNA expression of NME6 is found in most human tissues, particularly in kidney, prostate, ovary, intestine, and spleen [265]. Of all the members from Group II, only NME6 has been reported to possess NDPK activity [228, 231]. It has been shown that overexpression of NME6 in SAOS2 cells leads to growth suppression and generation of abnormally shaped multinucleated cells as a result of mitosis failure [266]. This suggests that NME6 may have important roles in the regulation of cell growth and cell cycle progression [266].

1.5.1.5 NME7 and NME8

NME7 and *NME8* genes were identified by Mehus and Lambeth (unpublished data, reviewed in [228]). The *NME7* gene contains 12 exons spanning over 180 kb, whereas the *NME8* gene is comprised of 17 exons spanning over 50 kb. Both NME7 and NME8 possess a tandemly repeat kinase domain. Tissue analysis reveals that NME7 and NME8 are predominantly expressed at the mRNA level in testes. Expression of NME7 is also detected in liver, heart, brain, ovary, small intestine, and spleen (reviewed in [228]).

1.5.1.6 NME9

The *NME9* gene encodes a protein of 330 amino acids consisting of two major domains: an amino-terminal domain typical of a thioredoxin (small 12 kDa protein that functions as a protein-disulfide reductase) and a carboxy-terminal domain belonging to the NME family [267]. Thus NME9 is also known as thioredoxin-like protein 2 (Txl-2). NME9 mRNA was ubiquitously expressed, with expression predominantly found in testis and cilia of lung airway epithelium [267]. Light electron microscopy analyses also reveal that NME9 protein is associated with microtubular structures [267].

1.5.1.7 NME10

The *NME10* gene encodes the XRP2 protein involved in X-linked retinitis pigmentosa, which is an inherited affliction of the retina due to photoreceptor degeneration [268]. NME10 possesses a partial NDPK domain which may explain the lack of NDPK activity in the protein [269]. In conjunction with its 3’-5’ exonuclease activity, cytoplasmic NME10 has been shown to relocate into the nucleus upon treatment with DNA damaging agent in the cells, suggesting a role of NME10 in DNA repair [269].

Table 1.5.1: Summary of the characteristics and properties of various isoforms of the human NME family. ND, Not determined. Table modified from [228].

Group	Isoform	Tissular expression	Sub-cellular localisation	NDPK activity	Remarks	Exo-nuclease activity	Ref.
I	NME1	Ubiquitous (kidney, liver, intestine, brain)	Cytoplasmic, microtubule, ER nuclear	Yes	Overexpressed in tumours; inverse correlation with metastatic potential	Yes	[228, 270-273]
	NME2	Ubiquitous (heart, liver, pancreas, kidney)	Cytoplasmic, microtubule, ER nuclear, nucleolar	Yes	Overexpressed in tumours; transcription factor (PuF); DNA repair	ND	[228, 232, 270, 272-274]
	NME3	Ubiquitous (pituitary gland, cerebellum, adrenal gland)	Cytoplasmic	Yes	Overexpression suppresses granulocyte differentiation and induces apoptosis of myeloid cells.	ND	[228]
	NME4	Ubiquitous (prostate, liver, muscle, ovary, heart)	Mitochondrial	Yes	Associated with inner mitochondrial membranes	ND	[228, 253, 259]
II	NME5	Testis (traces in brain and kidney)	ND	ND	Expressed in male germinal cells	Yes	[228, 272]
	NME6	Ubiquitous (skeletal muscle, placenta)	Cytoplasmic, mitochondrial	Yes	Indicated role in regulation of cell growth and cell cycle progression	ND	[228, 266]
	NME7	Mainly in testis	ND	ND	Duplicated NDPK kinase domain	Yes	[228, 272]
	NME8	Mainly in testis	Microtubule	ND	Triplicated NDPK domain	Yes	[228, 272, 275]
	NME9	Testis, lung	Microtubule	ND	Closely related to NME8	ND	[231, 267]
	NME10	Ubiquitous	Cytoplasmic, nuclear	ND	Partial NDPK kinase domain	Yes	[231, 269]
	NM23-LV	Ubiquitous (except kidney)	Cytoplasmic, nuclear	ND	Long variant, a read-through transcript of *NME1* and *NME2*	ND	[250]

1.5.2 Mechanism of nucleoside diphosphate kinase reaction

Originally identified as an essential housekeeping enzyme, NDPK plays an essential role in a number of cellular processes, including (1) maintenance of the cellular pool of nucleotides via utilising ATP as a phosphate donor for the biosynthesis of nucleoside triphosphate precursors of nucleic acid synthesis; (2) regulation of the homeostasis between GTP produced in the Krebs cycle and ADP; and (3) supplying GTP for G-protein signalling, protein synthesis, and tubulin polymerisation [228, 276, 277].

NDPK catalyses the reversible transfer of the terminal (γ) phosphate of nucleoside triphosphate (NTP) to nucleoside diphosphate (NDP), following a ping-pong kinetic reaction as shown in (Figure 1.5.2.1) [241, 278, 279]. It has been well documented that the NDPK reaction occurs via a covalent intermediate, in which the enzyme is first transiently phosphorylated at a conserved phospho-acceptor histidine 118 (H118) residue before transfering the high energy phosphate to an NDP [280]. Additionally, divalent metal ions, such as Mg^{2+}, Mn^{2+} and Ca^{2+}, are also important in the phospho-transfer reaction of NDPK since interaction with the metal ion helps to reduce electrostatic repulsion and stabilise the transition state [276, 281]. Although NDPKs are thought to be non-specific to the base moiety of the donor and acceptor nucleotides, steady-state experiments have demonstrated that guanine nucleotides are the most favourable substrates [276].

$$
\begin{array}{rclcll}
N_1TP + NDPK & \rightleftarrows & N_1DP + NDPK{\sim}P & & (1) \\
NDPK{\sim}P + N_2DP & \rightleftarrows & N_2TP + NDPK & & (2) \\
\hline
N_1TP + N_2DP & \rightleftarrows & N_1DP + N_2TP & & (3)
\end{array}
$$

Figure 1.5.2.1: Mechanism of nucleoside diphosphate kinase (NDPK) reaction. Enzymatic reaction catalysed by NDPK involving the transfer of the terminal phosphate of a nucleoside triphosphate (NTP) to nucleoside diphosphate (NDP), where N_1 and N_2 represent any nucleosides or their deoxy- derivatives [278, 279]. All NDPK reaction occurs via the formation of an enzyme-bound high energy phosphate intermediate (NDPK~P) [280].

Subtrates of the phosphohistidine modification from H118 in Group I members are not restricted to NDPs but also to histidines located in several other target proteins [276, 282]. For example, NME2 can phosphorylate the β-subunit of heterotrimeric G proteins (Gβγ) to regulate G protein abundance and function *in vivo* [283]. Both human NME1 and NME2 are relatively small proteins, each being only 152 amino acids long. However, the amino acid residues responsible for NDPK activity span almost the entire NME protein (Figure 1.5.2.2). In particular, H118 is the key site for the phospho-transfer reaction, as a point mutation at this site completely abolishes NME NDPK activity [284, 285]. The remarkable sequence similarity, as well as identical active sites and crystal structures shared between the Group I NMEs suggest that these protein members are likely to adopt identical mechanism for NDPK activity [276]. Nevertheless, studies have shown that NDPK enzyme is relatively non-specific with varying levels of activity, depending on the tissue type and sub-cellular localisation [228].

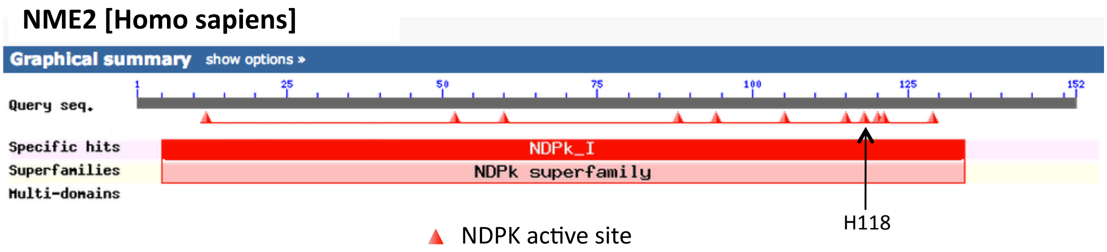

Figure 1.5.2.2: NDPK domain of NME2. Location of critical residues in the NDPK domain of NME2 (all sites are conserved in NME1) spanning almost the entire protein, including residues at positions 12, 52, 60, 88, 94, 105, 115, 118, 120, 121 and 129. Histidine at position 118 (H118) is the key site for the phospho-transfer reaction [284, 285]. Figure adapted from National Centre for Biotechnology Information at http://www.ncbi.nlm.nih.gov/Structure/cdd/wrpsb.cgi?INPUT_TYPE=live&SEQUENCE=CAG46519.1 accessed on 26th April 2014.

1.5.3 NME1 and NME2

NDPK enzyme was first discovered in 1953, and only later in 1988, the gene that encodes for NME1 was identified by Steeg *et al.* [240, 241, 246]. NME1 was identified based on its down-regulation in highly metastatic melanoma cell lines, leading to the speculation that NME1 constitutes a potential metastatic suppressor gene [246]. NME2 was subsequently discovered based on its high degree of homology to NME1 [286]. NME1 and NME2 proteins share 88% amino acid sequence identity, with a monomer mass of 17 kDa [280]. These proteins have different isoelectric points (6.13 and 8.64 for NME1 and NME2, respectively) and display two distinctly migrating protein bands when analysed by SDS-PAGE. The observed heterogeneity might be a consequence of differential proteolysis or post-translational modifications such as phosphorylation [280].

Although adult NME1 knockout mice exhibit an essentially normal phenotype, they are characterised by reduced birth weight and delayed mammary development [287]. On the other hand, NME2 knockout mice are also phenotypically normal at birth but are defective in cytokine production and have impaired activation of the Ca^{2+} activated potassium ion channel (KCa3.1) [288]. The fact that both NME1 and NME2 knockout mice are viable indicates that there might be some functional redundancy between them, although the synergistic function of both NME1 and NME2 may be required in the development of diseases, such as cancer. Double knockout mice of NME1 and NME2 are undersized and die perinatally, with defects in erythropoiesis [289]. It has been speculated that the impeded growth might be a consequence of the global effect of the NME1 and NME2 deletions causing a shortage of NTP precursors for nucleic acid synthesis [290].

In general, NME1 and NME2 proteins are ubiquitously expressed (Table 1.5.1) but the level of expression seems to be tissue-specific [280, 290]. NME1 and NME2 can form various complexes *in vivo* [280, 291]. For example, NME subunits can form dimers, which in turn assemble into a tetramer in *Myxococus xanthus*, or into a hexamer in eukaryotes [277, 292]. Hexamers can be described as three dimers arranged about a three-fold axis, or a dimer of trimers [277]. NME1 and NME2 in humans are active as homo- and hetero-hexamers and are believed to account for at least 80% of the cellular NDPK activity [280, 290]. Unpublished data from Schaertl *et al.* suggests that monomeric human NME contributes to less than 5% of the NDPK activity of the equivalent single isoform oligomers, highlighting the importance of the oligomeric form [293]. It has also been suggested that different oligomeric species of NME may participate in different cellular processes regardless of their essentially similar intrinsic enzymatic activity [294]. Both NME1 and NME2 are predominantly localised in the cytosol but other sub-cellular localisations have also been reported (Table 1.5.1) [270, 273, 290]. For example, NME1 and NME2 have been shown to be associated with the endoplasmic reticulum (ER) and nucleus [273]. Studies have also suggested that both proteins are associated with cytoskeletal structures such as intermediate filaments and the microtubular network [270, 295, 296]. In neuroblastoma cells, NME1 and NME2 (as well as NM23-LV) show similar cellular distribution [250]. The proteins were primarily located in the cytoplasm, with perinuclear localisation, but were completely absent from the nucleoli [250]. By contrast, in breast carcinoma cells, NME2 but not NME1 was found in the nucleus and nucleoli [270]. This suggests that the different localisations of NME proteins are cell-type specific and might reflect different NME functions in the particular cell types.

Although NME1 and NME2 share high sequence similarity and are capable of forming hetero-hexamers that possess housekeeping enzymatic activity, they have distinct cellular functions, largely owing to their substrate-specific enzymatic activity and interaction with other proteins [297]. Whilst low expression of NME1 is associated with aggressive types of breast and cervical carcinomas, melanomas and several other neoplastic lesions, overexpression of NME1 and NME2 have been reported to be linked with poor prognosis in neuroblastoma, lung cancers and thyroid carcinoma [294, 298-302]. These findings indicate that NME1 and NME2 may employ different mechanisms and have different roles in tumorigenesis, which will be discussed in the next section.

1.5.4 NME1 and NME2 in cancers

Tumour metastasis and aggressive tumour phenotype often result from a perturbed cell-matrix and/or cell-cell communication [303]. Deregulation of these highly regulated communication networks may lead to uncontrolled cell division, aberrant apoptosis, abnormal cell shape and cell adhesion properties, and degradation of the surrounding extracellular matrix [294]. Following identification of NME1 as the first metastasis suppressor gene by Steeg *et al.*, studies in which NME1 was overexpressed in metastatic cell lines (including melanoma, breast carcinoma, prostate, colon, hepatocellular and oral squamous cell carcinoma) demonstrated that these cells displayed reduced cell motility in *in vitro* assays and also reduced metastatic potential in xenograft models [246, 285, 298, 304-308]. In particular, Boissan *et al.* examined the role of NME1 in tumour development and metastatic dissemination by generating compound strains from NME1$^{-/-}$ mice mated with mice expressing the SV40 virus large T antigen (ASV40) in the liver, since the latter develop hepatocellular carcinoma (HCC) with pulmonary metastases [309]. The lack of NME1 gene had no effect on primary tumour formation despite a, possibly compensatory, increase in NME2 expression in the lesions of knockout mice [309]. However, the incidence of AVS/NME1$^{-/-}$ mice developing lung metastases was almost double that of AVS/NME1$^{+/+}$ mice, suggesting that the loss of NME1 contributes to an increase in metastasic spread [309]. In addition, most lung metastases in ASV/NME1$^{+/+}$ mice display considerably less labeling with an antibody specific to mouse NME1, indicating that metastatic dissemination of HCC is inversely associated with NME1 expression [309]. Interestingly, overexpression of NME1 was observed during primary tumour formation compared to the non-tumoral tissue, but the expression decreased concomitant with metastatic dissemination of the primary tumour [309]. Thus whilst NME1 plays an important role in metastasis suppression, it is likely that NME1 is also involved in primary tumour development, however, this remains to be further elucidated.

Although the role of NME2 in metastasis suppression seems to be less well understood, several studies have demonstrated that NME2 plays a key role in motility suppression, invasive growth and differentiation across different tumour types (reviewed in [310]). In particular, reduced NME2 expression was observed in metastatic breast, colon, lung and ovarian tumours (reviewed in [310]). Overexpression of NME2 has been shown to suppress lung metastasis in oral squamous carcinoma cells [307]. Histological analysis of the pulmonary metastatic foci in NME2 transfected clones revealed well-differentiated cells compared to control clones not expressing exogenous NME2 that were composed of anaplastic squamous cells [307]. A reduction in vascularisation into the metastatic foci was also observed in the NME2 transfected clones, suggesting that NME2 overexpression could inhibit tumour angiogenesis [307]. In addition, overexpression of NME2 has been shown to be involved in suppression of metastasis of breast cancer cells to lung [311, 312]; and to inhibit motility, invasiveness, and anchorage independent growth in highly metastatic breast cancer cells [313].

Nonetheless, as well as acting as metastasis suppressor genes, high levels of NME1 and NME2 have also been correlated with metastatic progression and poor prognosis in malignant lymphoma, neuroblastoma and osteosarcoma patients [314-316]. In a study comparing the level of NME1 protein with different types of lymphoma, patients with aggressive non-Hodgkin lymphoma and higher NME1 levels had worse overall and progression-free survival rates than those with lower NME1 levels [315]. NME1 expression was significantly increased in the pulmonary metastatic site in comparison with the osteosarcoma primary tumour, suggesting a correlation between NME1 and metastatic progression in osteosarcoma [314]. In addition, overexpression of both NME1 and NME2 has been detected in colorectal carcinogenesis and during primary tumour formation of HCC [309, 317].

The multifaceted effects of NME in cancers suggest a cancer type-specific role for NME that is likely to be governed by different mechanisms and through differential expression of interacting proteins or enzyme substrates [316]. In fact, multiple proteins involved in different molecular pathways have been identified as NME-interacting proteins. Some of these NME binding proteins seem to disrupt NME metastasis inhibitory activity, whilst other proteins appear to promote functional NME pathways [316]. The broad consequences of changes in levels of NTP generation catalysed by the NME enzyme may also explain the numerous effects in cancer phenotype that ensues from altered NME activity or expression. Here, we will focus on discussing the mechanisms employed by NME for its metastasis suppression function.

1.5.5 Cancer/Metastasis inhibitory roles for NME function

Despite extensive studies, the molecular mechanism underlying the ability of NME to regulate oncogenic transformation and metastasis is still poorly understood. Different functions of NME proteins have been suggested to contribute to its metastasis-suppressive effect, including NDPK activity, histidine protein kinase activity, 3’-5’ exonuclease activity, and interaction with DNA and proteins [247, 271, 316, 318-321]. Several studies have also demonstrated that NME is involved in the control of cellular responses to extracellular stimuli [294]. The mechanisms by which NME exerts its anti-metastatic function will be discussed in the following sections.

1.5.5.1 NME1 and NME2 in endocytosis and signalling and in cytoskeleton dynamics

1.5.5.1.1 Endocytosis and signalling

The role of NME in endocytosis and signalling pathway has been demonstrated in several studies [322-326]. For example, Krishnan *et al.* (2001) has shown that enzymatically active NME is required for synaptic vesicle internalisation at the stage that requires the GTPase dynamin, likely by supplying GTP required for Shibire (Shi; dynamin homolog)-mediated endocytosis [322]. This finding was later supported by Dammai *et al.* (2003) when they investigated the role of AWD (abnormal wing discs; *Drosophila* homolog of NME) during tracheal tube formation [323]. In particular, the authors demonstrated that in mutants lacking AWD, the Breathless (Btl; FGFR homolog) levels are dramatically elevated on the cell surface, leading to ectopic activation of downstream pathways and abnormal migration in cells [323]. This suggests that AWD is involved in the inhibition of Btl activity by vesicle transport-mediated turnover, therefore modulating the receptor tyrosine kinase signalling pathway, which is crucial for controlled cell migration [323]. Another study has also described AWD as a negative regulator of directional migration in border cells during *Drosophila* oogenesis by regulation of Pvf (the homolog of PDGF/VEGF) emanating from the oocyte [324]. AWD was shown to promote down-regulation of the Pvr (Pvf receptor) and Dome (essential for JAK/STAT functions in *Drosophila*), in collaboration with Shi, thus regulating the chemotactic signal strength to disrupt border cell migration [324]. In addition, AWD has also been indicated to be important for Notch signalling via its role in endocytic pathway [325]. Studies by Ignesti *et al.* (2014) have shown that AWD function is necessary for proper Notch signalling in follicle cells and imaginal disc cells [325]. It was also shown that loss of AWD function inhibits Notch from entry into late endosomes, causing accumulation of Notch in abnormal early endosomes [325]. Since Notch entry on the endocytic pathway is critical for proper Notch signalling, which may function either as a tumour suppressor or as an oncogene, the relationship between AWD and Notch may shed light into the role of NME in tumour progression [325]. More recently, Boissan *et al.* has also demonstrated that knockdown of NME1 and NME2 decreased clathrin-dependent endocytosis of the transferrin and EGF receptors, suggesting a role for NME1 and NME2 in dynamin-mediated membrane fission and signalling pathways [326].

1.5.5.1.2 Cytoskeleton dynamics

Since the dynamic changes to the cytoskeleton are involved in tumour cell motility, which is an important component of tumour invasion and metastasis, it is not surprising that NME proteins also have a role in the cytoskeleton machinery [316]. In fact, several cytoskeleton interactions of NME have been reported [238, 247, 270, 327, 328]. For example, NME1 and NME2 have been shown to co-immunoprecipitate with vimentin in a variety of tissues [328]. Vimentin, which is a member of the intermediate filament family of proteins, promotes changes in cell shape, adhesion, and motility during tumour invasion [329]. Activation of transmembrane receptors often affects cytoskeleton organisation and the association of NME proteins with structural proteins such as vimentin could have an impact on the dynamics of cytoskeleton remodeling upon external stimulation [327]. Studies by Otero *et al.* demonstrated that vimentin networks tend to form bundles and become more densely packed when assembled in the presence of NME [327]. The authors speculate that if NME has such an impact *in vivo*, it is possible that overexpression of NME could reduce cytoskeleton plasticity and cell movement, thus contributing to an anti-metastatic function [327]. Microtubules can be considered as a dynamic structure in cells which grow at one end by the polymerisation of tubulin dimers, and shrink at the other end by depolymerisation, and thus acting as a major contributor to cell motility [316]. It has also been demonstrated that NME1 and NME2 can associate with microtubules in interphasic, but not in mitotic human breast carcinoma cell lines [270]. Furthermore, changes in NME expression have also been shown to influence tubulin polymerisation, suggesting a regulatory role of NME in tubulin polymerisation [330, 331]. It is possible that NME could provide a high localised concentration of nucleotides needed for both microtubule polymerisation and vesicular-dependent movement along the microtubules powered by the kinesin and dynein motor proteins [316]. Through co-immunoprecipitation in breast cancer cells, Marino *et al*. have identified the actin-severing protein Gelsolin as a binding partner of NME1 [238]. Gelsolin modulates the assembly and disassembly of actin filament by directly interacting with actin and severing of actin filaments at their fast-growing ends [332]. When co-expressed in Gelsolin-transfected cells, NME1 inhibits the actin severing activity and dynamic functions of Gelsolin, thereby reducing the metastasis-stimulatory effect of Gelsolin [238]. The interaction of NME1 and Gelsolin would therefore appear to provide another possible mechanism for a tumour suppressive activity of NME1.

1.5.5.2 NME-interacting proteins

1.5.5.2.1 TGF-β

TGF-β is well known for being a tumour suppressor in early carcinogenesis but a tumour promoter in later stages of cancer development [333]. Studies by Hsu *et al*. have demonstrated that NME1 can inhibit TGF-β1-mediated cell adherence and growth arrest in weakly tumorigenic chicken erythroblast HD3 cells, but not in highly tumorigenic colon carcinoma U9 cells [334]. This observation may suggest a role for NME1 in TGF-β-mediated growth inhibition and differentiation but not in TGF-β-mediated proliferation and invasion [334]. Nonetheless, recent studies have shown that NME1 and NME2 are involved in the regulation of anti-proliferative function of TGF-β signalling in fibroblasts [335]. Both NME1 and NME2 have been reported to down-regulate TGF-β-stimulated induction of cyclooxgenase-2 (COX-2) [335]. COX-2 is a key enzyme in the syntheses of prostaglandin E_2 and is highly induced in response to cytokines, pathogens, irradiation, and growth factors [336, 337]. Up-regulation of COX-2 has been associated with tumour growth, angiogenesis, and metastasis [338-340]. Therefore, NME1 and NME2 inhibitory effect on COX-2 expression is consistent with NME roles as a metastasis suppressor, although the exact mechanism behind this connection with COX-2 expression remains elusive [335]. Paradoxically, NME1 has also been shown to up-regulate transcription of the COX-2 promoter in reporter assays, which is in line with the tumour-progressive property of NME1 considering the influence of COX-2 on tumour progression [335, 341]. Such contradictory results/differences are difficult to reconcile and it is possible that they will not be explained until functional genomic studies are performed *in vivo*. TGF-β is also a key inducer of epithelial-mesenchymal transition (EMT) during tumour progression. NME1 has been demonstrated to negatively regulate TGF-β-dependent induction of EMT in non-progressive lung cancer cell line [342]. Since EMT is often required for tumour cell migration and invasion, it is possible that NME1 acts as a tumour suppressor through inhibiting EMT induction [342].

1.5.5.2.2 Estrogen receptor (ER)

ERα and ERβ belong to the steroid hormone receptor superfamily and are important regulators of growth and differentiation. Upon activation by estrogen, ER translocates to the nucleus and regulates transcriptional activity through interactions with estrogen response elements (EREs) [343, 344]. Although ERα and ERβ are structurally similar, they can be functionally specific, partly through interactions with different co-regulatory proteins [345]. In fact, whilst ER-α is generally proliferative, ER-β has anti-proliferative properties [346]. Both NME1 and NME2 are able to interact with ER to regulate transcription from ERE in breast cancer and smooth muscle cells [347-349]. NME1 has been shown to interact with ER-α and decreases the transcription of an estrogen-responsive reporter plasmid [348]. A decrease in NME1 expression by siRNA leads to an increase in expression in a number of estrogen-responsive genes that inhibit apoptosis and promote metastasis, suggesting that NME1 may inhibit metastasis by repressing transcriptional activation by ERα [348]. On the other hand, NME2 selectively interacts with and acts as a co-activator of ERβ [347]. NME2 facilitates estrogen-induced gene transcription and attenuates cell migration by acting synergistically with estrogen [347]. As a result, both of these NME family members contribute to an the overall outcome of anti-proliferative response by coordinately modulating ER members [310].

1.5.5.2.3 Kinase suppressor of RAS (KSR)

The histidine protein-kinase activity of NME1 may also contribute to its metastatic-suppressive function [350, 351]. NME1 has been reported to co-immunoprecipitate with the kinase suppressor of RAS (KSR) protein, which acts as a molecular scaffold protein for the ERK-MAPK (extracellular signal-regulated kinase - mitogen-activated protein kinase) signalling pathway [352, 353]. ERK activation plays an important role in mediating tumour invasion and metastasis [354, 355]. NME1 is capable of phosphorylating KSR on a histidine residue, resulting in decreased ERK activation levels in response to signalling [352, 355]. Overexpression of NME1 in breast carcinoma cells results in diminution in ERK activation levels [352]. Consistently, expression of an NME1 mutant lacking the histidine kinase activity led to an increase in the levels of activated ERK [352]. Thus, these findings suggest that changes in NME1 levels in tumour cells can affect ERK activation and metastasis through interaction with the KSR scaffold protein [355]. Similarly, NME2 can also have an anti-cell proliferation effect through regulation of the ERK signalling pathway. A decrease in the level of NME2 can lead to activation of ERK signalling and promote cell proliferation, whereas high levels of NME2 inhibit proliferation induced by EGFR and Ras through counteracting the ERK signalling [356].

1.5.5.2.4 Guanine nucleotide exchange factors (GEFs)

The Rho family GTPases consists of Rho, Rac and Cdc42 subfamilies that are important mediators of cell signalling pathways involved in regulation of actin cytoskeleton and cell migration (Figure 1.5.5.2.4.1) [357]. Like all GTPases involved in signalling, the Rho family of GTPases function as binary switches by cycling between an inactive (GDP-bound) and an active (GTP-bound) conformational state [358]. Guanine nucleotide exchange factors (GEFs) activate GTPases by stimulating the exchange of GDP for GTP, in which the activated GTPases are then capable of recognising their downstream signalling targets [358]. On the other hand, GTPase activating proteins (GAPs) accelerate the intrinsic GTPase activity of GTPases to inactivate the switch through hydrolysis of GTP [358]. Rho family GTPases are important in regulating cell morphology and migration in different organisms through acting as a molecular switch between GDP-bound inactive and GTP-bound active forms [357, 359, 360]. Interestingly, a number of GEFs for the Rho family GTPases have been identified as NME-interacting proteins.

NME1 has been demonstrated to associate with a Rac1-specific GEF, Tiam 1 [361]. Overexpression of NME1 inhibits the Tiam-1-induced production of GTP-bound Rac1, a member of the Rho family of GTPases [361]. Thus, NME1 may exert its effect as a tumour metastasis suppressor by acting as a negative regulator of Rac1 [361]. In addition, NME2 has been found to directly interact with integrin cytoplasmic domain-associated protein 1α (ICAP-1α), an important regulator of cell adhesion, in the lamellipodia and peripheral ruffles during cell spreading [362]. Interestingly, Rac/Tiam-1 proteins also co-localise with ICAP-1α in the lamellipodia, linking NME2 to the cell adhesion and migration machinery [362].

Dbl-1 is another GEF that has been identified as an NME1-interacting partner [363]. Through interaction with Dbl-1, NME1 can modulate the activation of Cdc42 by inhibiting the GDP to GTP exchange activity by Dbl-1, which can negatively regulate cell migration and tumour metastasis by causing cytoskeletal reorganisation [363, 364]. On the other hand, NME2 but not NME1, has been identified as an Lbc-interacting protein [365]. Lbc is a product of a transforming gene with RhoGEF domain identified from leukaemia cells [365]. It has been shown that NME2 expression can negatively regulate and suppress the stress fibre formation induced by Lbc expression [360]. Using microarray analysis, it has been demonstrated that lysophosphatidic acid (LPA) receptor, a member of the G protein-coupled receptor group, is down-regulated by wild-type NME1 [366]. Down-regulation of LPA receptor by NME1 leads to suppression of tumour cell motility, and may thus play a role in NME1-mediated metastasis suppression [366].

A bi-directional interaction between NME1 and Ras-related GTPase Rad has also been identified [367]. In this complex, NME1 acts functionally as both Rad-GAP and Rad-GEF to stimulate both GTP hydrolysis and GTP loading of Rad, respectively [367]. Simultaneously, Rad regulates NME1 by promoting NME1 NDPK activity and decreasing NME1 autophosphorylation [367]. High expression of Rad has been shown in human breast cancer tissues and breast cancer cell line with high tumorigenic and metastatic potential [368]. The positive effects of Rad on tumour growth can be abrogated by co-expression of NME1, suggesting that interaction between Rad and NME1 may modulate growth and tumorigenicity in breast cancer [368].

1.5.5.3 DNA binding

NME2 can control the expression of c-MYC in cervical cancer, lung carcinoma, and Burkitt lymphoma cells [274, 370, 371]. However, the mechanism underlying this regulatory control is still unclear. Studies by Postel *et al.* demonstrated that NME2 can transactivate the human *c-MYC* oncogene through binding to a region upstream of the transcription start site, called the nuclease-hypersensitive element (NHE) (also termed CT element or the PuF site), in an NDPK activity-independent manner [274, 372]. More recently, NME2 has been shown to mediate *c-MYC* activation through interaction with a G-quadruplex DNA motif within the NHE in the *c-MYC* promoter [371]. However, the role of NME2 as a transcription factor is debatable since it lacks a DNA-binding domain that is common in transcription factors [373]. Furthermore, unlike typical DNA binding proteins that bind to a double-stranded DNA for transcriptional regulation, NME2 binds to single-stranded DNA [371, 374, 375]. These observations lead to the speculation that NME2 anti-metastatic functions are likely due to other biochemical activities [373]. Interestingly, NME1 possesses 3'-5' exonuclease activity, which is critical for DNA proofreading and maintenance of genome stability [271, 376]. Zhang *et* *al.* has demonstrated that NME1 mutant E_5A deficient in 3'-5' exonuclease activity, exhibited compromised suppressor activity in spontaneous metastasis of 1205LU melanoma cells *in vivo* [318]. This suggests that the 3'-5' exonuclease activity of the NME1 is essential for its anti-metastatic function [318].

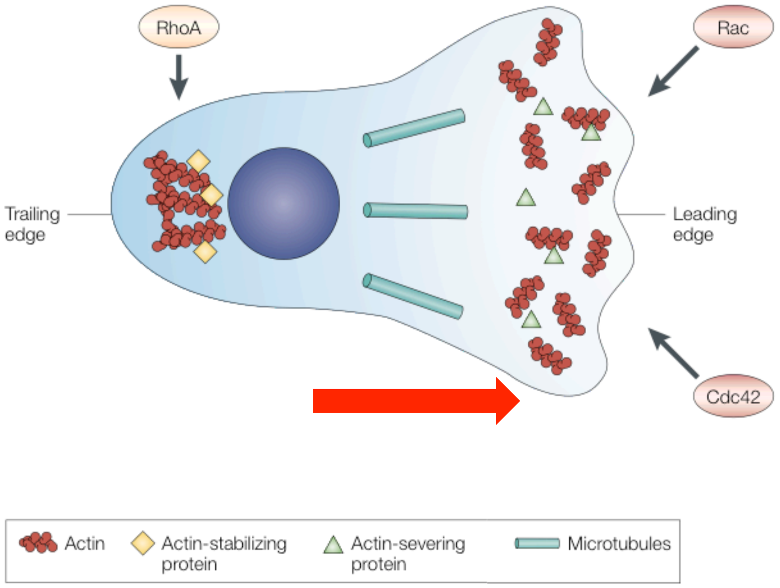

Figure 1.5.5.2.4.1: The role of Rho proteins in fibroblast migration. Rho is more active at the trailing end of the fibroblast, and this induces stress-fibre and focal-adhesion formation through actin polymerisation, which may stabilise the trailing end of the cell as it migrates towards the external stimulus (the direction of growth is indicated by the red arrow). On the other hand, Rac and Cdc42 are dominant at the leading edge and, by depolymerising actin, they promote the formation of protrusions that underlie the force-mediated movement towards the stimulus. The dynamics of polymerisation and depolymerisation depend on the balance between proteins that stabilise actin and sever microfilaments. Figure adapted from [369].

1.5.5.4 NDPK activity

To date, literature that correlates NDPK activity and metastasis suppression is very limited, which has led to speculation that NME enzymatic activity may not be required for its function as a metastasis suppressor [377, 378]. Nevertheless, a recent study by Conery *et al.* suggests that NME1 NDPK activity is required for supplying a local source of GTP for the activation of GTPase dynamin during cytokinesis [379]. Down-regulation of NME1 results in cytokinesis failure and chromosome instability regardless of the status of p53 signalling [379]. Chromosomal instability, or the inability to segregate chromosomes equally during cell division, plays critical roles in the development of the majority of solid tumours [380]. Chromosome instability may lead to aneuploidy and an increased susceptibility of loss of heterozygosity, which may provide tumorigenic advantages by increasing the mutation rate in oncogenes, tumour suppressors or genomic stability genes [381, 382]. Therefore it is possible that NME1 may have a role in maintaining normal cytokinesis to avoid chromosome missegregation, which may contribute to tumour development. The same study also showed that whilst loss of NME1 leads to tetraploidy regardless of p53 status, the reduced NME1 expression only leads to scenescence only in cells with intact p53. This suggests that continued cycling of tetraploid cells may only occur after the loss of p53 signalling [379].

1.5.6 NM23-LV (NME1-NME2)

NM23-LV (also known as *NME1-NME2*) was identified as a read-through transcript (or ‘cojoined genes’) of the tandemly located *NME1* and *NME2* genes on chromosome 17q (Figure 1.5.6.1) [250, 251]. The encoded NM23-LV fusion protein lacks exon 5 of NME1 and consists of the first 114 residues of NME1 fused in-frame to the N-terminus of the full-length NME2 [250, 251]. As the exon 5 of NME1 comprises of a β-sheet and an α-helix that play a critical role in oligomerisation, its absence in NM23-LV may be incompatible with hexamerisation [383]. Although the H118 site of the NME1 portion is also absent from NM23-LV, there has been no report on how this would affect NM23-LV NDPK activity [383]. The physiological function of NM23-LV has not been well characterised. A study by Valentijn *et al.* using qRT-PCR analysis of a panel of human tissues has demonstrated that NM23-LV is ubiquitously expressed at the mRNA level, with the exception of reduced expression in lung and barely any expression in kidney [250]. In the same study, high levels of NM23-LV mRNA expression have also been shown in eight neuroblastoma tumours, and this result is also analogous to NME1 and NME2 [250]. As discussed in Section 1.5.3, NME1 and NME2 may employ different mechanisms and have different roles in tumorigenesis, at least in part, owing to their specific interaction with other proteins [297]. Low expression of NME1 has been associated with aggressive types of cancers such as, breast carcinomas and melanomas, whereas high levels of NME1 and NME2 are linked with poor prognosis in neuroblastoma, lung cancers and thyroid carcinoma [294, 298-302]. Therefore the possibility emerges that the expression of NM23-LV, which contains part of the NME1 and the NME2 protein, may serve as potential prognostic marker in different types of cancer. Furthermore, studies on neuroblastoma cells show that NME1, NME2 and NM23-LV are mainly located in the cytoplasm, with some nuclear expression, but were absent from the nucleoli and plasma membrane [250]. By contrast, localisation of NME2 in breast carcinoma cells was observed in the nucleoli and plasma membrane [270]. Therefore, studying of the localisation of NM23-LV protein based on the cell type studies may also serve as surrogate indicators of its function and tumorigenic potential. Thorough understanding of the similarities and differences in molecular functions and physiological roles of NME1, NME2 and NM23-LV may provide great prognostic potential in cancers.

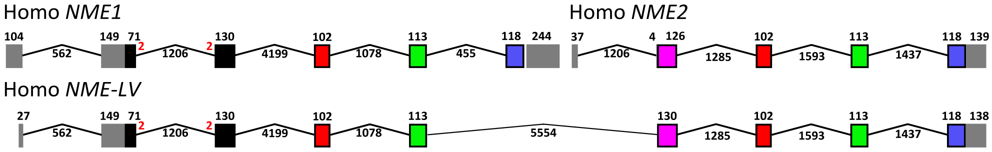

Figure 1.5.6.1: *NM23-LV* (or *NME1-NME2*) read-through transcript. *NM23-LV* is a read-through transcript of the *NME1* and *NME2* neighbouring genes [250]. NM23-LV lacks exon 5 of NME1, which contains the stop codon and H118 phospho-transfer site for NDPK activity. Additionally, NM23-LV also lacks exon 1 of NME2, which is an untranslated sequence. The encoded protein hence comprises of part of NME1 fused to a complete NME2 protein. Boxes represent exon sequences and are connected by thin lines, which represent the intron sequences. Non-coding exons are shown in grey boxes. Introns are not drawn to scale. Transcription starts from left to right. Figure reproduced from [231].

1.6 Aims of the study

RCC is a heterogeneous disease and patients typically display an unpredictably varied disease course, which is likely to be elicited by the acquisition of specific molecular alterations in the developing cancer. This has prompted us to focus on *p53* and *MDM2* genes that have previously been identified as predictors of disease progression. As mentioned in Section 1.4.3, a recent study by Noon *et al.* has demonstrated that there is a strong positive link between MDM2 and p53 co-expression in RCC and this is accompanied by reduced disease specific survival even though the up-regulated p53 is rarely mutated [139]. It remains unknown as to why cells could tolerate co-upregulation of p53 and MDM2 since an auto-regulatory feedback loop exists between p53 and MDM2. One explanation could be that there is a defect in the p53/MDM2 pathway that prevents high levels of MDM2 from degrading p53. More interestingly, it is unclear as to why up-regulation of the wild-type tumour suppressor p53 would be associated with promoting cancer. One explanation might be that the predominantly wild-type p53 in RCC promotes increased expression of MDM2 and that it is the MDM2 upregulation that provides the link with cancer progression. Considering that MDM2 expression has been shown to promote cell motility and invasiveness in RCC in a p53-independent manner [384], we hypothesised that up-regulation of MDM2 promotes disease progression in RCC, leading eventually to reduced disease specific survival and thus providing the association with poor prognosis in RCC.

Therefore, our overall aim has been to examine how MDM2 may contribute to a more aggressive phenotype in RCC cells. Whilst it will ultimately be critical to examine the function of MDM2 in renal cells, since these routinely retain wild-type p53 it is important to examine the effects of MDM2 in p53 null cells to simplify the interpretation of the results so that other pleiotropic effects of p53 do not confound the analysis. For this reason we have extensively utilised H1299 (non-small cell lung carcinoma cells that lack p53) as a system to study MDM2 function.

Aim 1: Investigate how MDM2 promotes cell motility using expression profiling

Based on the findings that MDM2 promotes increased cell motility and invasion in a p53- and RING-finger-independent manner [384], we aimed to investigate how MDM2 promotes cell motility by performing expression profiling to detect consequences of MDM2 expression in derivatives of H1299 cells expressing high levels of MDM2 (Clone 9) and lacking E3 ligase activity (RFM9). It was hypothesised that genes that are mutually altered by MDM2 and RFM expressions would be likely to promote cell motility via the same biological pathways and studying these genes could provide insights into the mechanism of MDM2 in promoting cell motility and invasion.

Aim 2: Investigation of the mechanisms and consequences of MDM2-NME2 interaction

It has been shown that MDM2 interacts with NME2 and abolishes the ability NME2 to suppress motility in RCC [183]. However, the mechanism of action behind this remains unknown. We therefore aimed to study the mechanism and consequences of MDM2-NME2 interaction for cell motility.

Aim 3: Investigation of the role of MDM2 on NME ubiquitination

In a study using stable cell lines expressing 6xHis-biotin-tagged ubiquitin for purification of the ubiquitinated proteome, Meierhofer *et al.* identified NME1 as one of the potential substrate for ubiquitination [385]. Furthermore, mass spectrometry analyses show that both NME1 and NME2 amino acid sequences contain a potential ubiquitination site (K100) [385]. In addition, our fractionation analyses of MDM2 and NME sub-cellular distribution suggest that NME proteins could be targets for MDM2-mediated ubiquitination. It is possible that MDM2 mono- or poly-ubiquitinates NME and then targets the modulated NME for protein shuttling or degradation, respectively. Therefore despite the finding that MDM2 motility promoting effect is independent of its E3 ligase activity [384], we aimed to examine whether NME1, NME2 and NM23-LV proteins could be subjected to MDM2-mediated ubiquitination to gain better understanding of the regulation of NME proteins by MDM2.

Understanding the mechanisms through which MDM2 expression promotes increased cell motility and invasiveness in cancer cells would provide valuable insights to allow for development of potential therapeutic targets for RCCs as well as other cancers.

Chapter 2

Materials and Methods

2. Materials and Methods

2.1 Molecular cloning

2.1.1 Agarose gel electrophoresis

Agarose gel electrophoresis was used to separate, purify and estimate the yield of DNA fragments. An agarose gel was prepared to an appropriate concentration (Table 2.1.1.1) in Tris-acetate-EDTA (TAE) buffer (40 mM Tris-Base (Calbiochem), 1.142% glacial acetic acid (MERCK) and 1 mM EDTA, pH 8.0 (BDH)). Genesieve LE agarose (Flowgen) was generally used, unless the DNA fragment of interest was to be extracted for downstream molecular cloning purposes, in which case, SeaKem®GTG®agarose (Lonza) was used instead. The agarose gel was supplemented with 0.5 μg/ml of ethidium bromide (Roche) so that DNA bands could be visualised under UV light. Gel electrophoresis was run in TAE buffer inside a horizontal electrophoresis unit (Scie-Plas) connected to a PowerPac power supply (Bio-Rad), at a voltage of 1-10 V/cm across the gel. All DNA samples to be run were supplemented with 10% (v/v) orange G loading buffer (50% glycerol with adequate orange G dye (BDH). DNA markers used are 100 bp DNA ladder (New England Biolabs, NEB) and/or 1 kb DNA ladder (Invitrogen). For qualitative analysis of RNA samples, the method was similar to that described above, except that the electrophoresis tank, gel cast and gel comb were immersed in 1 M HCl (VWR) for 1h and then washed with RNase/DNase free water before use.

Table 2.1.1.1: Concentrations of agarose gels for different sized DNA fragments.

% Agarose (w/v)	Effective resolution of DNA fragments (kb)
0.5	>12
0.7	1-12
1.0	0.5-8
1.2	0.2-5
2	<1

2.1.2 Polymerase Chain Reaction (PCR)

Amplification of DNA fragments of interest was performed using two suitable primers and a thermostable Phusion® High-Fidelity DNA polymerase (NEB). Briefly, all components of a PCR reaction (Table 2.1.2.1) were mixed and then loaded in a thermal cycler (Px2 Thermal Cycler, Thermo. Electron Corporation) and appropriate cycle conditions were used (Table 2.1.2.2). Typically, after 30 cycles, the presence or quantity of the PCR product was checked by gel electrophoresis (Section 2.1.1). Primers were designed using online tools, including Primer3 (http://frodo.wi.mit.edu/primer3/) or Primer-BLAST (http://www.ncbi.nlm.nih.gov/tools/primer-blast/index.cgi?LINK_LOC=BlastHome). In general, primers were designed to be 18-25 nt in length, with a GC content between 40-70% and a melting temperature (Tm) of approximately 60°C. All oligonucleotides were synthesized by Eurofins MWG Operon and were reconstituted in water.

Table 2.1.2.1: Standard components of a PCR reaction.

Component	**/ 25 µL**
Standard buffer	x 1
dNTPs	200 µM
Primers	0.05 µg each
DNA polymerase	0.5-1 unit
Template DNA	1 pg – 10 ng
Nuclease-free H_2O	To 25 µL

Table 2.1.2.2: Standard cycle conditions for Phusion® High-Fidelity DNA polymerase.

	Phusion High-Fidelity DNA polymerase	
Initial denaturation	98°C	30 sec
15-35 cycles		
Denaturation	98°C	10 sec
Anneal	50-65°C	30 sec
Extend	72°C	15-30 sec/kb
Final extension	72°C	5-10 min
Hold	4°C	

2.1.3 A-tailing reaction

Tag DNA polymerase (Invitrogen) was used to create the 3’ A-tail overhangs required for ligation of PCR product into pCR2.1 vector (known as TA-cloning). Typically, PCR reaction was left overnight at 4°C to reduce the efficiency of Phusion enzyme at removing A-tails freshly synthesised by *Tag* DNA polymerase. For A-tailing reaction, 1 μL of 10 mM dATPs and 1 μL of *Tag* DNA polymerase (10 units) were added to the completed PCR reaction, which already contained the required buffer. The reaction was mixed and briefly centrifuged before being incubated at 72°C for 20 min. Once the A-tailing reaction has finished, the PCR products were run on a GTG® agarose gel and the DNA extracted for downstream cloning applications.

2.1.4 Restriction endonuclease digestion

Restriction digest of DNA was performed either for ligation reactions or for identification of correctly targeted recombinant clones (diagnostic purposes). For DNA digest reactions, restriction endonucleases were used according to the conditions suggested by manufacturer (NEB). Typically, 0.5-3 μg of the plasmid containing the insert of interest and 1 μg of the vector ‘backbone’ DNA were digested routinely with 10-fold excess of restriction enzyme, for example, 10 U of enzyme were used to digest 1 μg of DNA. The digestion was incubated for 3h to overnight at the manufacturer's recommended temperature, usually 37°C. For ligation purposes, the backbone DNA was further dephosphorylated to avoid self-ligation by adding 0.5 μL Antarctic phosphatase (NEB) and 10x Antarctic Phosphatase Reaction Buffer (NEB) (to a final concentration of 1x) and incubating at 37°C for 15 min. The DNA digest was then examined by agarose gel electrophoresis (Section 2.1.1). In the case for ligation, DNA digest samples were run on GTG® agarose gel. The insert and backbone of interest were cut out of the gel using a sterile scalpel and purified using a GENECLEAN Turbo Kit (Qbiogene) according to the manufacturer's instruction.

2.1.5 Ligation of DNA fragments

DNA ligation reactions were performed with T4 DNA ligase (NEB) according to the manufacturer's protocols. Briefly, the components of the ligation reaction (50 ng vector DNA, x1 ligase buffer, 1 unit T4 ligase, and DNA insert of at least 1:1 molar ratio of vector:insert DNA) were added in a 0.2-ml PCR tube to a final volume of 20 μL. The reaction was mixed by a quick vortex and centrifuged briefly before incubation at 16°C for overnight or longer. After incubation, 1-5 μL of the ligation reaction was used for transformation of competent *E. coli* (Section 2.1.7.2).

2.1.6 Basic maintenance for bacteria

Different strains of bacteria with specific genotypes were used for different or specialised purposes. Typically, TOP10 (Invitrogen, #C4040) bacteria were used for routine cloning, whereas XL1-Blue (Stratagene, #200130) cells were used when better quality and yield of DNA were needed for downstream applications, such as transfection into mammalian cells. All bacterial work was performed using aseptic techniques. *E. coli* were cultured in Luria Broth (LB, Sigma-Aldrich) liquid media that was prepared by adding 25 g/L of LB to distilled water, and was subsequently sterilised by autoclaving at 122°C for 15 min. Appropriate antibiotics were added at their recommended working concentration (Table 2.1.6.1) once the medium has cooled down to ~ 55°C. Solid medium was prepared using a similar method and formulation, with the addition of 15 g/L of agar (Formedium). Antibiotics were added as required at about 55°C and then poured into 10-cm Petri dishes and allowed to set.

Initially, *E. coli* cells were propagated in small starter cultures and then diluted 1:100 for larger culture volumes. To set up a starter culture, an individual bacterial colony was picked from an LB-agar plate, inoculated into small 5 ml liquid cultures containing an appropriate antibiotic in 14-ml sterile Falcon 2059 tubes and incubated overnight at 37°C, with vigorous shaking at 230 rpm. For larger scale of *E. coli* culture, the bacteria were inoculated into a conical flask that was at least five times the size of the culture volume to ensure sufficient aeration and grown overnight at 37°C, with vigorous shaking at 230 rpm.

For long term storage of *E. coli*, a freshly grown overnight culture was mixed 1:1 with 50% glycerol (Sigma-Aldrich) and stored at -80°C. Frozen bacteria were revived by scraping off some of the frozen glycerol stock with an inoculation loop and streaking this onto an LB-agar plate which was then incubated overnight at 37°C until individual colonies have formed.

Table 2.1.6.1: Selective antibiotics. Each antibiotic was reconstituted in H_2O and prepared as a concentrated stock solution, which was sterilised by filtration. The stock solution was subsequently aliquoted and stored at -20°C.

Antibiotic	Stock solution	Working concentration	Source
Ampicilin	x 1000	100 μg/μL	Sigma-Aldrich
Kanamycin	x 250	50 μg/μL	Sigma-Aldrich

2.1.7 Introduction of plasmid DNA into bacterial cells

2.1.7.1 Generation of electrocompetent bacteria

To generate electrocompetent *E. coli*, aseptic technique was used throughout the following methods. A single colony of *E. coli* strain of interest was inoculated into

5 mL LB medium containing appropriate antibiotic and incubated overnight at 37°C, with shaking at 300 rpm. 2.5 mL of this starter culture was then inoculated into 500 mL of LB medium and incubated at 37°C, with shaking at 300 rpm. After about 3-4h when an OD600 nm of 0.5 to 0.7 was reached, cells were chilled in an ice water-bath for 10-15 min before harvesting. From this point onwards, all centrifugation steps were carried out at 2°C and all reagents and equipments were kept pre-chilled on ice. Cells were harvested in a 500-mL centrifuge bottle in a Sorvell RC 5C *Plus* (Du Pont) Centrifuge at 3000 x g for 20 min. Promptly, the supernatant was poured off and the cell pellet washed with 500 mL of ice-cold water by re-suspending initially with 5 mL to achieve a single cell suspension. The remaining water was added and the cell suspension was mixed well before being harvested as previous steps. The cell pellet was washed with 500 mL ice-cold water again and then the cells were re-suspended in 40 mL of 10% (v/v) glycerol. The cell suspension was transferred into a narrow bottom 50-mL Falcon tube and was harvested in an Eppendorf Centrifuge 5804R at 3000 x g for 10 min. The supernatant was immediately discarded and the cells mixed with (1:1) and re-suspended with 10% (v/v) glycerol. The electrocompetent *E. coli* were then aliquoted at 50 µL/1.5 mL micro-centrifuge tube and promptly frozen on dry ice or snap frozen in liquid nitrogen. The frozen cells were then kept at -80°C until needed.

2.1.7.2 Transformation by electroporation

Bio-Rad Gene Pulser II was used for the electro-transformation of *E. coli* by high voltage. Electroporation cuvettes (Bio-Rad) with a 0.1 or 0.2 cm gap were used and recycled between transformations using a washing protocol as described below. Super Optimal broth with Catabolite repression (SOC) media (0.5% yeast extract, 2% tryptone (BD Bioscience), 10 mM NaCl, 10 mM $MgCl_2$, 10 mM $MgSO_4$ (BDH AnalaR), 2.5 mM KCl (AnalaR NORMAPUR), 20 mM glucose (Formedium)) was prepared and sterilised by autoclaving in advance.

For electro-transformation of *E. coli*, competent cells were first thawed on ice and 1-2 µL of pre-chilled ligation mixture was added (or 10 pg of pUC19 control plasmid DNA). The transformation reaction was then carefully transferred, making sure that air bubbles were avoided, into an ice-cold eletro-cuvette. The outside of the cuvette was wiped to avoid condensation before being placed into the Bio-Rad Gene Pulser Xcell for pulse delivery (Table 2.1.7.2.1). Immediately after a single pulse was delivered, 1 mL of chilled SOC medium was added to the cuvette and the transformation mix was gently re-suspended before being transferred to a chilled 2-mL screw-cap Eppendorf tube. The cell suspension was then incubated for 1h at 37°C, with shaking at 230 rpm. Following incubation, the transformation mixture was spread onto LB-agar plates containing selective antibiotics and incubated overnight at 37°C to allow for the growth of transformants. Typically, 10% and 90% of the total transformants mixture volume were spread onto LB-agar plates. The reason for this is to optimise the growth of individual colonies for picking and screening of recombinant clones. Transformation efficiency (colony forming units per μg of pUC19 DNA) was calculated to check whether the transformation was performed satisfactorily. Using this protocol, the cells generally produced transformation efficiencies of > 1 x 10^{8-9} cfu/μg pUC19 DNA.

For recycle use, the electro-cuvette was washed by rinsing with H_2O five times, soaking in 0.2 M HCl for 10 min, and then rinsing with 70% ethanol for five times. Following the last rinse with 70% ethanol, the liquid was decanted under a sterile hood and air-dried for about an hour. The cuvette was re-capped and was ready to use again.

Table 2.1.7.2.1: Specifications for electroporation using Bio-Rad Gene Pulser Xcell

Gap size (cm)	0.1	0.2
Capacitance (μF)	25	25
Resistance (Ω)	200	200
Voltage (kV)	1.5	2.4
Pulse (kV/cm)	15	12
Expected time constant (ms)	4.6	4.6

2.1.8 DNA extraction

2.1.8.1 Basic small scale DNA extraction using alkaline lysis and PCI

This low cost and quality plasmid DNA extraction method was used for screening recombinant clones, but not for sequencing purpose. This method usually yielded between 30-50 μg from a 4 mL liquid culture, and met the quality for analysis by restriction digest (Section 2.1.4). This basic protocol has the advantage of being able to extract DNA quickly from many clones at once, allowing for express screening. All reagents were prepared in advance according to Table 2.1.8.1.1.

Accordingly, 4 mL of the *E. coli* overnight culture was harvested by batch in 2-mL micro-centrifuge tubes in an Eppendorf centrifuge 5415 at 6800 x g for 5 min at room temperature (RT). The cell pellet was re-suspended in 200 μL GTE solution by vortexing, and then 200 μL of the lysis buffer was added into each tube, followed by quick addition of 200 μL of K^+Ac^- solution and 500 μL of PCI (24:25:1). The tubes were mixed by inversion for 5 min, followed by centrifugation at 16,000 x g for 10 min. The aqueous phase was quickly transferred into a clean 1.5-mL micro-centrifuge containing 500 μL of isopropanol (VWR), and mixed well prior to incubation at RT for 5 min. The precipitated DNA was harvested by centrifugation at 16,000 x g for 10 min. DNA pellet was washed thoroughly by adding 1 mL of 70% ethanol and gentle vortexing to ensure that the pellet was dislodged into the solution. The samples were centrifuged briefly and the supernatant carefully removed. The pellet was air-dried for 5-10 min depending on the pellet size, or until the white pellet appeared translucent. DNA was re-suspended in 20 μL of TE buffer + Ribonuclease A (RNase A). The DNA solution could be incubated in a 37°C water-bath for 30-60 min to help the DNA dissolve. The dissolved DNA was stored at -20°C. Typically 2 μL of a 1:10 diluted (in H_2O) DNA solution was adequate for analysis by restriction enzyme digestion.

Table 2.1.8.1.1: Formulation of buffers for basic DNA extraction. GTE, lysis buffer and K^+Ac^- solution were stored at RT. The lysis buffer was warmed up in a 37°C water-bath before use to dissolve any precipitated sodium dodecyl sulphate (SDS). PCI (24:25:1) was stored at -20°C and defrosted before use. TE buffer + RNase A was stored at 4-8°C.

Solution	**Composition**	**Source**
GTE (re-suspension buffer)	50 mM Glucose 25 mM Tris (pH 7.4) 1 mM EDTA (pH 8.0)	AnalaR Calbiochem Sigma-Aldrich
Lysis buffer (AKA buffer P2)	1% SDS (w/v) 200 mM NaOH	VWR VWR
K^+Ac^- solution (neutralisation buffer)	3 M KAc 11.5% Glacial acetic acid (v/v)	BDH Biochemical MERCK
PCI (24:25:1)	24: Phenol 25: Chloroform 1: Isoamylalcohol	VWR VWR VWR
TE buffer + RNase A	10 mM Tris.Cl (pH 8.0), 1 mM EDTA 10 μg/ml RNase A	QIAGEN Sigma-Aldrich

2.1.8.2 Small scale, high quality plasmid DNA extraction

The QIAprep Spin Miniprep Kit (QIAGEN) was used to isolate plasmid DNA when small amounts of high quality DNA were required for downstream applications, such as DNA sequencing. DNA extraction was performed according to the manufacturer's guidelines and typically yielded 5-20 μg DNA from a 4 mL overnight bacteria culture. The concentration of DNA and its purity were determined using a UV spectrophotometer. Pure DNA should give a A_{260}/ A_{280} ratio value of 1.8. A value below 1.8 is indicative of protein contamination whereas a value of 2.0 is considered to be pure RNA.

2.1.8.3 Large scale, high quality plasmid DNA extraction

QIAGEN-tip 2500 EndoFree Megaprep Kit was used to isolate plasmid DNA when large scale, high quality and ultra-pure transfection grade DNA was required for downstream applications. The DNA isolation procedure was performed according to the manufacturer’s guidelines, with minor modifications, and typically yielded 1.5-2.5 mg of DNA. DNA was quantified and its purity was determined using a UV spectrophotometer (Section 2.1.8.2).

2.1.9 RNA isolation and quality testing

Cellular RNA was extracted using the RNeasy Mini Kit (QIAGEN) according to the manufacturer’s protocol. RNA was eluted in RNase-free water and was used for downstream applications such as microarrays or qRT-PCR. The quantity of RNA was estimated by spectrometry at 260nm and 280 nm using a BioPhotometer. RNA of high quality should have an A_{260}/A_{280} ratio of 2.0. The integrity of RNA was also examined by running 500 ng of RNA samples on a 1% (w/v) non-denaturing agarose gel.

2.1.10 DNA constructs and plasmids

Typically, 30-100 ng/µL in 20 µL (sufficient for 8 reactions) of purified plasmid DNA samples were sent to GATC Biotech for sequencing. The obtained sequence was compared to the reference sequence from the National Centre for Biotechnology Information (NCBI) database using NCBI Basic Local Alignment Search Tool (BLAST). BLAST allows for alignment of two sequences and provides statistical analysis of the sequence similarity.

Table 2.1.10.1: List of plasmids used in this study.

Plasmid	**Description**	**Source**
pCR2.1	A TA-Cloning vector for cloning amplified PCR products. It contains the lacZ gene which encodes for β-galactosidase, allowing for blue/white colony screening of transformants.	Invitrogen
pUC19	Control plasmid	Invitrogen
pβ-gal	An expression vector encoding β-galactosidase (β-gal) under the regulation of an SV40 promoter.	Laboratory stock
pGL4.11-p53RE-luc2	A p53 luciferase reporter construct. It drives firefly luciferase expression from a wt MDM2 promoter cloned into pGL4.11 which contains *Luc2*. *Luc2* is a mammalian codon optimised version of *Luciferase* for more efficient translation and expression in mammalian cells.	Laboratory stock
pRL-TK	A luciferase reporter constructs that drives constitutive *Renilla* luciferase expression from an HSV thymidine kinase promoter.	Kindly provided by Prof Mike White
pEGFP-N1	An expression vector encoding red-shift variant of green fluorescent protein (GFP) suitable for N-fusions.	Clontech
pEYFP-N1	Encodes an enhanced yellow-green variant of GFP suitable for N-fusions.	Clontech
pEYFP-C1	Encodes an enhanced yellow-green variant of GFP suitable for C-fusions.	Clontech
pECFP-N1	Encodes an enhanced cyan variant of GFP suitable for N-fusions.	Clontech
pECFP-C1	Encodes an enhanced cyan variant of GFP suitable for C-fusions	Clontech
pCMV-HA	A mammalian vector expressing hemagglutinin (HA)	Clontech
pFLAG-CMV-6b	A FLAG expression vector in mammalian cells	Sigma-Aldrich

pCEP4	A basic mammalian expression vector	Invitrogen
pcDNA3.1	A basic mammalian expression vector	Invitrogen
pCMVNeoBam	An empty vector that contains two independent transcription units, a CMV promoter and a HSV thymidine kinase promoter.	Kindly provided by Dr Bert Vogelstein
pCMVNeoBam-MDM2	Encodes full length human MDM2, used for expression in mammalian cells	Kindly provided by Dr Bert Vogelstein
pCMVNeoBam-MDM2C464A	Encodes human MDM2 that harbours a single point mutation (C464A) at the zinc-coordinating residue in the RING domain that is critical for its E3 ubiquitin ligase activity. Used for expression in mammalian cells.	Kindly provided by Dr Dimitris Xirodimas
pCEP4-p53	Encodes full length human p53	Kindly provided by Dr Dale Haines
pHis$_6$-Ub	Encodes ubiquitin tagged with six consecutive histidines	Kindly provided by Prof Mathias Treier
pcDNA3.1-NM23-LV	Encodes full length NM23-LV	Kindly provided by Dr Linda Valentijn
pcDNA3.1-HA-NM23-LV	Encodes HA-tagged full length NM23-LV	Kindly provided by Dr Linda Valentijn
pCEP4-NME1	Encodes for full length NME1 of isoform b.	Laboratory stock
pCEP4-NME2	Encodes for full length NME2 of isoform a.	Laboratory stock
pCEP4-HA-NME2	Encodes HA-tagged full length NME2 of isoform a.	Laboratory stock
pCEP4-	Encodes for full length NME2 of isoform a	Laboratory stock

NME2H118F	with a point mutation (H118F) at the phospho-acceptor residue critical for NDPK activity	
pCEP4-NME1H118C	Encodes for full length NME1 of isoform a with a point mutation (H118C) at the phospho-acceptor residue critical for NDPK activity	Laboratory stock

2.1.10.1 Constructs expressing fluorescence-labelled NME fusion proteins

In order to generate constructs that express fluorescence-labelled NME fusion proteins, NME1, NME2, NME2H118F and NM23-LV DNA fragments were cloned into pEYFP and pECFP vectors, to result in both C- and N- terminally fluorescent-tagged forms of NMEs, as illustrated in Figure 2.1.10.1.1. Based on DNA templates as listed in Appendix 1, primers for PCR reaction were designed to include two desired restriction sites (ECoRI and BamHI) compatible to the multiple cloning sites of the pEYFP/pECFP backbones, and in some cases, to delete STOP codon (dSTOP). Standard cloning procedures (Section 2.1) were followed.

Briefly, NME DNA fragments were amplified by PCR according to DNA templates and primers, as well as PCR conditions listed in Appendix 1. PCR products were ligated into pCR2.1 vector for transformation into XL1-Blue bacteria cells. Extracted DNAs from positive colonies were digested with ECoRI and BamHI restriction enzymes to check for insertion and sent for sequencing. The correct NME fragments were subcloned into pEYFP and pECFP vectors at ECoRI and BamHI restriction sites.

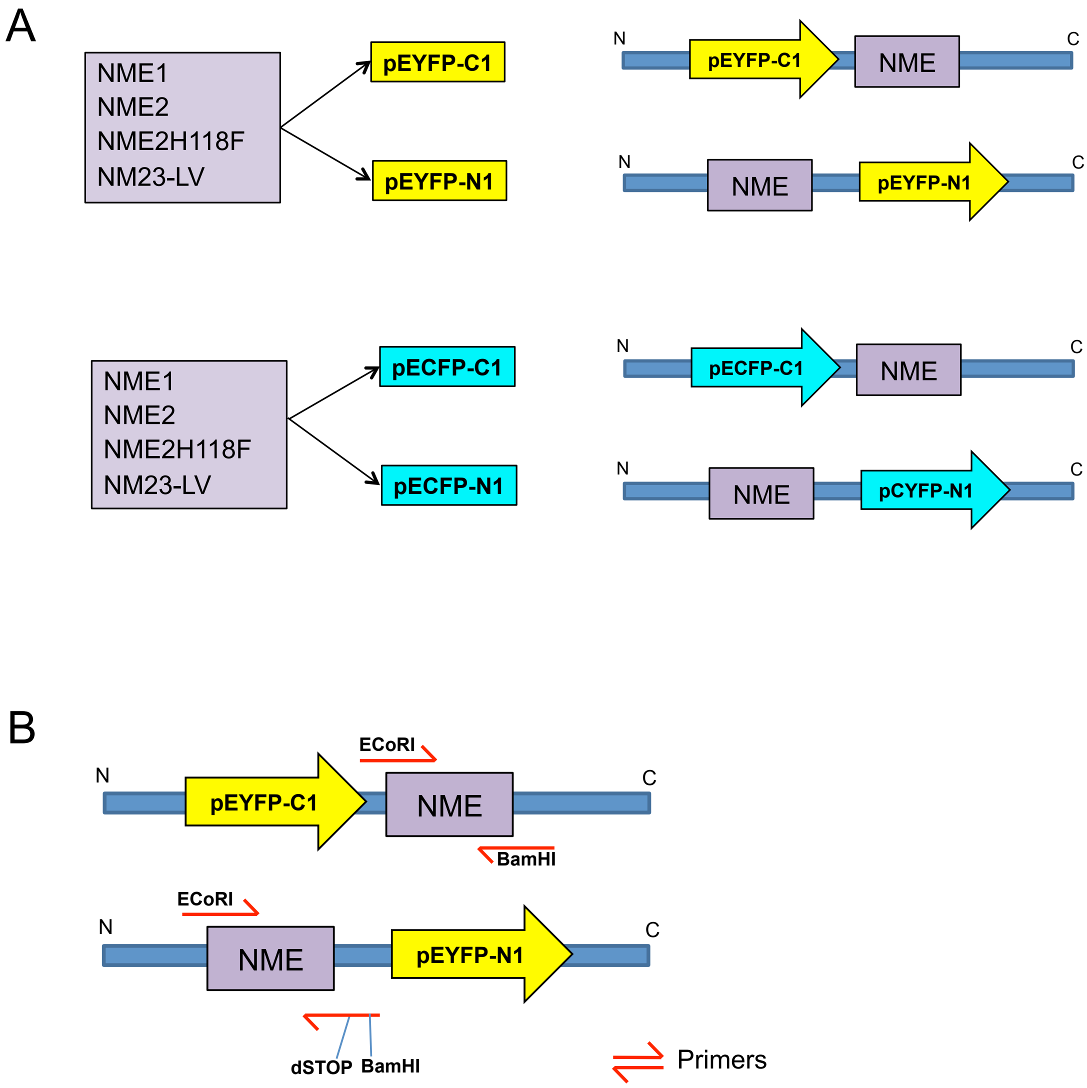

Figure 2.1.10.1.1: Schematic diagram illustrating the cloning strategy for **A.** generating constructs expressing EYFP/CFP-labelled NME fusion proteins **B.** designing primers that include deleted STOP codon (dSTOP) and/or restriction sites.

2.2 Cell Culture

Cell culture was performed in Class II safety cabinet using aseptic technique. All cells were grown at 37°C in a humidified incubator of 5% CO_2 and all reagents were pre-warmed to 37°C. Cells were routinely passaged 1:10 at 90-100% confluence. Once cells reached the desired confluence, the old media was discarded and the cells were washed with Dulbecco's Phosphate Buffered Saline (PBS, Sigma-Aldrich). PBS wash helps to remove any remaining traces of serum in the growing media which is capable of inhibiting Trypsin-EDTA activity. Trypsin-EDTA (Sigma-Aldrich) solution was then added to the cells and the flask was tilted gently to ensure even coverage. The cells were incubated, if required at 37°C, for 2-5 min. The flask was gently tapped at the side for a few times. Once the cells started to detach from the flask, the trypsin was inactivated by adding at least 1x volume of growth medium. The cells were then pipetted vigorously to ensure single cell suspension and applied into fresh culture vessel at the desired cell density with fresh medium.

To prepare cryostocks, cells were harvested by trypsinisation and pelleted by centrifugation at 300 x g for 5 min at RT. The media was aspirated and the pellets were gently re-suspended in 1 mL of freezing media (10% DMSO in FBS). The cell suspension was then transferred into cryovials (Nunc). To ensure slow freezing, the vials were placed into polystyrene containers and stored at -80°C overnight. After 24h, the cryovials were transferred to liquid nitrogen for storage. When recovering cells from liquid nitrogen, the stocks were defrosted as quickly as possible in a 37°C water-bath. The thawed cells were re-suspended in complete growth media in an appropriate tissue culture flask. The medium was changed when the cells adhered to the flask surface, usually on the following day.

Table 2.2.1: List of cell lines used in this study.

Cell line	Description and Maintenance	Source
H1299	H1299 (non-small cell lung carcinoma) cells were obtained from the American Type Culture Collection (Manassas, VA). H1299 cells are immortalised and p53-null. They were largely used in this study because they are well characterised, easily maintained and are relatively easy to transfect. The cells were maintained in RPMI-1640 medium (Sigma-Aldrich) supplemented with 10% Fetal Bovine Serum (FBS, Sigma-Aldrich).	American Type Culture Collection
H1299 Clone 9	A derivative of H1299 that overexpresses MDM2. Clone 9 cells were maintained as described above for H1299.	Laboratory stock
RFM9	A RING-finger mutant derivative of H1299 that lacks E3 ubiquitin ligase activity of MDM2. RFM9 cells were maintained as described above for H1299.	Laboratory stock
HEK293	Human embryonic kidney 293 cells was maintained in DMEM HEPES modification medium supplemented with DMEM HEPES modification (Sigma-Aldrich), 10% FBS and 2mM L-glutamine (Invitrogen).	Laboratory stock
U2OS	A human osteosarcoma cell line. The cells were maintained in RPMI-1640 medium (Sigma-Aldrich) supplemented with 10% Fetal Bovine Serum (FBS, Sigma-Aldrich).	American Type Culture Collection
Double null MEF	Mouse embryonic fibroblast with null p53 and MDM2 ($p53^{-/-}$, $Mdm2^{-/-}$). The cells were maintained in DMEM HEPES modification, 10% FBS and 2mM L-glutamine.	Laboratory stock

2.3 Introducing exogenous DNA into mammalian cells

2.3.1 GeneJuice transfection

GeneJuice (Novagen) was used to transiently transfect mammalian cells with plasmid DNA, according to the manufacturer's protocol. GeneJuice contains a non-toxic cellular protein and novel polyamine that allows for efficient entry of DNA into cells. Transfection was performed on 50-80% confluent cells, usually at 3 μL of GeneJuice per μg of DNA (ratio 3:1), with empty vectors added to ensure equal DNA content of transfections. Prior to transfection, GeneJuice, serum-free medium and DNA were equilibrated to RT. Appropriate volume of serum-free medium was added in a sterile tube. For each condition, DNA was prepared and mixed together (if performing co-transfection) in a sterile 1.5 ml screw-cap centrifuge tube. Then, GeneJuice was added directly and dropwise to the serum-free medium without touching the walls of the tube and mixed thoroughly by vortexing for a few seconds. The GeneJuice mixture was incubated for 5 min at RT then added to the DNA. The GeneJuice/DNA mixture was mixed by flicking the tube a few times and then incubated at RT for 15 min. The mixture was then added drop-wise to the cells in complete growth medium, covering the entire dish surface. The dish was rocked gently to ensure even distribution of the transfection mixture. The cells were kept in a tissue culture incubator at 37°C, normally for at least 24h before harvested for analysis or downstream experiments.

2.3.2 Lipofectamine transfection

Lipofectamine transfection is a cationic lipid-mediated transfection used in this study for introducing plasmid DNA or siRNA into mammalian cells. Lipofectamine can form liposomes in an aqueous environment and entrap negatively charge nucleic acid molecules to mediate the transport of transfection materials into cells. Typically, transfection was performed on approximately 90-95% confluent cells to enhance transfection efficiency and expression levels, and to minimise cytotoxicity. Before transfection, Opti-MEM Reduced Serum Medium (Invitrogen), Lipofectamine 2000 (Invitrogen) and DNA were equilibrated to RT. Lipofectamine was typically used at 2.5 μL per μg of DNA. For a 6-well plate, DNA and Lipofectamine were each diluted in 250 μL (1.5 ml for 10-cm dish) of

Opti-MEM medium in separate tubes and mixed well by a brief vortex. The mixtures were incubated at RT for 5 min. After incubation, the diluted Lipofectamine was added to the diluted DNA and the DNA/Lipofectamine mixture was mixed by flicking the tube several times. The DNA/Lipofectamine mixture was incubated for 20 min at RT. Then, all the transfection mixture was added drop-wise to cells in complete growth media, distributing the drops over the entire dish surface. The dish was gently rocked to ensure even distribution. The cells were incubated in a 37°C tissue culture incubator. Transfection mixture was removed 2-6h after incubation and replaced with complete growth medium to minimise cytotoxicity. Transfected cells were analysed at least 24h post-transfection.

2.3.3 siRNA transfection

siRNA transfection was performed on 40% confluent H1299 cells using Lipofectamine 2000 transfection reagent. Prior to transfection, Lipofectamine 2000 and Opti-MEM Reduced Serum Medium were equilibrated to RT. siRNA (Table 2.3.3.1) was defrosted just before transfection. Typically, cells were transfected with siRNA at a final concentration of 40 nM. For a 6-well plate, 80 pmoles of siRNA and 4 μL of Lipofectamine 2000 was each diluted in 250 μL Opti-MEM medium in separate tubes. The mixtures were incubated at RT for 5 min and then combined. The transfection mixture was mixed by flicking the tube for a few times and incubated for at RT for 20 min. The entire mixture was then added drop-wise to cells in complete growth media, distributing the drops evenly across the entire dish surface. The dish was rocked gently and then incubated at 37°C in a tissue culture incubator. Transfection mixture was removed 6h after incubation and replaced with complete growth medium. Transfected cells were analysed at least 24h post-transfection.

Table 2.3.3.1: Target sequence of siRNA. All of the siRNAs used in this study were synthesised by Dharmacon.

Name	**Target Sequence**	**Accession**	**Base No.**
Scrambled	5'- AAGGACGCAUCCUUCUUAAUU -3'	N/A	N/A
MDM2 oligo 1	5'- AAGCCACAAAUCUGAUAGUAU -3'	NM_002392	872-890
NME1 oligo 6	5'- GAGAUCGGCUUGUGGUUUCUU -3'	NM_198175	713-731
NME1 oligo 7	5'- CCGCCUUGUUGGUCUGAAAUU -3'	NM_198175	427-447
NME1 oligo 8	5'- GAGCGUACCUUCAUUGCGAUU -3'	NM_000269	121-140
NME1 oligo 9	5'- GAGAGAUUAUCAAGCGUUUUU -3'	NM_000269	173-192
NME2 oligo 7	5'- GCGAGAUCAUCAAGCGCUU -3'	NM_002512	295-313
NME2 oligo 8	5'- AAGGCGAGAUCAUCAAGCGCUU -3'	NM_001018137	315-334

2.4 Protein extraction and quantification (Bradford assay)

Bradford assay was performed to prepare and quantify protein samples [386]. Briefly, Cells were harvested by trypsinisation and pelleted by centrifugation at 300 x g for 5 min. The supernatants were discarded and the pellets were washed with 1 ml of PBS followed by centrifugation as previous step. The pellets were stored at -80°C before being further processed [386].

In order to extract protein, cell pellets were defrosted and then re-suspended on ice in lysis buffer supplemented with protease inhibitors (2 μg/mL aprotonin, 0.5 μg/mL leupeptin, 100 μg/mL soy bean trypsin inhibitor (STI), 1 μg/mL pepstatin (Roche), 1 mM phenylmethylsulphonyl fluoride (PMSF, Fluka)). Either Standard Lysis and Immunoprecipitation (SLIP) (50 mM HEPES, pH 7.5 (Calbiochem), 150 mM NaCl (VWR), 0.5 mg/mL bovine serum albumin (BSA, Fluka), 10% (v/v) glycerol, 0.1% (v/v) Triton X-100 (Sigma-Aldrich)) or radioimmunoprecipitation assay (RIPA), pH7.6 (50mM Tris. HCl (Calbiochem), 0.5% Na deoxycholate, 1% NP-40 (Sigma-Aldrich), 150mM NaCl, 0.1% SDS (VWR)) buffers was used as lysis buffer in this study. Following incubation on ice for 10 min, the lysates were centrifuged at 16,000 x g for 10 min at 4°C. The supernatants were then transferred to fresh pre-chilled 1.5-mL micro-centrifuge tubes and kept on ice.

To prepare protein standards, 20 mg of BSA was first dissolved in 1 mL of lysis buffer and then serial dilutions were generated to obtain the following concentrations: 10, 5, 2.5 1.25, 0.625, 0.3125 mg/ml. 2 µL of the standards (or samples) were then added to 1 mL of protein assay dye reagent (Bio-Rad) (diluted 1:5 with H_2O) mixed well by vortexing. 2 µL of the lysis buffer was also added to 1 mL of protein assay dye reagent and used as a blank. The addition of protein to Bradford reagent causes a change in the dye colour, which can be measured by a shift in absorbance at 595 nm. The absorbance of the known protein standards was measured using a BioPhotometer (Eppendorf) to create a standard curve. Protein concentrations of samples of interest were then determined based on the calibrated spectrophotometer. Normally, 50 µg of total protein was made up in sample loading buffer (4x) (250 mM Tris, pH 6.8, 8% (w/v) SDS, 40% (v/v) glycerol, 4 mg/mL bromophenol blue, 1% (v/v) β-mercaptoethanol (Sigma-Aldrich)) to a total volume of 20 µL, to achieve a final concentration of 1x buffer.

A micro-Bradford assay was performed when low protein yields were expected. A micro-Bradford assay was essentially identical to the regular Bradford assay described earlier except the protein standards were created in Passive Lysis Buffer (PLB, Strategen) as follows: 5, 2.5, 1.25, 0.625, 0.3125, 0.156, 0.078 mg/mL. 5 µL of standards (or samples) were added to 1 mL of protein assay dye reagent. The spectrophotometer was calibrated and protein concentrations of the samples were estimated as previously described.

2.5 Sodium dodecyl sulphate polyacrylamide gel electrophoresis (SDS-PAGE)

SDS-PAGE was performed using two-gel Mini-PROTEAN® Tetra cell (Bio-Rad) in an electrophoresis tank filled with running buffer (25 mM Tris, 220 mM glycine, 0.1% SDS). Protein samples and pre-stained protein markers (NEB) were denatured by boiling for 5-10 min, vortexed and centrifuged at 16,000 x g for 2 min at 4 °C. The samples were kept on ice while being loaded into the wells of polyacrylamide gel. Typically, SDS-PAGE was run at 200 V for approximately 1h.

2.6 Western blotting

Western blotting is used to detect and quantify specific proteins in the studied sample using specific antibodies. Proteins are first separated based on their molecular size using SDS-PAGE (Section 2.5) and then transferred to a Hybond ECL nitrocellulose membrane (GE Healthcare) using Mino Trans-Blot® Electrophoretic Transfer Cell (Bio-Rad). Briefly, the gel was placed on the nitrocellulose membrane in the cassette between sponges and Whatman paper. The cassette was placed in the tank filled with transfer buffer (25 mM Tris, 192 mM glycine, 20% methanol) along with an ice pack (to prevent overheating during the transfer). The transfer was run for 1h at 100 V. Following the transfer, the membrane was briefly stained with Ponceau S (0.1% (w/v) in 5% acetic acid (Sigma-Aldrich)) followed by several rinses with water. Stained membrane was cut according to the size of the proteins of interest by referencing the protein marker. After that, the membrane was destained with PBS/Tween (0.075 M NaCl, 0.065 M Na_2HPO_4, 0.015 M $NaH_2PO_4xH_2O$, 0.1% Tween 20 (Sigma-Aldrich)) and blocked in 5% (w/v) non-fat dried milk in PBS/Tween solution at 4°C overnight to prevent nonspecific antibody binding to the membrane. After blocking, the membrane was incubated with primary antibodies (in 5% milk/PBS/Tween solution) for 1h at RT with agitation (Table 2.6.1). The membrane was washed for at least 3 times for 15 min in PBS/Tween. The horseradish peroxidase (HRP)-conjugated secondary antibodies (in 5% milk/PBS/Tween solution) were applied and the membrane was incubated for 1h at RT with agitation. The membrane was again washed at least 3 times for 15 min in PBS/Tween. After the final wash, the membrane was incubated with Western Lightning Chemiluminescence Plus ECL reagent (Perkin Elmer) for 1 min. After the supply of Western Lightning Chemiluminescence Plus ECL reagent had been discontinued, ECL Prime (or Select for enhanced signal) Western blotting detection (Amersham) was used as replacement. The signal was detected by chemiluminescence using a Kodak IM4000 image station.

Table 2.6.1: A. Primary and B. secondary antibodies for Western blotting.

A

Primary antibodies			
Antibody	**Source**	**Raised in**	**Working concentration**
Anti-β-Actin (AC-15)	Santa-Cruz	Mouse monoclonal	1:10,000
Anti-α-tubulin (DM1A)	Sigma-Aldrich	Mouse monoclonal	1:2,000
*Anti-β-gal (OB02)	Merck	Mouse monoclonal	3 μg/mL
Anti-β-gal (AB986)	Milipore	Rabbit polyclonal	1:1,000
Anti-GFP (Clone 7.1 and 13.1)	Roche	Mouse monoclonal	0.4 μg/mL
Anti-p53 (DO-1/Ab-6)	Calbiochem	Mouse monoclonal	3 μg/mL
Anti-MDM2 (IF2/Ab-1)	Calbiochem	Mouse monoclonal	3 μg/mL
Anti-NME1 (NM301)	Santa-Cruz	Mouse monoclonal	3 μg/mL
Anti-NME2 (L15)	Santa-Cruz	Goat polyclonal	3 μg/mL
*Anti-NME1/2 (ab31019)	abcam	Rabbit polyclonal	6 μg/mL
Anti-NME1/2 (C1C3)	GeneTex	Rabbit polyclonal	1:1,000
Anti-HA (12CA5)	abcam	Mouse monoclonal	3 μg/mL
Anti-HA (16B12)	abcam	Mouse monoclonal	3 μg/mL
Anti-Histone H3 (ab1791)	Santa-Cruz	Mouse monoclonal	3 μg/mL
Anti-Lamin A/C (636)	Santa-Cruz	Mouse monoclonal	1:200
Anti-B23 (NA24)	Santa-Cruz	Mouse monoclonal	1:200

* Supply discontinued and replaced with alternatives

B

Secondary antibodies (HRP-conjugated)		
Antibody	**Source**	**Working concentration**
Sheep anti-mouse IgG	Amersham	1:2,500
Donkey anti-rabbit IgG	Amersham	1:5,000
Rabbit anti-goat IgG	Jackson ImmunoResearch Laboratories	1:20,000

2.7 Densitometry

When necessary, densitometry was performed to quantitatively measure chemiluminescence signal intensity using the Kodak Molecular Imaging Software. The areas for analysis were defined by manually creating regions of interest (ROIs) on the image using the software tools. Volumes of the ROIs selected were calculated by the software according to the recorded pixel information. A blank area of the blot was selected as background ROI. The signal intensity for each sample was calculated by deducting the sum intensity of the background ROI from the sum intensity of each of the sample ROIs.

2.8 Dual-luciferase reporter assays

Luciferase reporter assay is commonly used to study eukaryotic gene expression. The Dual-Luciferase® Reporter Assay System (Promega) was used to simultaneously detect the expression of firefly and *Renilla* luciferase constructs which had been transfected into mammalian cells. Briefly, the luciferase assay was performed on a 48-well plate which had been co-transfected with luciferase constructs, pGL4.11-p53RE-luc2 (firefly luciferase) and pRL-TK (*Renilla* luciferase). At least 24h post-transfection, the old medium was aspirated and cells were washed twice with 300 μL of PBS. 150 μL of Passive Lysis Buffer (diluted 1 in 5 in H_2O before use) was then added to each well and incubated with agitation for 10 min at RT. The cell lysates were re-suspended and transferred into 1.5-mL micro-centrifuge tubes and centrifuged at 16,000 x g for 1 min. The supernatants were transferred into fresh 1.5-mL micro-centrifuge tubes and examined for firefly luciferase activity. 30 µL of LAR II (Luciferase Assay Reagent II) was added in a fresh tube. 6 µL of the sample was added and vortexed for 1 sec. Immediately, luminescence was measured at 560 nm in a Glomax 20/20 luminometer (Turner BioSystems). The reaction was then quenched and the *Renilla* luciferase reaction was initiated by adding 30 µL of Stop & Glo® Buffer (supplemented with 50x Stop & Glo® Substrate). The tube was vortexed for 5 sec and the luminescence generated by *Renilla* luciferase was measured with an integration period of 10 sec. The results were normalised to protein concentrations in the samples, which had been determined using a micro-Bradford assay (Section 2.4).

2.9 *In situ* β-galactosidase (β-gal) assay

In situ β-gal assay was performed in this study to examine transfection efficiency. Cells were transfected with pβ-gal containing the lacZ gene. LacZ gene encodes for β-gal that cleaves the glycosidic linkage in X-Gal into galactose and 5-bromo-4-chloro-3-hydroxyindole, which upon dimerisation and oxidation generates an insoluble blue product. The dimerisation and oxidation reactions require the transfer of an electron facilitated by ferric and ferrous ions.

Briefly, 24-72h post-transfection, tissue culture medium was aspirated off the cells. Transfected cells were washed gently with 2 mL of PBS. Then, 2 ml of fixation solution (0.5% (v/v) glutaraldehyde (BDH) in PBS) was added to each well and incubated at RT for 15 min. In the meantime, substrate buffer (3 mM potassium ferrocyanide, 3 mM potassium ferricyanide, 2% (w/v) X-Gal (BDH), 1 mM $MgCl_2$) was made up in PBS. After incubation, the fixation buffer was aspirated and cells were washed with PBS. Then, 1 mL of substrate buffer was added to each well and incubated in a tissue culture incubator at 37°C for 8-10h. After that, substrate buffer was removed and cells were rinsed twice with H_2O before allowed to air-dry. Cells were then examined using light microscopy. Typically, untransfected cells were also assayed to determine baseline levels of endogenously expressed β-gal.

2.10 Live cell imaging

The live cell imaging system used in this study was developed and maintained by Dr Carlos Rubbi (University of Liverpool) (Figure 2.10.1). The imaging system was designed in a way that throughout the imaging process, cell culture vessel was kept in a microscope chamber, which was maintained at 37°C and supplied with a humidified CO_2-filled atmosphere.

Typically, cells were cultured to about 40-50% confluence on the day of experiment to allow sufficient room for cell migration, taking cell proliferation rate into account. 5 mL of fresh complete growth medium was added into each well and 2 mL of H_2O was applied in the gap between the wells to maintain humidity in the chamber. The cell culture plate was placed and secured inside the microscope with the temperature probe submerged in the water-filled gap between the wells.

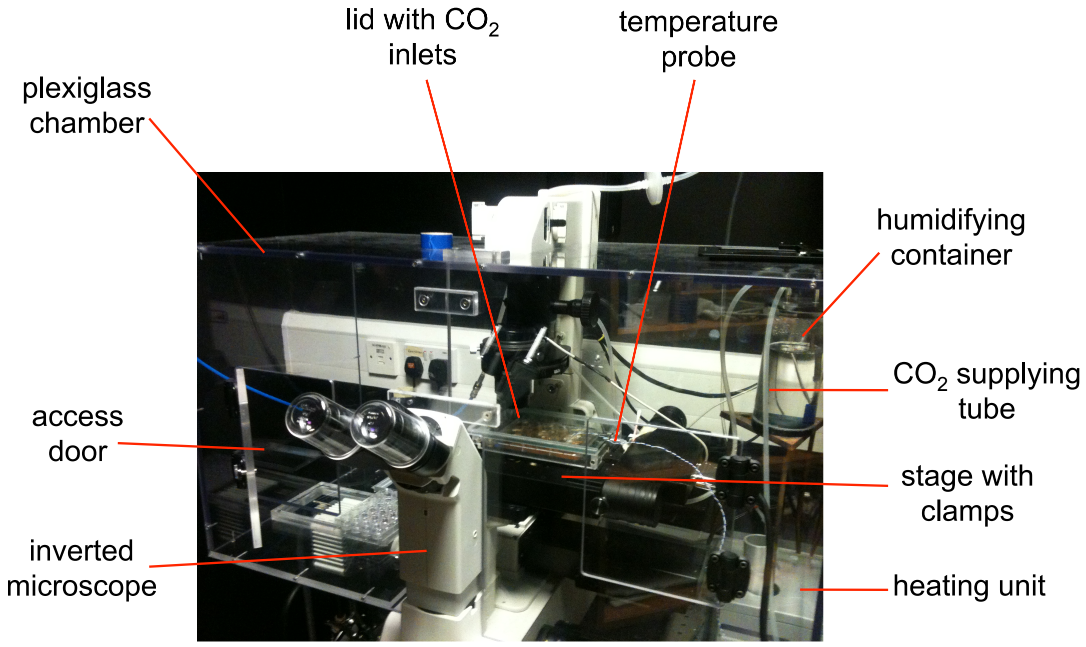

Figure 2.10.1: Microscope chamber for live cell imaging.

To examine cell migration using the live cell imaging system, at least 2 positions were selected per well and imaged with a time-lapse of 3-5 min for 24h (unless otherwise stated) using Simple PCI software (Hamamatsu Corporation). The recorded images were then combined to create movies and analysed using ImageJ software (National Institutes of Health). Plugins enabling tracking and analysis of cell motility of individual cells were written by Dr Carlos Rubbi. Whenever possible, 20 cells were selected and tracked for each condition. The following parameters were determined and compared:

- Total distance travelled – the length of the entire track of each cell
- Net distance travelled – distance in straight line between the first and last position of each cell
- Speed – total distance travelled divided by the duration of experiment in min
- Persistence – net distance travelled divided by total distance travelled

2.11 Boyden chamber migration assay

Boyden chamber migration assay was performed to measure the migratory potential of cells by examining their ability to migrate from one medium-filled compartment to another through a microporous membrane. BD Falcon^{TM} Cell Culture Inserts for 24-well plates with a polyethylene terephthalate (PET) membrane containing 8.0 μm at a density of $6 \pm 2 \times 10^4$ /cm^2 (BD Biosciences) were used for migration assays. 600 μL of complete growth medium was added to the wells of a 24-well Companion Plate (BD Biosciences). The cell culture inserts were placed in the companion plate and then pre-gassed in the tissue culture incubator for at least 30 min before seeding. Meanwhile, cells were harvested in complete growth media and counted. Typically, 15,000 cells in 300 μL of medium were seeded into the insert and the plate was incubated at 37°C, 5% CO_2 for 18h. After incubation, the inner side of the insert was cleaned rigorously with a cotton bud to remove cells that did not migrate through the porous membrane. The insert was soaked in PBS and its inner side was further cleaned with a fresh cotton bud. Using the REASTAIN Quick-Diff Kit (Reagena), cells successfully migrated through the porous membrane were fixed with 1 mL of REASTAIN Quick-Diff Fix solution for 10 min. The membrane was then stained with 500 μL of

REASTAIN Quick-Diff Red solution for 2 min, followed by 500 μL of REASTAIN Quick-Diff Blue solution for 2 min. The insert was rinsed with plenty of H_2O and left upside down to air-dry. The dried membrane was then carefully cut off the insert using a sharp scalpel blade and mounted on a microscope glass slide under a cover slip using DPX Mountant (Sigma-Aldrich). Once the slide was dry, cells that migrated through the membrane were counted on a microscope.

2.12 Expression microarrays

DNA microarray is a useful tool for measuring the expression levels of large numbers of genes simultaneously. In this study, the expression profiles of Clone 9 (over-expressing MDM2) and RFM9 (RING-finger mutant Clone 9) were compared with their parental H1299. The RNA samples for each cell line were prepared in triplicate on three separate occasions by previous members of our lab (Dr Anna Behrendt and Hubert Pakula). Microarray hybridisation of biotinylated cDNA was performed using an Affymetrix GeneChip® Human Exon 1.0 ST Array by members of the Applied Biology team (led by Prof. Ross Sibsons, University of Liverpool). Data analysis was performed by Dr Bryony Lloyd (University of Liverpool). Quality control analysis was performed on the raw array data using Expression Console software (Affymetrix). Normalisation was performed to minimise systemic errors so that the majority of observed differences originate from biological variation. The data was then analysed to identify differentially expressed genes and validated by quantitative real-time PCR (Section 2.13). All of the experimental work and analysis for microarray (except validation of expression using quantitative real-time PCR) were performed before I joined the lab.

2.13 Quantitative real-time PCR

2.13.1 Reverse transcription (RT)

RNA samples were reverse-transcribed to generate complementary DNA (cDNA) using the RNA-directed DNA polymerase Moloney Murine Leukemia Virus Reverse Transcriptase (M-MuLV RT, NEB). To reverse transcribe RNA, the initial reaction components (0.5-2 μg RNA solution, 40 μM Primer: oligo dT

(MWG Eurofins), 2.5 mM of each dNTPs (GE Healthcare), nuclease-free H_2O) were mixed together in a sterile, nuclease free, 0.2-mL PCR tube. The initial reaction mixture were heat-denatured at 80°C for 5 min and placed immediately onto ice. The remaining components (x10 RT buffer, 10 U/ μL RNase inhibitor, M-MuLV RT (NEB)) were then added to the tube and the reverse transcription reaction was performed at 42°C for 1h. A reaction without adding the reverse transcriptase was also included for each sample as negative control. After 1h, the reaction was terminated by heat-inactivating the enzyme at 90°C for 10 min. cDNA samples were stored at -20°C for future use.

2.13.2 Standard preparation

A standard curve can be calculated from external standard samples of known amounts and is used to determine the concentration of the target molecule in the unknown. Genes of interest selected from the expression microarray analysis were amplified by PCR from the cDNA using the primers listed in Appendix 2, after performing a gradient PCR to determine their optimum annealing temperatures. The PCR products were cloned into pCR2.1 vector using standard cloning protocols as described in Section 2.1. Once the identity of the PCR products were confirmed by sequencing, plasmids were purified using QIAPrep Spin Miniprep Kit (QIAGEN). The DNAs were quantified using NanoDrop ND-1000 (Thermo Scientific). Typically 7 standard amounts of each plasmid were prepared by 1:10 serial dilution on the day of experiment as follows: 5, 5×10^{-1}, 5×10^{-2}, 5×10^{-3}, 5×10^{-4}, 5×10^{-5} and 5×10^{-6} ng per reaction.

2.13.3 qRT-PCR

Quantitative Real-Time PCR (qRT-PCR) was performed on cDNA samples using the iQ^{TM} SYBR® Green Supermix and iQ5 multicolor real time PCR detection system (Bio-Rad). qRT-PCR was performed for the genes of interest selected from the expression microarray analysis and a housekeeping gene (*HPRT1*) to standardise the data. The reactions were set up in clear 96-well PCR microplates by combining the reaction components (2x iQ^{TM} SYBR® Green Supermix, forward primer (0.1 μg/μL), reverse primer (0.1 μg/μL), H_2O) except for the template cDNA. 50 ng in 5 μL of test cDNA samples, as well as the prepared standards (Section 2.13.2) were pipetted into designated wells of the PCR microplate. qRT-PCR was performed in triplicate for each reverse transcription, including for minus RT and only H_2O negative controls. Following the addition of cDNA, the reaction plate was sealed with a Microseal® 'B' film (Bio-Rad). The plate was briefly centrifuged and then placed into the iQ5 multicolor real time PCR detection system to begin the qRT-PCR reaction. The thermal cycling parameters and primers used for each gene are shown in Table 2.13.3.1 and Appendix 2, respectively.

Table 2.13.3.1: Standard cycling parameters for qRT-PCR.

Initial denaturisation	95°C	3 min
40 cycles		
Denaturisation	94°C	30 sec
Anneal	64°C	30 sec
Melt curve	95°C to 55°C	1°C per 10 sec

2.13.4 Data analysis

Data analysis was performed using the CFX Manager^{TM} Software (Bio-Rad). Briefly, the cycle number (C_T) at which the fluorescence passes a certain threshold was determined and reflects the quantity of the sample. To generate a standard curve, C_T for the 7 standards were determined and plotted against the log of the standard amounts, producing a regression line. Using this standard curve, the amount of product in the unknown samples within the same real-time PCR run was determined.

Melting curve analysis was also performed to determine whether the desired PCR product is free from non-specific by-products such as primer-dimer. PCR products can be characterised by melting curve analysis because each double-stranded DNA molecule has a characteristic melting temperature (Tm), at which 50% of the DNA is double-stranded and 50% is melted (i.e. single stranded). A sharp decrease in SYBR Green I fluorescence occurs when the temperature reaches the Tm of a

PCR product. If the PCR generated only one amplicon, melting curve analysis will show only one melting peak (Figure 2.13.4.1). If primer-dimers or other non-specific products are present, additional melting peaks (normally at a lower temperature due to shorter product) will be shown and the corresponding data will be eliminated from analysis.

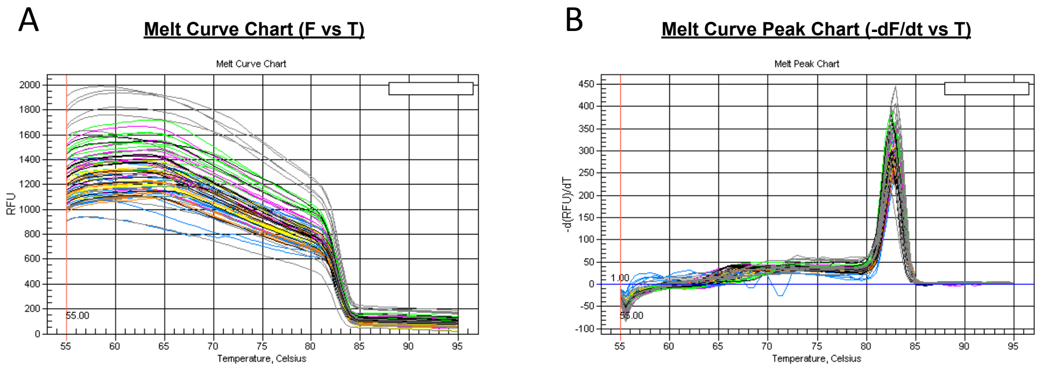

Figure 2.13.4.1: Melting curve graphs for real-time PCR. A. Melting curve showing a sharp drop in fluorescence signal when the temperature reaches the Tm of a PCR product. **B.** Melting curve peak chart will show only one melting peak if only one amplicon was generated by PCR.

For each transcription reaction, the average values were determined and normalised by dividing the average gene expression value by the expression value of the reference gene (HPRT) for the corresponding reverse transcription reaction. The normalised relative value was then averaged between the three transcription reactions. Since the RNA samples were also present in triplicate, the normalised relative values for each gene were averaged between the triplicates and the standard deviation was calculated. The relative gene expression was obtained by dividing the gene expression level in the test sample by the gene expression level in the control sample.

2.14 Nucleoside diphosphate kinase (NDPK) assay

NDPK assay was performed based on the protocol described by Agarwal et al. 1978 with minor modifications [279]. Accordingly, NDPK activity was determined by a coupled pyruvate-lactate dehydrogenase system, with ATP as the phosphate donor and thymidine diphosphate (dTDP) as phosphate acceptor nucleotides (Figure 2.14.1). The oxidation rate of nicotinamide adenine dinucleotide (NADH) was determined by spectrophotometrically measuring the decrease in absorbance at 334 nm over time. The consumption of NADH can thus act as a surrogate indicator of NDPK activity.

$$\text{dTDP} + \text{ATP} \xrightarrow{\text{NDPK}} \text{dTTP} + \text{ADP}$$

$$\text{ADP} + \text{PEP} \xrightarrow{\text{PK}} \text{ATP} + \text{pyruvate}$$

$$\text{pyruvate} + \text{NADH} \xrightarrow{\text{LDH}} \text{lactate} + \text{NAD}^+$$

Figure 2.14.1: NDPK assay principle. NDPK activity was determined by measuring the rate of oxidation of NADH spectrophotometrically following the formation of ADP from ATP in a coupled pyruvate-lactate dehydrogenase system. The consumption of NADH reflects the ADP formation by NDPK. dTDP, thymidine diphosphate; dTTP, thymidine triphosphate; PEP, phosphoenol pyruvate; ATP, adenosine triphosphate; ADP adenosine diphosphate; LDH, lactate dehydrogenase; PK, pyruvate kinase; NADH, reduced nicotinamide adenine dinucleotide; NAD^+, oxidised nicotinamide adenine dinucleotide.

Briefly, 250,000 cells were harvested and centrifuged at 16,000 x g for 5 min at 4°C. The supernatant was discarded and the cell pellet was washed with 1 ml of PBS, followed by centrifugation at 16,000 x g for 5 min at 4°C. The PBS was discarded and the cell pellet was lysed with 100 µL of RIPA buffer (Section 2.4), followed by centrifugation at 16,000 x g for 5 min at 4°C. The lysate was then transferred to a fresh micro-centrifuge tube and kept on ice. For each reaction, 200 µL of 5x buffer reagent (250 mM HEPES, 25 mM $MgCl_2$, 375 mM KCl, 5 mg/mL BSA), 10 µL of each 100 mM ATP (Sigma-Aldrich), 10 mM NADH (Santa Cruz), 100 mM phosphoenol pyruvate (PEP, Santa Cruz) and 40 mM dTDP (Sigma-Aldrich), and 750 µL of H_2O (pH7) were mixed and equilibrated at RT. To avoid contamination from adenylate kinase activity, 100 µM of adenylate kinase inhibitor, P1,P5-Di(adenosine-5')pentaphosphate (Ap5A, Sigma-Aldrich), was added to the reaction mixture. Next, 12.5 U/ml of each pyruvate kinase (Sigma-Aldrich) and 22.5 U/mL of L-lactate dehydrogenase (Sigma-Aldrich) were added to the mixture. Typically 3-5 µL of the lysate was used per 1 mL reaction. The reaction mixture was vortexed and then transferred to a UV compatible cuvette. The decrease in absorbance (or O.D.) was measured using a Biochrom Libra S32 spectrophotometer at 334 nm every 12 sec for 2 min. The reaction should be linear. If not, the extract was diluted or prepared in a more concentrated form. To measure the basal activity, the same amount of RIPA solution was added instead of the lysed sample. All measurements were performed in triplicate. The change in O.D. per minute was calculated by subtracting the basal activity and then converted to enzyme activity, considering the O.D. of a 1 mM NADH solution is 6.29. A unit of activity is defined as the amount required to convert 1 µmol of NADH to NAD^+ per minute.

$$\underset{(\text{U/ml})}{\text{Enzyme Activity}} = \frac{\Delta\text{O.D./min} \times \text{Final Vol. } (\mu\text{l}) \times \text{Dilution Factor}}{6.29 \times \text{Extract Vol. } (\mu\text{l})}$$

2.15 *In vivo* ubiquitination assay

In vivo ubiquitination assay was performed to identify target substrates subjected to ubiquitination in the cell. Essentially, the assay utilises Ni-NTA agarose beads (QIAGEN) to purify 6xHis-tagged ubiquitin (His_6-Ub) covalently bound to its protein substrates. Histidine residues in the His_6-Ub bind to the vacant positions in the coordination sphere of the immobilised nickel ions with high specificity and affinity. When cell lysates are loaded onto the matrix, His_6-ubiquitinated proteins are bound whereas other proteins pass through the matrix. Proteins subjected to His_6-ubiquitination can then be eluted in buffer under denaturing conditions.

The protocol used was adapted from [117]. Briefly, H1299 cells were transfected with 15 μg of His_6-Ub expression plasmid per 15-cm dish in addition to other expression constructs using GeneJuice transfection reagent. 24h post-transfection, cells were split 1:2 and further grown for an additional 24h. Cells were then harvested into two aliquots: 10% for Western blotting to confirm expression and possible degradation of transfected proteins; and the remaining 90% was used in the assay for purification with Ni-NTA agarose beads.

To perform the purification assay, cell pellet (90%) was lysed in 2 mL of Buffer A, pH8.0 (1 mL per 15-cm dish) (6 M guanidinium-HCl (Fluka), 0.1 M NaH_2PO_4, 0.01 M Tris-Cl, 10 mM β-mercaptoethanol, 5 mM imidazole (BDH)) supplemented with 10 mM N-ethylmaleimide (NEM, Sigma-Aldrich) to avoid deubiquitination. 100 μL/mL of Ni-NTA agarose beads was added to the lysate and incubated for 4h on the rotator at RT. Following incubation, Ni-NTA beads were washed with 1 mL of each Buffer A, Buffer B, pH8.0 (8 M urea (Fluka), 0.1 M NaH_2PO_4, 0.01 M Tris-Cl, 10 mM β-mercaptoethanol), and Buffer C (same composition as Buffer B, except at pH6.3), successively. These buffers contain strongly denaturing buffers, such as 8 M urea or 6 M guanidinium hydrochloride, to prevent co-purification of non-covalently bound proteins. After the washes, proteins bound to the beads were eluted into 80-120 μL of 1x sample buffer supplemented with 200 mM imidazole and analysed by SDS-PAGE and Western blotting.

2.16 Immunoprecipitation

Briefly, H1299 cells in 15-cm dishes were transfected with plasmids of interest using GeneJuice transfection reagent. 48h post-transfection, cells were harvested and the pellets were frozen at -80°C for at least 1h. The pellets were thawed and lysed using SLIP buffer supplemented with protease inhibitors for at least 10 min on ice. The lysates were clarified by centrifugation at 16,000 x g for 10 min at 4°C. The supernatant was immediately transferred into a fresh pre-chilled micro-centrifuge tube. Bradford assay was performed to determine the protein concentration of the samples. A small proportion of the lysate, usually just sufficient for conventional Western blot, was used to confirm expression of transfected plasmids. The remaining lysates, typically about 4 mg of total protein, were used for each point of immunoprecipitation. For immunoprecipitation, the lysate volume was made up to 500 μL with SLIP buffer. Protein G Sepharose beads (100 μL of 50% slurry per sample) were washed 3 times with 1 mL of SLIP buffer and collected by centrifugation at 16,000 x g for 30 sec at 4°C. After the last wash, the beads were re-suspended in SLIP buffer to obtain 50% slurry. 50 μL of the 50% slurry of washed Protein G Sepharose beads were added to each protein sample. The samples were incubated for 1h at 4°C on the rotator to remove non-specific proteins bound to the beads. After incubation, the samples were centrifuged for 30 sec at 4°C at 16,000 x g and the supernatants were transferred to pre-chilled fresh tubes. 2 μg of antibody was added to each of the samples and incubated for 1h on rotator at 4°C to allow the antibody to bind to its antigen. After that, 50 μL of the 50% slurry of Protein G Sepharose beads was added to each of the samples and incubated for 2h at 4°C on a rotator to capture the antibody/antigen complex on the beads. The samples were then centrifuged for 30 sec at 16,000 x g. The supernatants were discarded and the beads were washed 3 times with 500 μL of SLIP buffer. Following the last wash, the collected beads were re-suspended in 40-80 μL of 1x protein sample buffer and stored at -80°C for conventional SDS-PAGE and Western blotting analysis. For NDPK assay, 80-100 μL of RIPA buffer was added to the collected beads containing the immunoprecipitated proteins and was immediately used for the assay.

2.17 Flow cytometry

Typically, approximately 1 x 10^6 cells were harvested in a 15-mL Falcon and washed twice with cold PBS by centrifugation at 150 x g for 5 min. Following the final wash, PBS was aspirated carefully leaving about 100 µL above the pellet. The tube was flicked vigorously for several times to dislodge the cells and to create a single cell suspension. In order to allow propidium iodide (PI), a fluorochrome, to pass through the cell membrane and intercalate with DNA, cell membranes were permeabilised by fixation. For fixation, cells were gently vortexed while slowly adding drop-wise 5 mL of 70% ice-cold ethanol. The samples were left on ice for at least 1h (or up to two weeks at 4°C) before being further processed. Fixed cells were pelleted by centrifugation at 150 x g at 4°C and washed twice in cold PBS/0.1% Tween (Sigma-Aldrich) to remove residual ethanol.

As PI is also able to bind non-specifically to RNA, specific staining of DNA requires RNase A treatment. A solution of RNase A was prepared in advance as follows. 10 mg/mL of RNase A (Sigma-Aldrich) was made up in 0.01 M sodium acetate (pH 7.4), followed by boiling at 100°C for 15 min to inactivate DNase contaminants. The solution was cooled and 1/10th volume of 1 M Tris HCl (pH7.4) was added. The RNase A solution was aliquoted and stored at -20°C.

After the last wash, PBS/Tween was removed and the cell pellets were re-suspended in 100 µL of 10 mg/mL RNase A and left on ice for 5 min. Staining solution containing 850 µL of PBS and 50 µL of 1 mg/mL PI (Sigma-Aldrich) in PBS was added to each sample and left on ice in the dark for 30 min. Flow cytometry was performed on the samples using the Becton Dickinson FACSCalibur™ flow cytometer. Typically, 20,000 events were recorded for each run. Analysis was performed using FlowJo Analysis Software. The flow cytometry parameters used for analysis in this study were as follows: FL2 linear to detect PI, FL1-Height (EYFP Log), FL2-Width linear, FL2-Area linear, FS linear and SS linear.

2.18. Hypotonic lysis and sub-cellular fractionation

The hypotonic lysis and sub-cellular fractionation methods were performed based on the nucleolar isolation protocol described by Lam and Lamond 2006 [387]. Briefly, cells were harvested by trypsinisation and collected in a 50-mL Falcon tubes. The cells were washed three times with ice-cold PBS at 218 x g at 4°C. After the final wash, the cells were re-suspended in 5 mL of Buffer A (10 mM HEPES (pH7.9), 10 mM KCl, 1.5 mM $MgCl_2$, 0.5 mM Dithiothreitol (DTT, Sigma-Aldrich)), supplemented with protease inhibitors (Section 2.4), and incubated on ice for 5 min. A small drop of the cell suspension was put on a glass slide and checked under a phase-contrast microscope, using a 20x objective. The cells should be swollen, but not burst. The cells were maintained in this hypotonic condition by being incubated at 4°C. The cell suspension was transferred to a pre-cooled 7-mL Potter homogeniser and homogenized on ice for 10 times using a tight pestle. The homogenised cells were checked under a phase-contrast microscope after every 10 strokes. Homogenisation was stopped when more than 90% of the cells were burst, leaving intact nuclei with various amounts of cytoplasmic material attached. In most cases, the presence of this cytoplasmic contamination does not affect the final purity of the isolated nucleoli. The homogenised cells were centrifuged at 218 x g at 4°C for 5 min. For NDPK assay, the supernatant was kept on ice and used immediately as a hypotonic lysed cell sample.

For preparation of different sub-cellular fractions, the supernatant was retained as cytoplasmic fraction and stored at -80°C. The pellet contains enriched, but not highly pure, nuclei. The pellet was re-suspended with 3 mL of S1 solution (0.25 M sucrose (Sigma-Aldrich), 0.5 mM $MgCl_2$, supplemented with protease inhibitors (Section 2.4)). The re-suspended pellet was carefully layered over with 3 mL of S2 solution (0.35 M sucrose, 0.5 mM $MgCl_2$, supplemented with protease inhibitors (Section 2.4)), making sure the two layers were cleanly separated. The sample was then centrifuged at 1,430 x g for 5 min at 4°C to obtain a cleaner nuclear pellet. The pellet was re-suspended with 3 mL of the S2 solution. The nuclear suspension was sonicated with 6 burst, with 10-sec intervals between each burst, using a sonicator. The sonicated nuclei were checked under a phase-contrast microscope.

They should be virtually no intact cells and nucleoli should be readily observed as dense, refractile bodies. The sonicated sample was then layered over 3 mL of the S3 solution (0.88 M sucrose, 0.5 mM $MgCl_2$, supplemented with protease inhibitors (Section 2.4)) and centrifuged at 3,000 x g for 10 min at 4°C. The pellet contains nucleoli, whereas the supernatant was retained as nucleoplasmic fraction and stored at -80°C. The nucleoli were re-suspended with 0.5 mL of S2 solution, followed by centrifugation at 1,430 x g for 5 min at 4°C, to obtain a pellet containing highly purified nucleoli. The nucleoli was re-suspended in 0.5 mL of the S2 solution and stored at -80°C.

The cytoplasmic, nucleoplasmic and nucleoli fractions of U2OS cells used in this study were kindly provided by Dr Carlos Rubbi. A Bradford assay (Section 2.4) was performed for the U2OS cell fractions to quantify their protein levels. The samples were added with appropriate amounts of sample buffer for SDS-PAGE and Western blotting analysis.

2.19 MTT assay

MTT assay was used as a measure of cell viability/growth. Typically, cells were harvested by trypsinisation and re-suspended in complete growth medium. Either a haemocytometer or Beckman coulter counter (Z2 Coulter® Particle Count and Size Analyser) was used to count the concentration of cells. 2,000 cells in 200 µL of growth media were seeded into each well of a 96-well plate. Typically, cell proliferation was monitored over 7 days. Accordingly, cells were seeded into 7 plates and let proliferate with medium changing every day. After 24h (Day 0), 20 µL of 5 mg/mL sterilised MTT (Molekula) in PBS was added to each well, in addition to the existing medium. The plate was incubated for 3h at 37°C in a tissue culture incubator. After incubation, 190 µL of solution was aspirated off each well and discarded. 100 µL of DMSO was added to each well. The plate was then incubated for a further 30 min at 37°C. The absorbance was measured at an OD of 595 nm using a plate reader. The procedure was repeated for plates Day 1 to Day 6 in order to generate a growth curve.

Chapter 3.1

Results

3.1 Microarray analysis of the effects of MDM2 on gene expression

Following the findings that MDM2 promotes cell motility in a RING-finger-independent manner [384], gene expression profiles were studied using exon array analysis to identify the differences and overlaps in the expression changes induced by wt MDM2 (Clone 9) and a RING-mutant (RFM) of MDM2 (C464A) in parental H1299 cells. It was hypothesised that there is a possibility that genes that are mutually regulated in both Clone 9 and RFM9 represent genes that are involved in the same pathways to promote cell motility. RNAs were extracted from these cells (by Mr Hubert Pakula, a former member of the laboratory) for expression analysis by Dr Bryony Llyod. Two attempts at the microarray analysis experiment were made. In the initial experiment, 32 genes were found to be mutually regulated for more than 2.25-fold in Clone 9 and RFM compared to H1299 cells. A complete list of differentially regulated genes is shown in Appendix 3. However, since there was a high variability in the control H1299 RNA samples (Batch 1), the microarray experiment was repeated using freshly extracted H1299 RNA (by Dr Anna Behrendt, a former member of the laboratory) (Batch 2) as a control. In the second microarray analysis experiment, 151 genes were identified to be mutually regulated in Clone 9 and RFM. The list of differentially regulated genes identified in the second attempt is represented in Appendix 4. All of the experimental work and analysis for microarray (except validation of expression using quantitative real-time PCR) were performed before I joined the laboratory.

3.1.1 Validation of exon array analysis

Following the identification of two lists of genes that are mutually regulated in Clone 9 and RFM9, validation for the expression differences obtained from microarray analysis was performed. For this purpose, four genes were selected from these lists based on the relative mRNA expression level (normalised to the expression level in the parental H1299 cells) and a literature review that suggested a role in regulating motility/invasion/metastasis and that therefore they could be involved in the observed migratory phenotype of MDM2 overexpressing cells. The selected genes are TUBA1B, RPS24, ADAMTS1, and PCDHB2. A brief summary of the functions of the selected genes is presented in Table 3.1.1.1

Table 3.1.1.1: The list of genes selected for validation by qRT-PCR based on the expression differences identified by microarray analysis.

Gene symbol	Full name	Fold change		Function
		Clone 9 vs H1299	RFM9 vs H1299	
TUBA1B	Tubulin alpha 1b	22.29	32.34	- Major constituent of microtubules - Essential in cell division - Increased expression is associated with poor prognosis in HCC [388]
RPS24	Ribosomal protein S24	8.69	8.89	- A component of the 40S ribosomal subunit - Upregulated in HCC [389] - Important in rRNA processing and proliferation [390]
ADAMTS1	A disintegrin and metallopeptidase with thrombospondin type 1	6.43	3.34	- Member of the matrix metalloproteinase family - Impairs angiogenesis, tumour growth, and metastasis [391, 392] - May contribute to the metastatic program [393]
PCDHB2	Protocadherin beta 2	6.82	4.41	- Roles in tissue morphogenesis and formation of neuronal circuits [394]

In order to validate the expression differences observed in the selected targets presented in Table 3.1.1.1, qRT-PCR was performed using RNA extracted from H1299, Clone 9, RFM9 and EV Cl.1 of H1299 (as a negative clonal control). RNA extraction was performed in triplicates and the quality of RNA was examined before proceeding to qRT-PCR analysis. Whilst it is difficult to detect mRNA since it comprises only 1-3% of total RNA, main components of the ribosomal RNA (rRNA) 28S and 18S are easily detectable because they comprise more than 80% of total RNA. 28S and 18S rRNAs can be visualised as two clear separate bands on agarose gel stained with ethidium bromide. Since 28S and 18S rRNAs are derived from the same precursor rRNA, both molecules have the same number of copies. Thus the ratio of 28S:18S rRNA depends only on their size, which is approximately 5 kb and 1.9 kb (in mammals), respectively. Theoretically, the ratio of 28S:18S is estimated at 2.7:1 but a ratio of 2.1 is indicative of good quality, intact RNA. The ratio of the intensity of these bands can be used as a measure of the integrity of the extracted RNA since these two rRNA species have different degradation rates, in which 28S rRNA is more susceptible to degradation than 18S rRNA [395]. The ratio of the 28S:18S rRNA in the analysed RNA samples was approximately 2:1 (Figure 3.1.1.1) suggesting that the RNAs were not degraded.

An OD 260/280 ratio is used to estimate the nucleic acid purity and an ideal value for RNA is 2.0. The ratios obtained for the extracted samples (Table 3.1.1.2) are slightly lower (above 1.83), which could be due to the presence of protein contaminants. The OD 260/230 ratio is an alternative indicator of nucleic acid purity. The ratio should be higher than 2.0 and lower ratios may indicate the presence of inorganic contaminants that absorb at 230 nm (such as guanidinium thiocynate and EDTA). As shown in (Table 3.1.1.2), most of the obtained OD 260/230 ratios are mostly above 2.0, suggesting that the samples are essentially free of inorganic contaminants. Overall, the RNAs extracted were suitable for qRT-PCR analysis.

Table 3.1.1.2: Spectrophotometrical quantification of the RNA used for qRT-PCR. RNA was extracted from the indicated cell lines on three separate occasions (I-III).

Samples	OD 260/280	OD 260/230
H1299 I	1.88	2.35
H1299 II	1.90	2.28
H1299 III	1.91	2.35
Clone 9 I	1.92	1.79
Clone 9 II	1.90	2.13
Clone 9 III	1.88	2.29
RFM9 I	1.89	2.20
RFM9 II	1.84	2.40
RFM9 III	1.83	2.34
EV I	1.86	2.28
EV II	1.88	2.34
EV III	1.89	2.14

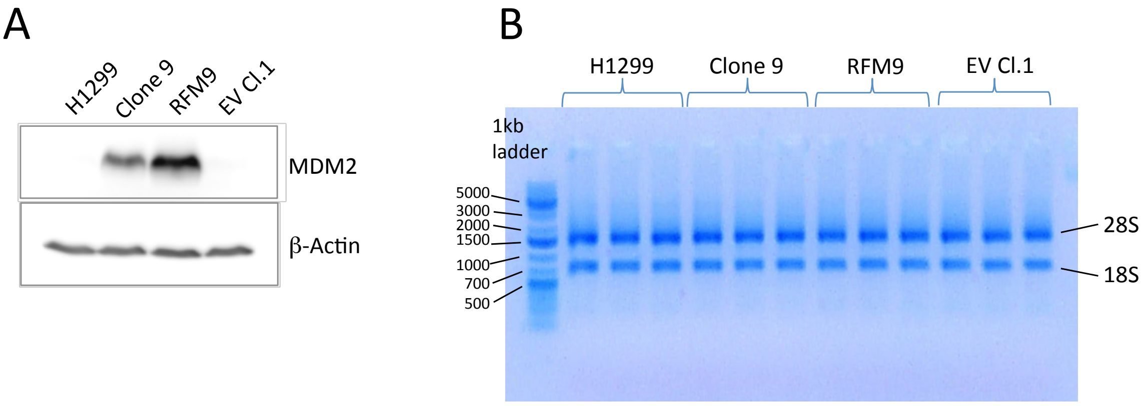

Figure 3.1.1.1: Analysis of the integrity of RNA used for qRT-PCR. RNA was extracted from H1299, Clone 9, RFM9 and EV Cl.1 (derived from H1299) on three separate occasions. **A.** Western blot of the lysate samples of the indicated cells used for RNA extraction. Primary antibodies used were anti-MDM2 (IF2) and anti-β-actin (AC-15). **B.** The RNA integrity was examined by running 500 ng of total RNA on a 1.2% (w/v) agarose gel stained with EtBr and visualized using UV light. The 28S and 18S RNA bands are indicated.

qRT-PCR was performed as described in Materials and Methods Sections 2.13.3 and 2.13.3. The relative expression levels (normalised to HPRT) of the four selected targets in H1299, Clone 9, RFM9 and EV Cl.1 are represented in Figure 3.1.1.2. Most of the determined relative gene expression levels of the four selected genes in the indicated cells did not validate gene expression obtained from the exon array analysis. No difference in mRNA expression of TUBA1B was detected in Clone 9 or RFM9, even though exon array indicates a 22- and 32-fold change in expression, respectively, compared to H1299. Only ADAMTS1 expression in Clone 9 was significantly higher than in parental H1299 (p=0.012). However, no difference in ADAMTS1 expression level was observed in RFM9.

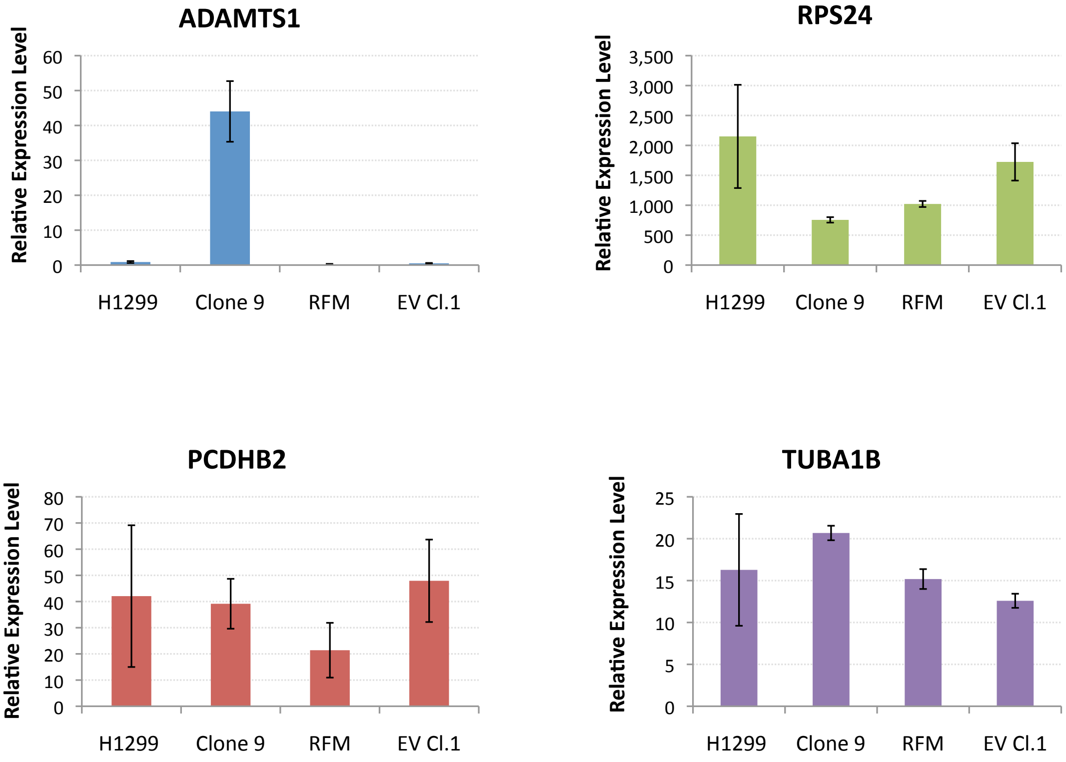

Figure 3.1.1.2: Relative expression levels of the ADAMTS1, PCDHB2, RPS24, and TUBA1B in the indicated cell lines. qRT-PCR was performed on RNA extracted from H1299, Clone 9, RFM9 and EV Cl.1. The histograms show mean of the average expression levels (normalised to HPRT expression) in three replicate RNA samples. Error bars indicate standard errors of mean.

3.1.2 Validation of gene expression changes in transiently transfected cells

To exclude the possibility of clonal variation affecting ADAMTS1 gene expression observed in Clone 9, qRT-PCR was repeated in transiently transfected H1299 cells. H1299 cells were transfected with plasmids expressing wt MDM2, RFM and EV, using both GeneJuice and Lipofectamine 2000, as described in Figure 3.1.2.1B. A small aliquot of cells from each condition was used for western blot analysis. Figure 3.1.2.1A shows the expected expression of MDM2 in transfected cells. Higher levels of MDM2 were detected in cells transfected with RFM compared to wt MDM2. This is because RFM lacks an E3-ligase activity for targeting MDM2 for proteasomal degradation. In addition, in comparison to GeneJuice, transfection using Lipofectamine 2000 also leads to a marginally higher expression of the plasmids. RNA was extracted from the transfected samples and the RNA quality was tested as described previously in Section 3.1.1. Based on the 28S:18S rRNA, OD 260/280 and OD 260/230 ratios of the analysed samples (Figure 3.1.2.1B and Table 3.1.2.1), the extracted RNA was suitable for qRT-PCR analysis. The relative expression levels (normalised to HPRT) of the four selected targets in transfected H1229 cells are represented in Figure 3.1.2.2. No difference in expression of the selected genes was observed in all the transfected cells, regardless of the transfection reagents used (Figure 3.1.2.2**).** This observation is in accordance with analysis of RNA extracted from stable clones, but in contradiction to the exon array analysis.

Table 3.1.2.1: Spectrophotometrical quantification of the RNA extracted from transfected cells used for qRT-PCR. RNA was extracted from transiently transfected H1299 for qRT-PCR analysis. GJ, GeneJuice; Lipo, Lipofectamine 2000.

Samples	OD 260/280	OD 260/230
EV-GJ	2.10	1.38
MDM2-GJ	2.02	2.23
RFM-GJ	2.06	2.16
EV-Lipo	2.05	2.11
MDM2-Lipo	2.05	2.21
RFM-Lipo	2.04	2.23

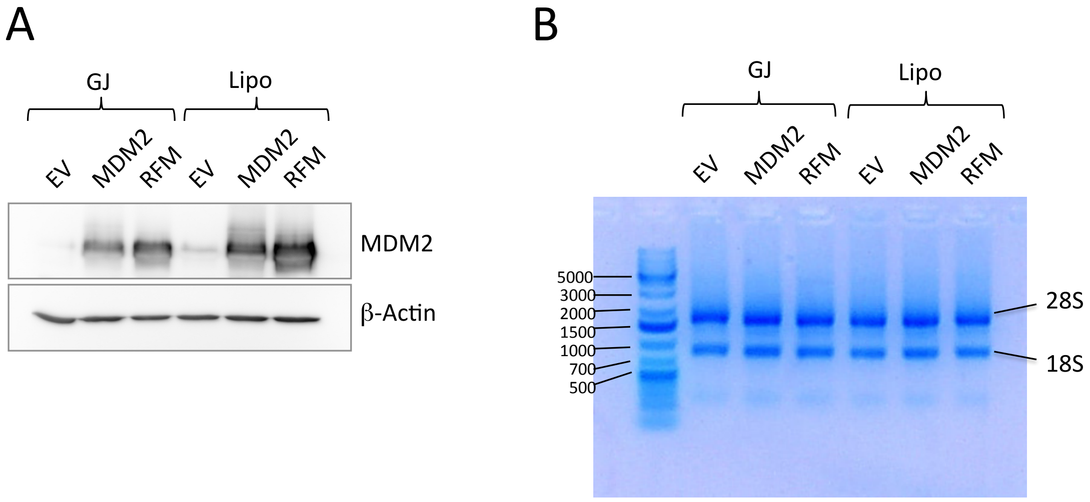

Figure 3.1.2.1: Analysis of the integrity of RNA extracted from transiently transfected cells. H1299 cells were transfected with either 10 μg of wt MDM2, RFM, or EV in 10-cm dishes, using GeneJuice (GJ) or Lipofectamine 2000 (Lipo), as indicated. **A.** Western blot of the lysate samples of the indicated cells used for RNA extraction. Primary antibodies used were anti-MDM2 (IF2) and anti-β-actin (AC-15). **B.** RNA integrity of RNA extracted from transfected cells was examined by running 500 ng of total RNA on a 1.2% (w/v) agarose gel stained with EtBr and visualized using UV light. The 28S and 18S RNA bands are indicated.

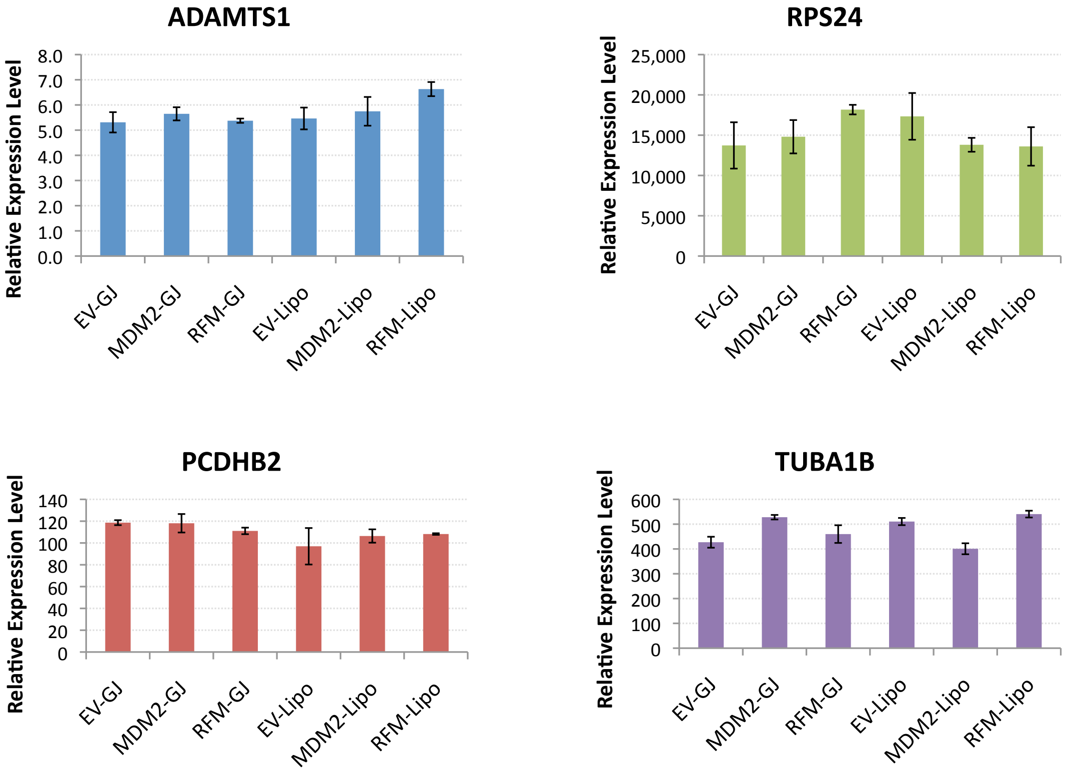

Figure 3.1.2.2: Relative expression levels of the ADAMTS1, PCDHB2, RPS24, and TUBA1B in transiently transfected H1299 cells. qRT-PCR was performed on RNA extracted from H1299 transfected with wt MDM2, RFM, or EV, using GeneJuice (GJ) or Lipofectamine 2000 (Lipo). The histograms show mean of the average expression levels (normalised to HPRT expression) in RNA samples. Error bars indicate standard error of mean.

3.1.3 Validation of gene expression changes in transient transfected cells

qRT-PCR analysis presented in Section 3.1.1 suggests that mRNA expression of ADAMTS1 in Clone 9 is more than 40-fold greater than H1299 and EV Cl.1 controls. However, concerns were raised as this result was not reproducible in H1299 transfected with wt MDM2 (Section 3.1.2). In order to eliminate the possibility of this result being an effect of clonal selection, qRT-PCR was repeated for ADAMTS1 using two additional clones that express high levels of MDM2 (MDM2 Cl.1 and Cl.3). EV Cl.2 was also included as an additional negative control. RNA extraction was performed in triplicates for H1299, EV C1.1 and Cl.2, Clone 9, and MDM2 Cl.1 and Cl.3. The quality of RNA was examined, as described in Section 3.1.1, before proceeding to qRT-PCR analysis. Based on the 28S:18S rRNA, OD 260/280 and OD 260/230 ratios of the analysed samples (Table 3.1.3.1 and Figure 3.1.3.1), the extracted RNA was suitable for qRT-PCR analysis. The relative expression levels (normalised to HPRT) of ADAMTS1 in indicated clones are represented in Figure 3.1.3.2. Only Clone 9 shows higher mRNA expression compared to H1299 and H1299 clonal derivatives EV Cl.1 and Cl.2 (about 150-fold). No difference in ADAMTS1 expression was observed in the other two high MDM2 expressing clones (Figure 3.1.3.2**).** This observation indicates that the expression changes of ADAMTS1 observed in Clone 9 were most likely a result of chance differences selected through cell cloning. An alternative explanation might be related to the difference in dynamic range between microarray platforms and qRT-PCR. The dynamic range represents the range of the initial mRNA concentrations, over which accurate expression levels can be determined. Most commercially available microarray platforms have a dynamic range that is lower by several orders of magnitude than that achievable by qRT-PCR. Therefore, it is unlikely that the larger dynamic range of qRT-PCR assays, which provides a more sensitive detection of expression changes, would have under-represented the differences in expression observed through microarray analysis. Instead, we question the reliability of the microarray analysis, considering we had issues with control variability in the first instance (Section 3.1). As we were unable to validate the expression differences obtained from microarray analysis, we decided to terminate this particular line of investigation.

Table 3.1.3.1: Spectrophotometrical quantification of the RNA used for qRT-PCR. RNA was extracted from the indicated cell lines on three separate occasions (I-III).

Samples	**OD 260/280**	**OD 260/230**
H1299 I	1.81	2.37
H1299 II	1.76	2.39
H1299 III	1.74	2.38
EV Cl.1 I	1.82	2.42
EV Cl.1 II	1.85	2.34
EV Cl.1 III	1.79	2.23
EV Cl.2 I	1.87	2.39
EV Cl.2 II	1.82	2.3
EV Cl.2 III	1.77	2.33
Clone 9 I	1.86	2.39
Clone 9 II	1.82	2.31
Clone 9 III	1.84	2.38
MDM2 Cl.1 I	1.87	2.39
MDM2 Cl.1 II	1.8	2.32
MDM2 Cl.1 III	1.8	2.37
MDM2 Cl.3 I	1.8	2.32
MDM2 Cl.3 II	1.79	2.37
MDM2 Cl.3 III	1.82	2.35

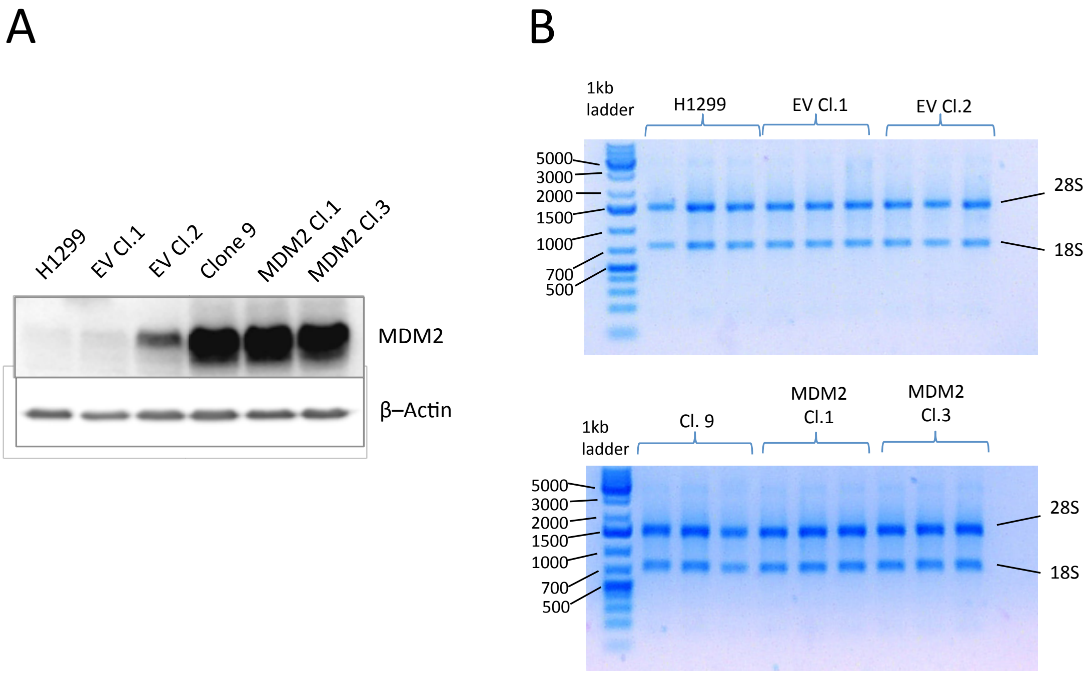

Figure 3.1.3.1: RNA integrity of RNA extracted from clonal cells for qRT-PCR. RNA was extracted from H1299, EV Cl.1 and Cl.2, Clone 9, MDM2 Cl.1 and Cl.3 on three separate occasions (I-III). **A.** Western blot of the lysate samples of the indicated cells used for RNA extraction. Primary antibodies used were anti-MDM2 (IF2) and anti-β-actin (AC-15). **B.** The RNA integrity was examined by running 500 ng of total RNA on a 1.2% (w/v) agarose gel stained with EtBr and visualized using UV light. The 28S and 18S RNA bands are indicated.

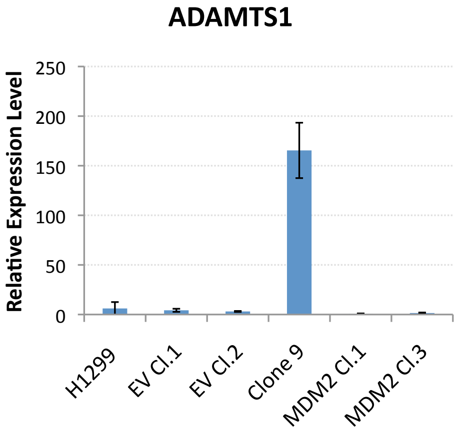

Figure 3.1.3.2: Relative expression levels of the ADAMTS1 in clonal cells. qRT-PCR was performed on RNA extracted from H1299, EV Cl.1 and Cl.2, Clone 9, MDM2 Cl.1 and Cl.3. The histograms show mean of the average expression levels (normalised to HPRT expression) in three replicate RNA samples. Error bars indicate standard errors of mean.

Chapter 3.2

Results

3.2 Investigation of the mechanisms of action of MDM2 in antagonising NME2 motility suppressive effect

3.2.1 RCC 117 cells are refractory to transfection using GeneJuice

In order to study the effect of high levels of MDM2 in promoting cell motility in RCC, cells had to be engineered to overexpress exogeneously introduced MDM2 or other genes of interest. This could be achieved through transient transfection of the cells. To establish the optimal conditions for transfection using GeneJuice, RCC cell line 117 (p53 wild-type) and non-small cell lung carcinoma cell line H1299 (positive control, since we know that these cells transfect well) were transfected with 1 μg of pβ-gal per well of a 6-well plate using different ratios of DNA:GeneJuice. Following transfection, the transfection efficiency was estimated based on *in situ* β-gal staining. Consistent with previous observations by past members from our laboratory, 117 cells were refractory to transfection, regardless of the DNA:GeneJuice ratios used (Figure 3.2.1.1). On the other hand, H1299 cells are easy to transfect and maintain. They possess a homozygous partial deletion of *TP53* gene and are therefore *p53* null, which makes them an excellent system for studying p53-independent processes. Since they are also easy to transfect, this makes them a good cell line for transient transfection experiment to examine the effects of protein of interest on cell motility. A decent transfection efficiency can aid the elucidation of the effect of cell population expressing exogenous proteins of interest.

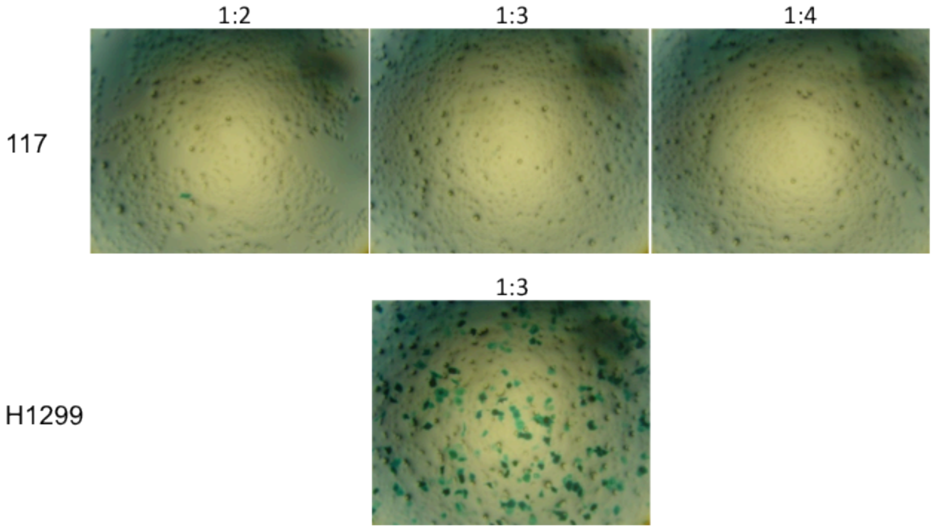

Figure 3.2.1.1: *In situ* β-gal staining on RCC 117 and H1299 cells 24h post-transfection using GeneJuice. 117 cells were refractory to transfection, regardless of the DNA:GeneJuice ratios used whereas H1299 cells were easily transfectable, with transfection efficiency of about 30% in this case.

3.2.2 Optimisation of co-transfection efficiency for live cell imaging motility assay

Investigation of the effect of a protein on cell motility using live cell imaging often involves co-transfection of plasmid of interest with a fluorescent plasmid, based on the assumption that transfected cells that express fluorescent protein also express the protein of interest. Hence it was important to estimate the proportion of plasmid of interest co-transfected with fluorescent plasmid. We also aimed to examine whether the percentage of co-transfection was dependent upon (a) the ratio of the plasmid of interest to fluorescent plasmid used and; (b) the duration for which transfected cells were incubated before imaging. For this purpose, a co-transfection experiment was performed using pEGFP-N1 as a surrogate indicator for the plasmid of interest and pCEP4-mCherry as the fluorescent plasmid for cell tracking. Using GeneJuice transfection reagent, 1.75 μg or 3 μg of pEGFP-N1 were co-transfected with a constant amount of pCEP4-mCherry (0.25 μg) in H1299 cells. Transfected cells were imaged at 24h, 36h and 48h post transfection, as shown in Figure 3.2.2.1A. Transfected cells were split from a mother plate (P1), which was used for 24h and 36h post-transfection imaging, into a new plate (P2) for 36h and 48h post-transfection imaging.

As shown in Figure 3.2.2.1B, of all the transfected cells, more than 70% of cells expressed both EGFP and mCherry (Average = 82.9% +/- (S.E.M.) 2.43). The co-transfection efficiency does not seem to depend upon the amount of EGFP used and the duration of incubation after transfection. Since only cells that are fluorescent with mCherry will be tracked, it is reasonable to only take mCherry transfected cells into account to calculate the percentage of cells co-transfected with EGFP. More than 85% of the cells transfected with mCherry were also transfected with EGFP, with an average co-transfection efficiency of approximately 93.6 +/- 1.39 (S.E.M)%. This suggests that there is more than 9 out of 10 chance that, when selecting a cell amongst cells expressing mCherry, the selected cell will also express the protein of interest. This is useful for the experimental design of our live cell imaging system since it is important to ensure that cells selected for tracking represented cells that have also uptaken the gene of interest.

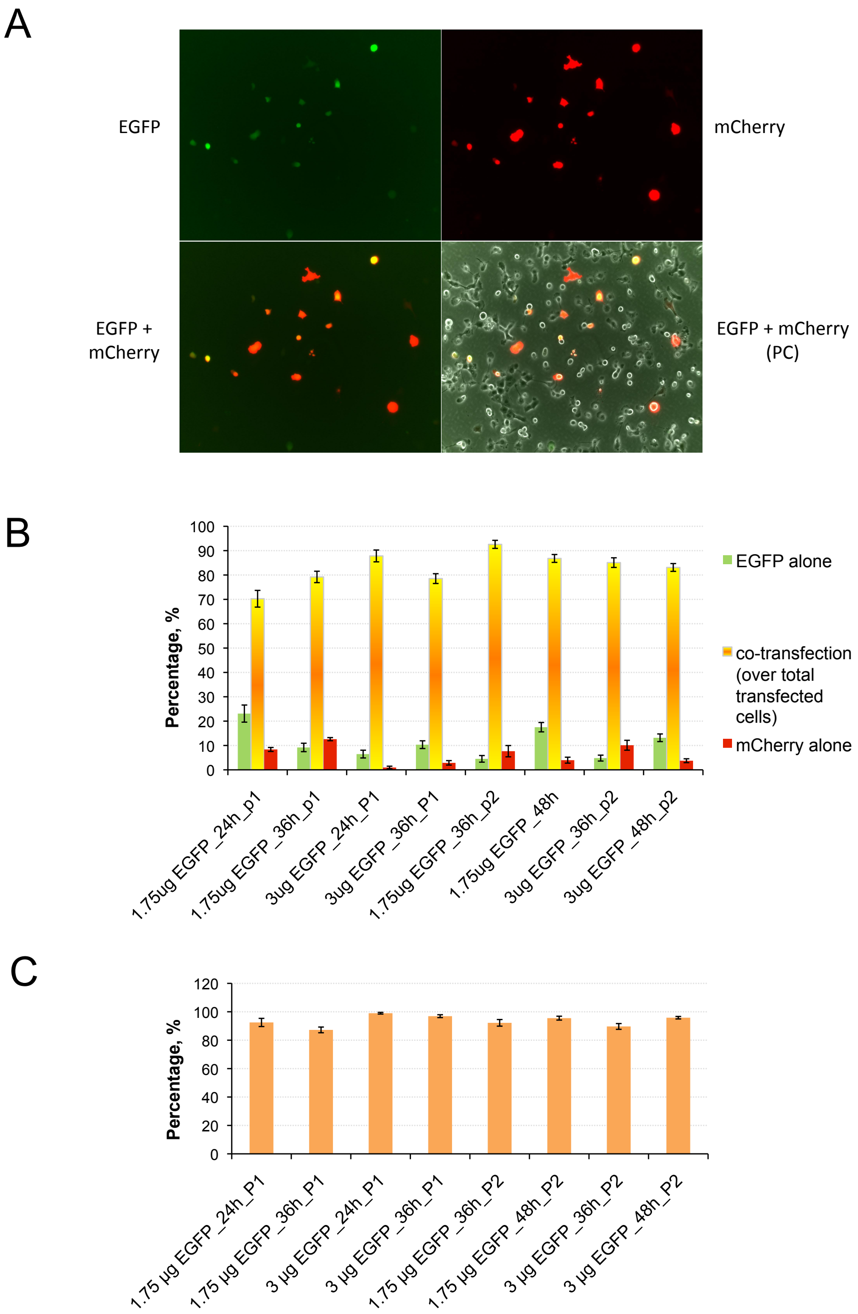

Figure 3.2.2.1: Co-expression of mCherry and EGFP. Using GeneJuice transfection reagent, H1299 cells were transfected with either 1.75 µg or 3 µg of pEGFP-N1 and 0.25 µg pCEP4-mCherry as indicated. Transfected cells were imaged at 24h, 36h and 48h post-transfection. Transfected cells were split from a mother plate (P1), which was used for 24h and 36h post-transfection imaging, into a new plate (P2) for 36h and 48h post-transfection imaging. **A.** Image of the same transfected cells expressing mCherry and EGFP, viewed with individual and

combined fluorescence and/or phase contrast (PC). **B.** Percentage of EGFP only, mCherry only and both EGFP and mCherry transfected cells. **C.** Percentage of EGFP expressing cells over total mCherry expressing cells. P-values were derived from statistical analyses by Student's *t*-test. Error bars indicate standard error.

3.2.3 Live cell imaging of cell motility

3.2.3.1 Analysis of the effects of NME2, NME2 kinase dead mutant NME2H118F, MDM2 and MDM2 RING finger mutant on cell motility

MDM2 has been shown to promote cell motility independently of its E3 ligase activity [384]. MDM2 has also been shown to promote cell motility through antagonising NME2 motility suppressive effect [183]. Both studies utilised Boyden chamber motility assay method to examine cell motility. In the light of these studies, we aimed to examine the effects of MDM2 and NME2 on cell motility using live cell imaging system to see whether live cell imaging system would be a reliable method for such investigation in the future. Accordingly, the effects of NME2, NME2H118F (kinase dead mutant), MDM2 and MDM2 RING-finger mutant (RFM) that lacks E3 ligase activity on motility were examined. In a 6-well plate, H1299 cells were co-transfected with 1.75 μg of plasmids encoding the aforementioned proteins and 0.25 μg of pCEP4-mCherry, which serves as an indicator of transfected cells for cell tracking. Live cell imaging was performed (as described in Materials and Methods Section 2.10) on transfected cells 30h post-transfection for a duration of 20h (Please see Appendix 5 for movies). Two positions were selected from each well for imaging. About 10-20 of each mCherry expressing and non-mCherry expressing cells were tracked for each position selected and then analysed in terms of total distance travelled, average speed, and net distance travelled (Figure 3.2.3.1.1A, B and C). Transfected cells were also harvested for western blot analysis 30h after transfection to confirm proteins expression as shown in Figure 3.2.3.1.1D. Non-mCherry expressing cells (indicated in grey) were also tracked in each well for motility analysis to ensure that any difference detected in mCherry expressing cells was not due to mCherry itself but to the ectopically introduced NME2 or MDM2. However, no obvious difference was observed in terms of total distance, average speed, net distance travelled, and persistence (net distance/ total distance) of cells transfected with NME2 or MDM2, in comparison to their corresponding empty vectors. Persistence can be used as an indicator of the directionality of cell migration, in which persistence is positively correlated with directionality. However, it is difficult to interpret the motility data obtained here, since there appears to be great variability, especially in terms of net distance travelled (Figure 3.2.3.1.1C).

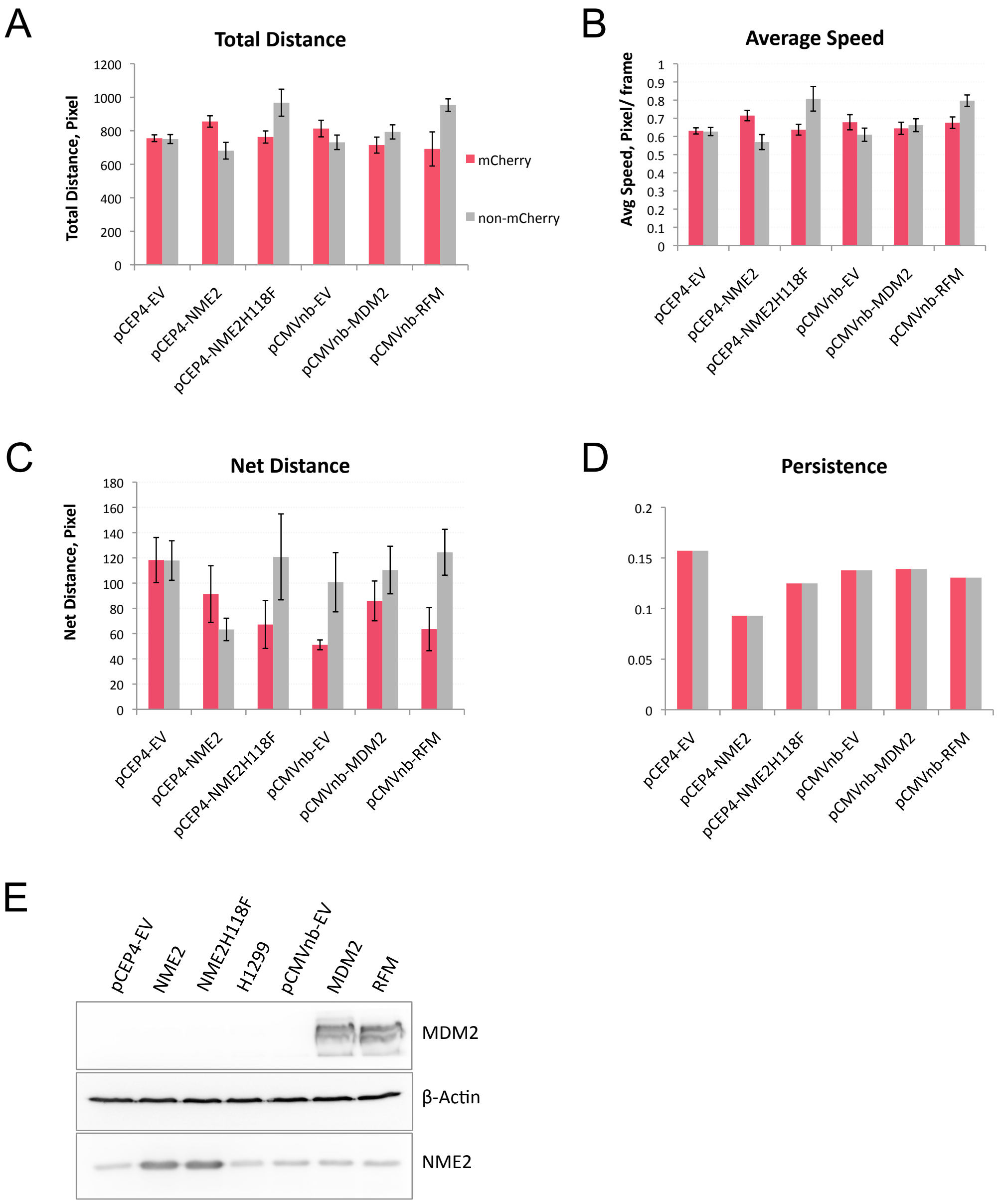

Figure 3.2.3.1.1: Analysis of the effects of NME2, NME2 kinase dead mutant NME2H118F, MDM2 and MDM2 RING finger mutant on cell motility. H1299 cells were co-transfected with 1.75 µg plasmids of interest and 0.25 µg pCEP4-mCherry, which serves as an indicator of transfected cells for cell tracking purpose. Live cell imaging was performed on the transfected cells 30h post-transfection for a duration of 20h. mCherry expressing cells were tracked for motility analysis in terms of **A.** total distance, **B.** average speed, **C.** net distance travelled, and **D.** persistence (net distance/ total distance) for mCherry expressing

cells. Non-mCherry expressing cells (indicated in grey) were also tracked in each well for motility analysis to ensure that any difference detected in mCherry expressing cells were not due to mCherry itself but the ectopically introduced NME2 or MDM2. **E.** Western blot analysis for transfected cells 30h post-transfection. Anti-MDM2 (IF2), anti-β-actin (AC-15) and anti-NME2 (L15) primary antibodies were used. Error bars indicate standard error.

3.2.3.2 Analysis of the effects of MDM2 overexpression on cell motility

Since the motility results generated using live cell imaging system (Section 3.2.3.1) were not consistent with those obtained using the more widely used Boyden chamber motility assay, it was questionable whether the live cell imaging system used in this study was a reasonable method for measuring cell motility. Since high levels of MDM2 have been shown to promote cell motility using Boyden chamber motility assay in a published paper by Polański *et al.* [384], we aimed to use the effect of MDM2 on cell motility as a control to examine whether the co-transfection method described in Section 3.2.2 can be used for examining cell motility using the live cell imaging system.

H1299 cells were transfected, as described in Figure 3.2.3.2.1, with an increasing amount of MDM2 and 0.25 μg of mCherry using GeneJuice to examine whether increased MDM2 levels would result in a positive correlative change in cell motility as measured using live cell imaging. Motility assay was performed using live cell imaging 30h post-transfection for a duration of 12h (Please see Appendix 6 for movies). Cell motility was analysed in terms of total distance travelled, average speed, net distance travelled, and persistence (net distance/ total distance) (Figure 3.2.3.2.1A, B, C and D). Contrary to the cell motility promoting effect of MDM2 observed when Boyden chamber motility assay was used, no difference in cell motility was observed with increasing amount of MDM2, using the co-transfection coupled with live cell imaging system (Figure 3.2.3.2.1). Cells expressing mCherry were also tracked in their phase contrast mode (indicated in green), as concerns were raised as to whether mCherry saturation could affect cell tracking and therefore motility. However, when mCherry expressing cells were tracked using phase contrast mode, the levels of different cell motility parameters examined here were comparable to those seen in the presence of mCherry fluorescence, indicating that mCherry saturation does not affect cell motility. Overall, we failed to confirm the effect of MDM2 on cell motility using live cell imaging system.

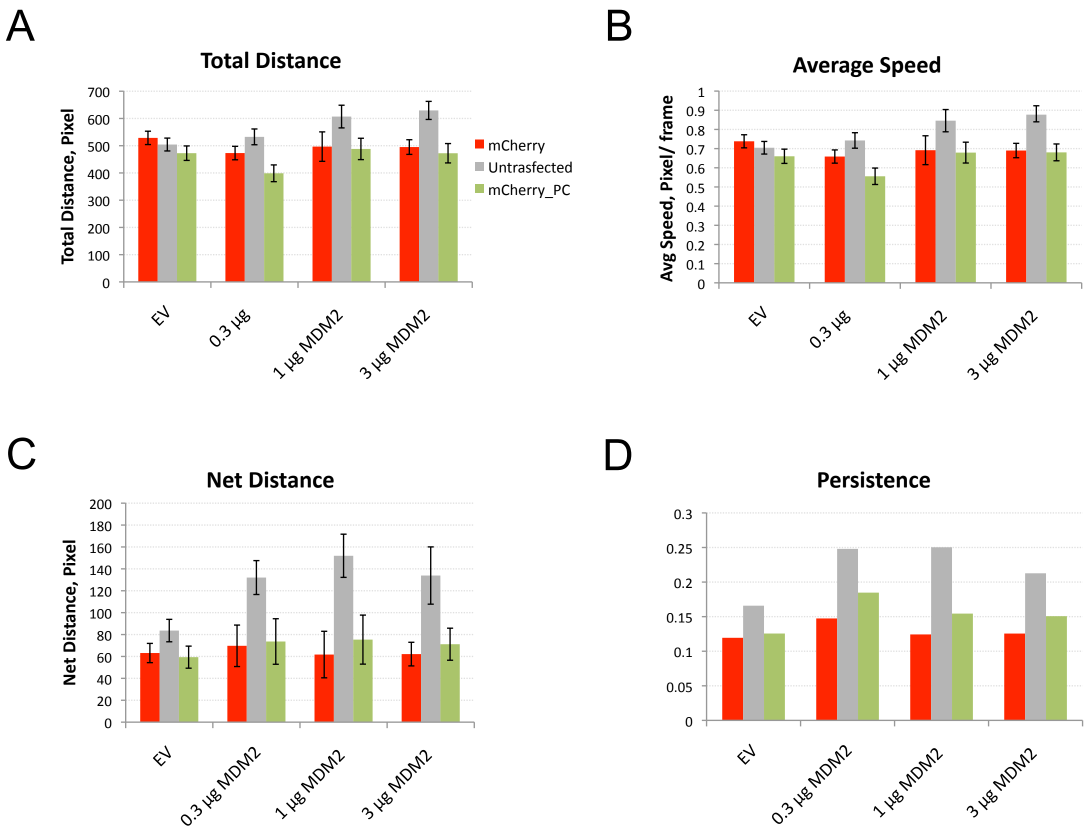

Figure 3.2.3.2.1: Analysis of the effects of increasing level of MDM2 on cell motility using live cell imaging. Motility assay was performed using live cell imaging on transfected H1299 cells with an increasing amount of MDM2 and 0.25 µg of pCEP4-mCherry using GeneJuice 30h post-transfection for 12h. Non-mCherry expressing cells (indicated in grey) were also tracked in each well for motility analysis to ensure that any difference detected in mCherry expressing cells were not due to mCherry itself but the ectopically introduced MDM2. Two positions were selected from each well for imaging. About 10-20 of each mCherry expressing and non-mCherry expressing cells were tracked for each position selected and then analysed in terms of total **A.** distance travelled, **B.** average speed, **C**. net distance travelled, and **D.** persistence (net distance/ total distance).

In an independent experiment, the effect of high levels of MDM2 on cell motility was examined using Boyden chamber motility assay as described in Materials and Methods (Section 2.11). Essentially, H1299 cells were transfected in triplicates with MDM2, RFM or an EV control followed by Boyden chamber motility assay and western blot analysis 30h after transfection. As shown in Figure 3.2.3.2.2, cells expressing high levels of MDM2 demonstrate increase in cell motility and this effect was independent of MDM2 RING-finger. This result is consistent with the published data in Polański *et al.* (2010) which showed that MDM2 promotes cell motility and invasiveness in a RING-finger independent manner [384]. This result also suggests that Boyden chamber is a more reliable method compared to live cell imaging for assessing cell motility in our study.

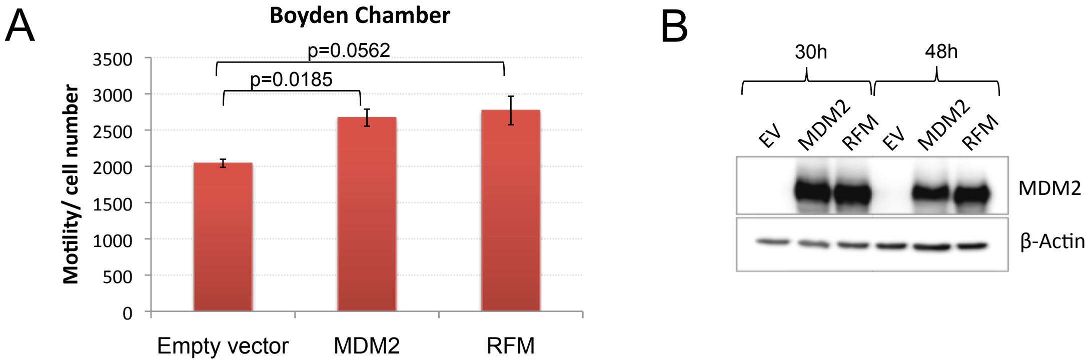

Figure 3.2.3.2.2: Analysis of the effects of increasing level of MDM2 on cell motility using Boyden chamber. A. H1299 cells were transfected in triplicates with MDM2, RFM or an empty vector (EV) control followed by Boyden chamber motility assay 30h after transfection. P-values were derived from statistical analyses by Student's *t*-test (n=3). Error bars indicate standard error. **B.** Western blot showing the levels of MDM2 and RFM protein expression after transfection. Actin was used as a loading control. Anti-MDM2 (IF2) and anti-β-actin (AC-15) primary antibodies were used.

3.2.4 Analysis of the effects of a stable NME2 knockdown on cell motility and NDPK activity

Since we were unable to establish a reliable live cell imaging system to assay cell motility, a more widely used Boyden chamber motility assay was used instead to examine the effects of NME2 on cell motility. Stable knockdown clones expressing short hairpin (sh)RNA NME2 in H1299 and Clone 9 (H1299 over-expressing MDM2) cell lines (generated by Dr Maria Maguire, a past member of our laboratory) were used for this purpose. Clones generated using H1299 as parental cell line were named with a preceding 'H' whereas clones generated using Clone 9 with '9'. Together with Scrambled (Scr) clones as negative controls, the NME2 knockdown clones were examined for NME2 expression by Western blot using a primary antibody specific for NME2 (L15) (Figure 3.2.4.1A). Western blot analysis shows substantial down-regulation of NME2 in the knockdown clones, as well as high expression of MDM2 in Clone 9 and its derivatives, as expected. These clones were further characterised by examining the levels of NDPK activity. NDPK activity assay was performed as described in Materials and Methods (Section 2.15) for each cell lines using 250,000 cells per sample (n=3). As expected, all the NME2 knockdown clones show considerably lower NDPK activity levels compared to NDPK activity observed for their respective parental cell line and Scrambled controls (Figure 3.2.4.1B). Interestingly, NDPK activity for Clone 9 is lower compared to NDPK activity observed for H1299 cells.

Boyden chamber motility assay was performed using each cell line with n≥4. In the absence of NME2, both HNME2:Cl.2 and Cl.7 cells are significantly more motile compared to H1299 and Scrambled controls (Figure 3.2.4.1C), consistent with the role of NME2 as a tumour suppressor. On the other hand, all of the Clone 9 cell lines demonstrate significantly higher motility than that of their parental H1299. This is expected since overexpression of MDM2 has been shown to promote cell motility [103, 384]. However, knockdown of NME2 in Clone 9 cells did not further promote cell motility, with motility levels comparable to Clone 9. One possible explanation for this could be that there is no real difference in motility in these cell lines. Alternatively, it is possible that, upon MDM2 transfection, the cells reach as high mobility as possible and are not capable of being more motile even when NME2 was down-regulated.

In order to ensure that the cell motility results obtained above were not affected by the rate of cell proliferation, which might be caused by the absence of NME2 and overexpression of MDM2, MTT cell proliferation assay (Section 2.25) was performed for NME2 knockdown clones. Growth curves in Figure 3.2.4.1 show that all cell lines used in the motility assay have comparable proliferation profiles. Cell proliferation rates were particularly similar from Day 0 to Day 2, i.e. the time frame during which Boyden chamber motility assay took place, suggesting that cell proliferation rate is unlikely a determinant for the increase in motility observed in NME2 knockdown clones. In summary, knockdown of NME2 promotes increased cell motility and abrogates most of the endogenous NDPK activity in cells, supporting the role of NME2 as a metastasis suppressor and that this function may be NDPK activity-dependent.

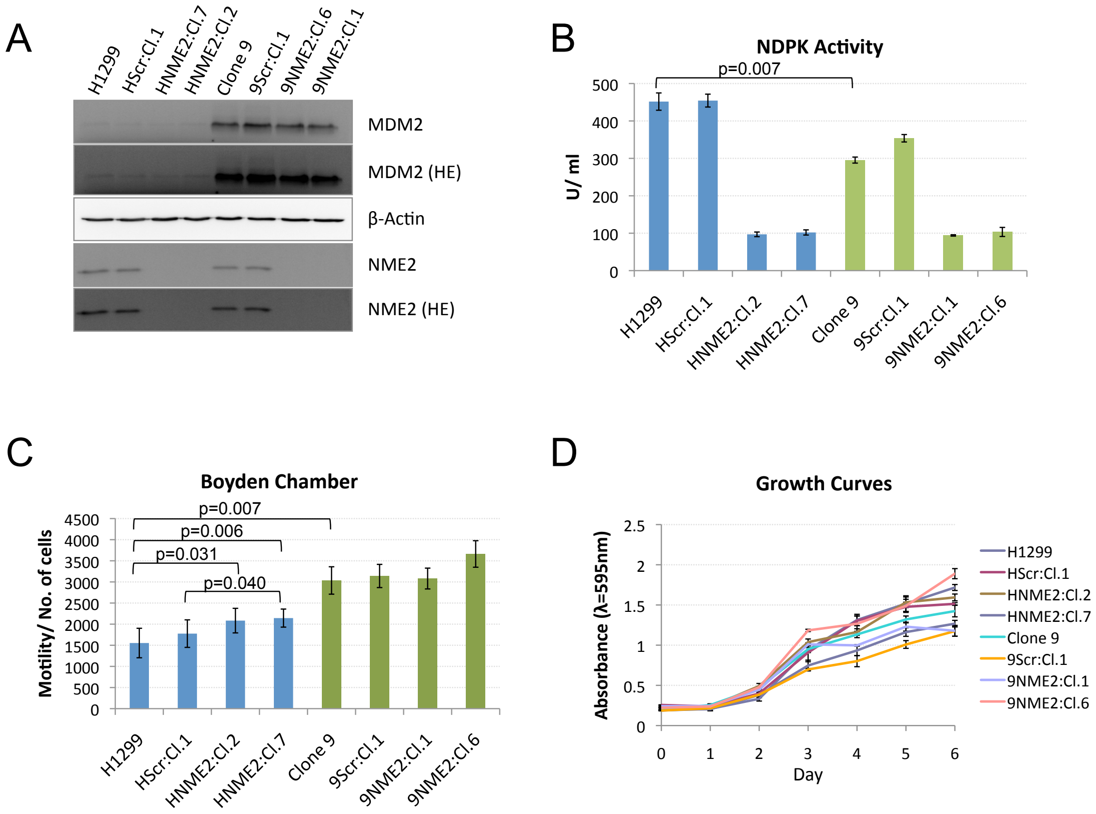

Figure 3.2.4.1: Analysis of the effects of a stable NME2 knockdown on cell motility and NDPK activity. A. Western blot analysis for stable knockdown clones expressing shRNA NME2 showing decent knockdown of NME2. Anti-MDM2 (IF2), anti-β-actin (AC-15) and anti-NME2 (L15) primary antibodies were used. HE, high exposure. **B.** NDPK activity assay for the NME2 knockdown clones. 250,000 cells per sample were used for each NDPK activity assay (n=3). Blue, H1299 parental cell line; Green, Clone 9 (H1299 overexpressing MDM2) as parental cell line. **C.** Boyden chamber assay for the clones (n≥4). **D.** Growth curves, examined using MTT assay, showing similar proliferation profile for the clones. In other words, the increase in motility seen in the knockdown clones is unlikely due to a difference in proliferation rate. P-values were derived from statistical analyses by Student's *t*-test. Error bars indicate standard error.

3.2.5 Analysis of the NDPK activity in MDM2 overexpressing cells

Since results presented in Section 3.2.4 indicated that NDPK activity is lower in cells expressing high levels of MDM2 (Clone 9) and also that the effect of NME2 on cell motility is NDPK activity-dependent, we hypothesised that overexpression of MDM2 might lower cellular NDPK activity to promote cell motility. Therefore, the effect of MDM2 levels on NDPK activity was investigated. Accordingly, additional clones (MDM2 Cl.1 and Cl.3) that express high levels of MDM2 were included in the study to ensure that the result seen in Clone 9 has not occured by chance. Furthermore, RFM Cl.9, Cl.8 and Cl.6 were included as well, to examine whether the effect of MDM2 on NDPK activity is RING-finger-dependent. Empty vector (EV) clones were used as control. All of these clones used for this assay are derivatives of H1299. As shown in Figure 3.2.5.1, NDPK activity of Clone 9 appears lower than that of H1299, which is consistent with result represented in Figure 3.2.4.1B, even though the decrease was not statistically significant in this experiment ($p=0.1228$). However, since the levels of NDPK activity in all other MDM2 and RFM clones are on a par with H1299 and EV clones, the result seen in Clone 9 may be due to clonal selection. Therefore, the results presented here fail to demonstrate that high levels of MDM2 reduce NDPK activity in cells.

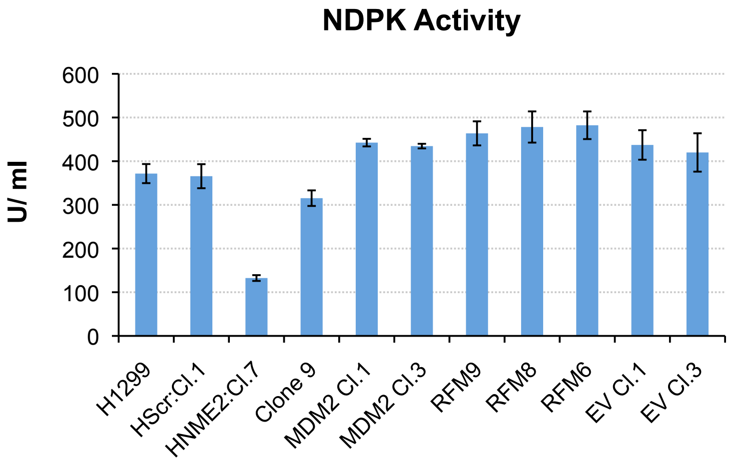

Figure 3.2.5.1: Analysis of the effects of high levels of MDM2 on NDPK activity. NDPK assay was performed for clones that express high levels of MDM2 (MDM2 Cl.1, Cl.3 and Cl.9) and RFM Cl.9, Cl.8 and Cl.6. Empty vector (EV) clones were used as control. HNME2:Cl.7 was also included as negative control. All of these clones were derivatives of H1299. Error bars indicate standard error.

3.2.6 Analysis of the effects of NME2H118F, MDM2 and RFM on NME2 protein levels and NDPK activity

NME2 is a relatively small protein (152 aa) with active sites responsible for NDPK activity spanning almost the entire protein, and this leads us to hypothesise that NME2 might exert its motility suppressive effect through NDPK activity. In addition, a preliminary study performed by a past member of our laboratory (Dr Radoslaw Polański) has demonstrated that NME2H118F kinase mutant does not inhibit cell motility, suggesting that the effect of NME2 on motiltiy is NDPK activity-dependent. Since high levels of MDM2 have been shown to promote cell motility independently of its RING-finger [384], we aimed to examine the effect of MDM2 on cellular NDPK activity. H1299 cells were transfected with 1 μg of each pCEP4-NME2, pCEP4-NME2H118F, pCMVNeoBam-MDM2 and pCMVNeoBam-MDM2C464A (RFM) using GeneJuice. Transfected cells were harvested 24h post-transfection for NDPK activity assay and Western blotting. Western blot analysis presented in Figure 3.2.6.1A shows higher expression of MDM2 in RFM transfected cells compared to wild-type MDM2 transfected cells, as expected, since RFM is unable to target MDM2 for degradation, resulting in accumulation of MDM2 in the cells. Furthermore MDM2 does not appear to have any effect on NME protein levels. As shown in Figure 3.2.6.1B, NDPK activity of NME2 transfected cells was significantly higher compared to that of EV transfected cells, indicating that the NME2 plasmid used was functionally active. However, NDPK activity of NME2H118F kinase mutant is on par with EV control, suggesting that it is unlikely that kinase mutant promotes cell motility through the loss of kinase activity. It is also possible that the change in activity could not be detected in this assay since NME2 proteins were abundantly expressed in the cells.

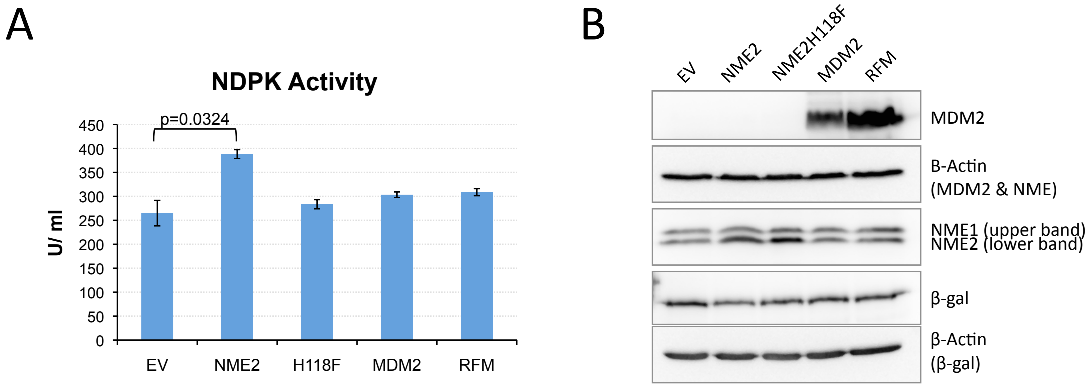

Figure 3.2.6.1: Investigation of the effects of NME2H118F, MDM2 and RFM on NME2 protein levels and NDPK activity. H1299 cells were transfected with 1 µg of pEV, pCEP4-NME2, pCEP4-NME2H118F, pCMVNeoBam-MDM2 and pCMVNeoBam-MDM2C464A (RFM) using GeneJuice. 0.2 µg of β-gal was used as a transfection efficiency control. Transfected cells were harvested 24 hours post transfection for NDPK assay (n=3) and western blot analysis. P-values correspond to statistical analyses by Student's *t*-test (n=3). Error bars indicate standard error. **A.** NDPK actity **B.** Western blotting using anti-MDM2 (IF2), anti-β-actin (AC-15), anti-NME1/2 (ab31019) and anti-β-gal (OB02) primary antibodies.

3.2.7 Analysis of the *in trans* effect of NME2H118F on cellular NDPK activity

Since NME2 can form homo- or hetero-hexamers comprised of individual active subenzymes, we wanted to investigate whether the NME2 kinase dead mutant has any *in trans* effect on the NDPK activity of the wt NME2. For example, the kinase mutant may exert an allosteric, possibly dominant negative effect and suppress wt NME2 NDPK activity by oligomerisation with wt NME2. To address this question, H1299 cells were transfected with 0.5 μg of pCEP4-NME2, pCEP4-NME2H118F or both using GeneJuice, followed by NDPK activity assay 24h, 48h and 72h after transfection (n=3). EV was used as a control. As expected, NME2H118F does not induce any NDPK activity due to the lack of a crucial phospho-acceptor histidine 118 residue required for NDPK activity (Figure 3.2.7.1). On the contrary, NDPK activity levels of NME2 transfected cells increase dramatically over time, proportionally to its protein expression levels. When co-expressed with wild-type NME2, the kinase mutant does not seem to affect NDPK activity induced by wild-type NME2 (p=0.1222, p=0.0865 and p=0.2429 for 24h, 48h and 72h post-transfection, respectively). This indicates that kinase dead mutant NME2H118F has no effect *in trans* on cellular NDPK activity.

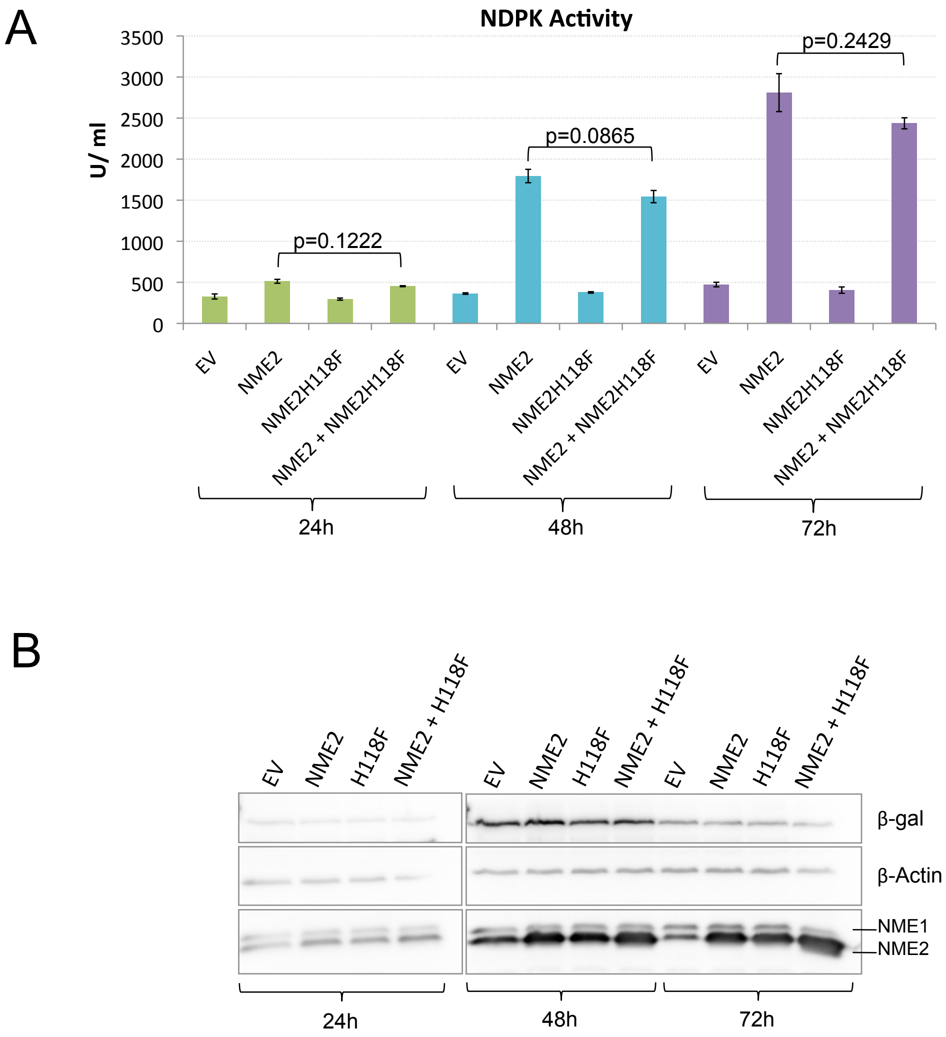

Figure 3.2.7.1: Analysis of the *in trans* effect of NME2H118F on cellular NDPK activity. A. NDPK activity assay for H1299 cells transfected with indicated plasmids followed by NDPK activity assay 24h, 48h and 72h after transfection (n=3). EV and NME2H118F were used as negative controls. As expected kinase dead mutant NME2H118F does not induce any NDPK activity due to the lack of a crucial phospho-acceptor histidine 118 residue for NDPK activity. When co-expressed with wild-type NME2, the kinase mutant does not seem to affect NDPK activity induced by the wild-type. 0.2 μg of β-gal was used as a transfection efficiency control. P-values correspond to statistical analyses by Student's *t*-test (n=3). Error bar indicates standard error. **B.** Western blot analysis of samples from panel A, with actin as a loading control. Primary antibodies used were anti-β-actin (AC-15), anti-NME1/2 (ab31019) and anti-β-gal (OB02).

3.2.8 Analysis of the effect of denaturing- or detergent-based lysis method on NDPK activity

The majority of the cellular NDPK activity is contributed by NME in oligomeric forms [290, 293]. The NDPK assay used in our study measures the overall NDPK activity in cells and is not able to determine the relative contributions of different NME forms In other words, the assay does not distinguish whether monomer or oligomer contributes more to the overall activity. In previous experiments presented in this thesis, RIPA buffer, both detergent-based and denaturing, was used for cell lysis when preparing samples for NDPK assay. There is a concern that this lysis method may disrupt the interactions between NME2 subunits and thus the NDPK activity measured might not be a true representation of the actual NDPK activity in the cells.

To address this question, H1299 cells were lysed using different lysis buffers varying in denaturing strength to compare their effects on observed cellular NDPK activity. Hypotonic extraction assay method is designed to minimise disruption of protein-protein interaction to preserve the protein oligomeric structure. It is both non-denaturing and non-detergent-based. SLIP lysis buffer is detergent-based but non-denaturing.

As shown in Figure 3.2.8.1, no difference in NDPK activity was observed between using a denaturing (RIPA) or non-denaturing (SLIP) lysis buffers. Although the laborious hypotonic lysis method gives a statistically higher NDPK activity in comparison to that of the detergent-based lysis methods, the difference is not dramatic enough to give us concern about our previous interpretation of NDPK activity in the cells. For result consistency and assay simplicity, RIPA buffer was used for cell lysis in all NDPK assays presented in this thesis.

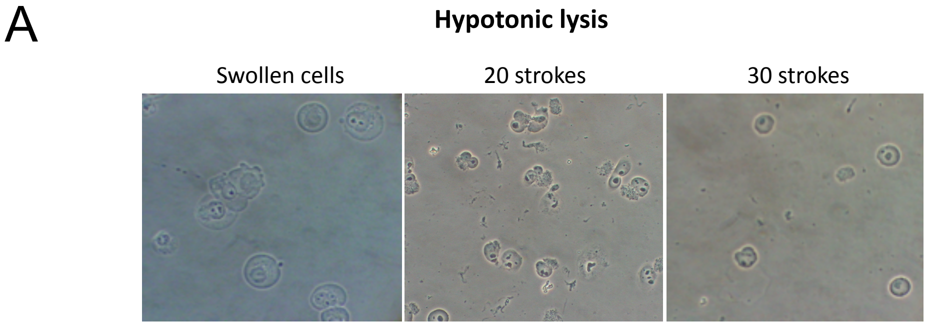

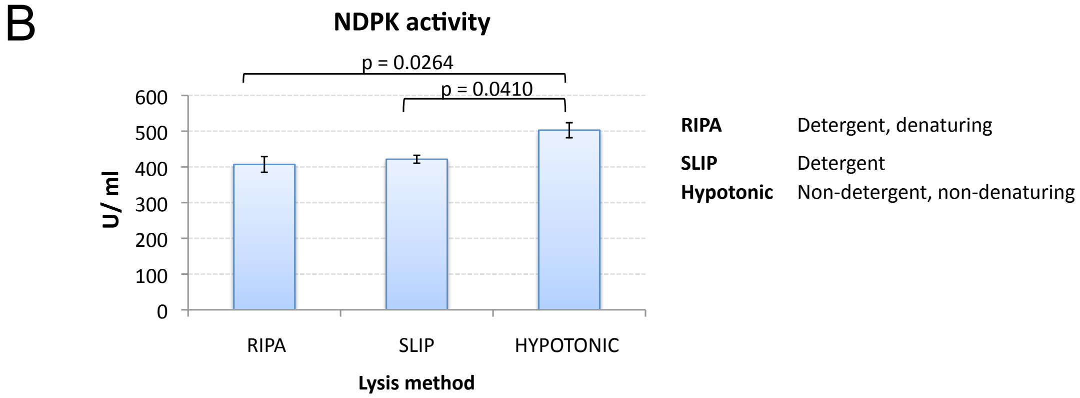

Figure 3.2.8.1: Analysis of the effect of denaturing- or detergent-based lysis method on NDPK activity. A. Hypotonic lysis of H1299 cells. Cells were incubated in a hypotonic buffer until swollen. After 20 strokes of homogenisation the cells were burst, leaving intact nuclei with various amounts of cytoplasmic material attached. After 30 strokes, a more homogenised solution was obtained, leaving cleaner nuclei. **B.** No difference in NDPK activity was observed between using a denaturing (RIPA) or non-denaturing (SLIP) lysis buffers. The NDPK activity resulted from hypotonic method is slightly but statistically higher that of the denaturing lysis methods. P-values correspond to statistical analyses by Student's *t*-test (n=3). Error bar indicates standard error.

3.2.9 Analysis of the effect of MDM2 overexpression on cellular NDPK activity level

It has been demonstrated that up-regulation of MDM2 in RCC opposes the motility suppressive effect of NME2 [183]. However, it is unclear whether this was an NDPK activity-dependent phenomenon. Therefore, we wanted to examine the effect of MDM2 overexpression on cellular NDPK activity level. In order to determine the time point post-transfection when MDM2 is expressed at the highest level, different time-points were studied. In addition, considering that different transfection reagents may vary in their transfection efficiency, both GeneJuice and Lipofectamine 2000 were used and compared. Accordingly, H1299 cells were transfected with 1.5 μg MDM2 using GeneJuice or Lipofectamine 2000 followed by NDPK activity assay 30h and 48h after transfection (n=3). As demonstrated in Figure 3.2.9.1B, when cells were transfected with GeneJuice, the highest expression of MDM2 was detected at 48h post-transfection, whilst with the Lipofectamine, the expressions seems to decrease at 48h. However, no difference in NDPK activity level was observed when MDM2 was overexpressed, regardless of the transfection reagents used Figure 3.2.9.1A.

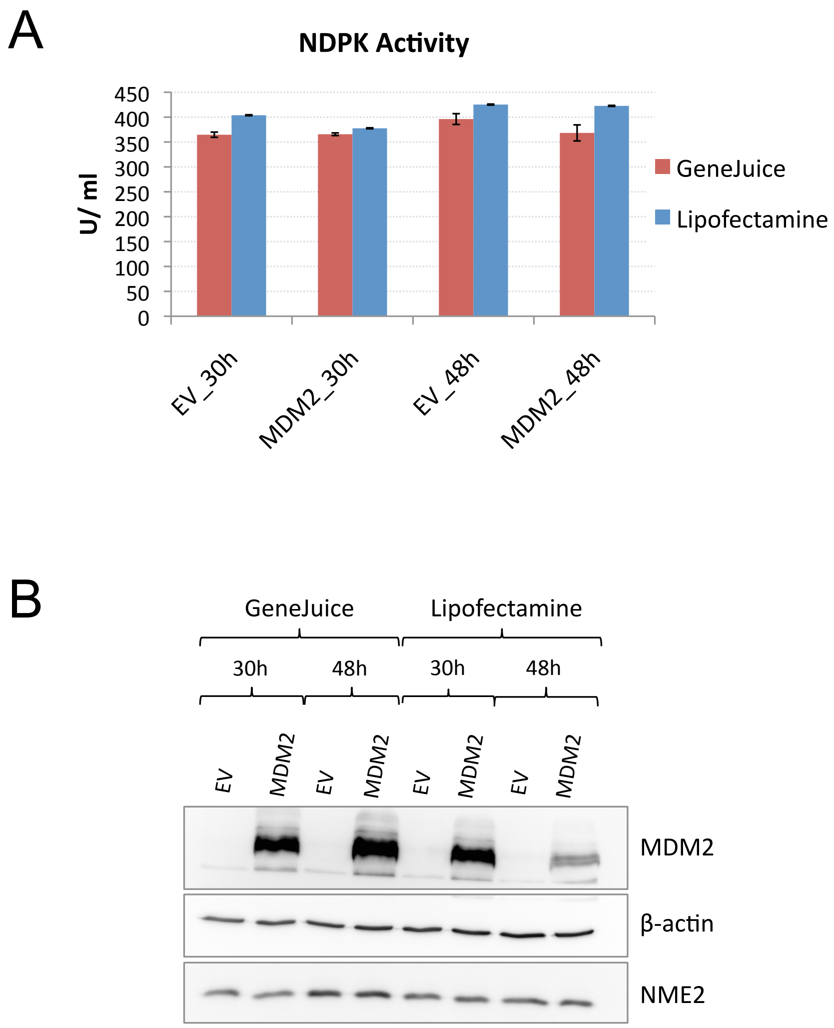

Figure 3.2.9.1: Analysis of the effect of MDM2 overexpression on cellular NDPK activity level. **A.** NDPK activity assay for H1299 cells transfected with 1.5 μg MDM2 using GeneJuice or Lipofectamine 2000 as transfection reagents. NDPK activity assay was performed 30h and 48h after transfection (n=3). EV was used as a control. P-values correspond to statistical analyses by Student's *t*-test (n=3). Error bar indicates standard error. **B.** Western blot analysis of samples from panel A. Primary antibodies used were anti-MDM2 (IF2), anti-β-actin (AC-15) and anti-NME1/2 (ab31019).

3.2.10 Examining whether MDM2 opposes the motility suppressive effect of NME2 through inhibition of NDPK activity

Considering that NMEs are very small proteins, it is hard to believe that NMEs have any other biochemical activity other than their defining NDPK activity. In order to investigate whether NME2 suppressive effect on motility is ascribed to its NDPK activity and whether MDM2 oppose NME2 motility suppressive effect through suppression of the NDPK activity, NME2 was transfected with or without MDM2 into NME2 knockdown clones from both H1299 and Clone 9 parental lines, followed by NDPK assay. Two previous experiments (performed in 9NME2:Cl.6 and HNME2:Cl.2) show that NDPK activity was significantly reduced in the presence of MDM2, suggesting a role of MDM2 in modulating NME2 kinase activity. However, these experiments were performed as part of pilot studies without clear evidence from Western blots that the expression of NME2 protein in all conditions was equal. In other words, the reduction in NDPK activity may not simply be explained by the presence of MDM2 since fluctuation in NME2 protein levels is a major determinant of NDPK activity. In light of these results, the experiment was repeated in wild-type H1299, Clone 9, and the NME2 KD clones from the two parental lines (HNME2:Cl.2, HNME2:Cl.7, 9NME2:Cl.1 and 9NME2:Cl.6). NME2 knockdown clones were used because as NME2 is abundantly expressed in cells, it may be easier to detect changes in NDPK activity in a system that has minimal NME2 expression.

The main goal was to examine whether MDM2 opposes the suppressive effect of NME2 on motility through suppressing NDPK activity. 1 μg of pCEP4-NME2 was co-transfected with either 1.5 μg pCMVNeoBam-MDM2 or 0.75 μg pCMVNeoBam-MDM2C464A (RFM) into the afore-mentioned cell lines. EV and NME2H118F were included as controls. The reason for using RFM is to examine whether RF, crucial for E3 ubiquitin ligase activity, is required for MDM2 effects on NDPK activity, if there are any. Please note that the amount of RFM plasmid used was half of the wt MDM2 plasmid to compensate for increased stability of RFM protein because of the absence of auto-ubiquitination. Transfected cells were harvested 24h post-transfection for NDPK assay and western blot analysis.

In H1299 cells (Figure 3.2.10.1A), the NDPK activity level of NME2 was lower in the presence of wt MDM2 compared to that of NME2 alone (p=0.0182). On the other hand, an increase in NDPK activity was observed in the presence of RFM (p=0.0274), which suggests that MDM2 may suppress NDPK activity in an E3 ligase-dependent manner. The results in Clone 9 mimic that of H1299 (Figure 3.2.10.1D), although no significant difference in NDPK activity was observed in the presence of MDM2 (p=0.2156) and RFM (p=0.0635). As shown in Figure 3.2.10.1, the levels of NDPK activity were dramatically reduced when NME2 is downregulated in NME2 stable knockdown clones. In comparison to their parental cell lines, only about 20-30% of NDPK activity remains in the knockdown clones suggesting that the majority of cellular NDPK activity is atributed to NME2 either in the forms of monomer, homo-oligomer or hetero-oligomer with other isoforms. Unfortunately, we were unable to analyse the results obtained from the knockdown clones since it was rather difficult to detect the expression of transfected NME2, as shown in the western blots. This is not surprising considering the cells already contain short hairpin RNA (shRNA) for NME2. Nevertheless, we have observed some potential inhibitory effect of MDM2 on NDPK activity in 9NME2Cl.1 and Cl.6 (p=0.04988 and p=0.0367, respectively).

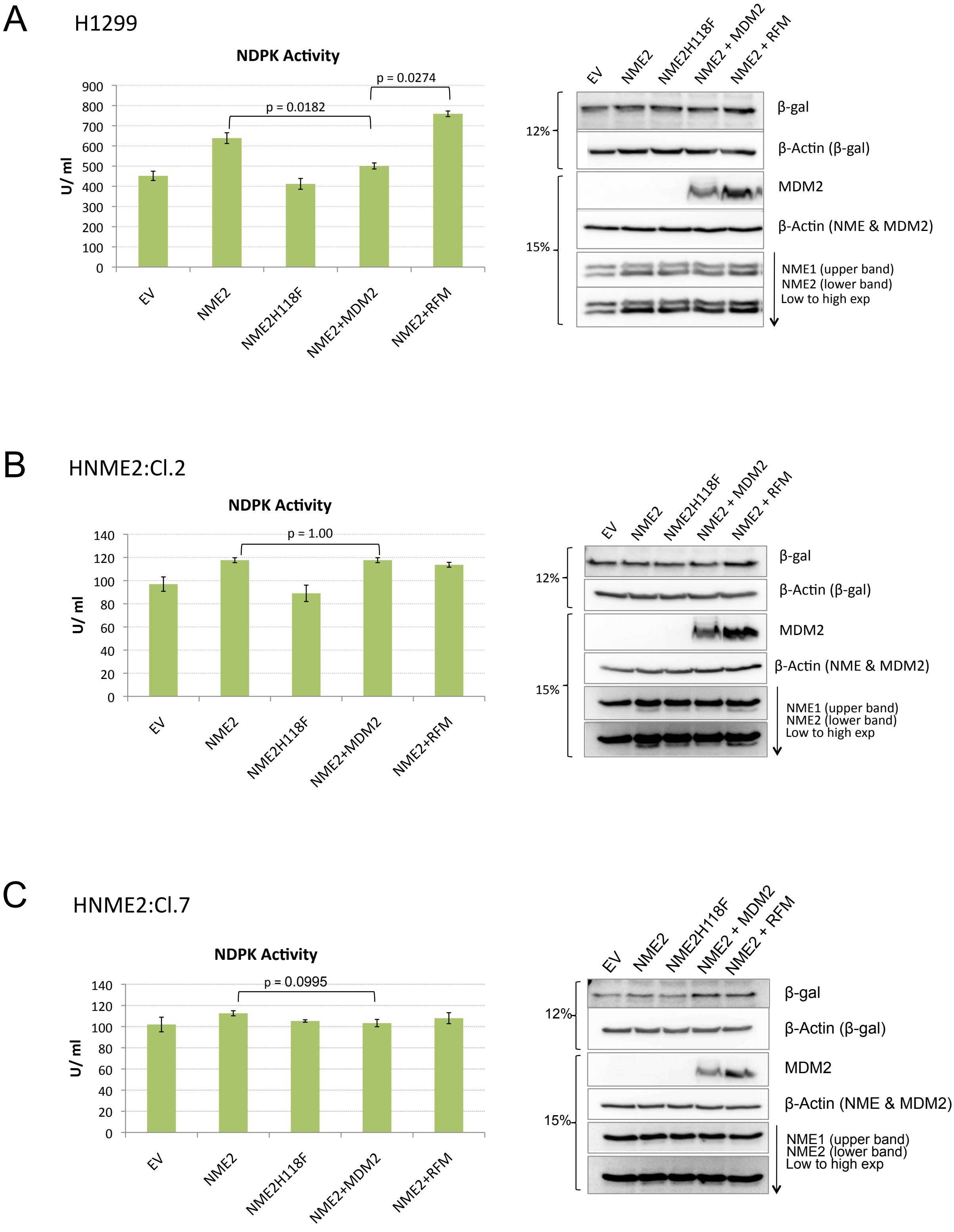

Figure 3.2.10.1 (To be continued)

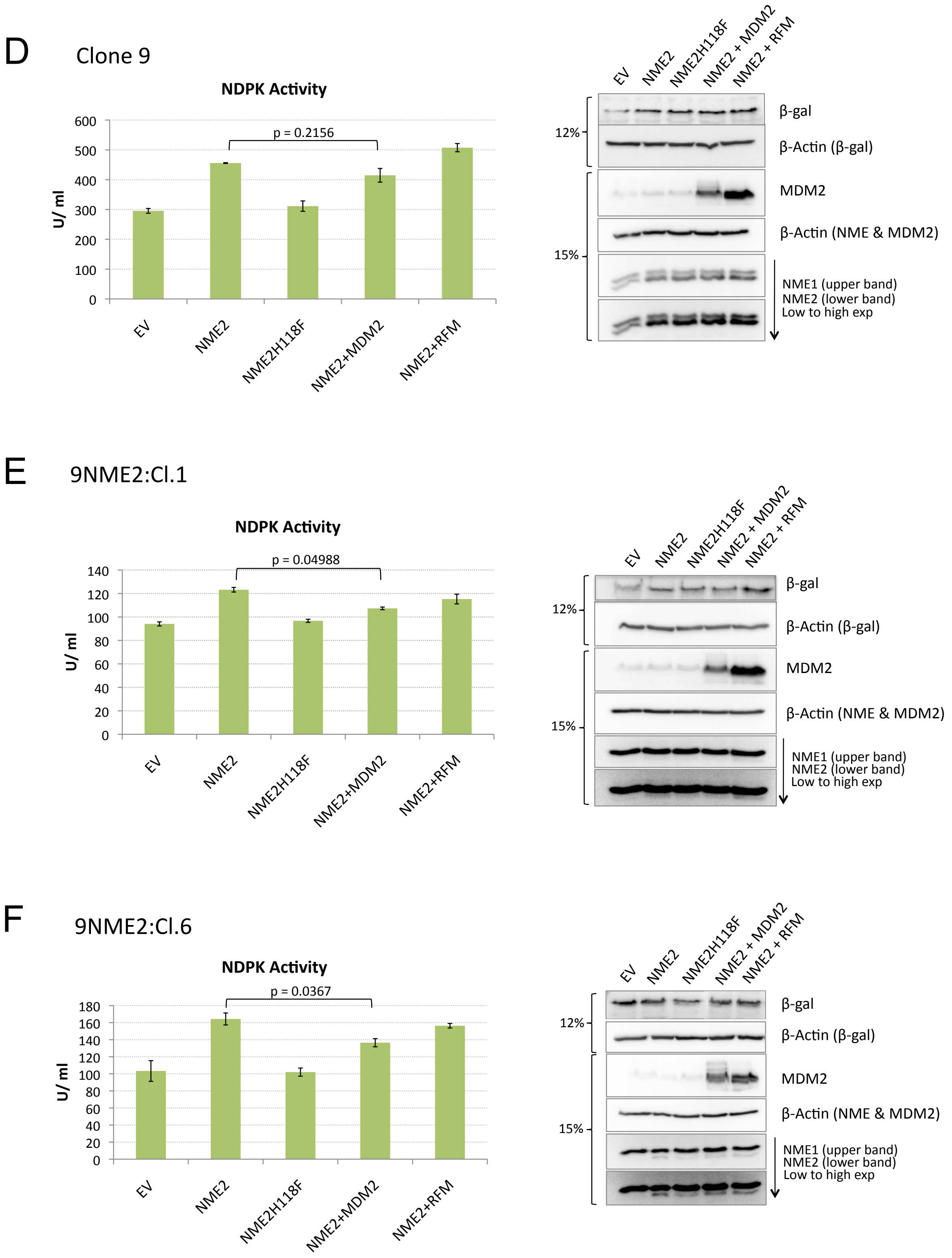

Figure 3.2.10.1 (To be continued)

Figure 3.2.10.1: Examining whether MDM2 opposes the motility suppressive effect of NME2 through inhibition of NDPK activity. 1 μg of pCEP4-NME2 was co-transfected with either 1.5 μg pCMVNeoBam-MDM2 or 0.75 μg pCMVNeoBam-MDM2C464A (RFM) into NME2 knockdown clones from both H1299 and Clone 9 parental lines using GeneJuice. EV and NME2H118F were included as negative controls. 0.2 μg of β-gal was used as a transfection efficiency control. Transfected cells were harvested 24h post-transfection for NDPK assay (n=3) and Western blot analysis. P-values correspond to statistical analyses by Student's *t*-test (n=3). Error bars indicate standard error. For Western blotting, samples were separated on 12% and 15% gels and actin was used as a loading control. Primary antibodies used were anti-MDM2 (IF2), anti-β-actin (AC-15), anti-NME1/2 (ab31019) and anti-β-gal (OB02). Results are shown in **A.** H1299 **B.** HNME2:Cl.2 **C.** HNME2:Cl.7 **D.** Clone 9 **E.** 9NME2:Cl.1 **F.** HNME2:Cl.6. Downward arrow indicates low to high exposures.

3.2.11 Optimisation of the NDPK activity assay

3.2.11.1 Optimisation 1: Time-points

Previous results presented in this thesis (Figure 3.2.7.1A) have demonstrated that the levels of transiently transfected NME2 expression and NDPK activity increase over time, up to 72h post-transfection. As the MDM2 protein levels seem to peak at 30-48h post-transfection with pCMVNeoBam-MDM2 (Figure 3.2.9.1), it is therefore interesting to see whether the effect of MDM2 on NDPK activity may also gradually increase over time. The hypothesis was that with higher NDPK activity more effect of MDM2 could be detected.

H1299 were transfected with 1 μg of NME2 and either 1.5 μg of MDM2 or 0.75 μg of RFM using GeneJuice, followed by NDPK assay (n=3) and western blotting 24, 48 and 72h post-transfection. *In situ* β-gal staining was performed 24h after transfection for determination of transfection efficiency. As expected, the NDPK activity (Figure 3.2.11.1.1A) and NME2 protein expression (Figure 3.2.11.1.1B) levels in wt NME2 transfected cells increase with incubation time. Down-regulation of NME2 by MDM2 was also observed at 48h and the effect seems to be RING finger-dependent. No suppressive effect on NDPK activity was observed at 24h when cells were co-transfected with wild-type MDM2 (Figure 3.2.11.1A). However, MDM2 seems to have a subtle suppressive effect on NDPK activity at 48h and this effect gradually increases over time. A similar trend was observed in the presence of RFM. Nevertheless the inhibitory effects observed were not statistically significant.

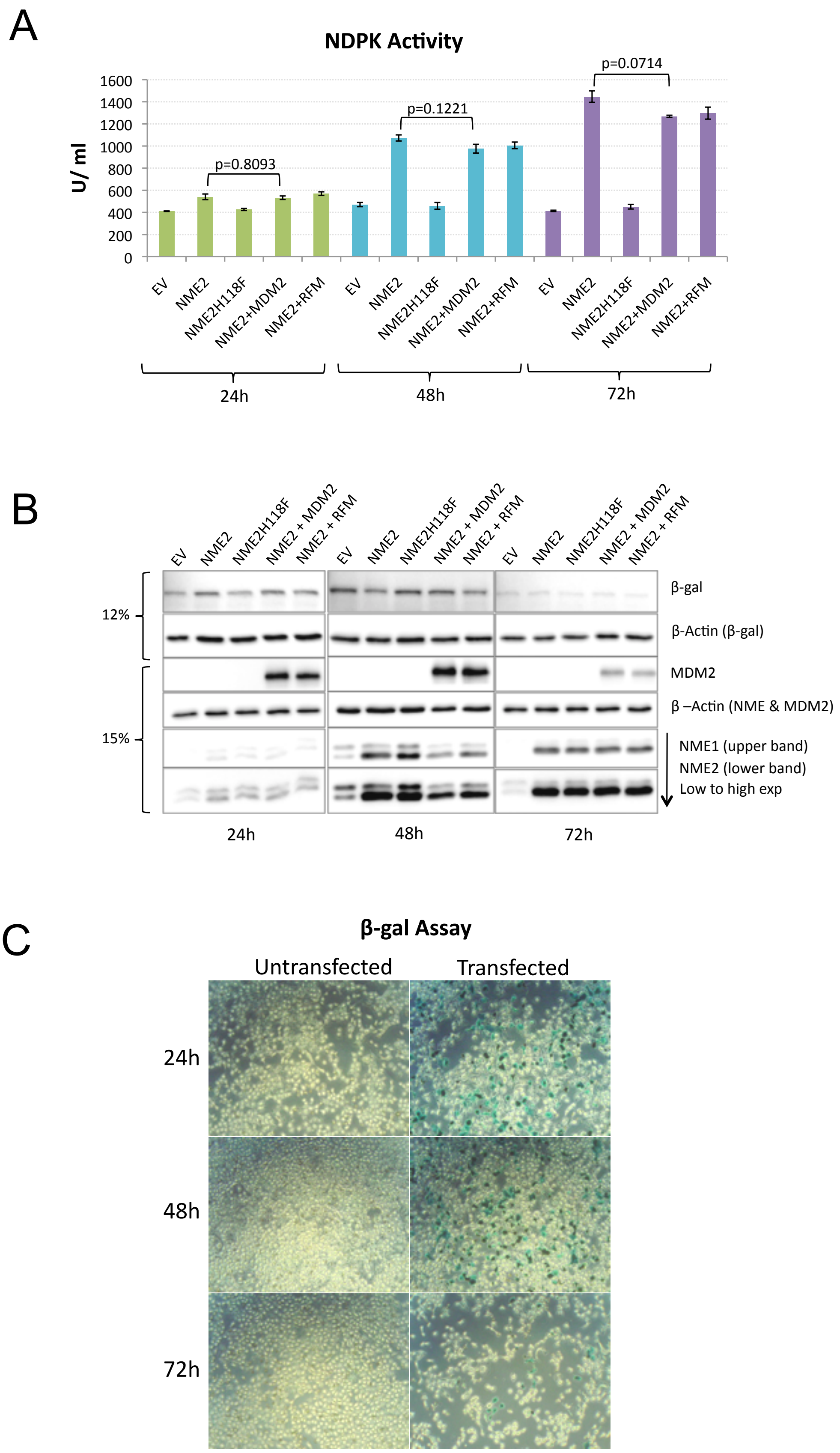

Figure 3.2.11.1.1 (To be continued)

Figure 3.2.11.1.1: Optimisation of NDPK activity assay: Time-points. A. NDPK activity assay for H1299 cells transfected with 1 μg of NME2 and either 1.5 μg of MDM2 or 0.75 μg of RFM 24h, 48h and 72h after transfection. EV and NME2H118F were included as controls. 0.2 μg of β-gal was used as a transfection efficiency control. When co-expressed with wild-type MDM2, no difference in NDPK activity was observed at 24h but there seem to be a suppressive effect on NDPK activity that gradually increases over time from 48h onwards. A similar trend was observed in the presence of RFM. P-values correspond to statistical analyses by Student's *t*-test (n=3). Error bars indicate standard error. **B.** Western blot analysis of samples from panel A separated on 12% and 15% gels, with actin as a loading control. Primary antibodies used were anti-β-actin (AC-15), anti-MDM2 (IF2), anti-NME1/2 (ab31019) and anti-β-gal (OB02). Downward arrow indicates low to high exposures. **C.** *In situ* β-gal staining (24h post-transfection) for determination of overall transfection efficiency.

3.2.11.2 Optimisation 2: NME2 to MDM2 ratios

So far, results presented in this thesis indicate that the suppressive effect of MDM2 on NDPK activity is not a consistent phenomenon. It was thought that the amount of MDM2 used for the assay was not sufficient for inducing a significant suppressive effect. In previous experiments performed in this thesis, NME2:MDM2 plasmid ratio (in µg) used for transfection was 1:1.5. Here, we aimed to use up to 1:6 of NME2 to MDM2 ratio for optimisation. NDPK activity assay was performed for H1299 cells transfected with 0.5 µg of NME2 and either 3 µg of MDM2 or 1.5 µg of RFM 24h, 48h and 72h after transfection, as described in Figure 3.2.11.2.1. As shown in Figure 3.2.11.2.1A, the suppressive effects of MDM2 on NDPK activity increase from 24h to 72h post-transfection. In particular, at 48h and 72h, the effect is statistically significant compared to NME2 alone, with ($p=0.0446$) and ($p=0.0280$), respectively. MDM2 expression level was observed to peak at 48h but diminished considerably at 72h (Figure 3.2.11.2.1B). This suggests that the effect of MDM2 may accumulate over time after transfection. Interestingly western blots also show that there is a hint of NME2 down-regulation in the presence of MDM2, particularly at 72h time point. Similar results were obtained (Figure 3.2.11.2.2) when the experiment was repeated using 1:3 ratio of NME2 to MDM2 for 48h and 72h (since these are the time points at which reaction effect seem to occur more noticeably).

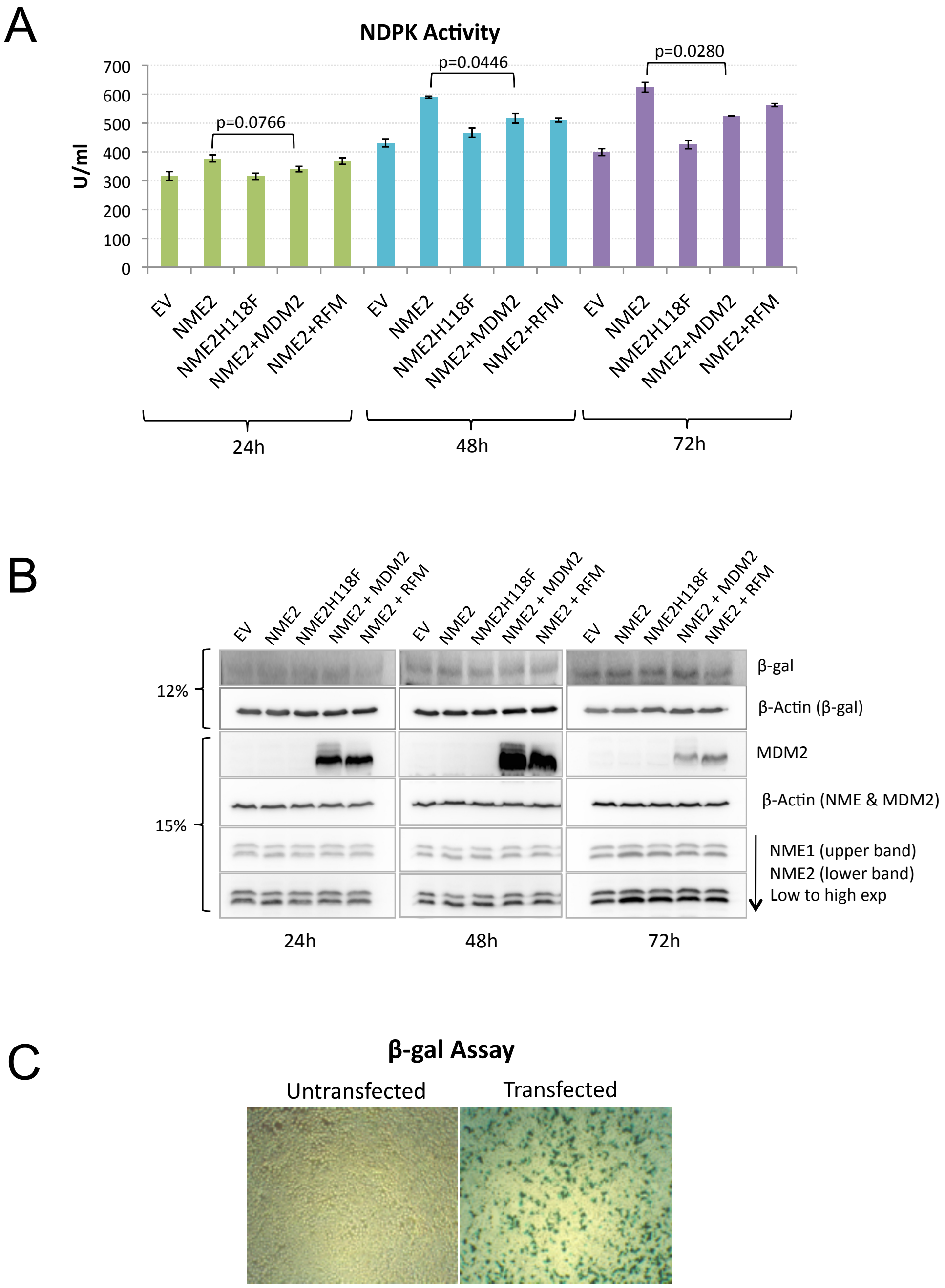

Figure 3.2.11.2.1: Optimisation: NME2 to MDM2 ratios. Experiment was performed as described in Section 3.2.11.1 but using 1:6 of NME2 to MDM2 plasmids for transfection. **A.** NDPK activity assay for H1299 cells transfected with 0.5 μg of NME2 and either 3 μg of MDM2 or 1.5 μg of RFM 24h, 48h and 72h after transfection. EV and NME2H118F were included as controls. 0.2 μg of β-gal was used as a transfection efficiency control. P-values correspond to statistical

analyses by Student's *t*-test (n=3). Error bars indicate standard error. **B.** Western blot analysis of samples from panel A separated on 12% and 15% gels, with actin as a loading control. Primary antibodies used were anti-β-actin (AC-15), anti-MDM2 (IF2), anti-NME1/2 (ab31019) and anti-β-gal (OB02). Downward arrow indicates low to high exposures. **C.** *In situ* β-gal staining (24h post-transfection) for determination of overall transfection efficiency. Magnification: x5.

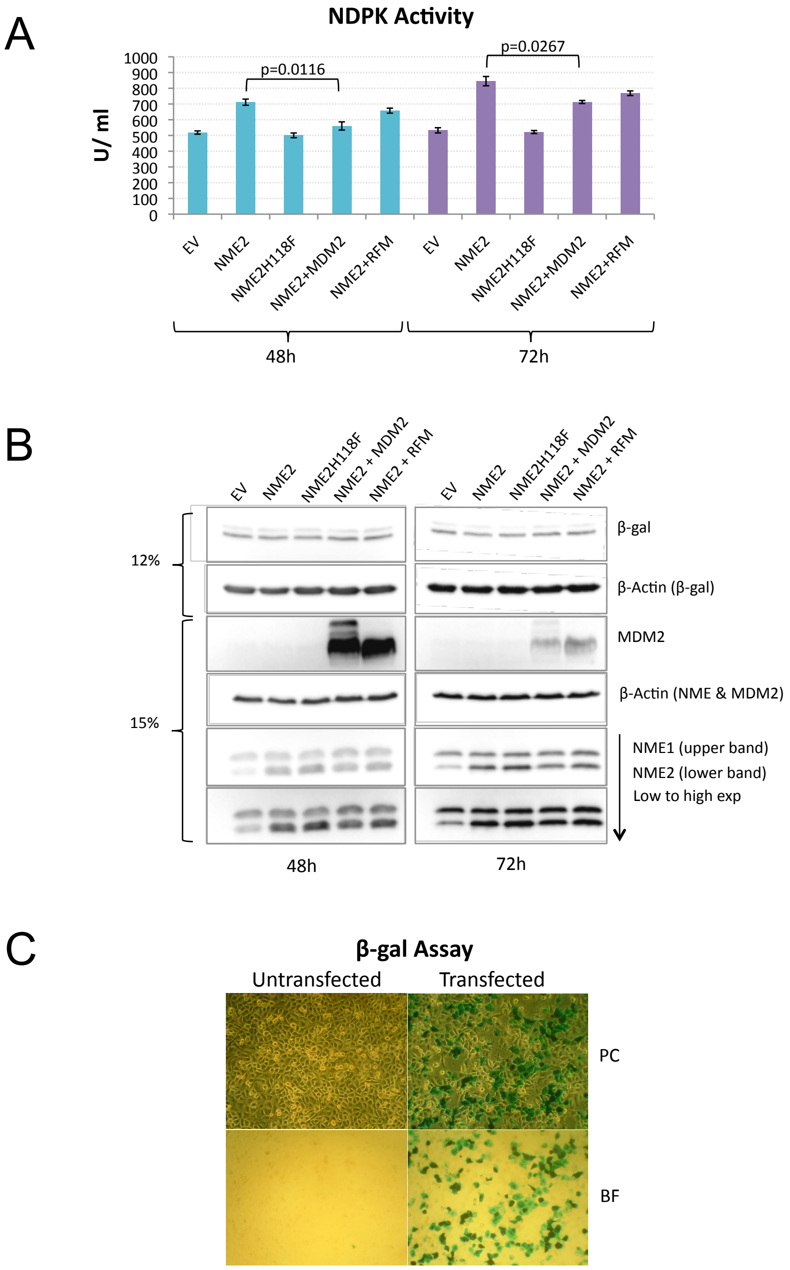

Figure 3.2.11.2.2: Optimisation: NME2 to MDM2 ratios. Experiment was performed exactly as described in Section 3.2.11.1 except using 1:3 of NME2 to MDM2 plasmids for transfection. **A.** NDPK activity assay for H1299 cells transfected with 1 μg of NME2 and either 3 μg of MDM2 or 1.5 μg of RFM 24h, 48h and 72h after transfection. EV and NME2H118F were included as controls. 0.2 μg of β-gal was used as a transfection efficiency control. P-values correspond to statistical analyses by Student's *t*-test (n=3). Error bar indicates standard error.

B. Western blot analysis of samples from panel A separated on 12% and 15% gels, with actin as a loading control. Primary antibodies used were anti-β-actin (AC-15), anti-MDM2 (IF2) anti-NME1/2 (ab31019) and anti-β-gal (OB02). Downward arrow indicates low to high exposures. **C.** *In situ* β-gal staining (24h post-transfection) for determination of overall transfection efficiency. PC, phase contrast; BF, bright field. Magnification: x10.

3.2.11.3 Optimisation 3: Transfection efficiency.

Transfection experiments for examining the effect of MDM2 on NDPK activity were thus far performed using GeneJuice, with transfection efficiency typically being between 15-40%. The low transfection efficiency could mean that only a small proportion of the cells assayed for NDPK activity were actually transfected with our plasmids of interest. In other words, the effect of MDM2 on NDPK activity could be underestimated due to low transfection efficiency. As a result, we wanted to examine whether higher transfection efficiency that can be obtained using Lipofectamine 2000 as a transfection reagent would have any effect on results obtained. In the first instance, we examined whether transfection incubation time before medium changing has any effect on cellular cytotoxicity and transfection efficiency when Lipofectamine 2000 is used. Accordingly, H1299 cells were transfected with 1 μg of pβ-gal. Medium containing transfection reagent was replaced at 2h, 4h and 6h post-transfection. β-gal assay was performed 24h post-transfection to determine the transfection efficiency. As shown in Figure 3.2.11.3.1, transfection efficiency increases with longer incubation time before medium changing. More than 90% of cells were expressing β-gal with medium changing after 6h of transfection. Although the transfection (6h) was also accompanied with a slightly higher number of cell deaths (result not shown), it was decided that medium would be changed 6h after transfection, in the interest of higher transfection efficiency.

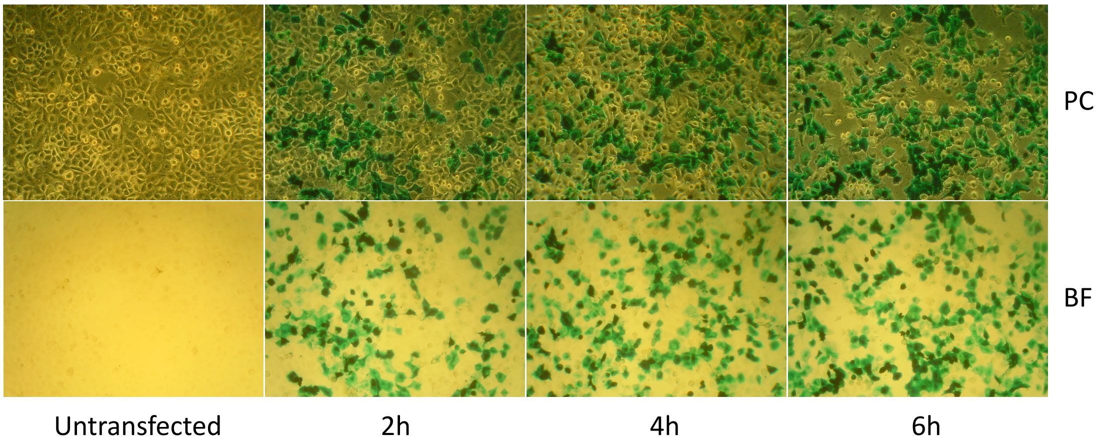

Figure 3.2.11.3.1: Optimisation: Transfection efficiency. H1299 cells were transfected with 1 μg of pβ-gal. Medium containing transfection reagent was replaced at 2h, 4h and 6h post-transfection. *In situ* β-gal assay was performed 24h post-transfection to determine the transfection efficiency. PC, phase contrast; BF, bright field. Magnification: x10.

3.2.12 MDM2 down-regulates NME2 in a dose-dependent manner

Following a series of optimisation experiments, the effect of MDM2 on NME2 level and NDPK activity was further investigated using the optimised conditions. It was assumed that if MDM2 has a suppressive effect on NDPK level and/or activity, the effect would, to some extent, be relative to the amount of MDM2 used. For this purpose, experiment was repeated as described in Section 3.2.11.1, except that H1299 were co-transfected with an increasing amount of MDM2 and a constant amount of NME2 (0.25 μg) using Lipofectamine 2000. Transfection medium was changed 6h post-transfection and cells were harvested 48h after transfection for NDPK assay (n=3).

As shown in Figure 3.2.12.1A**,** MDM2 seems to have negligible suppressive effect on NDPK activity even when the transfection efficiency was high (about 90%). There is a marginal but statistically significant difference in the NDPK activity when cells were transfected with 1.5 μg of MDM2 (p=0.0356). However, Western blot and densitometry analyses (Figure 3.2.12.1B&C) suggest that MDM2 down-regulates NME2 in a dose-dependent manner, since NME2 protein levels decrease in the presence of increasing amount of MDM2. This effect does not seem to be a consequence of uneven transfection efficiency. Interestingly, when co-expressed with the same amount of RFM (1.5 μg), some degree of NME2 down-regulation was observed, but the extent was much lower than that incurred by wild-type MDM2.

In a reverse manner, when MDM2 was down-regulated using siRNA (MDM2 oligo 1) followed by NDPK activity assay 48h post-transfection (n=3), a marginal but statistically significant increase in NDPK activity was observed (p=0.0203) (Figure 3.2.12.2A). Western blot also demonstrates an increase in NME2 level upon down-regulation of MDM2 (Figure 3.2.12.2B). These results suggest that MDM2 has an ability to down-regulate NME2 protein level and, perhaps by doing so, inhibit the NDPK activity of NME2.

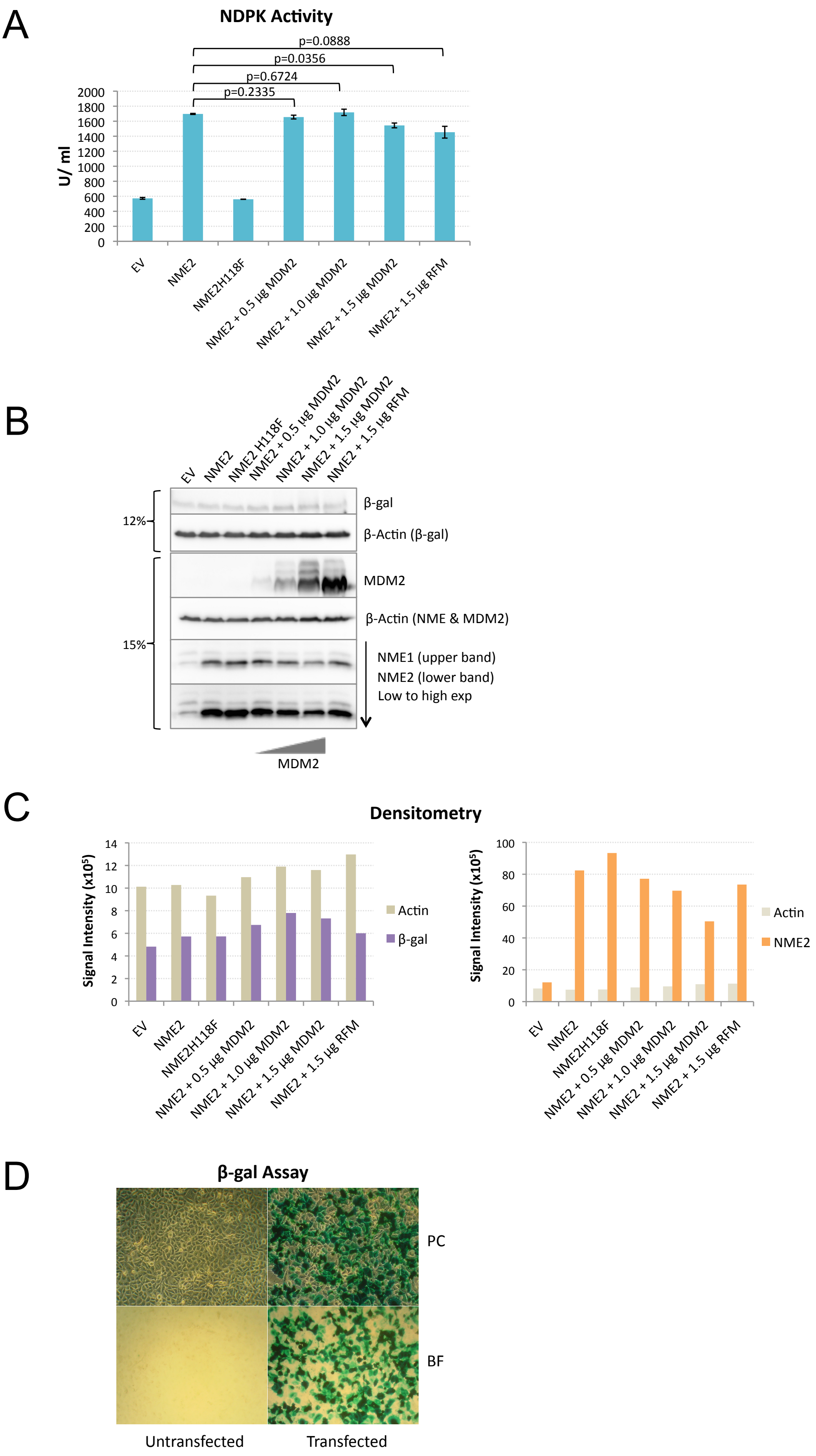

Figure 3.2.12.1 (To be continued)

Figure 3.2.12.1: MDM2 down-regulates NME2 in a dose-dependent manner. To examine the effect of MDM2 on NME2 level and NDPK, H1299 were co-transfected with 0.25 μg of NME2 and an increasing amount of MDM2 or 1.5 μg RFM using Lipofectamine 2000. EV and NME2H118F were included as controls. 0.2 μg of β-gal was used as a transfection efficiency control. Transfection media was changed 6h post-transfection. **A.** NDPK activity assay for transfected cells 48h post-transfection (n=3). P-values correspond to statistical analyses by Student's *t*-test. Error bar indicates standard error. **B.** Western blot analysis of samples from panel A separated on 12% and 15% gels, with actin as a loading control. Primary antibodies used were anti-β-actin (AC-15), anti-MDM2 (IF2), anti-NME1/2 (ab31019) and anti-β-gal (OB02). Downward arrow indicates low to high exposures. **C.** Densitometry analysis was performed on Western blot in panel B to estimate the signal intensities of β-gal and NME2 relative to their corresponding actin controls. **D.** *In situ* β-gal staining (24h post-transfection) for determination of overall transfection efficiency. PC, phase contrast; BF, bright field. Magnification: x10.

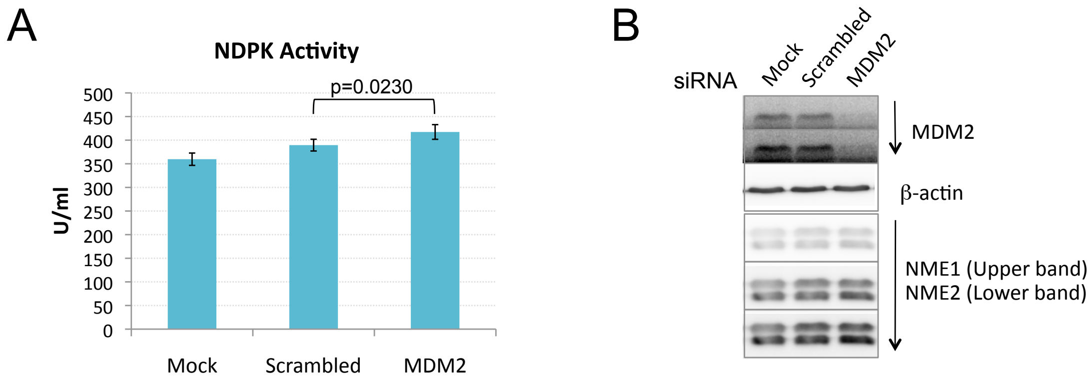

Figure 3.2.12.2: Down-regulation of MDM2 leads to an increase in NDPK activity supporting the potential role of MDM2 in suppressing NDPK activity. A. Down-regulation of MDM2 in H1299 cells using siRNA (MDM2 oligo 1, used at 80 pmol per well of a 6-well plate) followed by NDPK activity assay 48h post-transfection (n=3). Mock (transfection reagent only) and Scrambled siRNA were used as negative controls. P-values correspond to statistical analyses by Student's *t*-test. Error bar indicates standard error. **B.** Western blot analysis of samples from panel A showing decent down-regulation of MDM2 expression and a rise in NME2 level upon MDM2 down-regulation. Downward arrows indicating low to high exposures. Primary antibodies used were anti-β-actin (AC-15), anti-MDM2 (IF2) and anti-NME1/2 (ab31019).

3.2.13 Analysis of the effect of MDM2 on NME2 level and NDPK activity in siRNA NME1 knockdown cells

Both NME1 and NME2 are abundantly expressed in cells and can contribute to cellular NDPK activity through homo- and/or hetero-oligomerisation. Furthermore, since our assay does not discriminate between NDPK activity contributed by NME1 or NME2, it was questioned whether the effect of MDM2 measured was the effect on NDPK activity contributed by NME2 alone. To examine this, NME1 was down-regulated using transiently transfected siRNA NME1 oligo 9 (80 pmol for each well of a 6-well plate) in H1299 cells. Mock (only transfection reagent) and Scrambled siRNA were used as negative controls. 24h later, the NME1 down-regulated cells were transfected with 0.25 μg of pCEP4-NME2 and 1.5 μg of MDM2 or 1.5 μg of RFM using Lipofectamine 2000. The transfected cells were harvested 48h after the second transfection (72h post siNME1 KD) for NDPK activity assay (n=3). Western blot in Figure 3.2.13.1A and β-gal assay in Figure 3.2.13.1C show that NME1 knockdown followed by subsequent transient transfections have worked quite well. In the event of bypassing NDPK activity from endogenous NME1, both wt MDM2 and RFM seem to down-regulate NME2 protein expression, an observation supported by densitometry analysis (Figure 3.2.13.1B). However, unlike previous observation in Figure 3.2.11.2.1, no significant difference in NDPK activity was observed in the presence of either wt MDM2 or RFM. This suggests that even though MDM2 does not seem to inhibit NME2 NDPK activity in the absence of NME1, MDM2 still has an effect on NME2 protein levels.

It is worth mentioning that when NME1 is down-regulated, not much difference was observed in NDPK activity (mean activity for EV = ~380 U/ml), which is on par with the activity of EV transfected H1299 (mean activity = 350-500 U/ml). This is consistent with our previous NDPK activity results in which there was a massive reduction in NDPK activity in NME2 KD clones (Figure 3.2.11.1B and C). This suggests that the endogenous NME1 contributes relatively little to the cellular NDPK activity measured in our assay and that the majority of the NDPK activity comes from NME2 or at least that NME2 is required for the hexamerisation with NME1 that contributes to the overall NDPK activity.

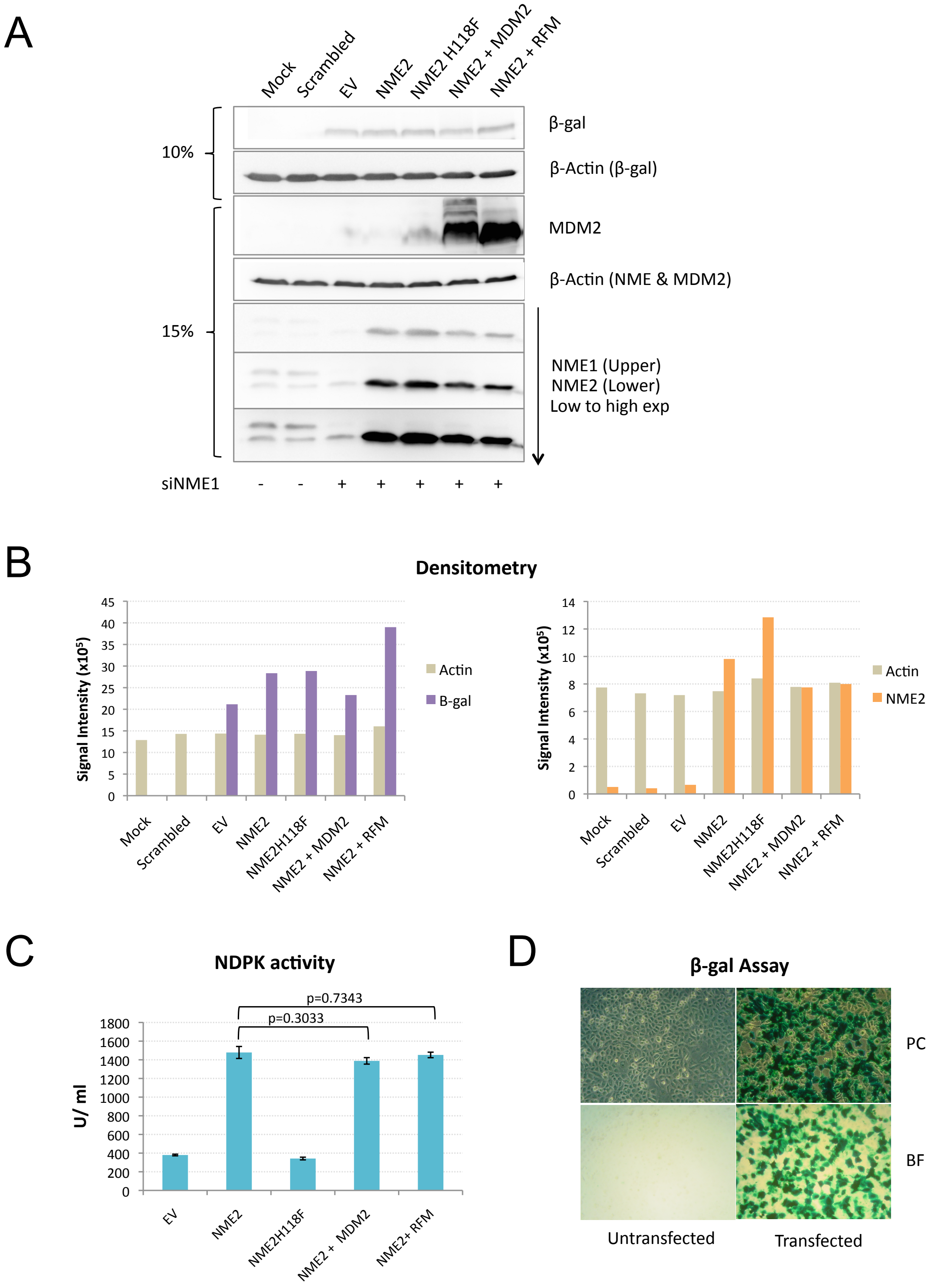

Figure 3.2.13.1: Analysis of the effect of MDM2 on NME2 level and NDPK activity in siRNA NME1 knockdown cells. A. NME1 was first down-regulated using siRNA NME1 oligo 9 (80 pmol for each well of a 6-well plate) in H1299 cells. Mock (only transfection reagent) and Scrambled siRNA were used as

negative controls. 24h later, the NME1 down-regulated cells were transfected with 0.25 μg of pCEP4-NME2 and 1.5 μg of MDM2 or 1.5 μg of RFM using Lipofectamine 2000. 0.2 μg of β-gal was used as a transfection efficiency control. Transfected cells were harvested 48h after the second transfection (72h post siNME1 KD) for NDPK activity assay (n=3). **A.** Western blot analysis of samples separated on 12% and 15% gels, with actin as a loading control. Primary antibodies used were anti-β-actin (AC-15), anti-MDM2 (IF2), anti-NME1/2 (ab31019) and anti-β-gal (OB02). Downward arrow indicates low to high exposures. **B.** Densitometry analysis was performed on western blot in panel A to estimate the signal intensities of β-gal and NME2 relative to their corresponding actin controls. **C.** NDPK activity assay. P-values correspond to statistical analyses by Student's *t*-test. Error bar indicates standard error. **D.** *In situ* β-gal staining (24h post-transfection) for determination of overall transfection efficiency. PC, phase contrast; BF, bright field. Magnification: x10.

3.2.14 Analysis of the effect of MDM2 on NME1 level and NDPK activity

Results presented in Section 3.2.13 suggest that NDPK activity of NME2 was unaffected by MDM2 in the absence of NME1. This raises the question of whether the effect of MDM2 on NDPK activity seen intermittently in previous sections was actually dependent and/or is a direct effect on NME1. Therefore the effect of MDM2 on NME1 protein level and NDPK activity was examined. Accordingly, H1299 were transfected with 0.25 μg pCEP4-NME1 and 1.5 μg of MDM2 or RFM using Lipofectamine 2000. EV and NME2H118C (kinase mutant) were used as negative controls. Transfected cells were harvested for NDPK activity assay 48h post-transfection (n=3).

Apart from kinase mutant, the expression of ectopically introduced NME1 could be detected, as shown in Figure 3.2.14.1A. Since the transfected NME1 plasmid encodes a longer form of NME1 (isoform a), its corresponding protein band on western blot can be easily separated and distinguished from endogenous NME1. In the presence of wt MDM2, NME1 expression levels decrease, with the most prominent effect at 72h post transfection. However, the effect was not seen in the presence of RFM, suggesting that MDM2 down-regulates NME1 in a RING-finger-dependent manner. Similarly, Figure 3.2.14.1B suggests that wt MDM2 has a suppressive effect on NME1 NDPK activity ($p=0.0211$), although the effect from RFM was less prominent ($p=0.0780$).

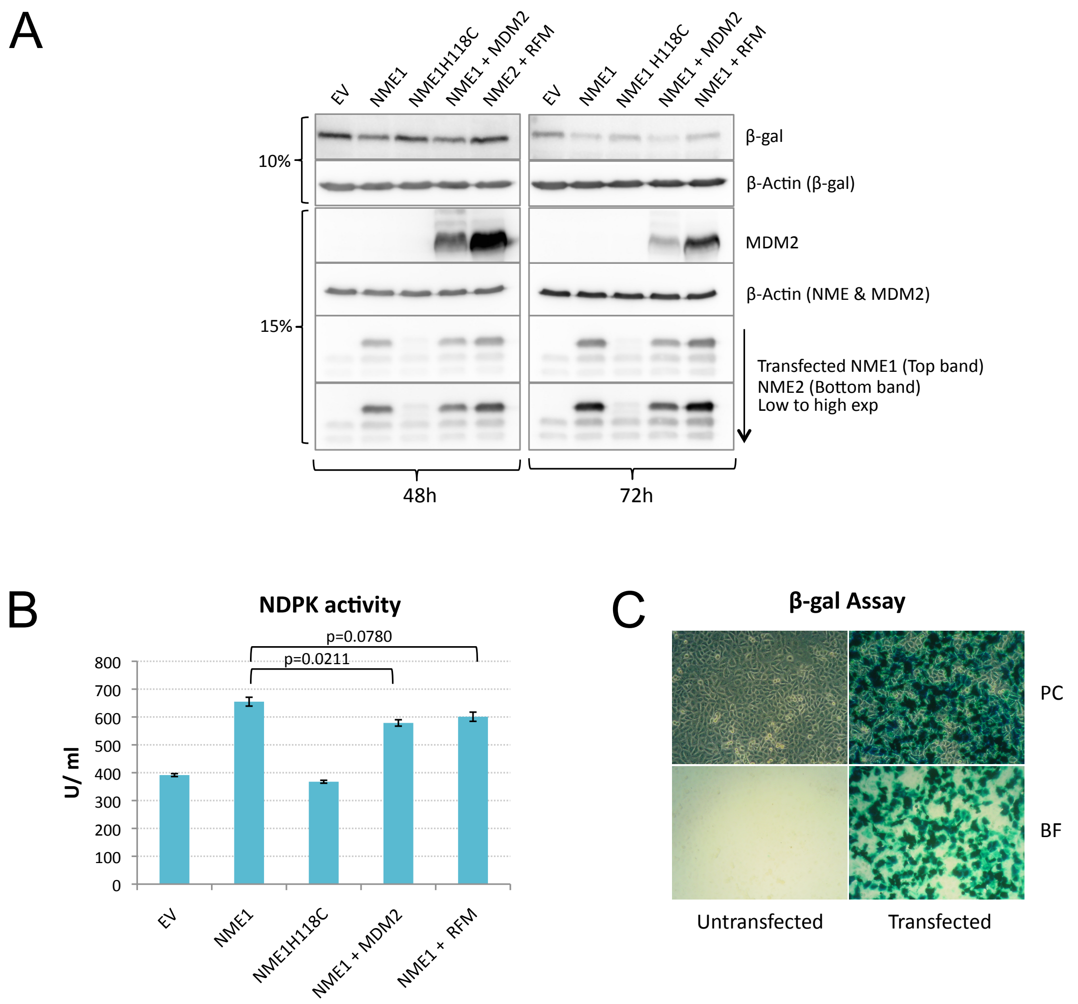

Figure 3.2.14.1: Analysis of the effect of MDM2 on NME1 level and NDPK activity. H1299 cells were transfected with 0.25 μg pCEP4-NME1 and 1.5 μg of MDM2 or RFM using Lipofectamine 2000. EV and NME2H118C (kinase mutant) were used as negative controls. **A.** Western blot analysis of samples separated on 10% and 15% gels, with actin as a loading control. Primary antibodies used were anti-β-actin (AC-15), anti-MDM2 (IF2), anti-NME1/2 (ab31019) and anti-β-gal (OB02). Downward arrow indicates low to high exposures. **B.** Transfected cells were harvested for NDPK activity assay 48h post-transfection (n=3). P-values correspond to statistical analyses by Student's *t*-test (n=3). Error bar indicates standard error. **C.** *In situ* β-gal staining (24h post-transfection) for determination of overall transfection efficiency. PC, phase contrast; BF, bright field. Magnification: x10.

3.2.15 Analysis of the contribution of NME1 and NME2 towards NDPK activity through siRNA down-regulation

As mentioned before, our method of measuring NDPK activity is not selective and does not discriminate between isoforms of NME. However, we wanted to examine the relative contribution of NME1, NME2 and both in combination to cellular NDPK activity. For this purpose, NME1 and NME2 were down-regulated, individually or in combination, in H1299 cells using siRNAs NME1 oligo 9 and NME2 oligo 8 (40 pmol for each well of a 6-well plate, i.e. a total of 80 pmol of siRNA/well), respectively. Mock (only transfection reagent) and Scrambled siRNA were used as negative controls. Transfected cells were harvested 48h and 72h post-transfection for NDPK activity assay (n=3) and western blot purpose.

As demonstrated on Western blot in Figure 3.2.15.1A, down-regulation of NME1, at both 48h and 72h, does not seem to affect NME2 expression level. Similarly, no difference was observed on NME1 expression level when NME2 was down-regulated. In terms of NDPK activity level, there was a decline of about 50 U/ml compared to that of Scrambled control when NME1 alone was down-regulated (Figure 3.2.15.1B). On the other hand, down-regulation of NME2 alone leads to a greater decrease in activity, of about 150 U/ml. Interestingly, the largest decrease in cellular NDPK activity was observed when both NME1 and NME2 were down-regulated, indicating that whilst NME2 may play a greater role in contributing to NDPK activity compared to NME1, it is the combination of both NME1 and NME2 that provides the majority of cellular NDPK activity. Similar results for NDPK activity were obtained for both 48h and 72h post-transfection.

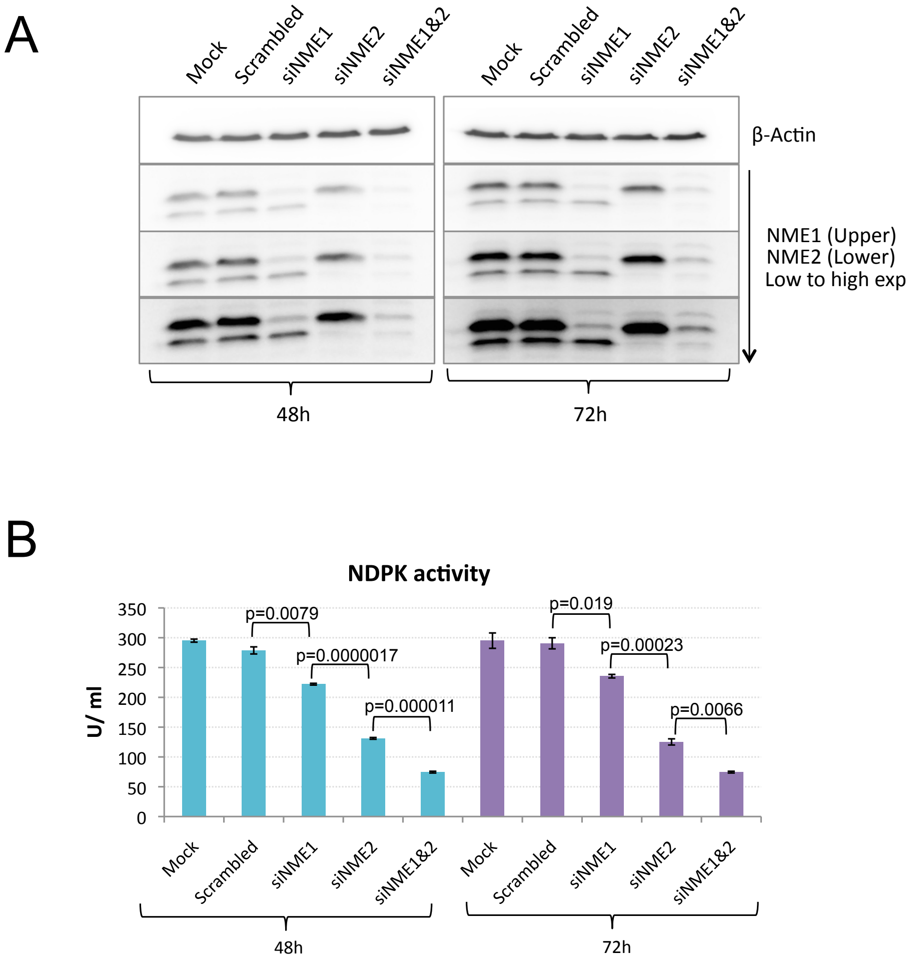

Figure 3.2.15.1: Analysis of the contribution of NME1 and NME2 towards NDPK activity through siRNA downregulation. NME1 and NME2 were down-regulated, individually or in combination, in H1299 cells using siRNAs NME1 oligo 9 and NME2 oligo 8 (40 pmol for each well of a 6-well plate, i.e. a total of 80 pmol of siRNA/well), respectively. Mock (transfection reagent only) and Scrambled siRNA were used as negative controls. Transfected cells were harvested 48h and 72h post-transfection for NDPK activity assay and western blot purpose. **A.** Western blot analysis of samples separated on 15% gels, with actin as a loading control. Primary antibodies used were anti-β-actin (AC-15) and anti-NME1/2 (ab31019). Downward arrow indicates low to high exposures. **B.** NDPK activity assay (n=3). P-values correspond to statistical analyses by Student's *t*-test (n=3). Error bar indicates standard error.

Chapter 3.3

Results

3.3 Investigation of whether NME proteins are substrates for MDM2-mediated ubiquitination

3.3.1 Sub-cellular localisation of NME proteins

Results presented in Section 3.2 have suggested that overexpression of MDM2 may negatively regulate NME1 and NME2 expression levels, although the suppressive effects of MDM2 on NDPK activity were inconsistent. This has led us to question whether the suppressive effect of MDM2 was localised to a specific cellular compartment, which could be missed by the assay used for measuring NDPK activity in this study. Therefore, cellular localisation of MDM2 and NME proteins was examined in order to gain more information on the mechanisms of interaction between MDM2 and NME2. U2OS cells were fractionated (by Dr Carlos Rubbi) into cytoplasmic, nucleoplasmic, and nucleolar fractions according to the protocol of Lam and Lamond [387].

Figure 3.3.1.1 shows the MDM2 levels in all of the fractions from untreated and proteasome inhibitor MG132-treated U2OS cells. 90-kDa MDM2 was abundant in the cytoplasm even without the stabilising effect of MG132. As expected, the 90-kDa band was highly enriched after stabilisation by MG132, particularly in the nucleolar fraction. Furthermore, it appears that the 60-kDa MDM2 was more abundant in the nucleoplasmic fraction compared to cytoplasmic and nucleolar fractions under normal conditions. Interestingly, sub-cellular distribution of the 60-kDa isoform changes after treatment with MG132. Upon treatment with MG132, more of the 60-kDa MDM2 was detected in the cytoplasm and particularly in the nucleoli, but less in the nucleoplasm. Treatment with MG132 was also accompanied by stabilisation of a ladder of what appear to be unknown MDM2 isoforms in the nucleoli. These MDM2 isoforms have molecular weight typically lower than 60 kDa.

The fractionation samples were also probed with three different anti-NME antibodies specific for either NME1 or NME2, or both (Figure 3.3.1.1), in order to increase our confidence that the bands detected were genuine. As the supply of anti-NME1/2 (ab31019), which recognises both NME1 and NME2, had been discontinued, a replacement antibody (C1C3) was used instead after testing has demonstrated that this antibody also recognises both NME1 and NME2 (Appendix 7).

Figure 3.3.1.1 shows that the 17-kDa NME1 and NME2 forms were found almost exclusively in the cytoplasm. Unexpectedly, both NME1 and NME2 levels were considerably lower in the cytoplasmic fraction upon treatment with MG132. This suggests that NME1 and NME2 are not likely to be subjected to proteasomal degradation in cytoplasm. Interestingly, when the three different NME antibodies mentioned earlier were used, a common banding pattern was observed at molecular weight above 17 kDa. Two distinctive bands, one at ~50 kDa (indicated with ◁) and the other at ~30 kDa (indicated with ◀), were found abundant in both nucleoplasmic and nucleolar fractions in both treated and untreated samples. In particular, when membranes were probed with anti-NME1 and anti-NME1/2 antibodies, the ~30 kDa band is more abundant in the nucleolar fractions (Figure 3.3.1.1C, E). More interestingly, a ladder of bands was detected in the nucleolar fractions, indicating that some post-translational events modifying NME2 may take place in the nucleoli. The ladder was particularly visible when membranes were probed with anti-NME1 and anti-NME1/2 antibodies and appeared to be slightly more abundant after treatment with MG132 (Figure 3.3.1.1C, E). The fractionation data therefore suggest that some unknown isoforms of NME could be ubiquitinated in nucleoli and that this might be mediated by MDM2.

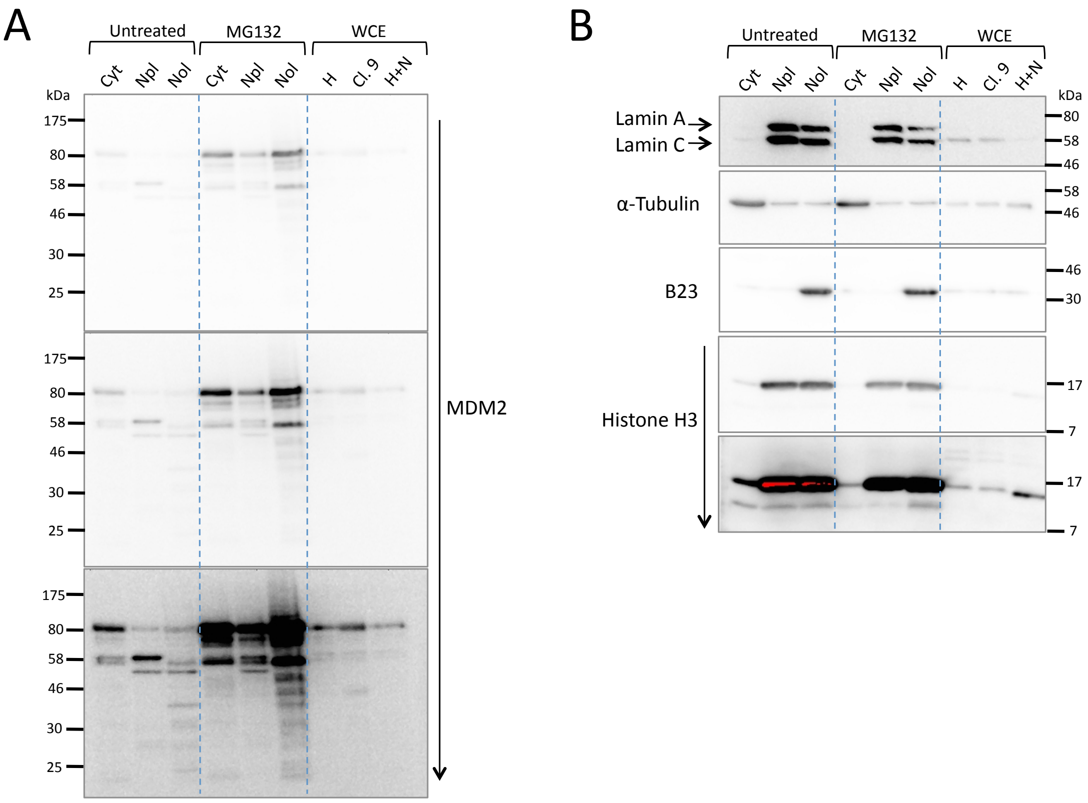

Figure 3.3.1.1: Sub-cellular fractionation of U2OS cells. Western blots of fractions of U2OS cells untreated and treated with 10 μM MG132 for 4h probed with anti-MDM2 (IF2) (**A**); fraction markers for nucleolus: B23 (sc-53175), cytoplasm: α-tubulin (DM1A) and lamin A/C (sc-7297), and nucleus: histone H3 (ab1791) (**B**). **C.** Western blots as in panel A probed with anti-NME1 (SC-465). **D.** Western blots as in panel A probed with anti-NME2 (L15). **E.** Western blots as in panel A probed with anti-NME1/2 (C1C3). Except for histone H3, 30 μg of fractionation samples were loaded in each well. Whole-cell extracts (WCE) of H1299, Clone 9 and H1299 transfected with 1 μg pCEP4-NME2 (H+N) were used as controls, with their loading amounts adjusted for visualisation purpose. WCE of H1299 and Clone 9 were loaded at 3 μg/well, whereas H+N was loaded at 5 μg/well. For histone H3, fractionation samples were loaded at 6 μg/well, and WCE at 15 μg/well. Western blot samples were separated on different gels for each primary antibody. Downward arrow indicates low to high exposures. Red area represents saturation of signal as a result of overexposure. Cyt, cytoplasmic; Npl, nucleoplasmic; Nol, nucleolar; H, H1299; Cl.9, Clone 9.

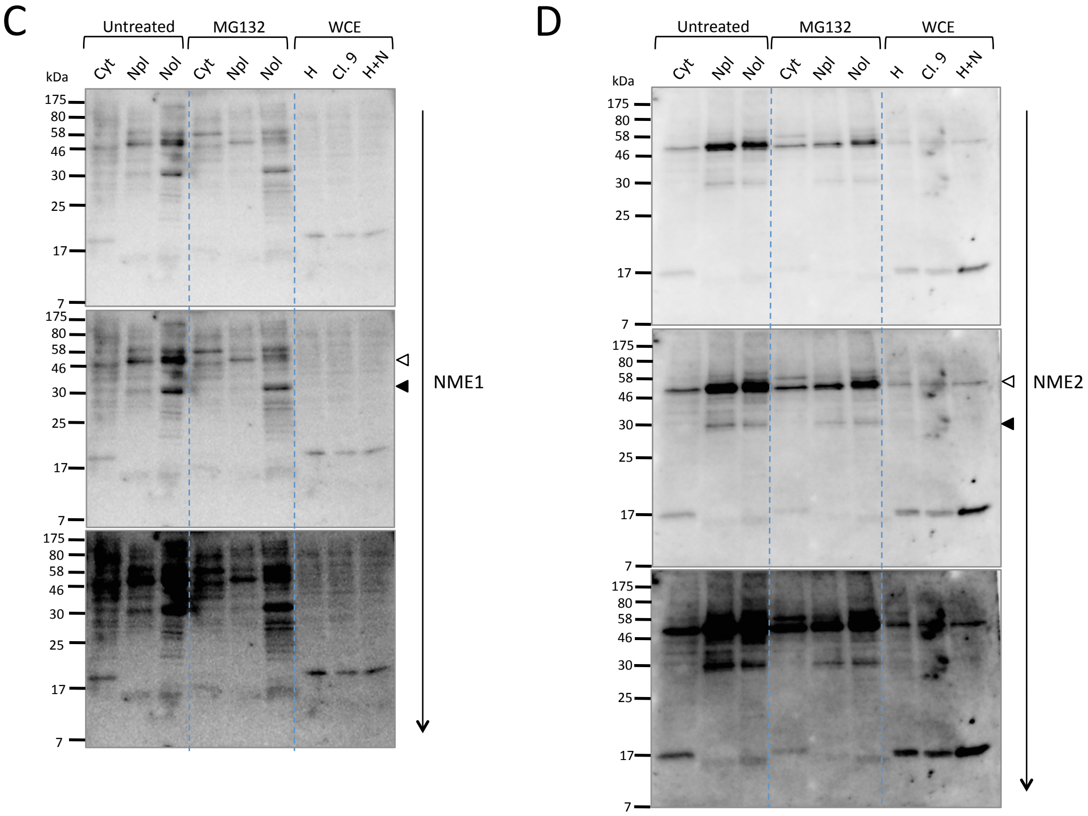

Figure 3.3.1.1 (Continued): Sub-cellular fractionation of U2OS cells. Western blots of fractions of U2OS cells untreated and treated with 10 μM MG132 for 4 hours probed with anti-MDM2 (IF2) (**A**); fraction markers for nucleolus: B23 (sc-53175), cytoplasm: α-tubulin (DM1A) and lamin A/C (sc-7297), and nucleus: histone H3 (ab1791) (**B**). **C.** Western blots as in panel A probed with anti-NME1 (SC-465). **D.** Western blots as in panel A probed with anti-NME2 (L15). **E.** Western blots as in panel A probed with anti-NME1/2 (C1C3). Except for histone H3, 30 μg of fractionation samples were loaded in each well. Whole-cell extracts (WCE) of H1299, Clone 9 and H1299 transfected with 1 μg pCEP4-NME2 (H+N) were used as controls, with their loading amounts adjusted for visualisation purpose. WCE of H1299 and Clone 9 were loaded at 3 μg/well, whereas H+N was loaded at 5 μg/well. For histone H3, fractionation samples were loaded at 6 μg/well, and WCE at 15 μg/well. Western blot samples were separated on different gels for each primary antibody. Downward arrow indicates low to high exposures. Red area represents saturation of signal as a result of overexposure. Cyt, cytoplasmic; Npl, nucleoplasmic; Nol, nucleolar; H, H1299; Cl.9, Clone 9.

E

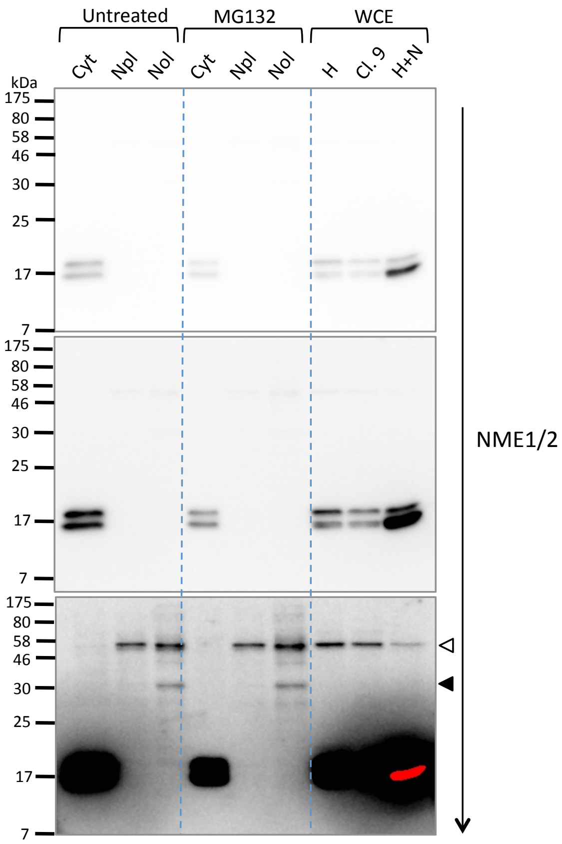

Figure 3.3.1.1 (Continued): Sub-cellular fractionation of U2OS cells. Western blots of fractions of U2OS cells untreated and treated with 10 μM MG132 for 4 hours probed with anti-MDM2 (IF2) (**A**); fraction markers for nucleolus: B23 (sc-53175), cytoplasm: α-tubulin (DM1A) and lamin A/C (sc-7297), and nucleus: histone H3 (ab1791) (**B**). **C.** Western blots as in panel A probed with anti-NME1 (SC-465). **D.** Western blots as in panel A probed with anti-NME2 (L15). **E.** Western blots as in panel A probed with anti-NME1/2 (C1C3). Except for histone H3, 30 μg of fractionation samples were loaded in each well. Whole-cell extracts (WCE) of H1299, Clone 9 and H1299 transfected with 1 μg pCEP4-NME2 (H+N) were used as controls, with their loading amounts adjusted for visualisation purpose. WCE of H1299 and Clone 9 were loaded at 3 μg/well, whereas H+N was loaded at 5 μg/well. For histone H3, fractionation samples were loaded at 6 μg/well, and WCE at 15 μg/well. Western blot samples were separated on different gels for each primary antibody. Downward arrow indicates low to high exposures. Red area represents saturation of signal as a result of overexposure. Cyt, cytoplasmic; Npl, nucleoplasmic; Nol, nucleolar, WCE, whole-cell extract; H, H1299; Cl.9, Clone 9.

3.3.2 *In vivo* His-ubiquitination assay

Fractionation analyses of MDM2 and NME sub-cellular distribution suggest that NME1 and NME2 proteins could be targets for MDM2-mediated ubiquitination taking place in nucleoli. Since down-regulation of NME proteins in the presence of MDM2 was consistently observed in experiments presented earlier in this thesis (Figure 3.2.12.1), it is possible that MDM2 mono-/poly-ubiquitinate NMEs and then targets the modified NME for protein shuttling or degradation. Furthermore, a publication by David Meierhofer *et al.* listed NME1 as one of the potential substrate for ubiquitination in Hela cells using a strategy that utilises stable cell lines expressing 6xHis-biotin-tagged ubiquitin for purification of the ubiquitinated proteome [385]. In the same study, peptide (VMLGETNPADS**K**PGTIR) containing potential ubiquitination site (K100), found in both NME1 and NME2 amino acid sequence was identified using mass spectrometry [385]. These data have led us to hypothesise that NME proteins could be subjected to MDM2-mediated ubiquitination. Therefore, we aimed to utilise an *in vivo* ubiquitination assay to examine whether MDM2 plays a role in mediating modification of NME proteins.

The *in vivo* ubiquitination assay is based upon purification of ubiquitin-conjugates by affinity chromatography. The *in vivo* ubiquitination assay utilised in this study allows for identification of substrates that are covalently modified by addition of 6xHis-tagged ubiquitin (His_6-Ub) moieties expressed in the cell. Ubiquitin conjugates can be purified by using Ni-NTA agarose beads due to high affinity binding of His residues to Ni ions (Please see Materials and Methods Section 2.15).

In order to test the validity of *in vivo* ubiquitination assay, a simplified control experiment was performed initially using a known target of MDM2 ubiquitination, i.e. p53. H1299 cells were transfected with constructs expressing His_6-Ub, MDM2 and/or p53, as described in Figure 3.3.2.1. Transfected cells were processed as described in Materials and Methods (Section 2.15), and harvested cells were processed for western blot analysis. A second aliquot consisting 90% of the sample was processed for the *in vivo* ubiquitination assay. In order to purify proteins conjugated to His_6-Ub, lysates were incubated with Ni-NTA beads for 4 hours, washed and eluted with sample buffer supplemented with 200 mM imidazole. Eluted samples along with cell lysates were subjected to SDS-PAGE followed by Western blot analysis with antibodies against p53 (DO-1) and MDM2 (IF2) as indicated in Figure 3.3.2.1.

As expected, Western blot analysis of the experiment lysate shows that p53 was markedly down-regulated upon MDM2 overexpression (Figure 3.3.2.1A). Western blot with anti-MDM2 for Ni-NTA pulled down (i.e. affinity purified) samples reveals a ladder of slowly migrating high molecular weight bands (Figure 3.3.2.1B, Lane 3). These bands indicate the presence of ubiquitinated MDM2, which is consistent with the ability of MDM2 to self-ubiquitinate. The presence of ubiquitinated p53 was also confirmed, especially when MDM2 is overexpressed, as indicated by the ladder of bands above 58 kDa (Figure 3.3.2.1C, Lane 3). The low level of ubiquitinated p53 observed in Figure 3.3.2.1C, Lane 2 is most likely due to ubiquitination by endogenous MDM2 in H1299 cells. These results show that the *in vivo* ubiquitination assay performed is applicable for future experiments.

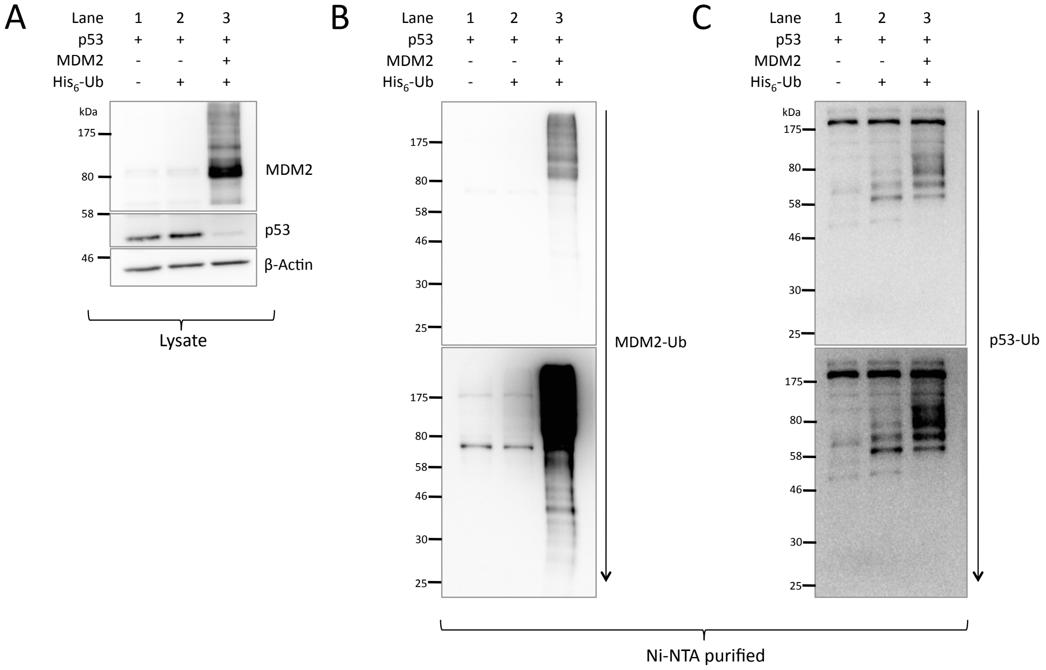

Figure 3.3.2.1: *In vivo* ubiquitination assay with His$_6$-Ub, p53 and MDM2. H1299 cells were transfected with 0.5 μg of pCEP4-wt p53, 5 μg pHis$_6$-Ub and 5 μg pCMVNeoBam-MDM2 in 10-cm dishes using GeneJuice in several combinations, as indicated. Transfected cells were harvested 32h post-transfection. **A.** Western blot for lysate samples of the transfected cells, illustrating the steady-state levels of the indicated proteins. Primary antibodies used were anti-β-actin (AC-15), anti-MDM2 (IF2), anti-p53 (DO-1). **B.** Western blot probed with anti-MDM2 (IF2) for proteins purified with His$_6$-Ub on Ni-NTA agarose beads. **C.** Same as panel B except that the blot was probed with anti-p53 (DO-1). Downward arrow indicates low to high exposures.

3.3.2.1 Examining whether MDM2 has a role in the ubiquitination of NME2

MDM2 has been shown to mediate ubiquitination of many of its interacting proteins, such as p53, MDMX, pRB and DHFR, just to name a few [80, 109, 110, 117]. Since NME2 has also been identified as an MDM2-interacting protein [183], it was examined whether NME2 was also ubiquitinated by MDM2.

H1299 cells were transfected with plasmids expressing His_6-Ub, MDM2 and/or NME2, as described in Figure 3.3.2.1.1B, to examine whether NME2 could be pulled down along with His_6-Ub, in either the absence or presence of transiently transfected MDM2 (Figure 3.3.2.1.1, Lanes 4 and 5/6 respectively). An increase in affinity purified NME2 levels in the presence of transfected MDM2 would suggest MDM2 involvement in NME2 ubiquitination. Furthermore, cells transfected only with His_6-Ub show the endogenous ubiquitination levels of the proteins of interest (Figure 3.3.2.1.1). Lanes 1 and 3 represent specificity controls for the assay, since His_6-Ub was not transfected and any proteins pulled down would be the consequence of non-specific interactions of these proteins with Ni-NTA agarose beads. In addition, the samples in Lanes 5 and 6 from cells transfected with MDM2 and His_6-Ub which should display detectable MDM2 E3 ligase activity, and therefore serve as a positive control for the assay (Figure 3.3.2.1.1).

As expected, MDM2 is detected in ubiquitinated forms in the presence of His_6-Ub (Figure 3.3.2.1.1B, Lanes 5 and 6). It is unclear why less MDM2 ubiquitination was detected when a higher amount of MDM2 plasmid (24 μg) was used for transfection. Considering that the total amount of DNA used for transfection in Lane 6 is higher than in the other conditions, one possibility might be that the chances of cells up-taking His_6-Ub plasmid are lower in the presence of such high amount of MDM2, resulting in less self-ubiquitination. Using antibody specific for NME2 (L15), bands at molecular weight of approximately 50 kDa were also detected under all conditions (Figure 3.3.2.1.1C). However, signal detected for NME in the presence of MDM2 (Lanes 5 and 6) seems to be stronger and seems to increase with the increasing amounts of MDM2. It is difficult to assess whether this is an indication of NME ubiquitination since the bands observed at 50 kDa would be too high a molecular weight for a ubiquitinated form of 17-kDa NME. Moreover, relatively weak bands were also present in Lanes 1, 2, 3 and 4, suggesting that NME can bind non-specifically to the Ni-NTA beads which makes this data difficult to interpret. It is possible that these bands are heavy chains of the secondary antibodies used in western blotting. It is also known that NME2 is capable to binding to metal ions such as Mg^{2+}, Mn^{2+} and $Ca^{2+}$to facilitate the catalysis process and this may provide an alternative explanation for the observed result [396]. Furthermore, when antibody that can detect both NME1 and NME2 (C1C3) was used to probe the Ni-NTA purified proteins, only bands with relatively even intensity were observed at about 50 kDa.

To examine whether the observed bands at 50 kDa were due to non-specific binding of secondary antibody, the corresponding secondary antibodies for L15 and C1C3 were used alone (i.e. without applying primary antibody) for probing western blot for the Ni-NTA purified proteins. Both types of antibodies display a band at about 50 kDa in all the lanes (Figure 3.3.2.1.1D), suggesting that the bands observed when developed with anti-NME antibodies were due to non-specific binding of secondary antibody used in western blotting. Interestingly, when only goat polyclonal secondary antibody was used, the band intensity in the presence of MDM2 was not greater Figure 3.3.2.1.1C, Lanes 5 and 6, in contrast to that observed using anti-NME2 (L15) primary antibody. This suggests that despite the presence of non-specific bands resulting from secondary antibodies used, our result does not eliminate the possibility of some unknown isoforms of NME being ubiquitinated by MDM2. Therefore, it was decided that it is worth studying the involvement of MDM2 in NME1 ubiquitination, to examine whether more information could be obtained by comparing the ubiquitination profiles of NME1 and NME2.

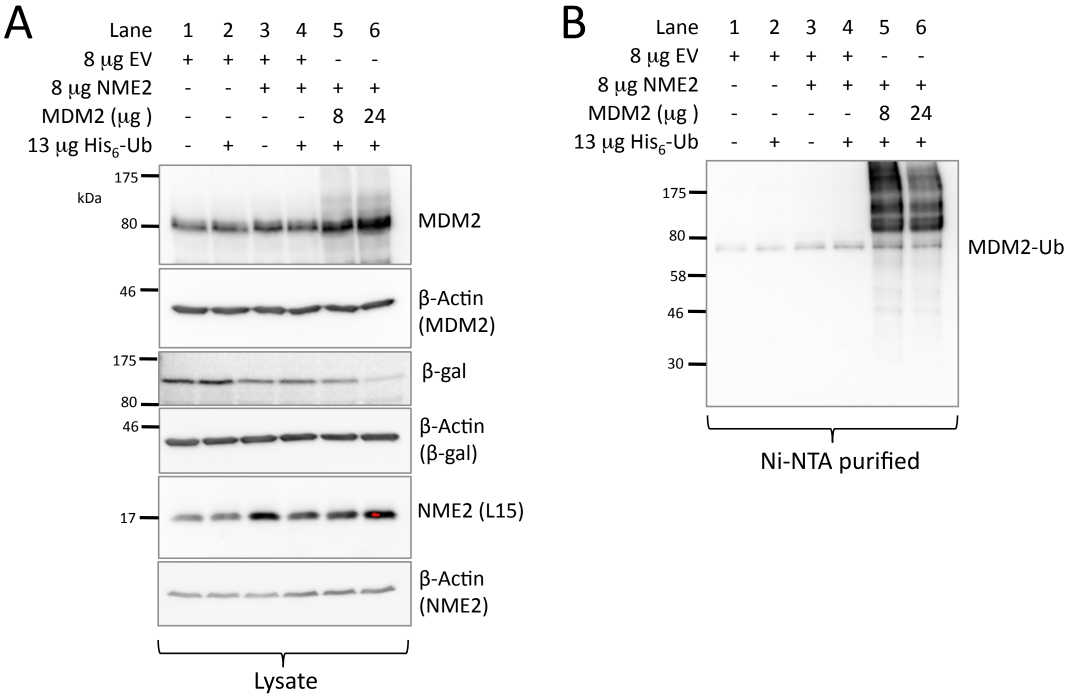

Figure 3.3.2.1.1: *In vivo* ubiquitination assay with His$_6$-Ub, NME2 and MDM2. H1299 cells were transfected with 8 μg of pCEP4-NME2, 13 μg pHis$_6$-Ub and indicated amount of pCMVNeoBam-MDM2 in 15-cm dishes using GeneJuice in several combinations, as indicated. All transfected samples included a plasmid that expresses β-gal (2 μg) to enable comparison of transfection efficiency and also actin to act as loading control. Transfected cells were harvested 48h post-transfection. **A.** Western blot for lysate samples of the transfected cells, illustrating the steady-state levels of the indicated proteins. Primary antibodies used were anti-β-actin (AC-15), anti-MDM2 (IF2), anti-NME2 (L15) and anti-β-gal (AB986). Red area represents saturation of signal as a result of overexposure. **B, C** and **D** represent proteins purified with His$_6$-Ub on Ni-NTA agarose beads. **B.** Western blot using anti-MDM2 (IF2) antibody **C.** Western blot probed with anti-NME2 (L15) and anti-NME1/2 (C1C3) primary antibodies. **D.** Western blot probed with solely secondary antibody (without incubation with primary antibody). Goat polyclonal (GP) was used for comparison with anti-NME (L15) and rabbit polyclonal (RP) for anti-NME1/2 (C1C3). This experiment was performed twice and results from both experiments were consistent.

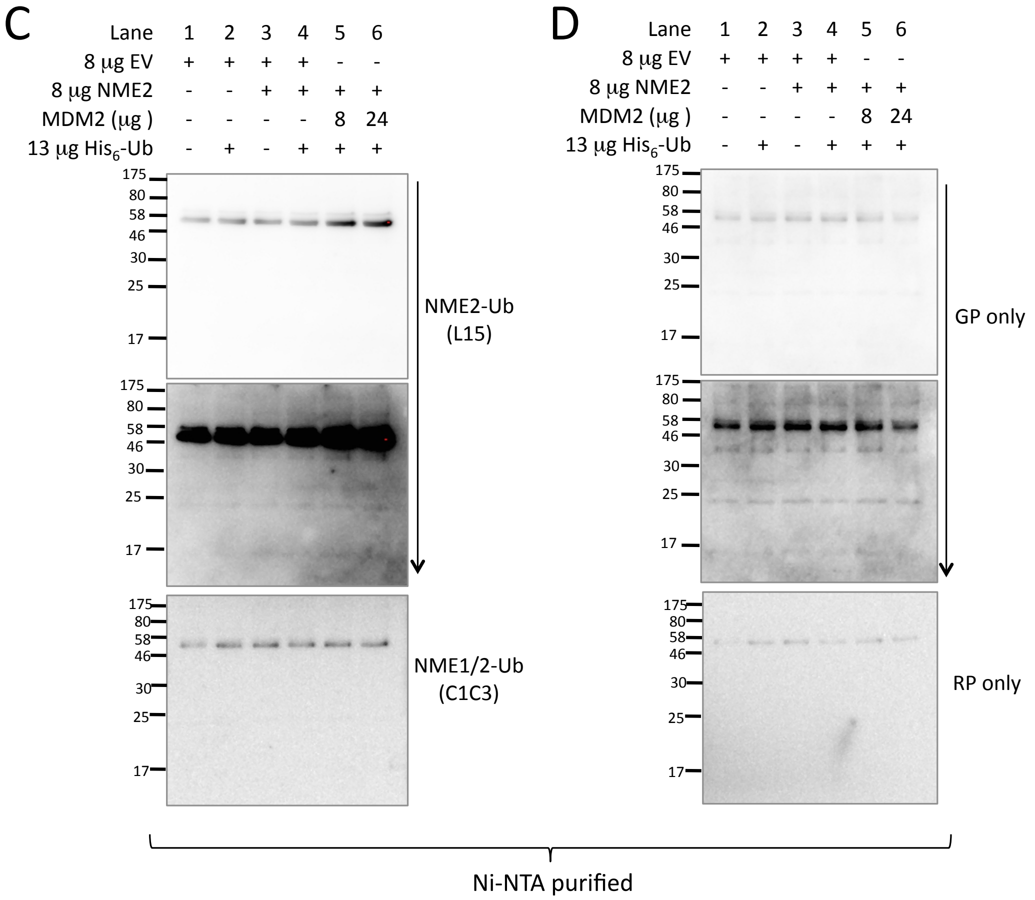

Figure 3.3.2.1.1 (Continued): ***In vivo*** **ubiquitination assay with His$_6$-Ub, NME2 and MDM2.** H1299 cells were transfected with 8 μg of pCEP4-NME2, 13 μg pHis$_6$-Ub and indicated amount of pCMVNeoBam-MDM2 in 15-cm dishes using GeneJuice in several combinations, as indicated. All transfected samples included a plasmid that expresses β-gal (2 μg) to enable comparison of transfection efficiency and also actin to act as loading control. Transfected cells were harvested 48h post-transfection. **A.** Western blot for lysate samples of the transfected cells, illustrating the steady-state levels of the indicated proteins. Primary antibodies used were anti-β-actin (AC-15), anti-MDM2 (IF2), anti-NME2 (L15) and anti-β-gal (AB986). Red area represents saturation of signal as a result of overexposure. **B,** **C** and **D** represent proteins purified with His$_6$-Ub on Ni-NTA agarose beads. **B.** Western blot using anti-MDM2 (IF2) antibody **C.** Western blot probed with anti-NME2 (L15) and anti-NME1/2 (C1C3) primary antibodies. **D.** Western blot probed with solely secondary antibody (without incubation with primary antibody). Goat polyclonal (GP) was used for comparison with anti-NME

(L15) and rabbit polyclonal (RP) for anti-NME1/2 (C1C3). Downward arrows indicate low to high exposures. This experiment was performed twice and results from both experiments were consistent.

3.3.2.2 Examining whether MDM2 has a role in the ubiquitination of NME1

Since NME1 shares a high degree of homology with NME2, we have also examined whether NME1 is a target for MDM2 ubiquitination. For this purpose, *in vivo* ubiquitination assay similar to Section 3.3.2.1 was performed to study whether MDM2 might modify NME1 by ubiquitination, along with NME2 for comparison. H1299 cells were transfected with constructs expressing His_6-Ub, MDM2, NME1 or NME2 in different combinations, as described in Figure 3.3.2.2.1A, to examine whether NME1 could be pulled down along with His_6-Ub, in either the absence or presence of transiently transfected MDM2.

Based on the western blot analysis of the transfected cell lysate (Figure 3.3.2.2.1B and C), both NME1 and NME2 appear to be down-regulated when co-transfected with His_6-Ub alone (Lane 3), and the down-regulation was more prominent in the presence of both ubiquitin and MDM2 (Lane 5). MDM2 has been demonstrated in this study to play a role in NME2 down-regulation, and thus it is not surprising that MDM2 also has the same effect on NME1. As expected, western blot analysis (Figure 3.3.2.2.1D) shows two distinctive ladders of slowly migrating bands in the presence of MDM2 (Lanes 5 and 8), suggesting that ubiquitinated MDM2 has been pulled down on Ni-NTA agarose beads and that MDM2 E3 ligase activity was present. However, western blot analyses of Ni-NTA purified proteins using anti-NME1 antibody does not seem to show any signs of NME1 ubiquitination by MDM2, as only what seems to be non-specific bands were observed (Figure 3.3.2.2.1E). Similarly, Figure 3.3.2.2.1F clearly shows that NME2 is also not ubiquitinated by MDM2. However, consistent with previous observation in this thesis (Figure 3.3.2.1.1C), the non-specific bands at 50 kDa seems to have greater intensity in the presence of His_6-Ub and MDM2.

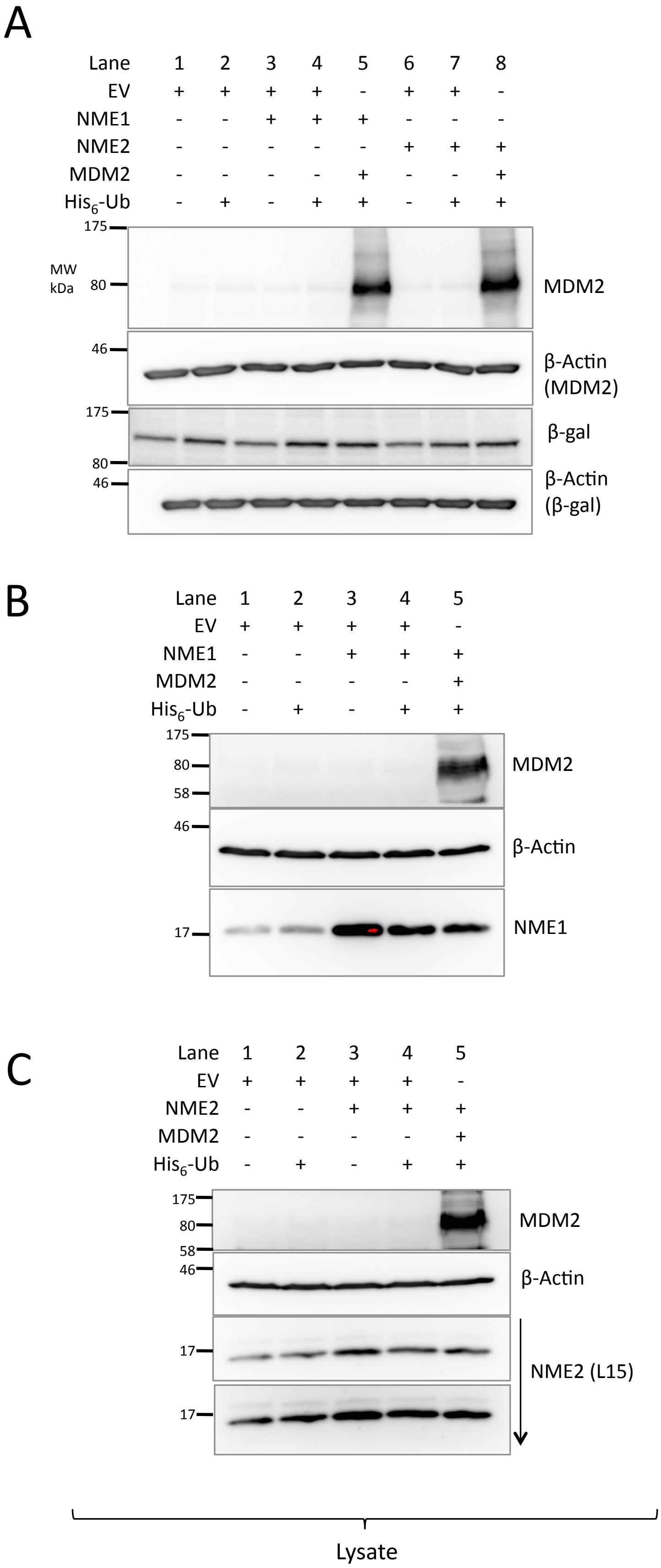

Figure 3.3.2.2.1 (To be continued)

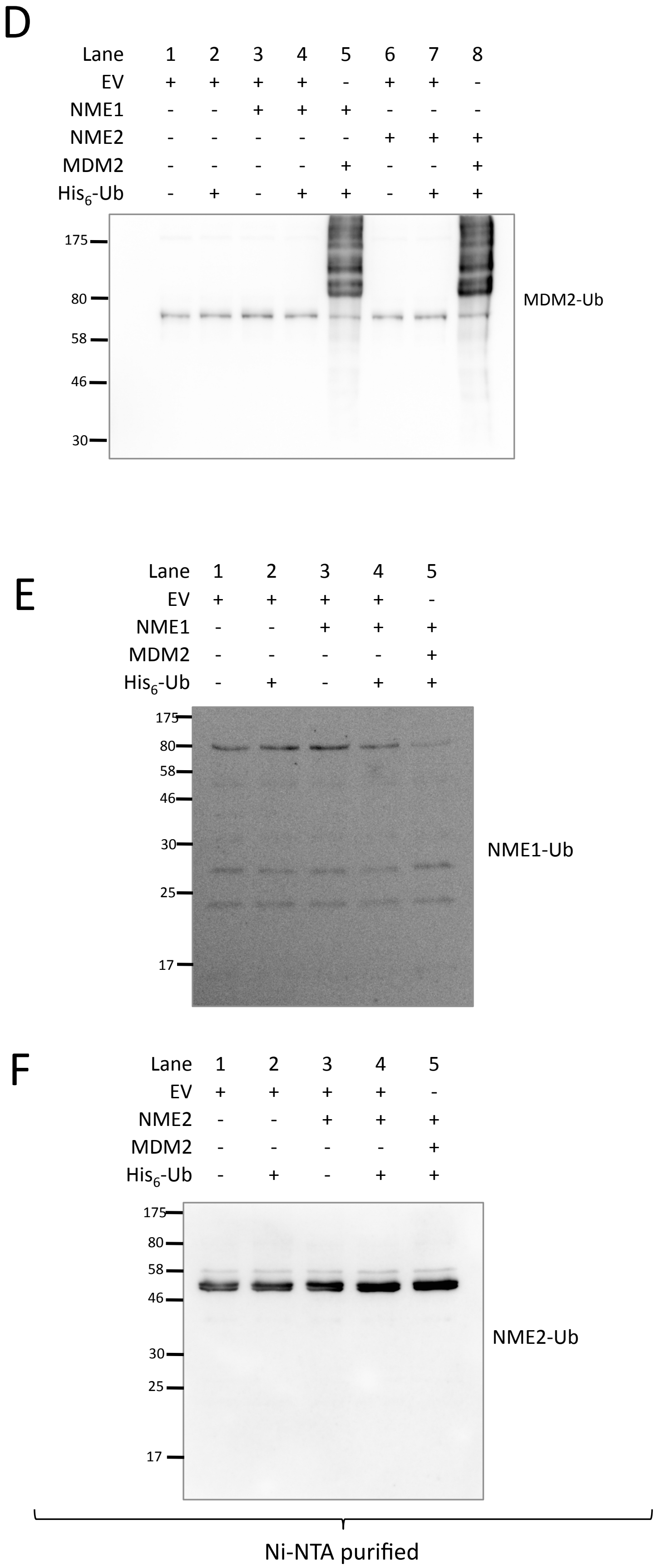

Figure 3.3.2.2.1 (To be continued)

Figure 3.3.2.2.1: *In vivo* ubiquitination assay with His$_6$-Ub, NME1 and MDM2. H1299 cells were transfected with 8 μg of pCEP4-NME1, 8 μg of pCEP4-NME2, 13 μg pHis$_6$-Ub and indicated amounts of pCMVNeoBam-MDM2 in 15-cm dishes using GeneJuice in several combinations, as indicated. All transfected samples included a plasmid that expresses β-gal (2 μg) to enable comparison of transfection efficiency and actin serves as loading control. Transfected cells were harvested 48h post-transfection. **A, B** and **C** Western blot for lysate samples of the transfected cells, illustrating the steady-state levels of the indicated proteins. Primary antibodies used were anti-β-actin (AC-15), anti-MDM2 (IF2), anti-NME1 (SC465), anti-NME2 (L15) and anti-β-gal (AB986). **D, E** and **F** represent western blots of proteins purified with His$_6$-Ub on Ni-NTA agarose beads using anti-MDM2 (IF2), anti-NME1 (SC465), and anti-NME2 (L15) antibodies, respectively. Downward arrows indicate low to high exposures. Red area represents saturation of signals as a result of overexposure.

3.3.2.3 Examining whether MDM2 has a role in the ubiquitination and NDPK activity regulation of NM23-LV

Results presented in this thesis have thus far shown no evidence for MDM2-mediated ubiquitination of NME1 or NME2. However, it remains unexplained as to why a 30 kDa band has been consistently detected in the nucleolar fractions, when Western blot of a fractionation study was probed with three different NME antibodies (Figure 3.3.1.1C, D and E). In addition, the fractionation data also suggest the possibility that some unknown NME isoforms might be ubiquitinated in the nucleoli (Figure 3.3.1.1C, E). Coincidently, *in vivo* ubiquitination assay described in Section 3.3.2.1 also implies that there is a possibility that an unknown isoform of NME is being ubiquitinated by MDM2 (Figure 3.3.2.1.1C). In the light of a study by Valentijn *et al.*, which described a novel protein of 33-kDa that was named NM23-LV and which is a product of a read-through transcript of *NME1* and *NME2* neighbouring genes [250], we hypothesised that the unknown band at 30 kDa might represent NM23-LV, and that this long variant may be subjected to MDM2 ubiquitination.

To examine whether NM23-LV is a target for MDM2 ubiquitination, H1299 cells were transfected with constructs expressing His_6-Ub, NM23-LV, wt MDM2 or RFM, as described in Figure 3.3.2.3.1. RFM was included to examine whether protein ubiquitination, if any, was dependent on MDM2 E3 ligase activity. Note that RFM was used at half of the amount of wt MDM2 in order to adjust for stabilisation effect of RFM, to achieve a similar expression level with wt MDM2 for comparison purpose. Along with the *in vivo* ubiquitination assay, transfected cells were also harvested 48h post transfection for NDPK activity, in order to examine the effect MDM2 on NM23-LV activity (Figure 3.3.2.3.2).

As shown in western blot in Figure 3.3.2.3.1A**,** NM23-LV was detected at about 28 kDa, unlike the published result by Valentijn *et al.* [250] suggesting that NM23-LV gives rise to a 33 kDa band on western blot. Prior to performing the *in vivo* ubiquitination assay, we have sequenced the plasmids kindly donated by Dr Linda Valentijn (Appendix 8) and also performed western blot analysis of cells transfected with these plasmids (Appendix 9). Based on these, we concluded that the 28-kDa band genuinely represents NM23-LV and that the observed difference in the size of the band could be due to a number of factors, for example, the way the gels were run. Perhaps different percentages of gels and molecular weight markers were used, which may result in the differences observed. Co-transfection with His_6-Ub seems to stabilise NM23-LV (Figure 3.3.2.3.1A Lanes 3 and 5) considering β-gal and β-actin levels were similar for these two conditions. A small degree of stabilisation of NM23-LV was also observed with the addition of wt MDM2 (Figure 3.3.2.3.1A Lanes 5, 6 and 7). However, this does not seem to be the case when NM23-LV was co-transfected with RFM (Lane 8). As shown in western blot with anti-MDM2 on Ni-NTA pulled down proteins (Figure 3.3.2.3.1B), ubiquitination of MDM2 in a dose-dependent manner was clearly demonstrated in the presence of transiently transfected MDM2 (Lanes 6 and 7). As expected, only a low level of MDM2 ubiquitination was detected in the presence of RFM (Figure 3.3.2.3.1B, Lane 8), since E3 ligase activity is crucial for auto-ubiquitination of MDM2.

Interestingly, when the affinity purified samples were analysed by western blot using anti-NME1/2 antibody (Figure 3.3.2.3.1B), two distinctive bands of estimated molecular weights of 36 kDa (as indicated with ◀) and 40 kDa (◁) were observed in Lane 6 and Lane 7 on the lower exposure blot. Since unmodified NM23-LV is normally detected at 28 kDa on western blot, it is likely that the doublet of bands described earlier were mono-ubiquitinated forms of NM23-LV, considering each ubiquitin moiety weighs about 8.5 kDa. It is also likely that the monoubiquitination occurred at different sites on NM23-LV, leading to the slight shift in molecular weight, resulting in the doublet formation. Followed behind these two bands was a ladder of slowly migrating bands (high exposure blot, Lane 6 and 7), indicating polyubiquitination of NM23-LV. The level of ubiquitination increases with the amount of wt MDM2 transfected, suggesting that NM23-LV is ubiquitinated by MDM2 in a dose-dependent manner. More interestingly, only a negligible amount of these bands was detected in RFM (Figure 3.3.2.3.1B, Lane 8), even at a higher exposure, suggesting that ubiquitination of NM23-LV is E3 ligase-dependent. Certain degree of NM23-LV ubiquitination was also detected in Lane 5 (high exposure blot), which is likely to be mediated by endogenous MDM2.

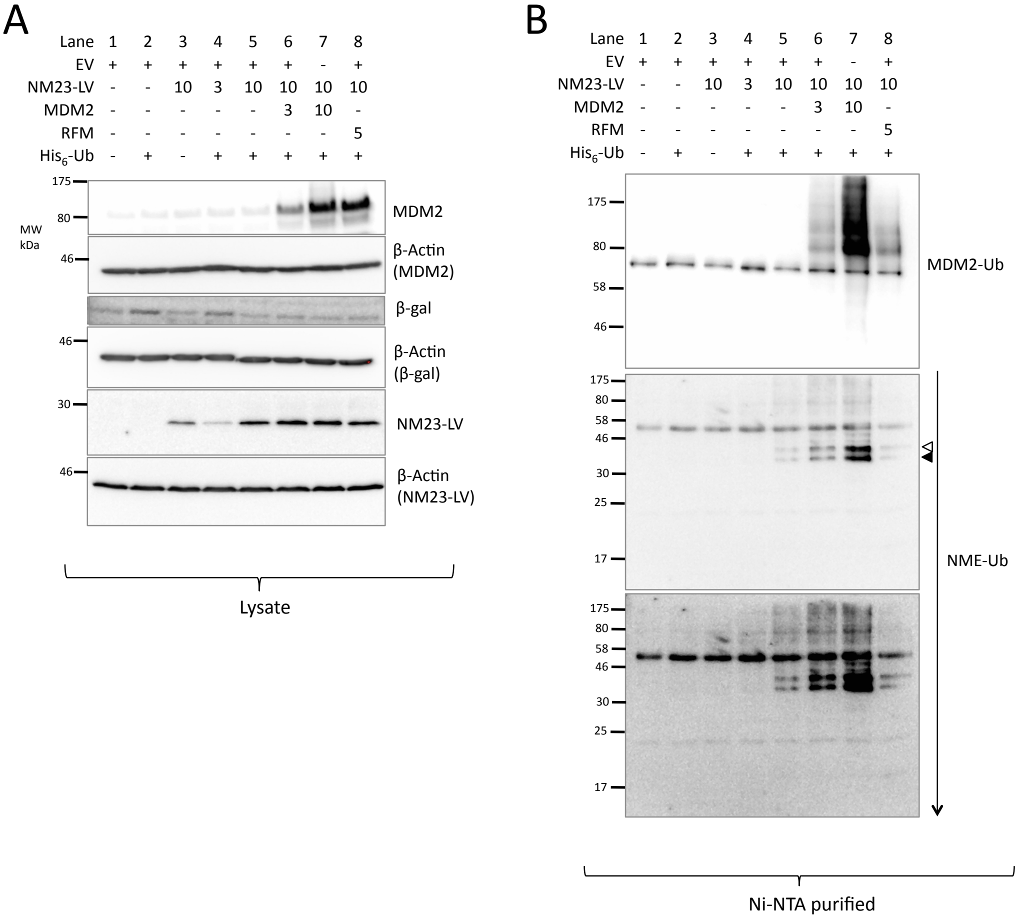

Figure 3.3.2.3.1: *In vivo* ubiquitination assay with His$_6$-Ub, NM23-LV and MDM2. H1299 cells were transfected with indicated amounts (μg) of pcDNA3.1-NM23-LV, pCMVNeoBam-MDM2, pCMVNeoBam-MDM2C464A and 13 μg pHis$_6$-Ub in 15-cm dishes using GeneJuice in several combinations, as indicated. Note that RFM was used at half amount of wt MDM2 in order to achieve a similar level of expression for comparison purposes. All transfected samples included a plasmid that expresses β-gal (2 μg) to enable comparison of transfection efficiency and also actin to act as loading control. Transfected cells were harvested 48h post-transfection. **A.** Western blot for lysate samples of the transfected cells, illustrating the steady-state levels of the indicated proteins. Primary antibodies used were anti-β-actin (AC-15), anti-MDM2 (IF2), anti-NME1/2 (C1C3), and anti-β-gal (AB986). **B.** Western blots of proteins purified with His$_6$-Ub on Ni-NTA agarose beads using anti-MDM2 (IF2) and anti-NME1/2 (C1C3) antibodies, as indicated. Downward arrows indicate low to high exposures.

In terms of NDPK activity, no difference was observed in the activity of NM23-LV when the levels were compared between cells transfected with NM23-LV alone or in combination with MDM2, and cells transfected with an empty vector control (Figure 3.3.2.3.2A). However, it is difficult to determine whether NM23-LV possess NDPK activity based on this result, since NM23-LV expression levels were extremely low amidst the considerably higher abundance of endogenous NME1 and NME2 in the cells (Figure 3.3.2.3.2B). Thus it would be difficult, through this experiment, to detect any changes in NDPK activity caused by NM23-LV even if NM23-LV did possess NDPK activity.

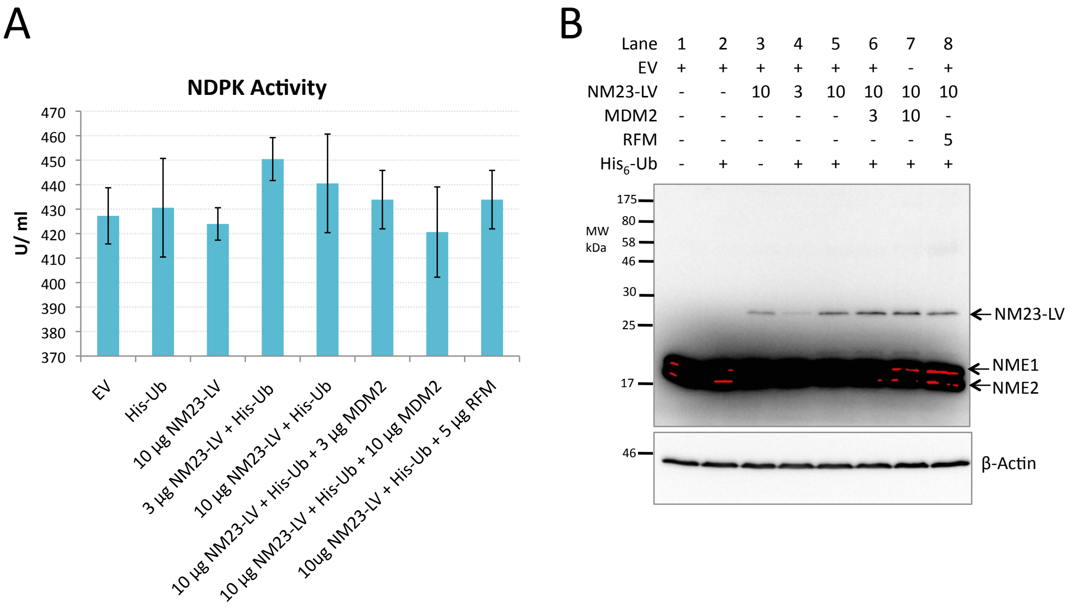

Figure 3.3.2.3.2: Analysis of the NDPK activity with His$_6$-Ub, NM23-LV and MDM2 transfection. Experimental design was the same as described in Figure 3.3.2.3.1, NDPK activity assay was performed 48h after transfection. **A.** NDPK activity. Error bars indicate standard error (n=3). **B.** Western blot with anti-NME1/2 (C1C3) and anti-β-actin (AC-15) showing the relative abundance of NM23-LV and NME1/2, as indicated by arrows. Red area represents saturation of signal as a result of overexposure.

In order to examine whether NM23-LV is a genuine target for MDM2-mediated ubiquitination, experiment described in Figure 3.3.2.3.1 was repeated, except for using HA-tagged NM23-LV plasmid (a kind gift from Dr Linda Valentijn). Since HA is not expressed endogenously, it can be used as an indicator for NM23-LV ubiquitination, if HA could be pulled down along with His$_6$-Ub, in the presence of transfected MDM2. As shown on western blot in Figure 3.3.2.3.3, HA-NM23-LV was detected at approximately 28 kDa (Figure 3.3.2.3.3B), at a similar position as NM23-LV (Figure 3.3.2.3.3A). This is as expected since HA (9 aa) only has an estimated molecular mass of 1.1 kDa, which would be difficult to detect on a western blot. There seems to be some stabilisation of NM23-LV in the presence of His$_6$-Ub and/or MDM2 (Figure 3.3.2.3.3B, Lanes 3, 4, 5 and 6) as observed in previous results presented in this thesis. However, this is more likely due to uneven transfection efficiency, as indicated by β-gal expression (Figure 3.3.2.3.3A). As expected, MDM2 was ubiquitinated in the presence of His$_6$-Ub and wt MDM2 (Figure 3.3.2.3.3D, Lane 5) but MDM2 ubiquitination was inhibited in cells transfected with RFM (Lane 6), indicative of polyubiquitination of MDM2 through E3 ligase activity. Consistent with observation in Figure 3.3.2.3.1B (Lanes 5, 7 and 8), a thick band of approximately 36 kDa, indicating mono-ubiquitinated NM23-LV accompanied by a ladder of polyubiquitinated NM23-LV, was observed in the presence of His$_6$-Ub and wt MDM2 (Figure 3.3.2.3.3E, Lane 5), based on western blot probed with anti-NME1/2 (C1C3) for Ni-NTA purified proteins. Mono- and polyubiquitination of NM23-LV was clearly inhibited in the presence of RFM (Lane 6). There were also signs of NM23-LV ubiquitination, most probably mediated by endogenous MDM2. This result is supported by western blot using anti-HA (12CA5) antibody (Figure 3.3.2.3.3F), which demonstrates an NM23-LV ubiquitination profile identical to Figure 3.3.2.3.3E. Overall, these results strongly suggest that NM23-LV is a substrate for MDM2-mediated ubiquitination and that this is E3 ligase- and dose-dependent phenomenon.

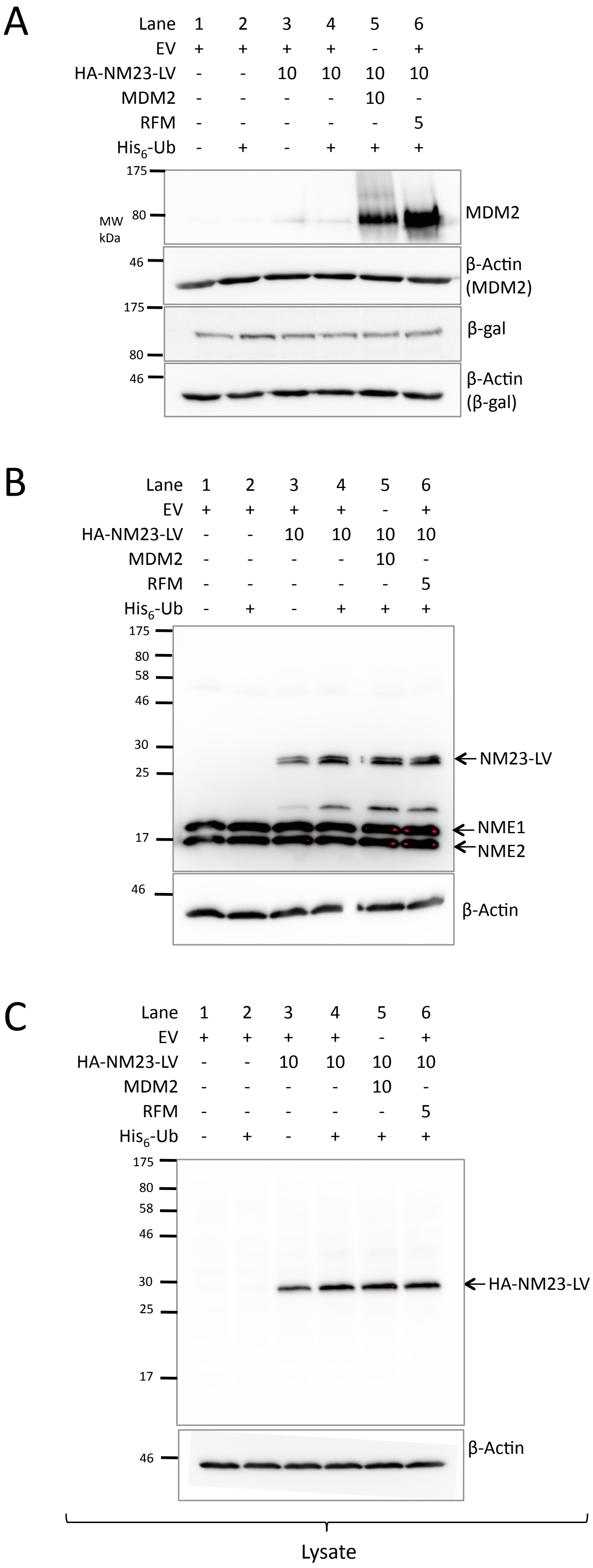

Figure 3.3.2.3.3 (To be continued)

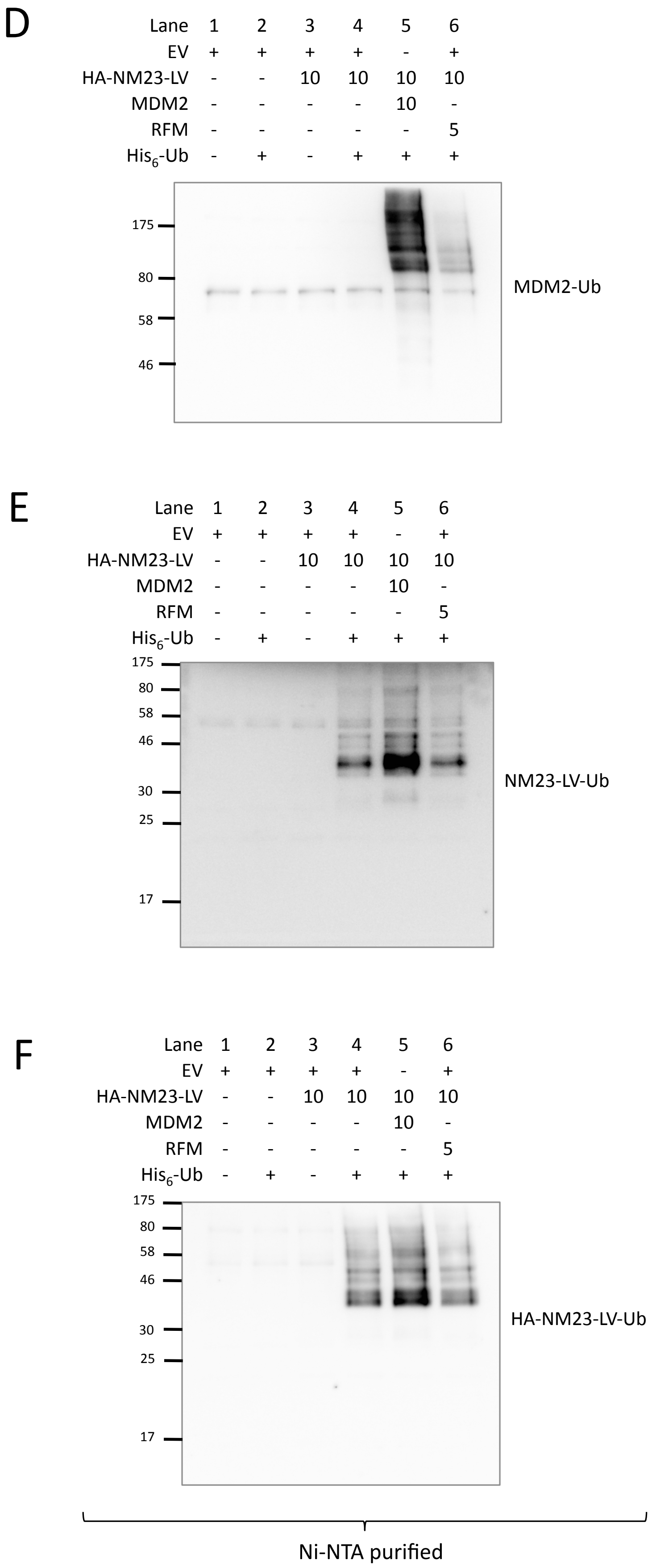

Figure 3.3.2.3.3 (To be continued)

Figure 3.3.2.3.3: *In vivo* ubiquitination assay with His$_6$-Ub, HA-NM23-LV and MDM2. H1299 cells were transfected with indicated amounts (μg) of pcDNA3.1-HA-NM23-LV, pCMVNeoBam-MDM2, pCMVNeoBam-MDM2C464A and 13 μg pHis$_6$-Ub in 15-cm dishes using GeneJuice in several combinations, as indicated. Note that RFM was used at half amount of wt MDM2 to adjust for RFM stabilisation. All transfected samples included a plasmid that expresses β-gal (2 μg) to enable comparison of transfection efficiency and also actin to act as loading control. Transfected cells were harvested 48h post transfection. **A, B** and **C.** represent western blots for lysate samples of the transfected cells, illustrating the steady-state levels of the indicated proteins. **A.** Western blots probed with anti-MDM2 (IF2), anti-β-actin (AC-15), and anti-β-gal (AB986). **B.** Western blot probed with anti-NME1/2 (C1C3). The split bands in Lane 4 were caused by a crack across a complete membrane due to human error. Red areas correspond to signal saturation caused by overexposure. **C.** Western blot probed with anti-HA (12CA5). **D, E,** and **F** represent western blots of proteins purified with His$_6$-Ub on Ni-NTA agarose beads using anti-MDM2 (IF2) antibody for **D**, anti-NME1/2 (C1C3) antibody for **E**, and anti-HA (16B12) antibody for **F.** This experiment was performed at least three times with consistent results.

3.3.2.4 Examining whether MDM2-mediated ubiquitination of NM23-LV results in proteasomal degradation

The results previously presented in this thesis (Figures 3.3.2.3.2 and 3.3.2.3.3) have shown that NM23-LV can be ubiquitinated by MDM2 in a RING-finger-dependent manner. We wanted to examine whether NM23-LV ubiquitinated by MDM2 is subjected to the proteasomal degradation, since one of the major roles of protein ubiquitination (particularly polyubiquitination) is to target proteins for proteasomal degradation. In order to examine whether NM23-LV ubiquitination by MDM2 follows the ubiquitin/proteasomal degradation pathway, *in vivo* ubiquitination assay was performed in the presence of proteasome inhibitor MG132. We expected to observe a shift in ubiquitination profiles upon inhibition of proteasome activity.

H1299 cells were transfected with combinations of plasmids expressing NM23-LV, MDM2 and pHis$_6$-Ub, as described in Figure 3.3.2.4.1. Transfected cells were processed as described in Materials and Methods (Section 2.15), and harvested 48h post-transfection. Transfected cells were treated with 100 μM of MG132 (in DMSO) 6h before harvesting in order to inhibit proteasome-dependent degradation and therefore increase the amount of cellular ubiquitinated proteins, or with DMSO as a negative control to test the effect of the drug vehicle on cells.

As shown in Figure 3.3.2.4.1A, stabilisation of MDM2 was observed in cells treated with MG132 (Lane 7), but not with DMSO (Lane 5). This observation is expected, since ubiquitinated MDM2 could not be degraded through proteasome and therefore accumulated in the cells. Interestingly, NM23-LV was also stabilised in the presence of MG132 (Figure 3.3.2.4.1A, Lane 7), indicating that NM23-LV is subject to proteasome-mediated degradation in the cell. In addition, a slight increase in ubiquitinated protein was observed for both MDM2 (as expected) and NM23-LV when cells were treated with MG132 (Figure 3.3.2.4.1B, Lane 7) in comparison to when only DMSO was used (Lane 5). This increase of NM23-LV polyubiquitination is more noticeable in the high exposure blot probed with anti-NME1/2 (C1C3). Taken together, our *in vivo* ubiquitination data demonstrate that NM23-LV is a target for MDM2-mediated ubiquitination, that this occurs in a dose- and E3 ligase-dependent manner, and that this modification by MDM2 might also mark NM23-LV for proteasomal degradation.

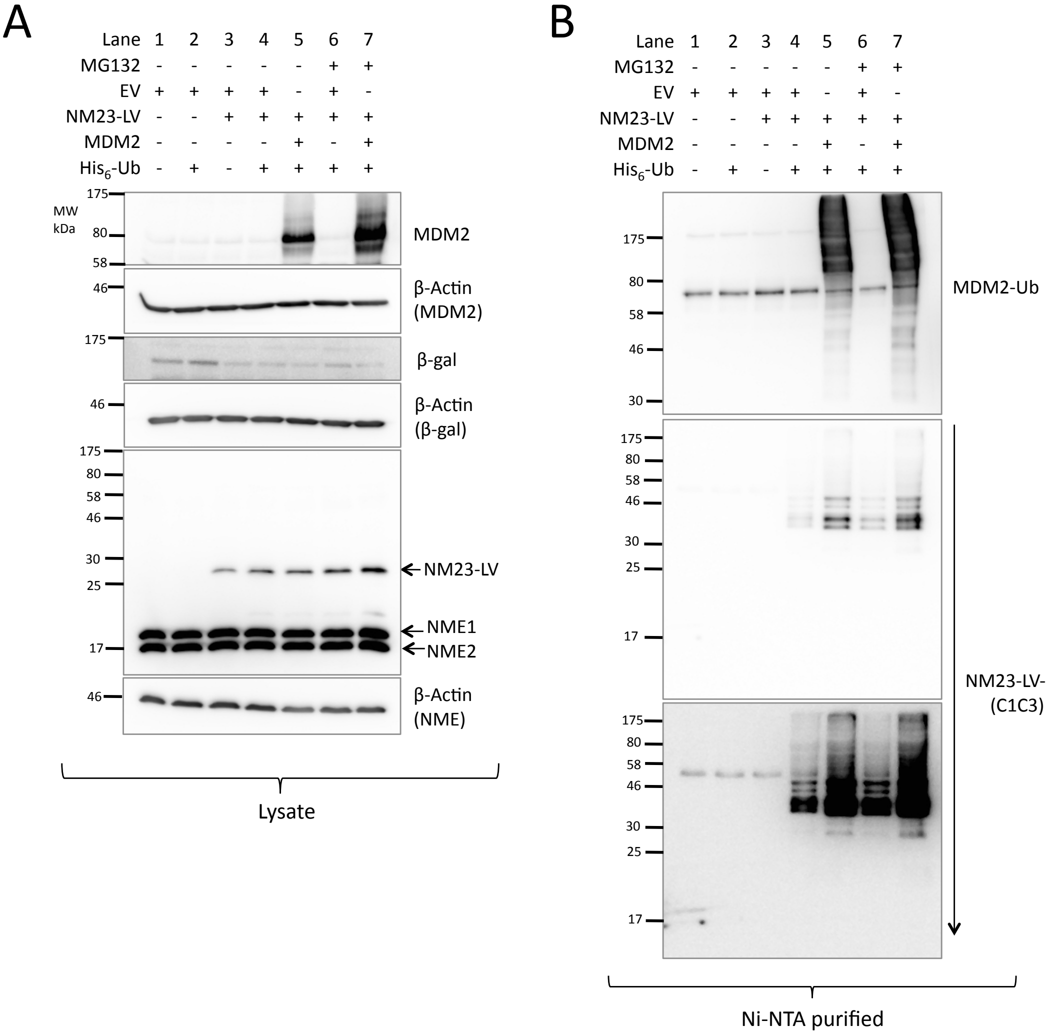

Figure 3.3.2.4.1: *In vivo* ubiquitination assay with His_6-Ub, HA-NM23-LV and MDM2 with addition of MG132. H1299 cells were transfected with 10 μg of pcDNA3.1-NM23-LV, 10 μg of pCMVNeoBam-MDM2, and 13 μg $pHis_6$-Ub in 15-cm dishes using GeneJuice in several combinations, as indicated. All transfected samples included a plasmid that expresses β-gal (2 μg) to enable comparison of transfection efficiency and also actin to act as loading control. 100 μM of MG132 was added to transfected cells 6h before harvest and DMSO was used as a control Transfected cells were harvested 48h post-transfection for *in vivo* ubiquitination assay. **A.** Western blots for lysate samples of the transfected cells, illustrating the steady-state levels of the indicated proteins. Primary antibodies used were anti-MDM2 (IF2), anti-β-actin (AC-15), anti-NME1/2 (C1C3), and anti-β-gal (AB986) **B.** Western blots of proteins purified with His_6-Ub on Ni-NTA agarose beads using anti-MDM2 (IF2) and anti-NME1/2 (C1C3) antibodies. Downward arrow indicates low to high exposures.

Chapter 3.4

Results

3.4 Functional consequences of NM23-LV and MDM2 interaction

3.4.1 Investigation of whether NM23-LV interacts with MDM2 and/or possesses NDPK activity

Results presented in Section 3.3 have demonstrated that NM23-LV, but not NME1 or NME2, is subjected to ubiquitination by MDM2. In order to perform its function as an E3 ligase and catalyse the covalent attachment of a ubiquitin moiety to a substrate, MDM2 generally needs to interact with its substrate. Therefore, since MDM2 seems to be able to ubiquitinate NM23-LV, it is very likely that MDM2 is also able to interact with NM23-LV. In addition, as reviewed in Section 1.5.5, little is known about the function of NM23-LV. NM23-LV is a member of the NDPK family and it possesses a H118 site crucial for NDPK activity which makes it likely that the main function of NM23-LV is to act as a kinase. However, to our knowledge, the role of NM23-LV as a kinase and furthermore its interaction with MDM2 have not been studied. Results presented in Figure 3.4.2.3.2 have suggested that it is difficult to detect any NDPK activity contributed by NM23-LV when NM23-LV was transfected in cells that are already abundant with NME proteins. Therefore, it is necessary to isolate NM23-LV from cellular NMEs when performing NDPK activity assay, in order to specifically measure NDPK activity contributed by NM23-LV alone. In light of this, we aimed to examine whether NM23-LV possesses any NDPK activity and/or interacts with MDM2 using the immunoprecipitation approach through a single experiment. The effect of MDM2 on NM23-LV NDPK activity was also investigated in this study.

H1299 cells were transfected with 36 μg of pCMV-HA-EV, 36 μg of pcDNA3.1-HA-NM23-LV, and 10 μg of pCMVNeoBam-MDM2 (as described in Figure 3.4.1.1) using GeneJuice. Transfected cells were harvested 48h post-transfection and was processed for the immunoprecipitation assay, as described in Section 2.16. As shown in Figure 3.4.1.1A, a striking MDM2 stabilisation was observed in cells co-transfected with HA-NM23-LV and MDM2 (Lane 4), despite having a lower transfection efficiency compared to that of in the absence of HA-NM23-LV (Lane 2), as illustrated by β-gal expression levels. Based on western blot of lysate samples shown in Figure 3.4.1.1C and E, HA-NM23-LV also appeared to be stabilised by MDM2, particularly when anti-NME1/2 (C1C3) antibody was used. As expected, Western blot of the samples immunoprecipitated with HA antibody (16B12), displays an approximately 28-kDa band in cells transfected with HA-NM23-LV (Figure 3.4.1.1D, Lanes 3 and 4) when probed with anti-HA (12CA5), indicating that NM23-LV has being immunoprecipitated. The presence of NM23-LV has also been shown when western blots for the immunoprecipitated samples were probed with anti-NME1/2 (C1C3) and anti-NME2 antibody (Figure 3.4.1.1F and G, respectively). As shown in Figure 3.4.1.1B, MDM2 was clearly detected in the samples immunoprecipitated with HA antibody (16B12), upon co-transfection with HA-NM23-LV (Lane 4), but not in the absence of HA-NM23-LV (Lane 2). This indicates that MDM2 co-immunoprecipitates with NM23-LV, suggesting that, at least, these two proteins exist in a complex in the lysate.

As shown in both Figure 3.4.1.1F and G, a noticeably greater amount of HA-NM23-LV has been immunoprecipitated in the presence of MDM2 (Lane 4), suggesting that MDM2 might have a role in stabilising NM23-LV. Interestingly, an approximately 17-kDa NME protein (as indicated by ◀) has also been pulled down with HA-NM23-LV (Figure 3.4.1.1F and G, Lanes 3 and 4), and also in greater abundance when cells were co-transfected with MDM2 (Lane 4). The 17-kDa band is most probably NME2 and not NME1, since a faint band at about 17 kDa (as indicated with ◁) could be detected using NME2 specific antibody (Figure 3.4.1.1 G, Lane 4), but not using NME1 specific antibody (Figure 3.4.1.1H, Lane 4). The presence of NME2 in Figure 3.4.1.1F, Lanes 3 and 4 could be as a result of NM23-LV oligomerisation with NME2. It is likely that the greater amount of NME2 that has been pulled down in Lane 4 is due to the interaction between NME2 and MDM2, since NME2 has been shown to interact with MDM2 [183].

The use of immunoprecipitation approach to isolate exogenous HA-NM23-LV for NDPK activity assay has demonstrated a negligible basal activity level in the absence of transfected HA-NM23-LV (Figure 3.4.1.1I). In the presence of both MDM2 and HA-NM23-LV, NDPK activity was significantly higher (93 U/ ml) in comparison to cells transfected with HA-NM23-LV alone (63 U/ ml). This suggests that MDM2 may promote NDPK activity of NM23-LV, probably as a result of NM23-LV up-regulation. However, the increase in NDPK activity could also be attributed to NME2 present in the immunoprecipitated samples, as indicated by ◀ in Figure 3.4.1.1F, Lanes 3 and 4.

Overall, this study has demonstrated that NM23-LV can be co-immunoprecipitated with MDM2 and is, at least, in the same complex with MDM2 within the cell lysate, suggesting that NM23-LV is likely to be an MDM2 interacting protein. More intriguingly, NM23-LV has been shown to strikingly up-regulate or stabilise MDM2. In addition, MDM2 seems to have an ability to up-regulate NM23-LV levels. The analysis of NDPK activity also suggests that there is a possibility that NM23-LV possess NDPK activity and that MDM2 could promote NDPK activity of NM23-LV, although further studies are required to examine this.

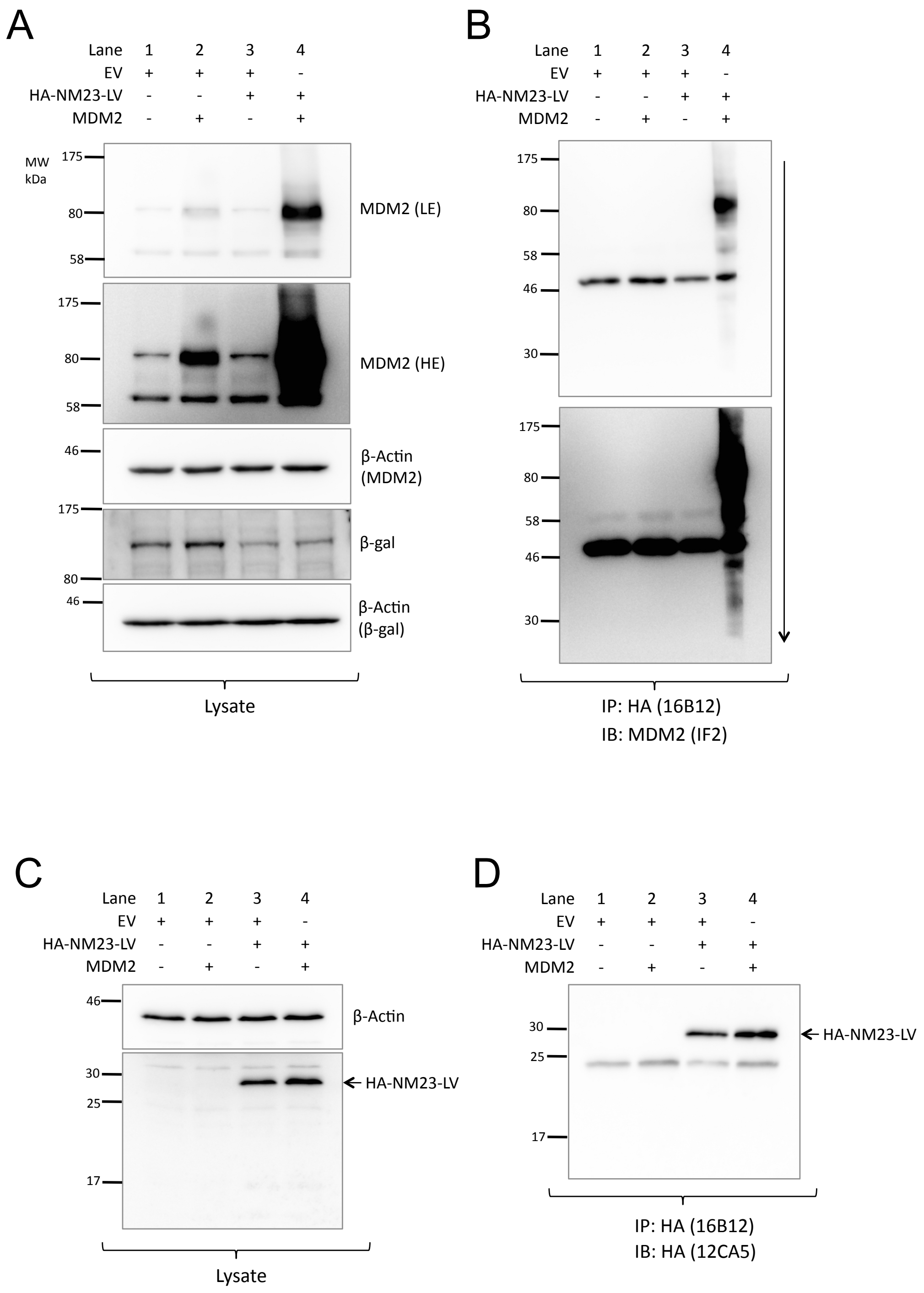

Figure 3.4.1.1 (To be continued):

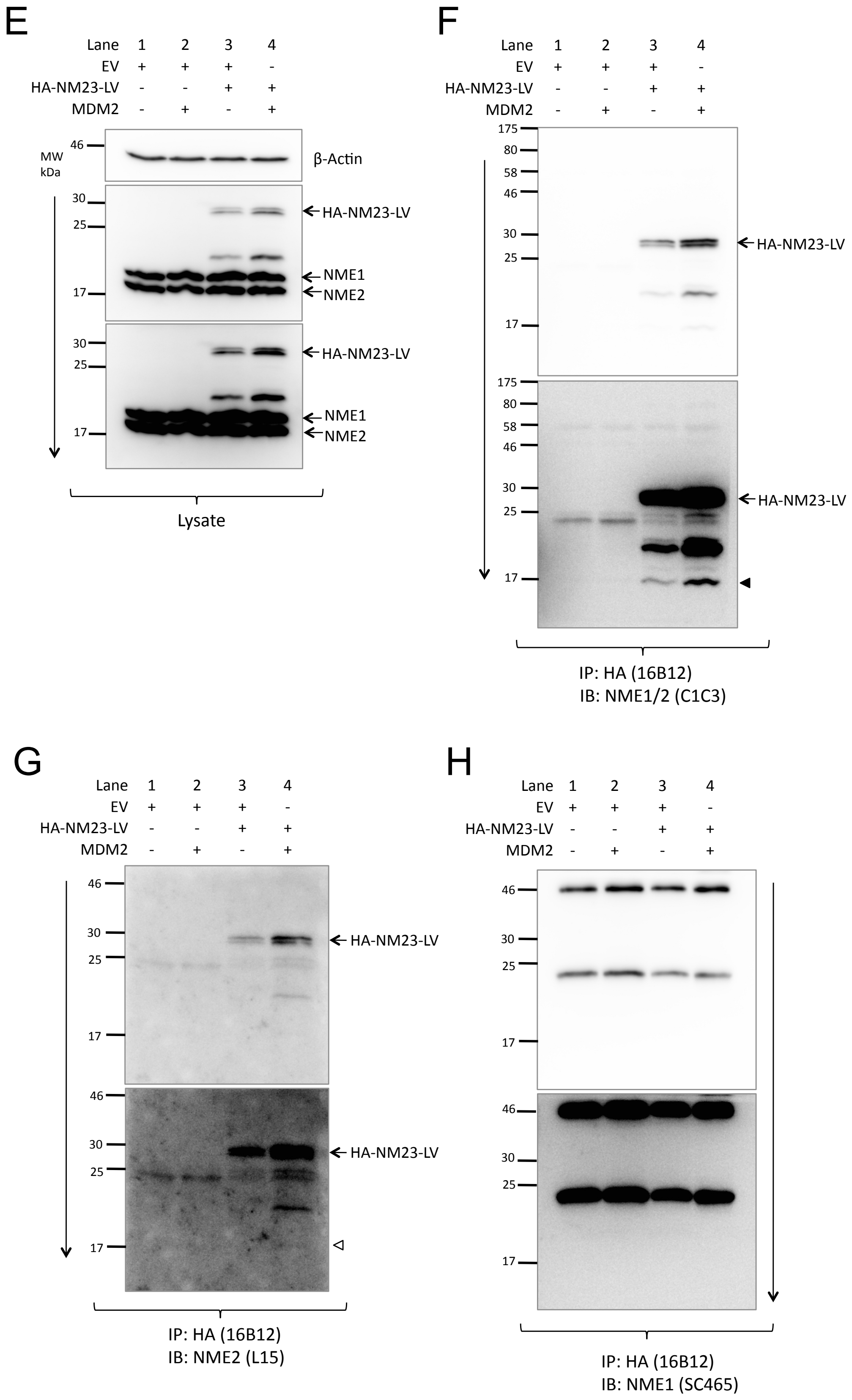

Figure 3.4.1.1 (To be continued):

I

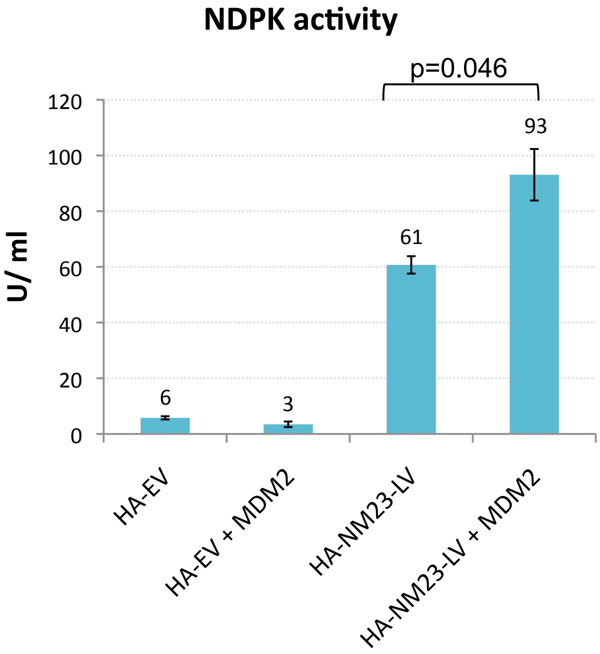

Figure 3.4.1.1: NDPK activity assay for HA-NM23-LV following immunoprecipitation. H1299 cells were transfected with 6 µg of pCMV-HA-EV, 36 µg of pcDNA3.1-HA-NM23-LV, and 10 µg of pCMVNeoBam-MDM2 in combinations in 15-cm dishes using GeneJuice. Transfected cells were harvested 48h post-transfection and divided into two aliquots. The first aliquot consisting of 10% of the samples was used for western blot analysis (Lysate), whereas the second aliquot containing the remaining samples was processed for the immunoprecipitation assay, as described in Section 2.16. 2 µg of anti-HA (16B12) antibody was added to the immunoprecipitation samples in order to allow antibody binding to HA-tagged NM23-LV (antigen) in the lysates. The samples were then incubated with Protein G Sepharose beads for 2h to capture the antibody/antigen complex on the beads. The washed beads were collected in two equal aliquots. One aliquot of the beads containing the immunoprecipitated proteins were re-suspended in 1x protein sample buffer for Western blotting analysis (IP panel). The second aliquot was added with 80 µl of RIPA lysis buffer and was immediately used for NDPK activity assay. **A, C,** and **E** represent Western blot of the lysate samples of the transfected cells, using **A.** anti-MDM2 (IF2), anti-β-actin (AC-15), and anti-β-gal (AB986) antibodies; **C.** anti-HA (12CA5) and anti-β-actin (AC-15) antibodies; **E.** anti-NME1/2 (C1C3) and anti-β-actin (AC-15) antibodies.

B, D, F, G, and **H** represent proteins purified with anti-HA (16B12) antibody on Protein G Sepharose beads, followed by immunoblotting with **B.** anti-MDM2 (IF2) antibody; **D.** anti-HA (12CA5) antibody; **F.** anti-NME1/2 (C1C3) antibody; **G.** anti-NME2 (L15); and **H.** anti-NME1 (SC465) antibodies. Note that only about half of Lane 4 (**B**) is shown due to human error. Downward arrows indicate low to high exposures. **I.** NDPK activity assay for the immunoprecipitated samples (n=3). P-values were derived from statistical analyses by Student's *t*-test. Error bars indicate standard errors. IP, Immunoprecipitation; IB, Immunoblotting.

3.4.2 Examination of NDPK activity of immunoprecipitated HA-tagged NME2 and NM23-LV in HNME2:Cl.7

Results presented in Section 3.4.1 suggest that it is likely that NM23-LV possesses NDPK activity and that MDM2 could promote NDPK activity of NM23-LV. However, we could not eliminate the possibility that the NDPK activity detected might be contributed, at least in part, by pulled down endogenous NME2, since NME2 can interact with both MDM2 and NM23-LV. Therefore, we aimed to perform an immunoprecipitation-NDPK activity assay experiment similar to one described in Section 3.4.1, except for using stable NME2 knockdown clones of H1299 parental cell line (HNME2:Cl.7). Characterisation of this cell line was described in Figure 3.2.4.1. We hypothesised that in the absence (or with negligible amount) of NME2 in the cells, the possibility of NME2 being pulled down with HA-tagged NM23-LV would be almost non-existent. Therefore, any NDPK activity detected from the immunoprecipitated samples would be solely contributed by NM23-LV.

HNME2:Cl.7 cells were transfected with an increasing amount of pcDNA3.1-HA-NM23-LV and 6 μg of pCEP4-HA-NME2, as described in Figure 3.4.2.1, using GeneJuice. pCMV-HA-EV was included as a negative control whereas HA-NME2 served as a positive control. The amount of HA-NME2 used was adjusted for comparison with HA-NM23-LV. Transfected cells were harvested 48h post-transfection and processed for immunoprecipitation and NDPK assay, as described in Figure 3.4.1.1.

Western blot analyses of lysate samples in Figure 3.4.2.1A and B showed that the levels of HA-NM23-LV were considerably lower in comparison to HA-NME2 levels, even though the amounts of HA-NM23-LV plasmids used for transfection were higher than HA-NME2 (Lanes 2, 3 and 4). When this experiment was designed, we wanted to minimise the amount of background NME2 and indeed, only a negligible amount of NME2 was present in the cells (Figure 3.4.2.1B). Note that there was a shift in HA-NME2 to approximately the same position as that of NME1 and this resulted in saturation of signal, as indicated by (*) in Figure 3.4.2.1B, Lane 4. Furthermore, as expected, the level of NM23-LV and NME2 proteins detected was consistent with their protein expression seen on western blots of the HA-immunoprecipitated samples using either anti-HA (12CA5) or anti-NME1/2 (C1C3) antibodies (Figure 3.4.2.1C and D, respectively). A very faint band of what could be NME2 protein was detected both in cells transfected with HA-EV and HA-NM23-LV, and these bands seem to be at similar signal intensities. As shown in Figure 3.4.2.1G, NDPK activity increases with the amount of HA-NM23-LV transfected, with 8 U/ ml and 14 U/ ml for 12 μg and 36 μg of HA-NM23-LV, respectively. On the contrary, NDPK activity for HA-NME2 (6 μg) was recorded at 43 U/ ml, which is about 3.3-fold higher than that observed in cells transfected with 36 μg of HA-NM23-LV. However, when comparing the signal intensity of 6 μg of HA-NME2 and 36 μg of HA-NM23-LV using densitometry analysis (Figure 3.4.2.1C and D), the signal for HA-NME2 proteins detected was at least 6.9-fold higher in the presence of HA-NM23-LV, using anti-NME1/2 antibodies for western blotting (Figure 3.4.2.1D, bands 'g' and 'h'). Therefore, taking the protein expression levels of these immunoprecipitated HA-tagged proteins into account, it is not unreasonable to conclude that NM23-LV could potentially contribute to NDPK activity at least two-fold higher than NME2, when an equal amount of NM23-LV and NME2 were used for NDPK activity assay.

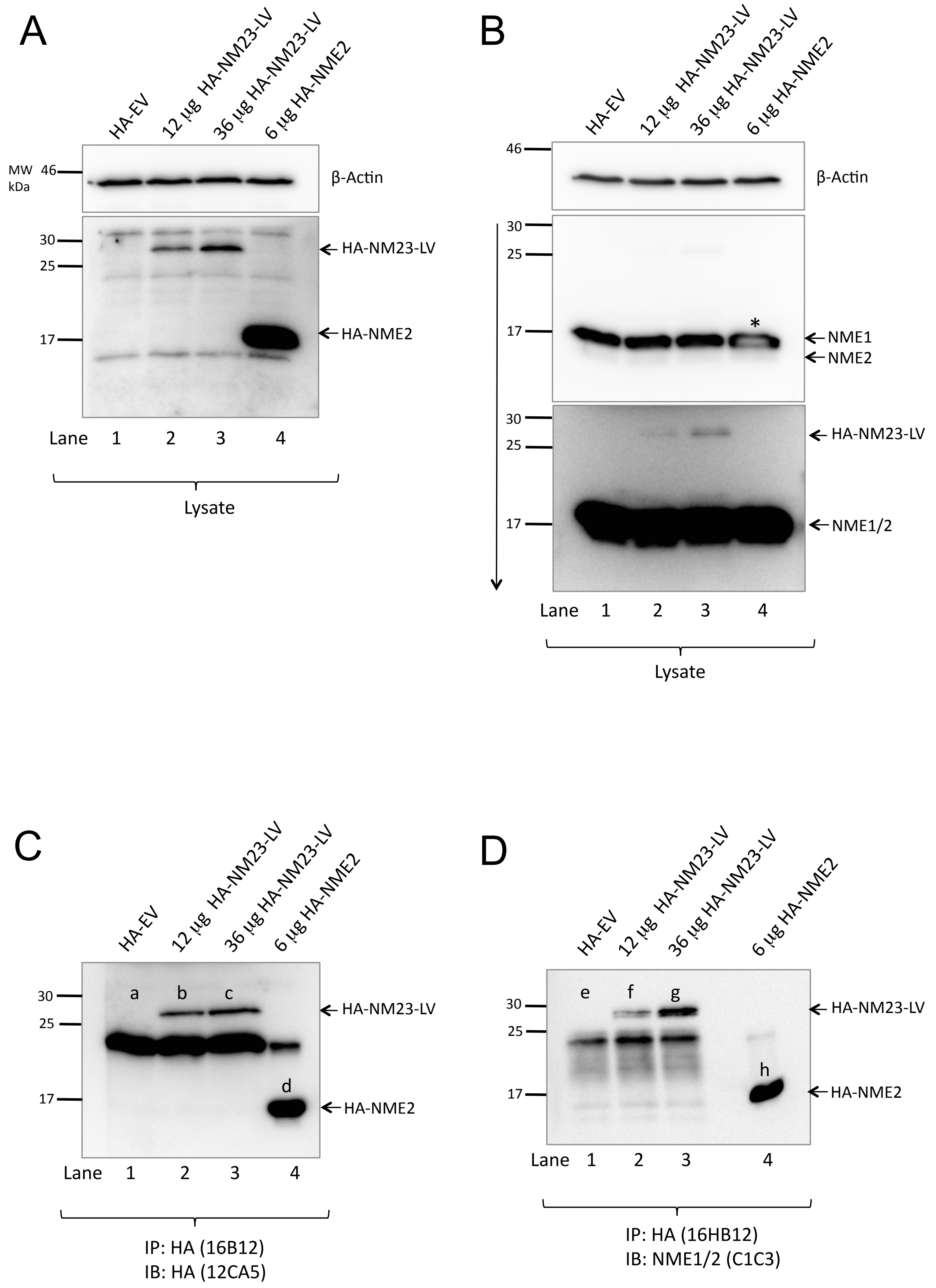

Figure 3.4.2.1 (To be continued):

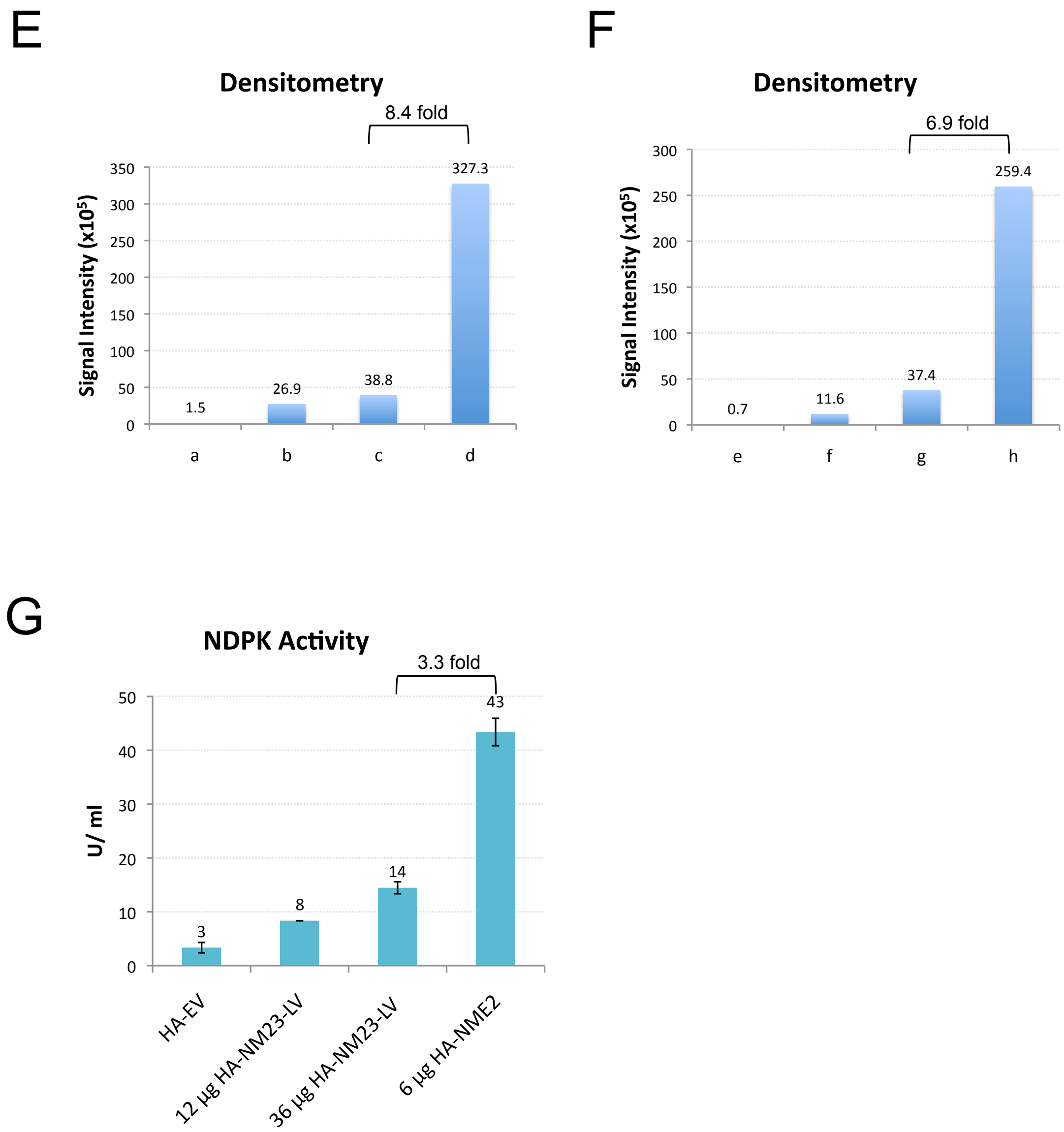

Figure 3.4.2.1: Examination of NDPK activity of immunoprecipitated HA-tagged NME2 and NM23LV in HNME2:Cl.7. NME2 stable knockdown clone, HNME2:Cl.7, was transfected with 12 µg or 36 µg of pcDNA3.1-HA-NM23-LV and 6 µg of pCEP4-HA-NME2 in 10-cm dishes using GeneJuice. pCMV-HA-EV was included as a negative control whereas HA-NME2 serves as a positive control. The amount of HA-NME2 used was adjusted for comparison with HA-NM23-LV. Transfected cells were harvested 48h post-transfection and processed for immunoprecipitation and NDPK assay, as described in Figure 3.4.1.1. **A** and **B** represent Western blot of the lysate samples of the transfected cells, using **A.** anti-

HA (12CA5) and anti-β-actin (AC-15) antibodies; and **B.** anti-NME1/2 (C1C3) and anti-β-actin (AC-15) antibodies. (*) represents a shift in HA-NME2 to approximately the same position of NME1 and thus resulting in saturation of signal. **C** and **D** represent proteins purified with anti-HA (16B12) antibody on Protein G Sepharose beads, followed by immunoblotting with **C.** anti-HA (12CA5); and **D.** anti-NME1/2 (C1C3) antibodies; **E** and **F** correspond to densitometry analysis of the immunoprecipitated HA-tagged proteins as alphabeted in Western blots in **C** and **D**, respectively**.** Downward arrows indicate low to high exposures. **G.** NDPK activity for HA-immunoprecipitated samples (n=3). P-values were derived from statistical analyses by Student's *t*-test. Error bar indicates standard error. IP, Immunoprecipitation; IB, Immunoblotting.

3.4.3 Analysis of the effect of MDM2 on NDPK activity of NM23-LV in NME2 knockdown clones

Results presented in Sections 3.4.1 suggest that MDM2 is likely to promote NM23-LV NDPK activity. However, the experiment shown in Figure 3.4.1.1 was performed in H1299 cells, which contain a high level of endogenous NME2. The presence of this endogenous NME2 could contaminate immunoprecipitated HA-tagged NM23-LV used for NDPK activity assay, making interpretation of NDPK activity measured difficult. Data described in Section 3.4.2 have demonstrated that stable NME2 knockdown clone HNME2:Cl.7 can be used in order to reduce cellular NME2 levels for immunoprecipitation-NDPK activity assay for HA-NM23-LV. Therefore, we aimed to examine the effects of MDM2 on NM23-LV NDPK activity in HNME2:Cl.7.

HNME2:Cl.7 cells were transfected with pCEP4-HA-EV, 12 μg of pcDNA3.1-HA-NM23-LV, and 3.5 μg of pCMVNeoBam-MDM2, as described in Figure 3.4.3.1, using GeneJuice. Transfected cells were harvested 48h post-transfection and processed for immunoprecipitation and NDPK assay, as described in Figure 3.4.1.1. Based on western blot analyses of the lysates samples, MDM2 does not appear to have any effect on NM23-LV expression levels (Figure 3.4.3.1A, Lanes 2 and 3), unlike previous results presented in Figure 3.4.1.1E. However, the up-regulation effect of MDM2 on NM23-LV levels becomes more obvious when the levels of immunoprecipitated NM23-LV (Figure 3.4.3.1B, Lanes 2 and 3) were analysed. Consistent with our findings that MDM2 can co-immunoprecipitate with NM23-LV (Figure 3.4.1.1B), MDM2 was also pulled down with HA-NM23-LV (Figure 3.4.3.1B, Lane 3).

NDPK activity was detected in the presence of NM23-LV even in the absence of endogenous NME2 in the immunoprecipitated samples, suggesting that the NDPK activity measured was genuinely contributed by NM23-LV. Furthermore, NDPK activity level increases in the presence of MDM2 ($p=0.0446$), suggesting a role of MDM2 in promoting NDPK activity of NM23-LV. It is therefore possible that the increase in NDPK activity is as a result of MDM2-mediated stabilisation of NM23-LV.

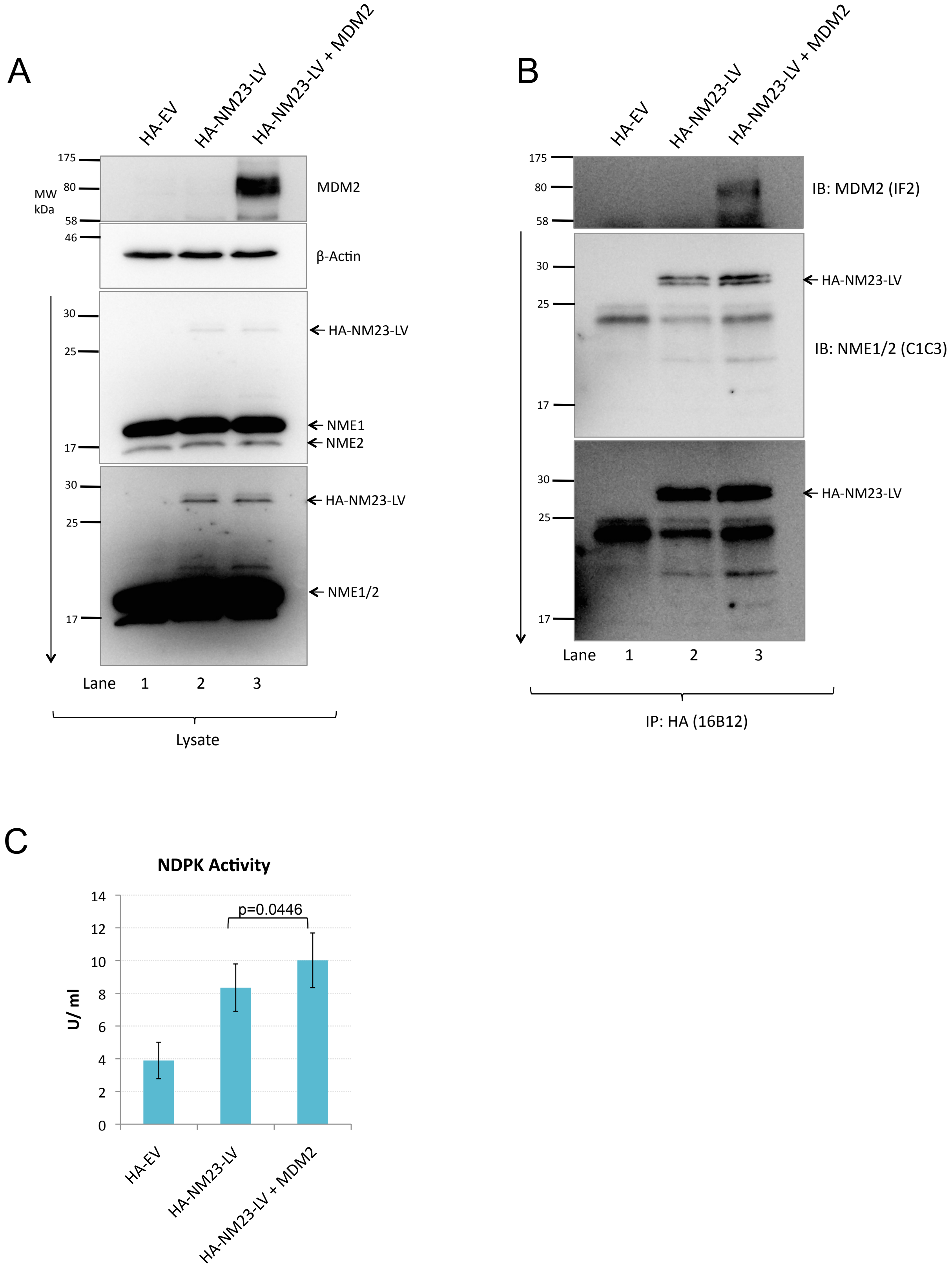

Figure 3.4.3.1: Examination of the effects of MDM2 on NM23-LV NDPK activity in NME2 knockdown clones. HNME2:Cl.7 cells were transfected in combinations with pCEP4-HA-EV, 12 μg of pcDNA3.1-HA-NM23-LV, and 3.5

μg of pCMVNeoBam-MDM2, in 10-cm dishes using GeneJuice. All transfected samples included a plasmid that expresses β-gal (1 μg) to enable comparison of transfection efficiency. Transfected cells were harvested 48h post-transfection and processed for immunoprecipitation and NDPK assay, as described in Figure 3.4.1.1. **A.** Western blot for lysate samples of the transfected cells, illustrating the steady-state levels of the indicated proteins. Actin serves as loading control. Primary antibodies used were anti-β-actin (AC-15), anti-MDM2 (IF2), anti-NME2 (L15) and anti-β-gal (AB986). **B.** Western blot for protein samples purified with anti-HA (16B12) antibody on Protein G Sepharose beads using anti-MDM2 (IF2) and anti-NME1/2 (C1C3) antibodies. Downward arrows indicate low to high exposures. **C.** NDPK activity for HA-immunoprecipitated samples (n=3). P-values were derived from statistical analyses by Student's *t*-test. Error bar indicates standard error.

3.4.4 Investigation of the effect of NM23-LV on p53 protein levels in H1299 and double null MEFs

Results presented in Section 3.4.1 have indicated that NM23-LV is able to stabilise or up-regulate MDM2 levels. Since MDM2 is one of the main regulators of p53, we wanted to examine whether NM23-LV has any effect on p53 protein levels. Considering the stabilising effect NM23-LV has on MDM2, the expectation was that NM23-LV would down-regulate p53.

To test this, p53-null H1299 cells were transfected with pCEP4-p53, pCMVNeoBam-MDM2 and pcDNA3.1-NM23-LV using GeneJuice, as described in Figure 3.4.4.1. 48h post transfection, cells were harvested and processed for SDS-PAGE and western blotting. Consistent with previous observations in this thesis (Figure 3.4.1.1A), co-transfection of MDM2 with NM23-LV leads to a marginal increase in NM23-LV levels and a dramatic increase in MDM2 levels (Figure 3.4.4.1A, Lane 4). As expected, MDM2 transfection leads to p53 down-regulation in the cells, as observed in Figure 3.4.4.1A, Lane 2. In addition, p53 levels decreased considerably more when both NM23-LV and MDM2 were transfected (Lane 4). This could be explained by the increase in the amount of MDM2 in the cells as a result of stabilisation by transfected NM23-LV. Interestingly, down-regulation of p53 by NM23-LV does not seem to be dependent upon MDM2 since a noticeable reduction in p53 levels has also been observed in cells transfected with NM23-LV (Figure 3.4.4.1A, Lane 3). However, it is possible that the observed reduction in p53 levels was due an increase in endogenous MDM2 level induced by transfected NM23-LV, even though the increase in MDM2 level could not be detected on western blot (Figure 3.4.4.1A, Lanes 1 and 3).

To examine whether the inhibitory effect of NM23-LV on p53 level was indeed MDM2-independent, the experiment was repeated using mouse embryonic fibroblasts that are null for both p53 and MDM2 ($p53^{-/-}$, $Mdm2^{-/-}$), called double null MEFs. However, as shown in Figure 3.4.4.1B, the transfection efficiency for the transfection performed in double null MEFs was very low. It was difficult to detect the expression of transfected plasmids on western blots even when 80 μg of protein samples (50 μg are normally used) were loaded into each lane for SDS-PAGE. An exception to this was p53, as p53 was clearly detected in transfected cells, suggesting that transfection did occur. In addition, despite the poor transfection efficiency, the same effect of NM23-LV on p53 as demonstrated in H1299 (Figure 3.4.4.1A) has also been observed in double null MEFs. In addition, as shown in Figure 3.4.4.1A, Lane 3, NM23-LV seems to be able to down-regulate p53 levels in a MDM2-independent manner. Therefore, based on the results observed in H1299 and double null MEFs, it is likely that NM23-LV can down-regulate p53 in a MDM2-independent manner.

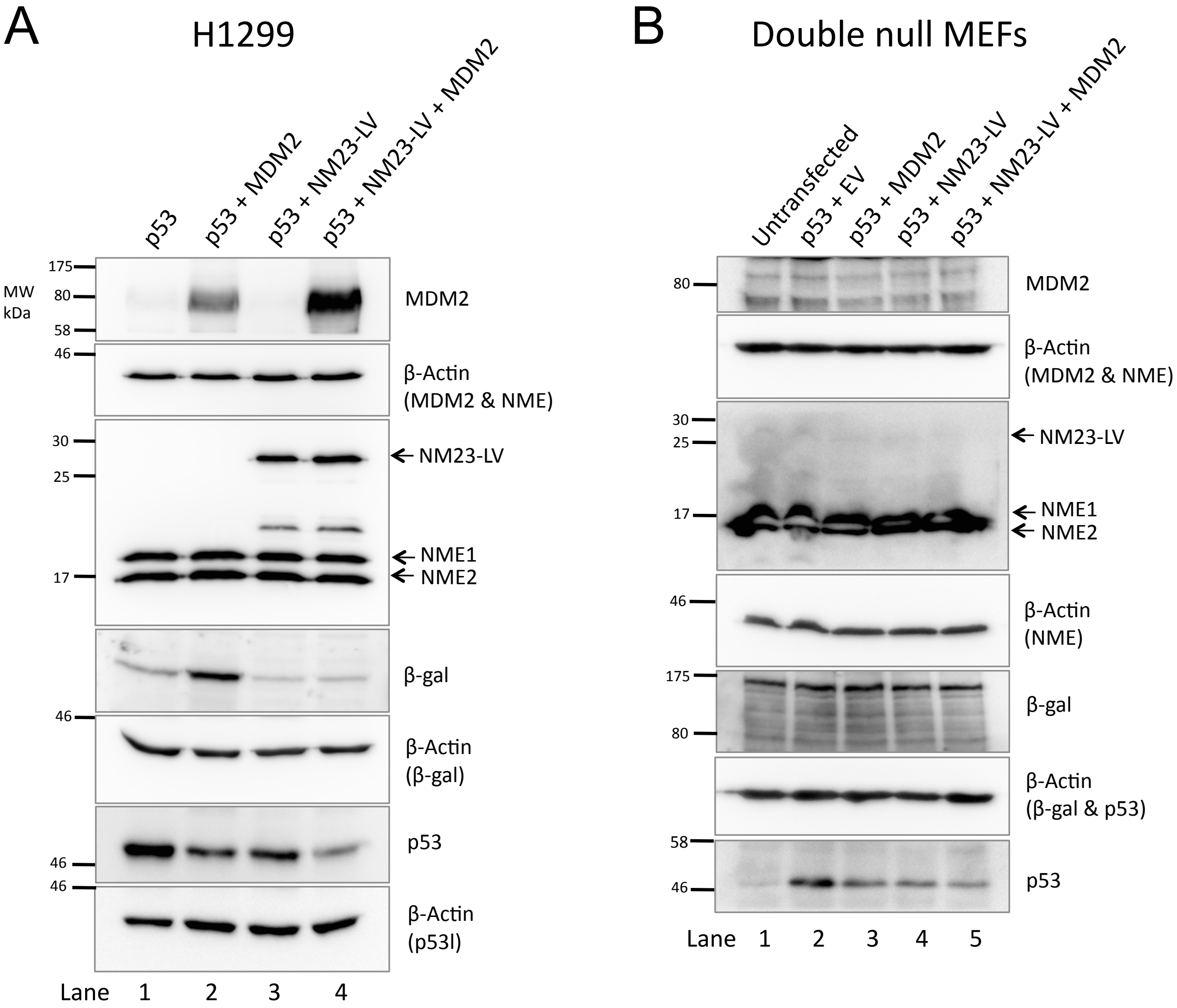

Figure 3.4.4.1: Investigation of the effect of NM23-LV on p53 protein levels in H1299 and double null MEFs. H1299 or mouse embryonic fibroblasts double null MEFs (p53$^{-/-}$, Mdm2$^{-/-}$) cells were transfected with 0.2 μg of pCEP4-p53, 0.67 μg pCMBNeoBam-MDM2 and 2.4 μg pcDNA3.1-NM23-LV in each well of a 6-well plate using GeneJuice (for H1299) or Lipofectamine 2000 (for double null MEFs). All transfected samples included a plasmid that expresses β-gal (0.15 μg) to enable comparison of transfection efficiency. 48h post-transfection, cells were harvested and processed for SDS-PAGE and western blotting. **A.** Western blot for lysate samples of transfected H1299 cells (protein samples loaded at 50 μg/well) **B.** Western blot for lysate samples of transfected double null MEFs (protein samples loaded at 80 μg/well). Primary antibodies used were anti-β-actin (AC-15), anti-MDM2 (IF2), anti-p53 (DO-1), anti-NME1/2 (C1C3), and anti-β-gal (AB986). This experiment was performed twice with consistent results.

3.4.5 Examination of NM23-LV effects on p53 transcriptional activity

Our data presented in in Section 3.4.4 suggest that NM23-LV may play a role in p53 down-regulation. To determine whether NM23-LV can exert an effect on p53 transcription activity, luciferase assay was performed in p53-null H1299 and double null MEFs ($p53^{-/-}$, $Mdm2^{-/-}$) in triplicate wells of a 48-well plate. Cells were transfected with pGL4.11-p53RELuc-2, pRL-TK, pCEP4-p53, pCMVNeoBam-MDM2, pcDNA3.1-NM23-LV as described in Figure 3.4.5.1. Transfected cells were harvested 16h and 24h post-transfection and processed for luciferase assay, as described in Materials and Methods (Section 2.8). The activity of the *Renilla* luciferase serves as an internal control for the transfection efficiency. As wild-type p53 was reported to modulate the activity of some promoters [397], including HSV-TK used in this study for *Renilla* expression, it is necessary to analyse our results with caution. In experiments shown in Figure 3.4.5.1A and B, although co-transfection of p53 and NM23-LV leads to a massive reduction in luminescence, it appears that *Renilla* activity also seems to decrease. Therefore, instead of normalising the firefly luciferase activity to *Renilla* activity as recommended by the manufacturer, the two luciferase activities were presented side by side for comparison. However, since the activity levels of *Renilla* activity were considerably lower than firefly luciferase activity, it is difficult to visualise *Renilla* activity on the graph, and thus a chart showing the amount of *Renilla* activity was also presented.

The luciferase activity profiles for H1299 were similar at both 16h and 24h, except that *Renilla* activity at 24h was uneven (Figure 3.4.5.1A and B). As expected, the positive control plasmid p53-RE-luc2 was considerably induced following co-transfection with p53 in both H1299 and double null MEFs at both 16h and 24h (Figure 3.4.5.1). Also, as expected, the presence of MDM2 results in a drop in luciferase luminescence. The presence of NM23-LV alone in H1299 at both 16h and 24h seems to reduce p53 activity to its basal level, comparable to that of EV. However, this effect is likely due to the lower transfection efficiency, as suggested by the corresponding *Renilla* activities. Therefore, it is difficult to conclude whether NM23-LV has any suppressive effect on p53 transcriptional activity. However, with similar *Renilla* activity at 16h, the presence of both NM23-LV and

MDM2 in H1299 leads to a massive reduction in luciferase activity to a level lower than in the presence of MDM2 alone (Figure 3.4.5.1A).

In double null MEFs, transfection efficiency and luciferase activity profiles for both 16h and 24h were relatively similar. Contrary to the results seen in H1299, no significant reduction in p53 activity was observed in the presence of NM23-LV. However, consistent to H1299, NM23-LV co-transfection with MDM2 in MEFs also results in a considerable decrease in luciferase activity (Figure 3.4.5.1C and D). These results indicate that NM23-LV alone is unlikely to exert inhibitory effect on p53 activity, but may act synergistically with MDM2 to inhibit p53 activity.

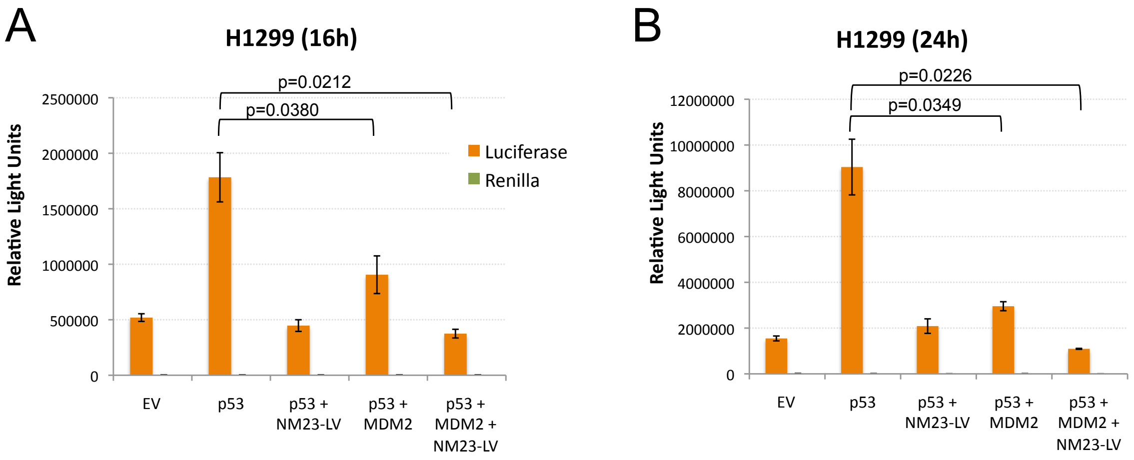

H1299 (16H))	Renilla (RLU)
EV	2929
p53	2692
p53 + NM23-LV	1440
p53 + MDM2	2702
p53 + MDM2 + NM23-LV	2158

H1299 (24H)	Renilla (RLU)
EV	10517
p53	8183
p53 + NM23-LV	4482
p53 + MDM2	7598
p53 + MDM2 + NM23-LV	3577

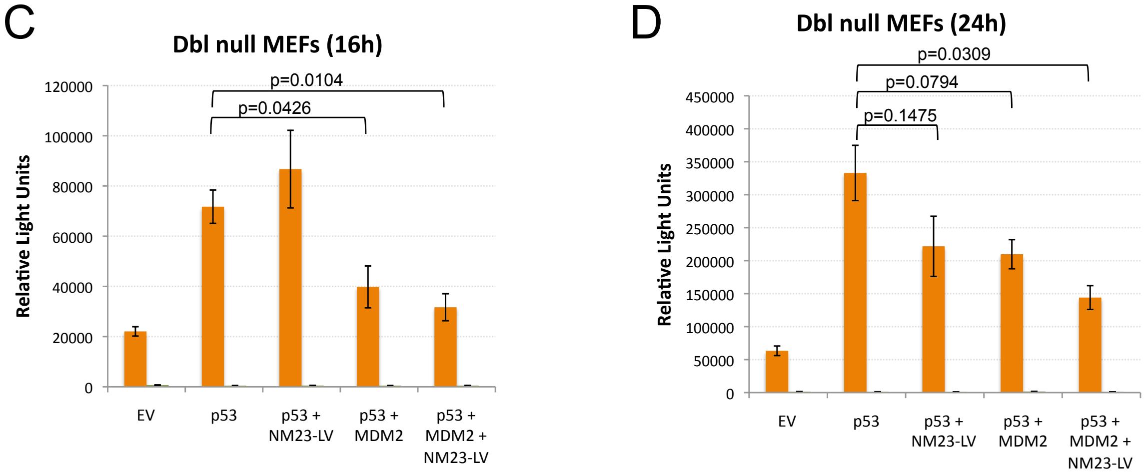

Dbl null MEFs (16H)	Renilla (RLU)
EV	677
p53	454
p53 + NM23-LV	495
p53 + MDM2	458
p53 + MDM2 + NM23-LV	475

Dbl null MEFs (24H)	Renilla (RLU)
EV	1376
p53	1199
p53 + NM23-LV	1019
p53 + MDM2	1688
p53 + MDM2 + NM23-LV	1112

Figure 3.4.5.1: Luciferase assay for examining the effect of NM23-LV on p53 transcriptional activity. Luciferase assay was performed in p53-null H1299 and double null MEFs ($p53^{-/-}$, $Mdm2^{-/-}$) in triplicate wells of a 48-well plate. Cells were transfected with 170 ng pGL4.11-p53RELuc-2, 17 ng pRL-TK, 5 ng pCEP4-p53, 10 ng pCMVNeoBam-MDM2, 75 ng pcDNA3.1-NM23-LV in combinations. Transfected cells were harvested 16h and 24h post-transfection and processed for

luciferase assay, as described in Materials and Methods (Section 2.8). **A** and **B** represent luciferase assay performed in H1299 cells at 16h and 24h post-transfection, respectively. **C.** and **D.** represent luciferase assay performed in double null MEFs at 16h and 24h post-transfection, respectively.

3.4.6 Analysis of the effects of NM23-LV on cell motility using Boyden chamber

NME proteins are well known for their non-metastatic properties, and thus we wanted to examine whether NM23-LV, as a member of the NME family, has any effects on cell motility. Boyden chamber motility assay was performed as described in Materials and Methods (Section 2.11) to examine the effect of NM23-LV on cell motility. H1299 cells were transfected with plasmids expressing either EV or NM23-LV in triplicates using GeneJuice, as described in Figure 3.4.6.1. Cells were harvested for Boyden chamber assay and western blot analysis 24h post-transfection. Interestingly, cells transfected with NM23-LV (Figure 3.4.6.1A) were shown to have significantly higher motility than EV (p=0.0064) (Figure 3.4.6.1B). In other words, in the presence of NM23-LV, there was a significantly higher number of cells that managed to travel through the membrane pores, as illustrated in Figure 3.4.6.1C.

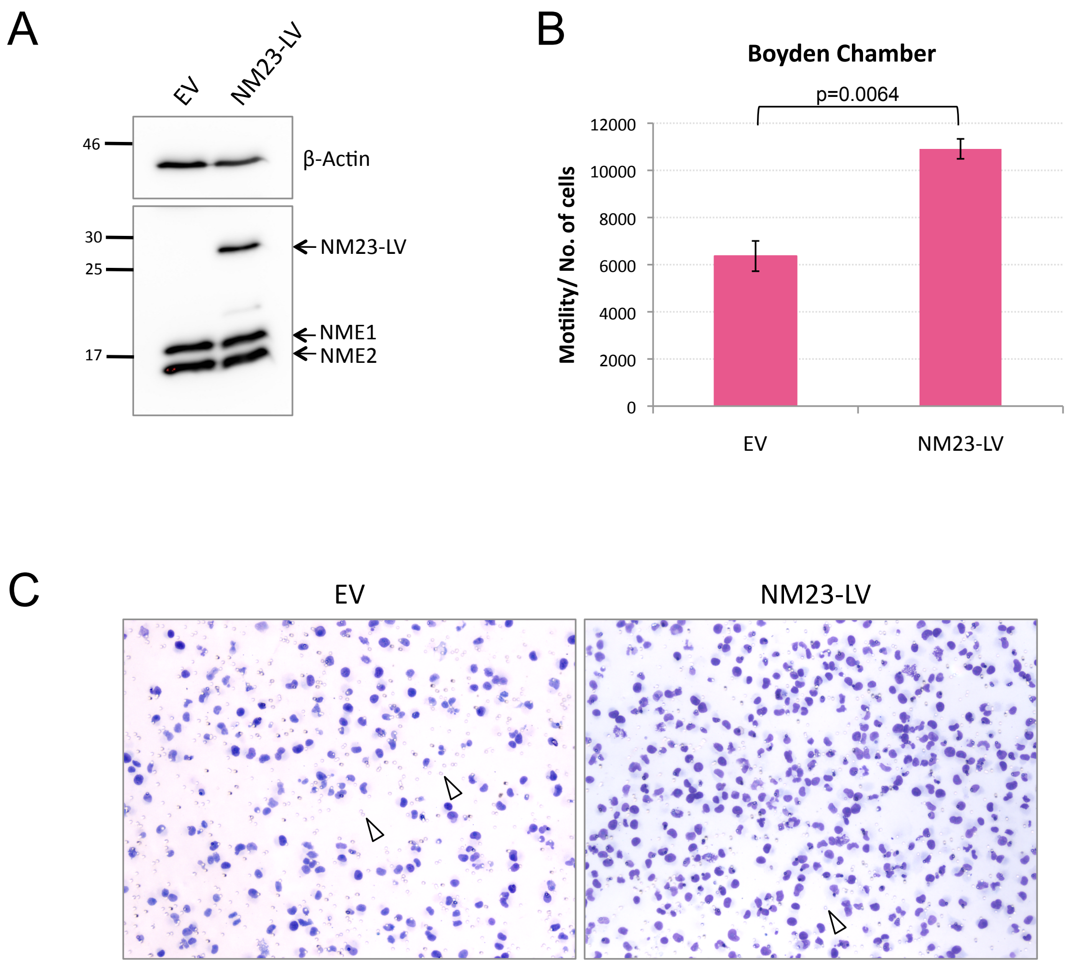

Figure 3.4.6: Boyden chamber motility assay for NM23-LV. To examine the effect of NM23-LV on cell motility, Boyden chamber motility assay was performed as described in Materials and Methods (Section 2.11). H1299 cells were transfected with 1 μg of pcDNA3.1-EV or pcDNA3.1-NM23-LV in each well of a 6-well plate using GeneJuice. Transfection was performed in triplicate. Cells were harvested for Boyden chamber assay and Western blot analysis 24h post-transfection. **A.** Western blot for lysate samples of the transfected cells, illustrating the steady-state levels of the indicated proteins. Primary antibodies used were anti-β-actin (AC-15), and anti-NME1/2 (C1C3). **B.** Analysis for Boyden chamber motility assay. **C.** Haematoxylin and eosin staining of the porous membranes excised from Boyden chamber after 18h of incubation. Cells that have travelled through the membrane would attach to the membrane and be stained for counting. Pictures were taken at randomly selected positions of stained membranes (Magnification: x10). Arrows indicate the membrane pores. This experiment was performed twice with consistent results.

3.4.7 Characterisation of NME fusion proteins

Fluorescent proteins are often used to tag a protein of interest in order to study the biology of proteins of interest *in vivo*. In order to study more functional implications of NM23-LV, constructs expressing fluorescence-labelled NME fusion proteins were generated, as described in Section 2.1.10.1. We aimed to fuse NME with enhanced cyan/yellow fluorescent proteins (ECFP/EYFP), which are variants of GFP with enhanced fluorescence properties, to study NME proteins behaviour in cells, particularly NM23-LV sub-cellular distribution and interactions with other proteins. ECFP is a blue-shifted emission variant of GFP whereas EYFP is a red-shifted emission variant of GFP. EYFP and ECFP were selected because they function as donor-acceptor pair for fluorescence resonance energy transfer (FRET), which could be used for monitoring direct protein-protein interactions between EYFP and ECFP fusion proteins in living or fixed cells [398]. In order to generate a functional and properly folded fluorescent fusion protein, two constructs were designed for each NME, one construct would contain NME at the C-terminal and the other at the N-terminal, since many proteins fold with their C- and N-terminals exposed on the protein surface, rather than embedded in the protein core [399, 400]. A small linker of 7-15 aa was included between the fluorescent protein and the NME protein, to provide flexibility and to promote proper folding and functioning of the two proteins [400].

As described in Materials and Methods (Section 2.1.10.1), constructs that express fluorescence-labelled NME fusion proteins, NME1, NME2, NME2H118F and NM23-LV were generated by cloning these NMEs into pEYFP and pECFP vectors, resulting in both C- and N- terminally fluorescence-tagged forms of NMEs, as illustrated in Figure 2.1.9.1.1. Following NME fragments being subcloned into pEYFP and pECFP vectors at ECoRI and BamHI restriction sites, the constructs were excised at these two restriction sites to check for insertions (Appendix 10).

Expression of the NME fusion constructs was also examined using fluorescence microscopy and western blotting (Figure 3.4.7.1). H1299 cells were transfected with each of these fusion constructs using GeneJuice. Plasmids expressing C-

ECFP, C-EYFP, N-ECFP and N-EYFP were included as controls. 24h post-transfection, cells were imaged using a fluorescence microscope before being harvested for Western blot analysis. As shown in Figure 3.4.7.1, cells transfected with NME fusion plasmids all expresses their corresponding fluorescent proteins. In general, NME proteins seem to fluoresce better when fused to C-terminal of ECFP/EYFP and fluorescence for NM23-LV fusion proteins was poorly detected. Molecular mass for EYFP/ECFP should be at 27 kDa using anti-GFP antibody. Thus NME1, NME2 and NME2H118F fusion proteins should each have a molecular mass at about 44 kDa, whereas NM23-LV fusion protein is expected to have a molecular mass at approximately 55 kDa. Western blot analyses using anti-GFP and different antibodies specific for each NMEs demonstrated bands that represent the fusion proteins (Figure 3.4.7.1). A summary of antibodies with their detectable NME fusion proteins is represented in Table 3.4.7.1. There seems to be a truncation of fusion proteins as observed on Western blots probed with anti-GFP antibody (Figure 3.4.7.1A). This was a cause for concern, since it might be possible that fluorescence detected may not actually be coming from NME fusion proteins. However, since different distribution of fluorescence was observed in cells transfected with fluorescence-tagged NME, compared to ECFP or EYFP controls (which have even distribution throughout the cells), it is likely that most of the fluorescence detected in cells represents the expression of NME fusion proteins.

Since C-EYFP-NM23-LV can be detected by both anti-GFP and anti-NME1/2 (C1C3) antibodies at appropriate molecular weights on western blot (Figure 3.4.7.1A and C) and its fluorescence expression was better than the other fluorescence-labelled NM23-LV, C-EYFP-NM23-LV and other C-EYFP fusion proteins were used for future transfection experiments.

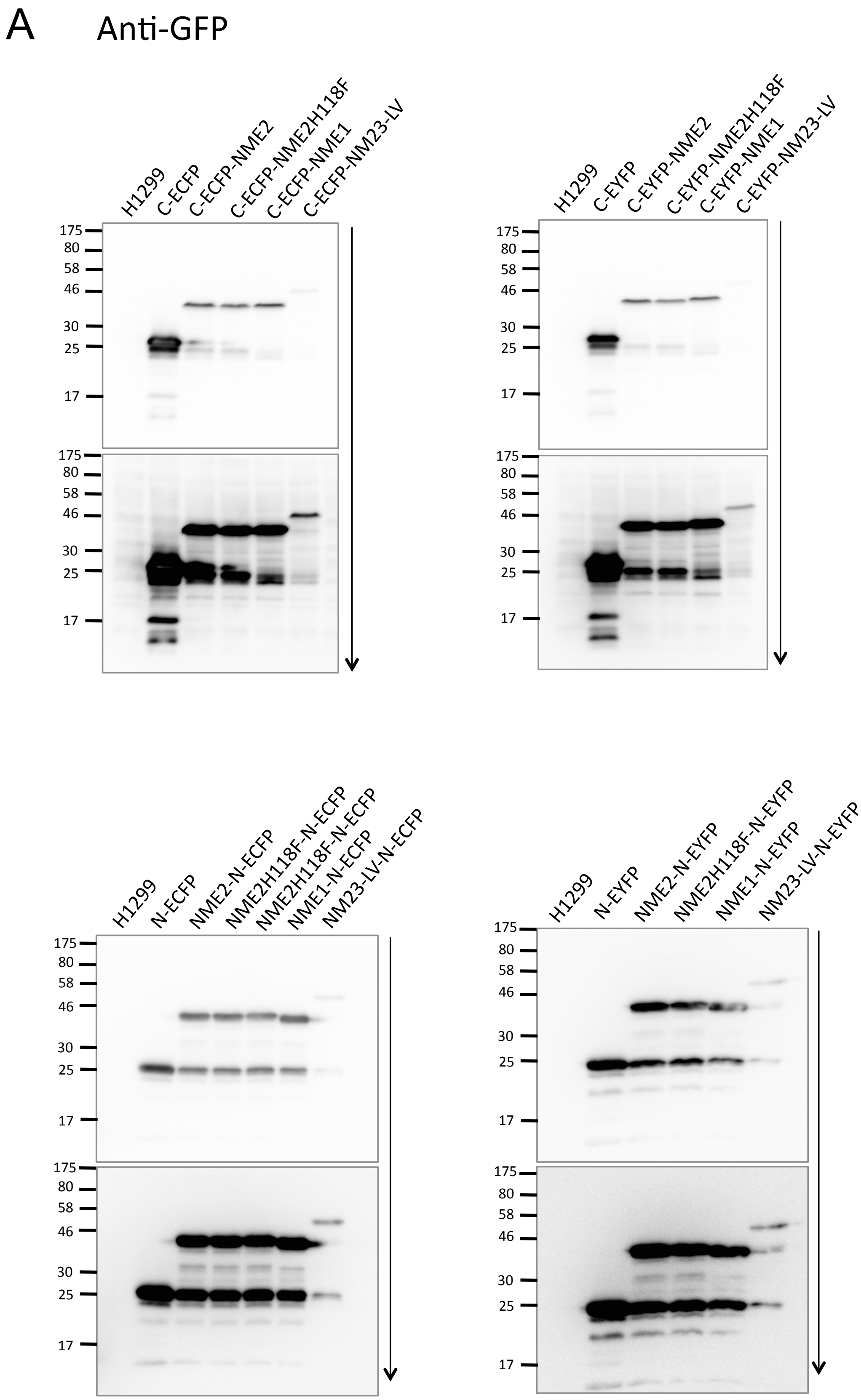

Figure 3.4.7.1 (To be continued)

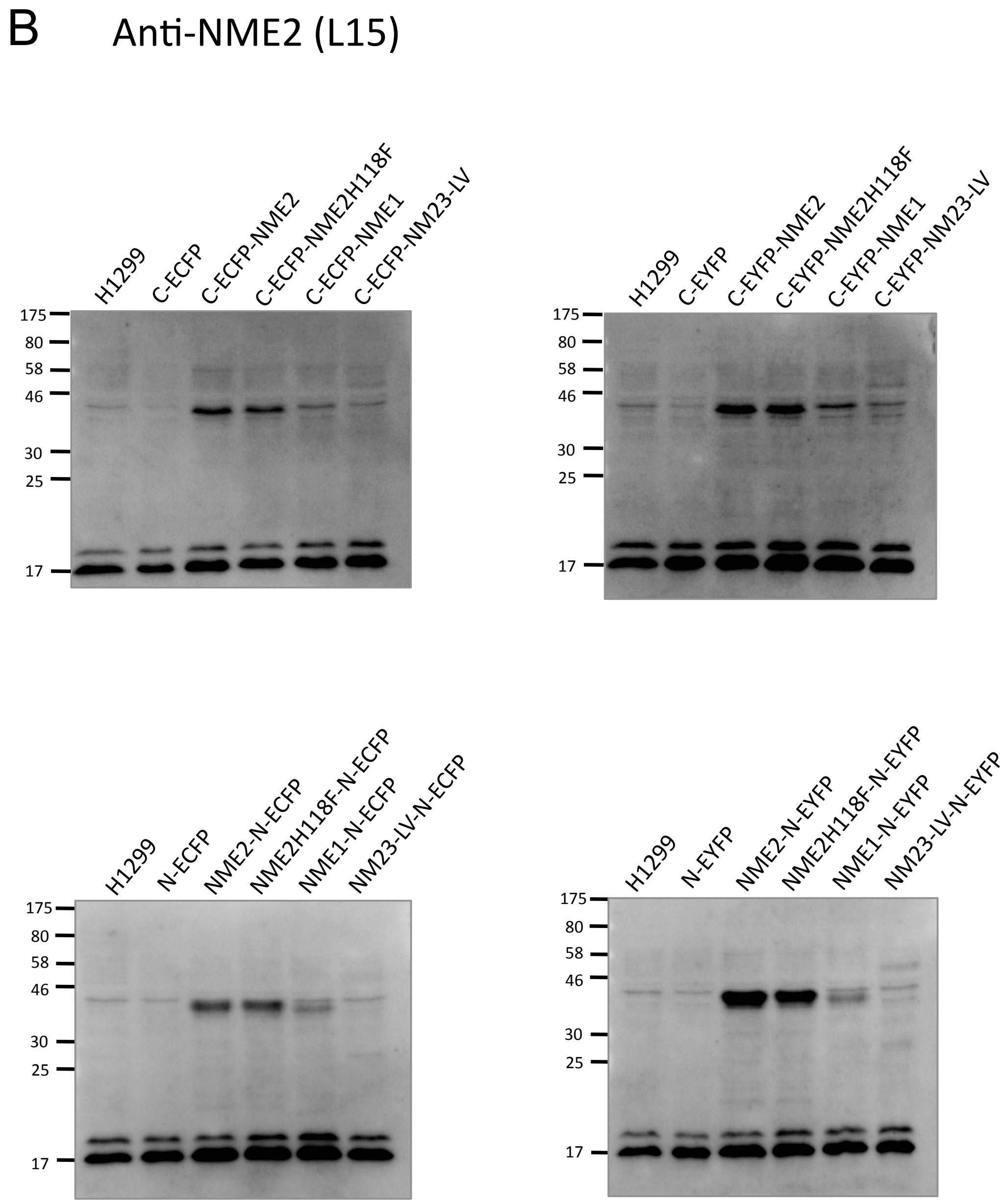

Figure 3.4.7.1 (To be continued)

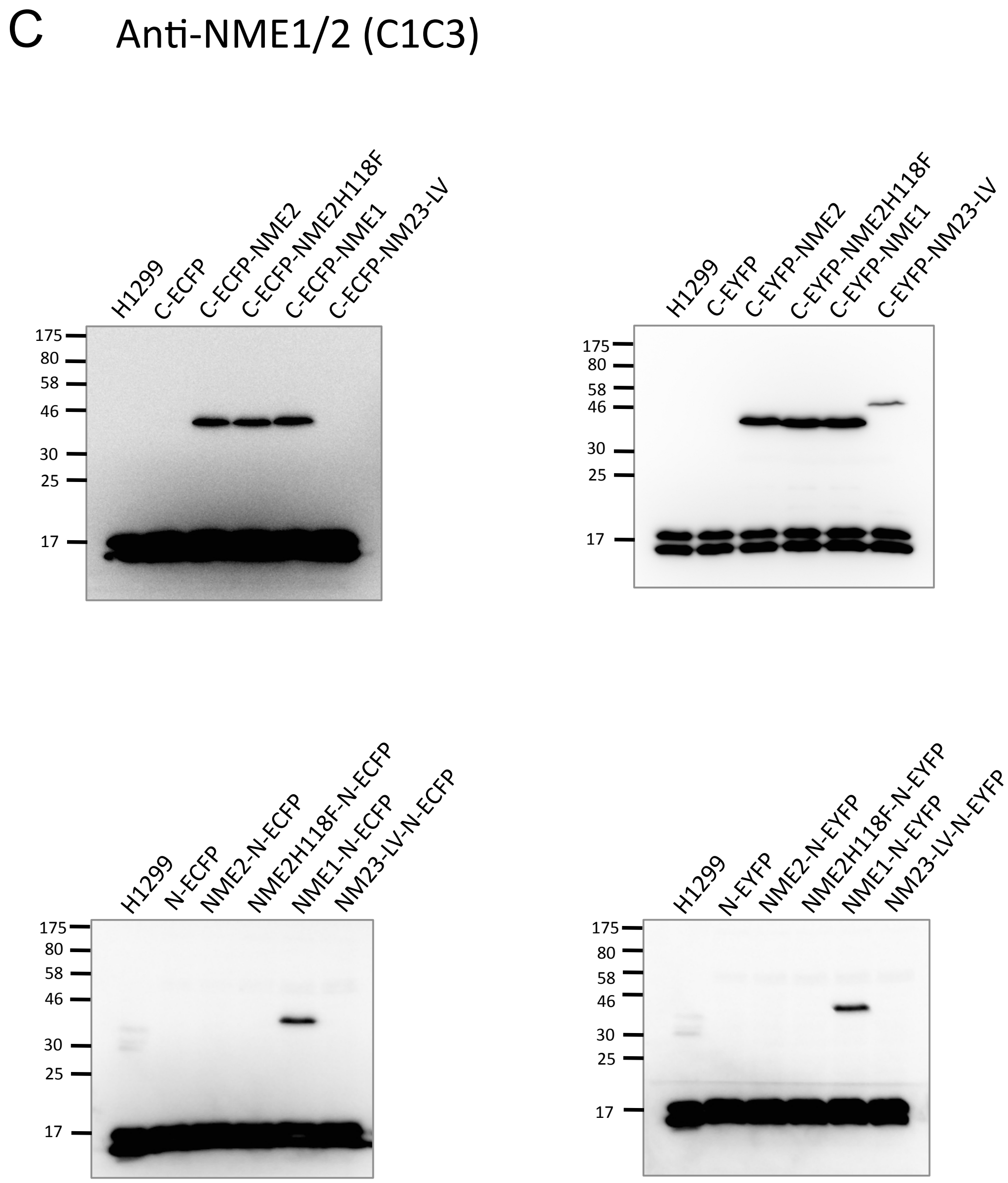

Figure 3.4.7.1 (To be continued)

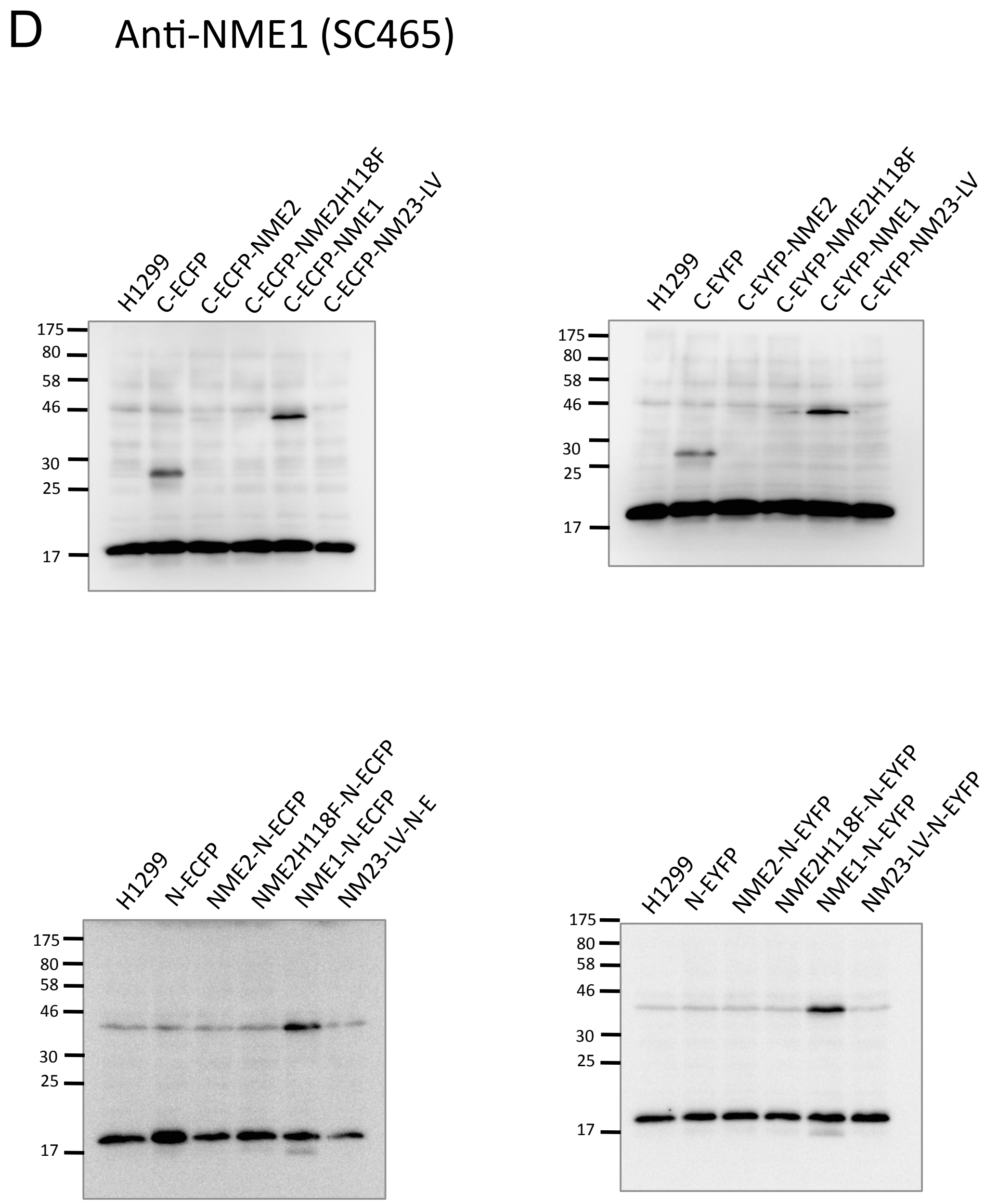

Figure 3.4.7.1: Characterisation of NME1, NME2, NME2H118F and NM23-LV fusion proteins. H1299 cells were transfected with 1 μg of constructs that express fluorescence-labelled NME1, NME2, NME2H118F and NM23-LV fusion proteins, in each well of a 6-well plate, using GeneJuice. Plasmids expressing C-ECFP, C-EYFP, N-ECFP and N-EYFP were included as controls. 24h post-transfection, cells were harvested for Western blotting using **A.** anti-GFP; **B.** Anti-NME2 (L15); **C.** Anti-NME1/2 (C1C3); and **D.** Anti-NME1 (SC465). Downward arrows indicate low to high exposures.

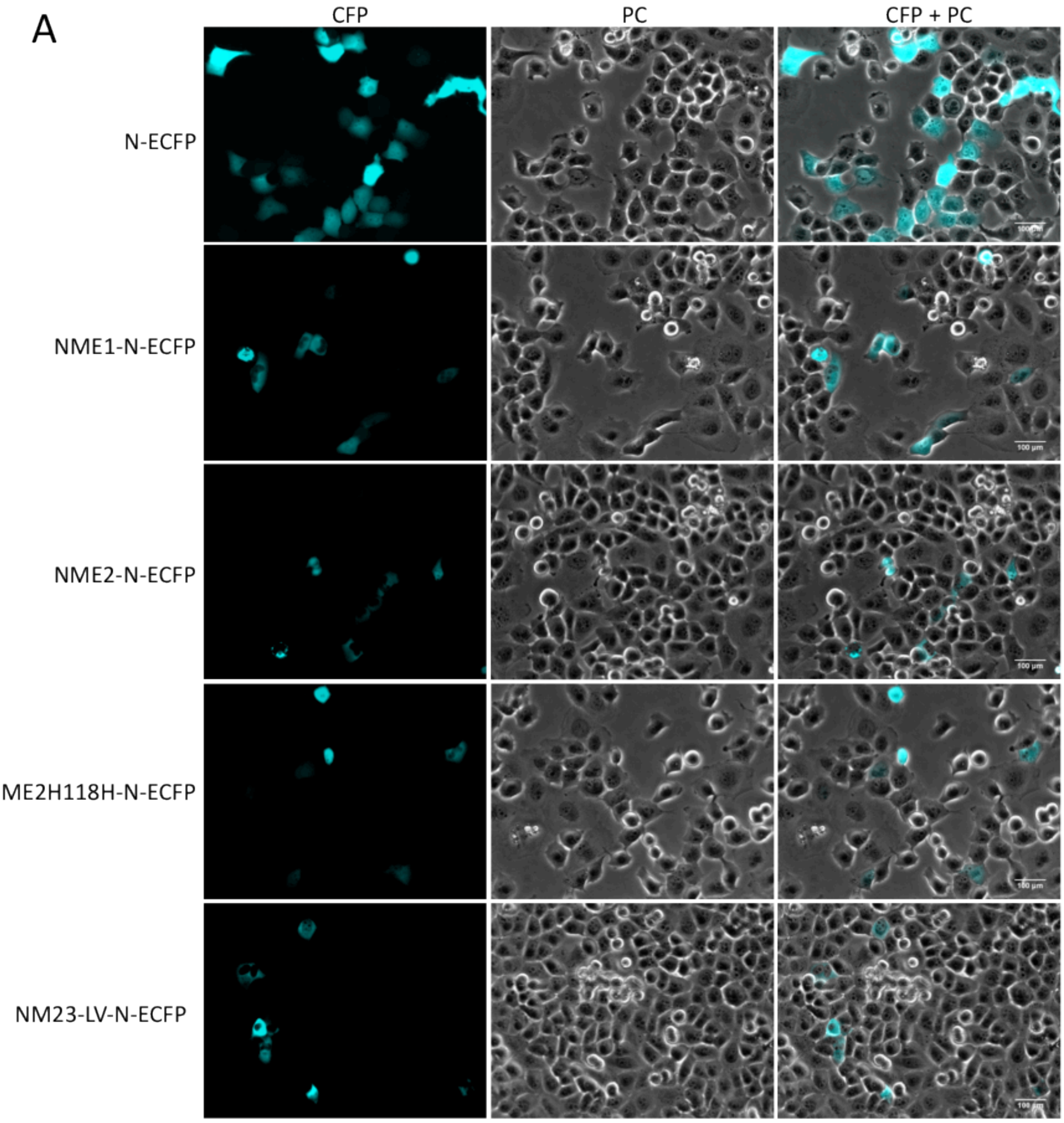

Figure 3.4.7.2 (To be continued)

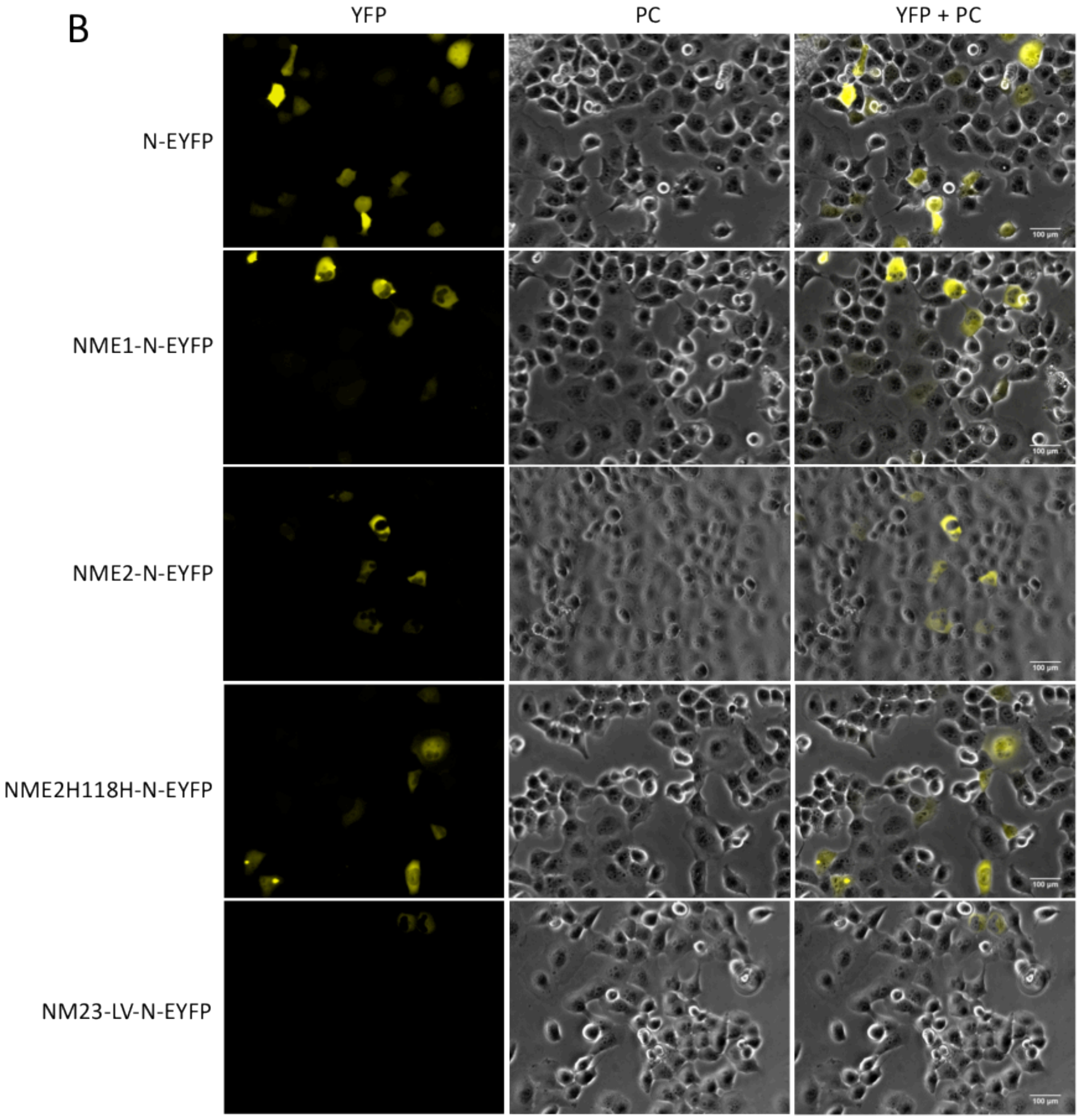

Figure 3.4.7.2 (To be continued)

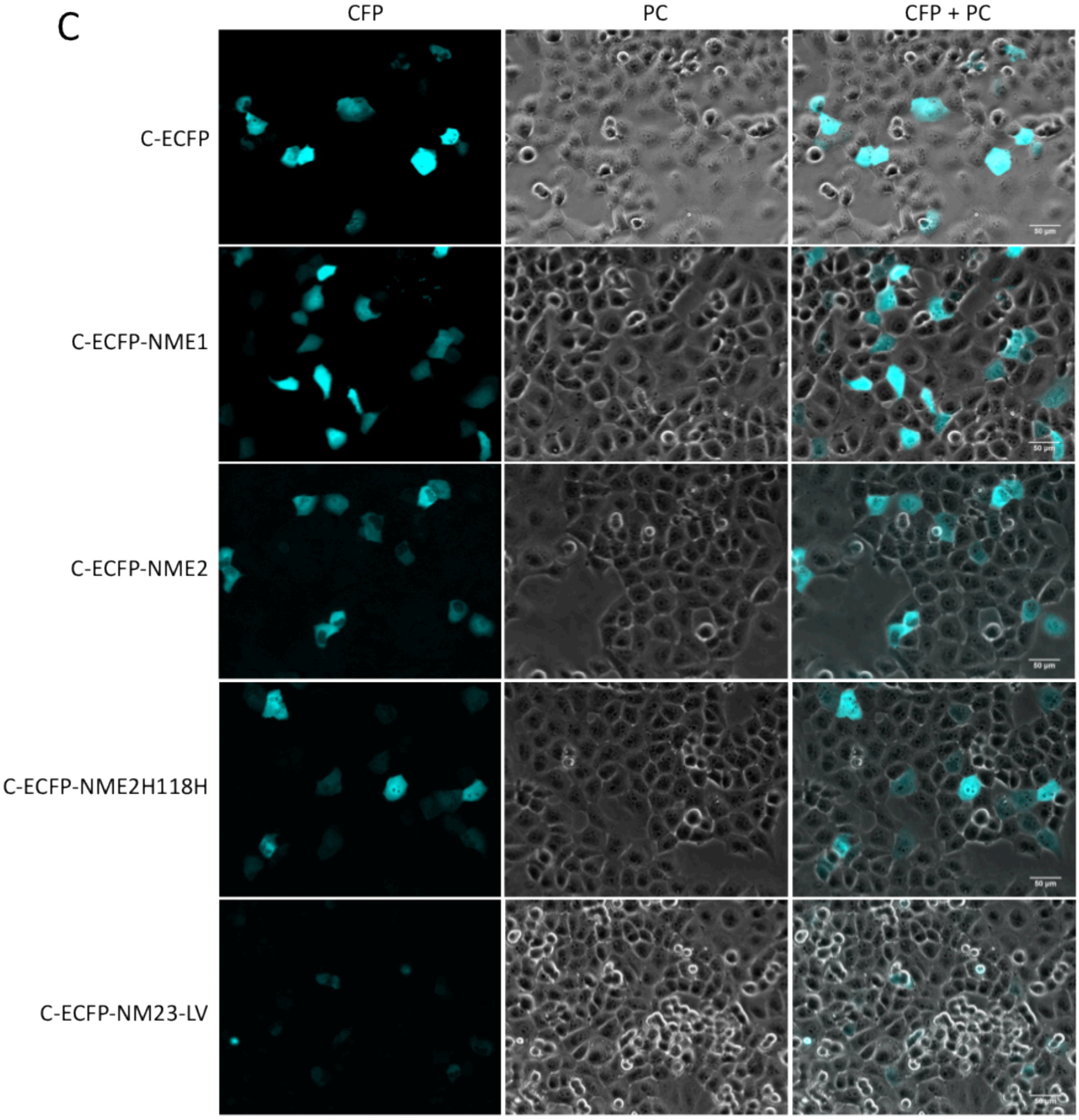

Figure 3.4.7.2 (To be continued)

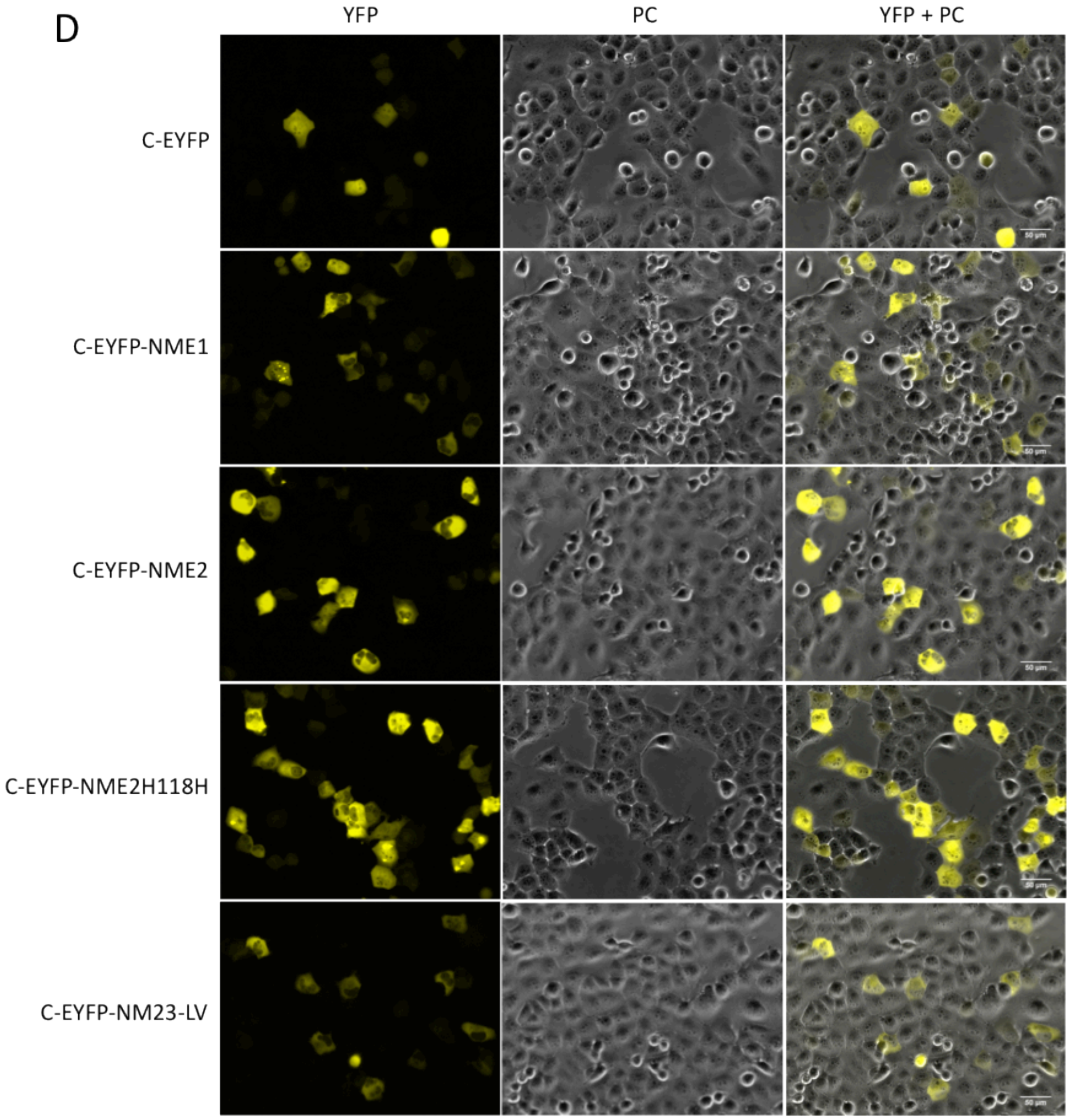

Figure 3.4.7.2: Fluorescence microscopy for NME1, NME2, NME2H118F and NM23-LV fusion proteins. H1299 cells were transfected with 1 µg of constructs that express fluorescence-labelled NME1, NME2, NME2H118F and NM23-LV fusion proteins, in each well of a 6-well plate, using GeneJuice. Plasmids expressing N-ECFP, N-EYFP, C-ECFP and C-EYFP were included as controls. 24h post-transfection, cells were imaged using a fluorescence microscope. NME proteins were fused to **A.** N-ECFP; **B.** N-EYFP; **C.** C-ECFP and **D.** N-EYFP. PC, phase contrast.

Table 3.4.7.1 Summary of antibodies and detected NME fusion proteins.

	Primary antibodies			
Fusion proteins	**Anti-GFP**	**Anti-NME2 (L15)**	**Anti-NME1 (SC465)**	**Anti-NME1/2 (C1C3)**
C-ECFP-NME1	✔	✔		✔
C-ECFP-NME2	✔	✔		✔
C-ECFP-NME2H118F	✔	✔	✔	✔
C-ECFP-NM23-LV	✔			
C-EYFP-NME1	✔	✔		✔
C-EYFP-NME2	✔	✔		✔
C-EYFP-NME2H118F	✔	✔	✔	✔
C-EYFP-NM23-LV	✔			✔
NME1-N-ECFP	✔	✔	✔	✔
NME2-N-ECFP	✔	✔		
NME2H118F-N-ECFP	✔	✔		
NM23-LV-N-ECFP	✔			
NME1-N-EYFP	✔	✔	✔	
NME2-N-EYFP	✔	✔		
NME2H118F-N-EYFP	✔	✔		✔
NM23-LV-N-EYFP	✔			

3.4.8 Examining the cellular localisation of NME fusion proteins using live cell imaging

In order to monitor the behaviour and distribution of NME proteins in cells, H1299 cells were transfected with plasmids expressing C-EYFP labelled NME1, NME2, NMEH118F and NM23-LV. 24h post-transfection, live cell imaging was performed on transfected cells for a duration of 34h, as described in Materials and Methods (Section 2.10). Representative movies are available on the attached CD (Appendix 11).

As expected, fluorescence signals for cells transfected with C-EYFP only were evenly distributed throughout the entire cell, including nucleus and cytoplasm (Figure 3.4.8.1A). The distribution of EYFP in cells was unchanged throughout the course of live cell imaging. C-EYFP-NME1 seems to predominantly reside in the cytoplasm, and has low expression in nuclei. Interestingly, our live cell imaging also show that C-EYFP-NME1 proteins slowly localise towards the nuclear periphery and the cells undergo apoptosis about 7h later (Figure 3.4.8.1B, Cell a). At the same imaging position (Figure 3.4.8.1B, Cell b), C-EYFP-NME1 was seen to migrate towards the nuclear membrane (Time 09:14:46), forming a ring-like structure around the nuclear membrane about one and a half hour later in Cell b. This was then followed by accumulation of C-EYFP-NME1 between two nuclei of Cell b (Time 12:09:46). However, the accumulation of C-EYFP-NME1 gradually disappeared within less than 2h and Cell b eventually died.

Live cell imaging for C-EYFP-NME2 transfected cells shows that C-EYFP-NME2 is also mainly localised in the cytoplasm (Figure 3.4.8.1C). Accumulation of C-EYFP-NME2 was seen to result in different outcomes. For example, some cells were observed to undergo cell death, as seen in Cell c. In Cell d, accumulation of C-EYFP-NME2 slowly diffused away and the cell remained viable until the end of the imaging. Interestingly, in Cell e, C-EYFP-NME2 proteins slowly localise towards the nuclear periphery, forming a ring-like structure around the nuclear membrane, as observed in C-EYFP-NME1 transfected Cell b (Figure 3.4.8.1B). However, the ring-like structure disappeared, and instead of undergoing cell death like Cell b, C-EYFP-NME2 expressing Cell e continued to undergo mitosis successfully to produce Cell e1 and e2 (Figure 3.4.8.1C). Interestingly, the NME2 fusion protein also seems be more readily found in the nuclei shortly before the mitosis process (Figure 3.4.8.1C).

C-EYFP fused with NME2H118F, which lacks kinase activity, seems to have similar sub-cellular distribution to NME1 and NME2, but appeared to be more readily found in nuclei. Accumulation of C-EYFP-NME2H11F protein generally leads to cell death (Figure 3.4.8.1D). Interestingly, similar to an observation in NME1 fusion protein (Appendix 11), no accumulation of C-EYFP-NME2H11F around the nuclear membrane was observed in Cell f (Figure 3.4.8.1D) before proceeding to a successful mitosis. Since fluorescence in Cell f was almost exclusive to the cytoplasm, it is likely that the fluorescence detected was not due to EYFP alone (as a truncation product of the NME2H118F fusion proteins).

On the other hand, C-EYFP-NM23-LV transfected cells appear to undergo cell death about 33h after transfection (Figure 3.4.8.1E). Before the cells die, NM23-LV proteins accumulate possibly in the endoplasmic reticulum, which indicates that the fusion proteins may not be processed properly in endoplasmic reticulum. In addition, C-EYFP-NM23-LV was also seen accumulating around the nuclear membrane, slowly migrating towards the furrow between two or three nuclei and then disappearing without the cell undergoing mitosis or apoptosis (Figure 3.4.8.1E, Cell g).

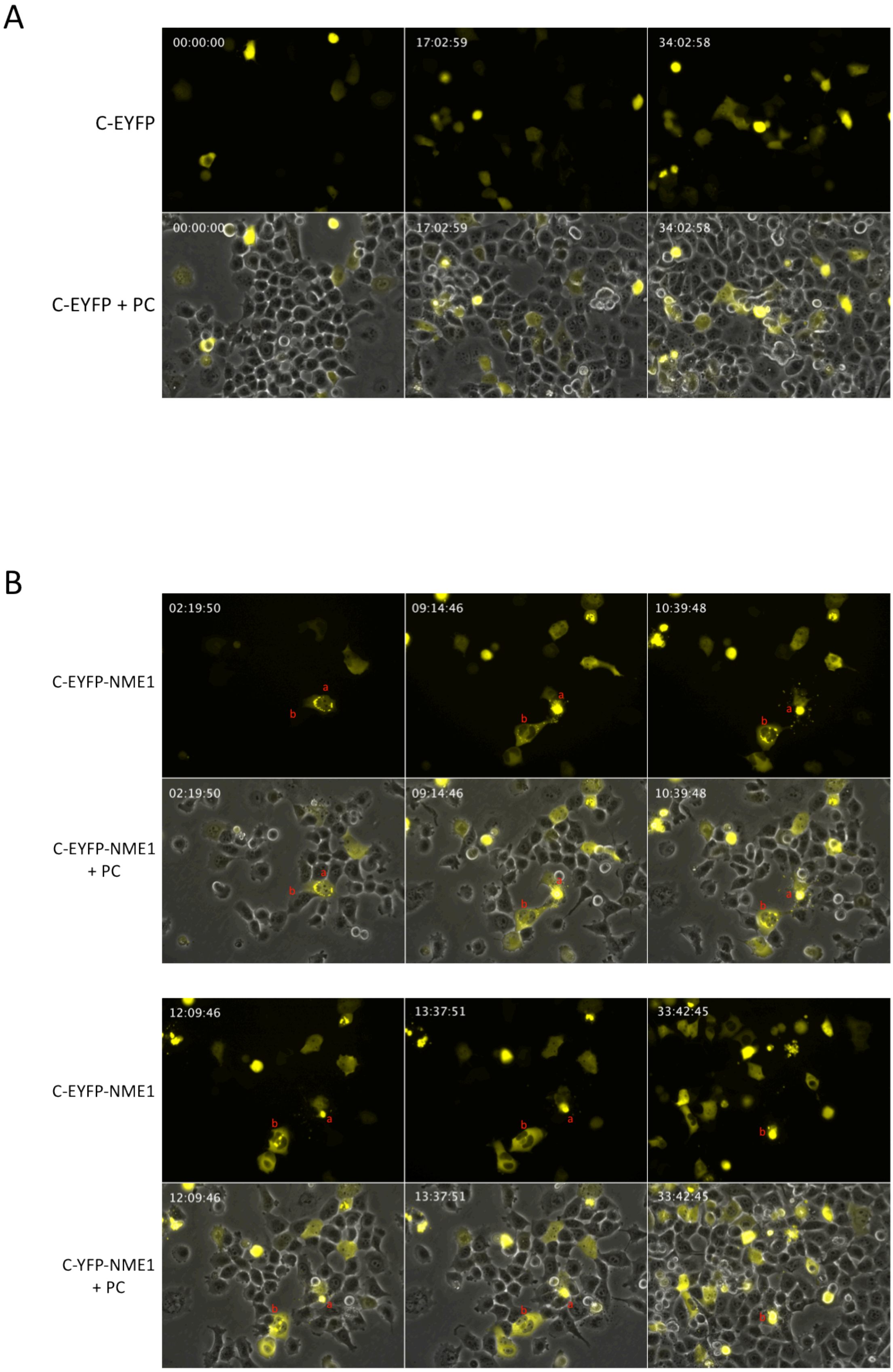

Figure 3.4.8.1 (To be continued)

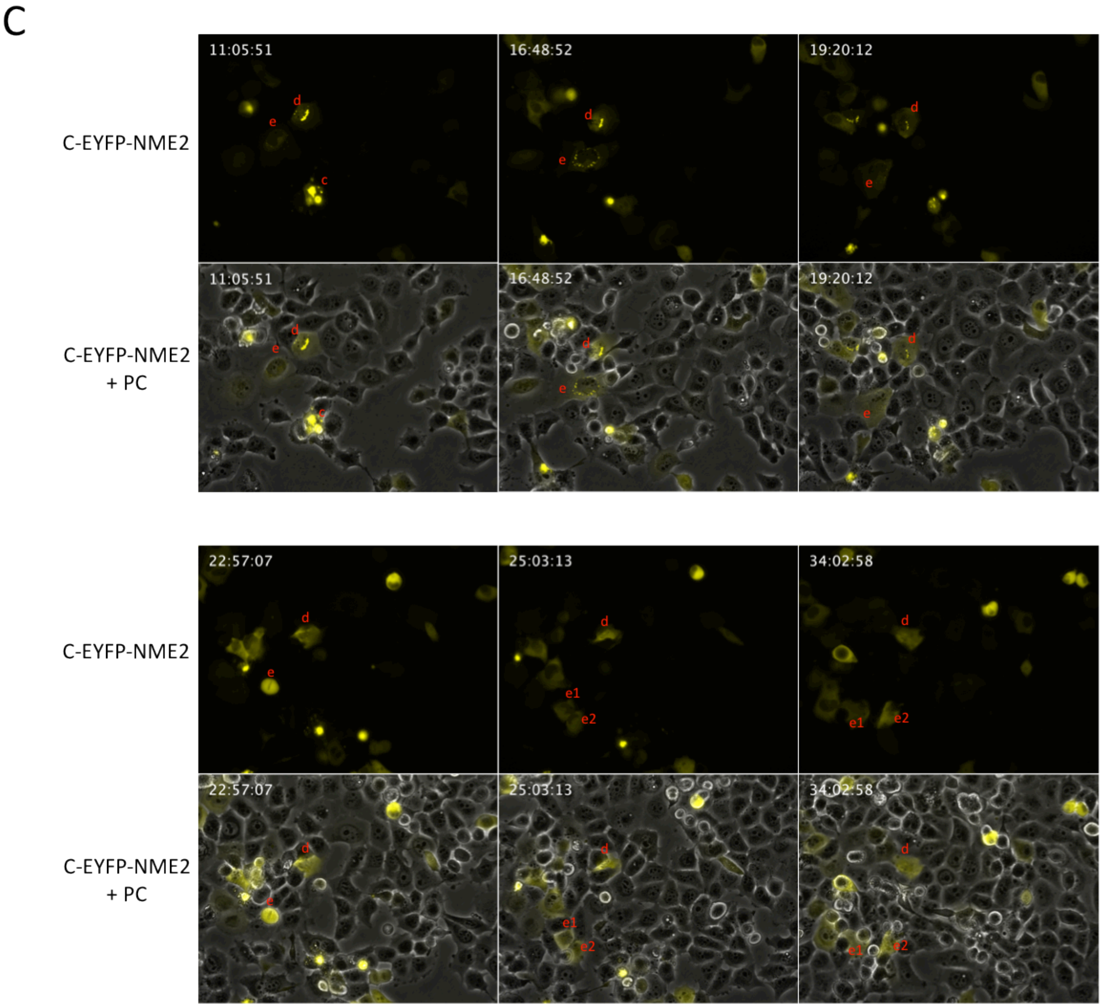

Figure 3.4.8.1 (To be continued)

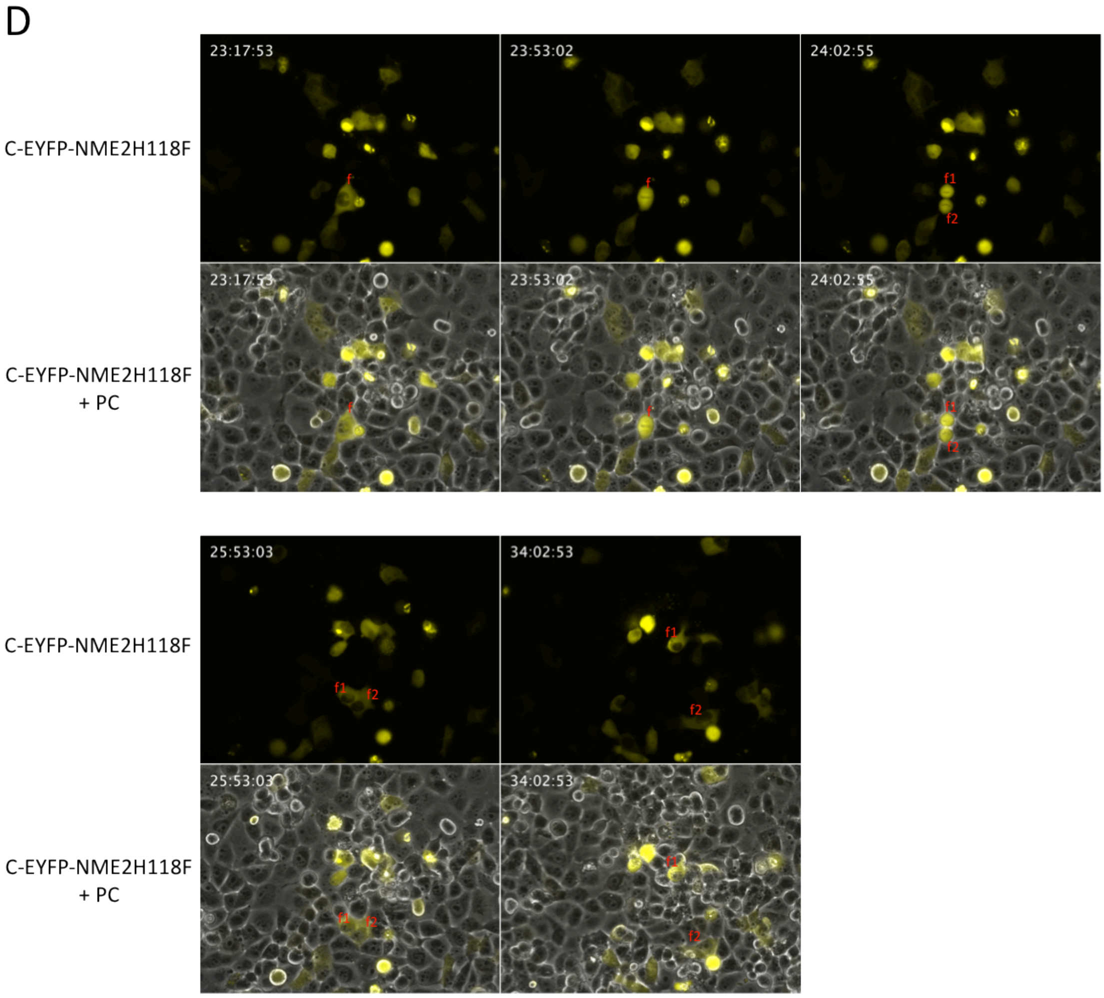

Figure 3.4.8.1 (To be continued)

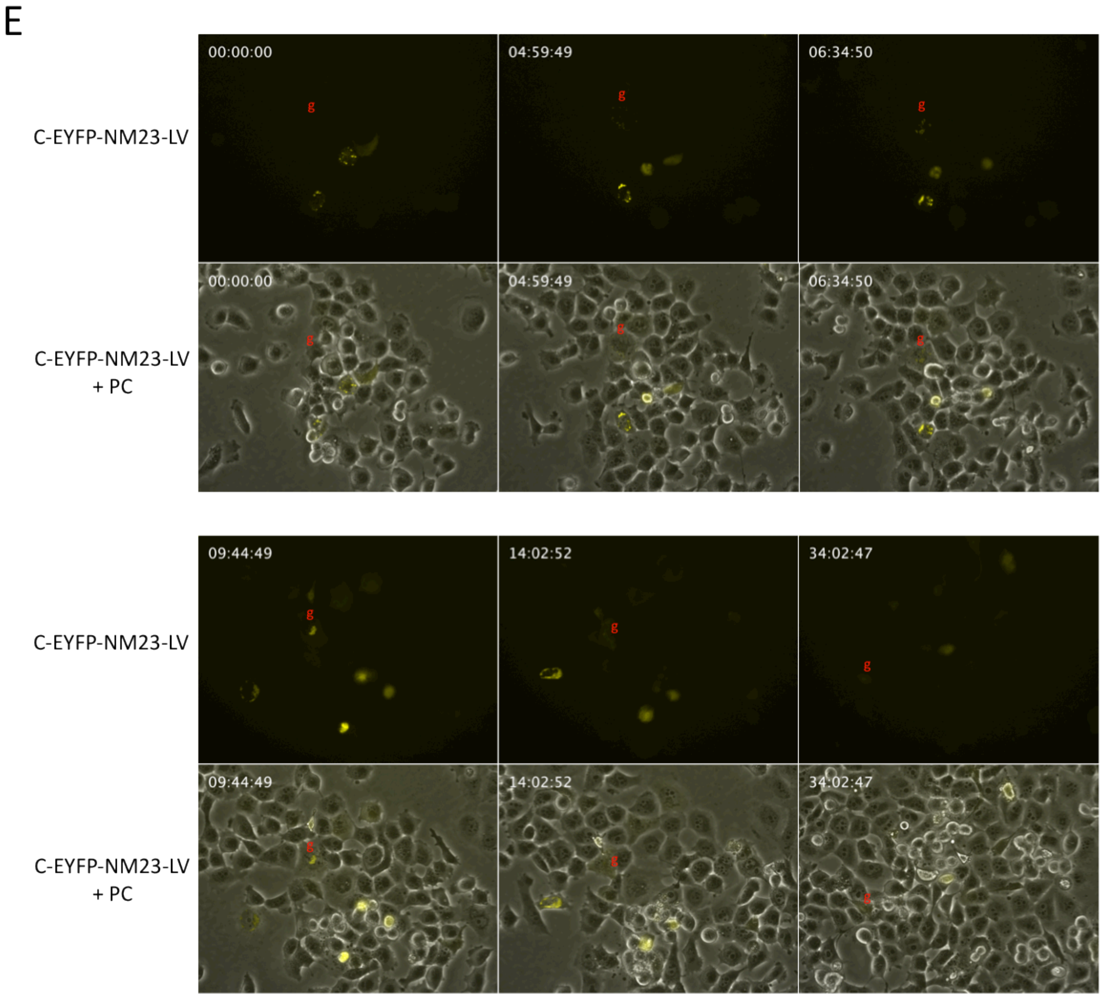

Figure 3.4.8.1: Examining the cellular localisation of NME fusion proteins using live cell imaging. In order to monitor the behaviour and distribution of NME proteins in cells, H1299 cells were transfected with 2 μg of plasmid expressing either C-EYFP labelled NME1, NME2, NMEH118F or NM23-LV, in each well of a 6-well plate, using GeneJuice. 24h post-transfection, live cell imaging was performed on transfected cells for a duration of 34h, as described in Materials and Methods (Section 2.10). Pictures of fluorescent cells at different time frame was illustrated above for cells transfected with **A.** C-EYFP, **B.** C-EYFP-NME1, **C.** C-EYFP-NME2, **D.** C-EYFP-NME2H118F and **E.** C-EYFP-NM23-LV. Time after transfection (Hours: Minutes: Seconds) was indicated in the top left corner of each picture. In the case of mitosis, daughter cells were numbered after the same alphabet as their parent cell. Representative movies are available on the attached CD (Appendix 11). PC, phase contrast.

3.4.9 Examining the effect of NME proteins on cell cycle using flow cytometry

Live cell imaging data presented in Section 3.4.8 have suggested that overexpression of NME proteins may lead to mitotic failure. As the mitotic failure seems to happen after accumulation of NME proteins around the nuclear periphery, which was often accompanied by multi-nuclei formation, we wanted to examine whether overexpression of NME proteins would have any effect on cell division. We aimed to examine the effect of NME proteins on cell cycle using flow cytometry.

H1299 cells were transfected with plasmids expressing fluorescent fusion proteins of NME1, NME2, NME2H118F and NM23-LV, as described in Figure 3.4.9.1. Lipofectamine 2000 was used as transfection reagent in order to achieve high transfection efficiency. Transfected cells were harvested 24h post-transfection and processed for flow cytometry analysis, as described in Materials and Methods (Section 2.17). Untransfected cells were used as negative control.

In order to generate cell cycle profiles, the following plots measuring the following parameters (x and y axis, respectively) were created for each sample: FSC-Area vs. SSC-Area, FL2-Area vs. FL2-Width, FL1-Height (EYFP Log) vs. PI, as shown in Figure 3.4.9.1. As single cells are the subjects of analysis, FL2-Area vs. FL2-Width plots were used to gate single cell and exclude debris and aggregates for analysis. Using the collection of single cells, FL1-Height (EYFP Log) was plotted to create a gate that is selective for only EYFP positive cells, using a threshold determined by the untransfected control. The EYFP gate was set so that no more than 0.5% of untransfected cells fall in the EYFP positive range. Since the emission spectra of EYFP overlaps with that of PI, it is possible that fluorescence from more than one fluorochrome was detected from a single channel. This could be a possible explanation for the top right-skewed dot-plot of FL1-Height (EYFP Log) vs. PI observed in the fluorescent fusion proteins. Since no compensation was used to correct this spectral overlap for this experiment, the right-skewed cells were gated out to ensure that only fluorescence detected from a particular fluorochrome is used for analysis. Cell cycle profiles for the samples were plotted as histograms of Cell Counts vs. PI Area for both singlets only and

EYFP positive only cells. A summary of cell cycle analysis for EYFP positive only cells is represented in Table 3.4.9.1.

As shown in Table 3.4.9.1, EYFP-NME1, -NME2 and -NM23-LV transfected cells appeared to have a slightly lower percentage of cells in G1-phase and a higher percentage of cells in S-phase, in comparison to EYFP alone. This is particularly noticeable in cells transfected with NM23-LV, with 4.6% less cells in G1-phase and 6.7% more cells in S-phase than EYFP. In addition, there are also 3.61% less cells in G2-phase for NM23-LV transfected cells, compared to EYFP. No noticeable difference in cell cycle subpopulations was observed in NME2H118F transfected cells compared to EYFP only. In addition, overexpression of the NME fusion proteins did not seem to have an effect on DNA contents of the cells. However, since this experiment was only performed once using n=1, no statistical analysis was produced.

A Untransfected

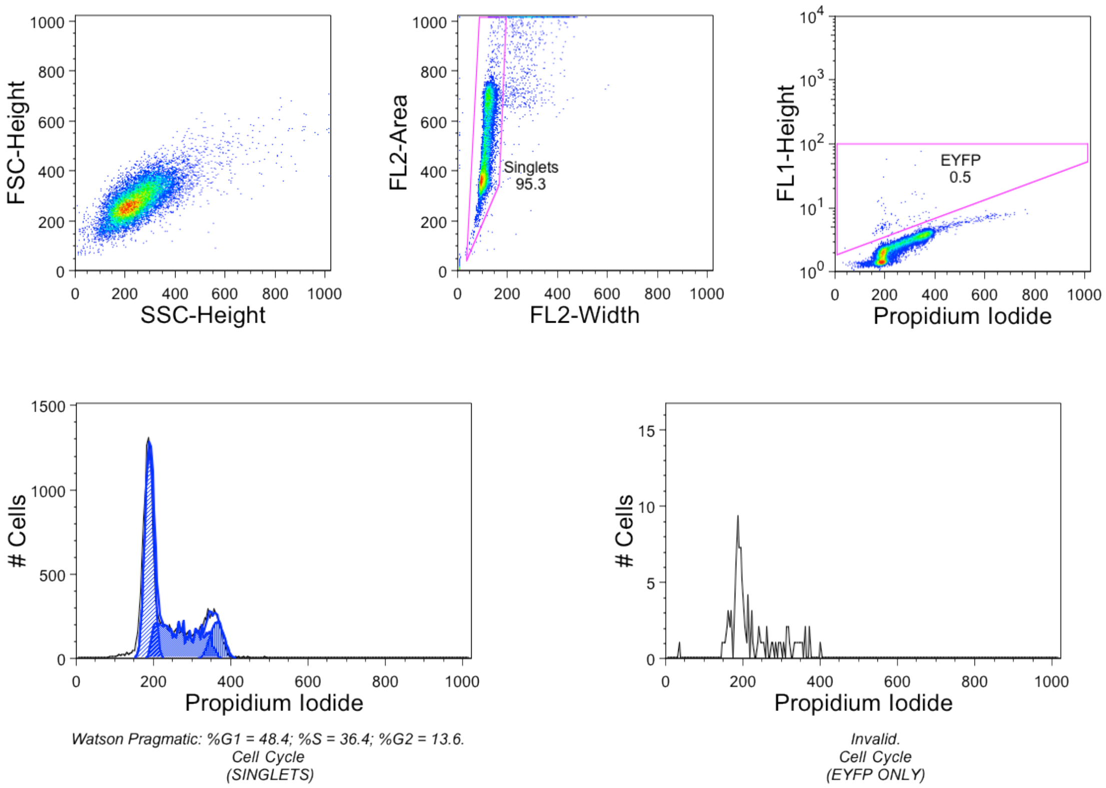

B C-EYFP

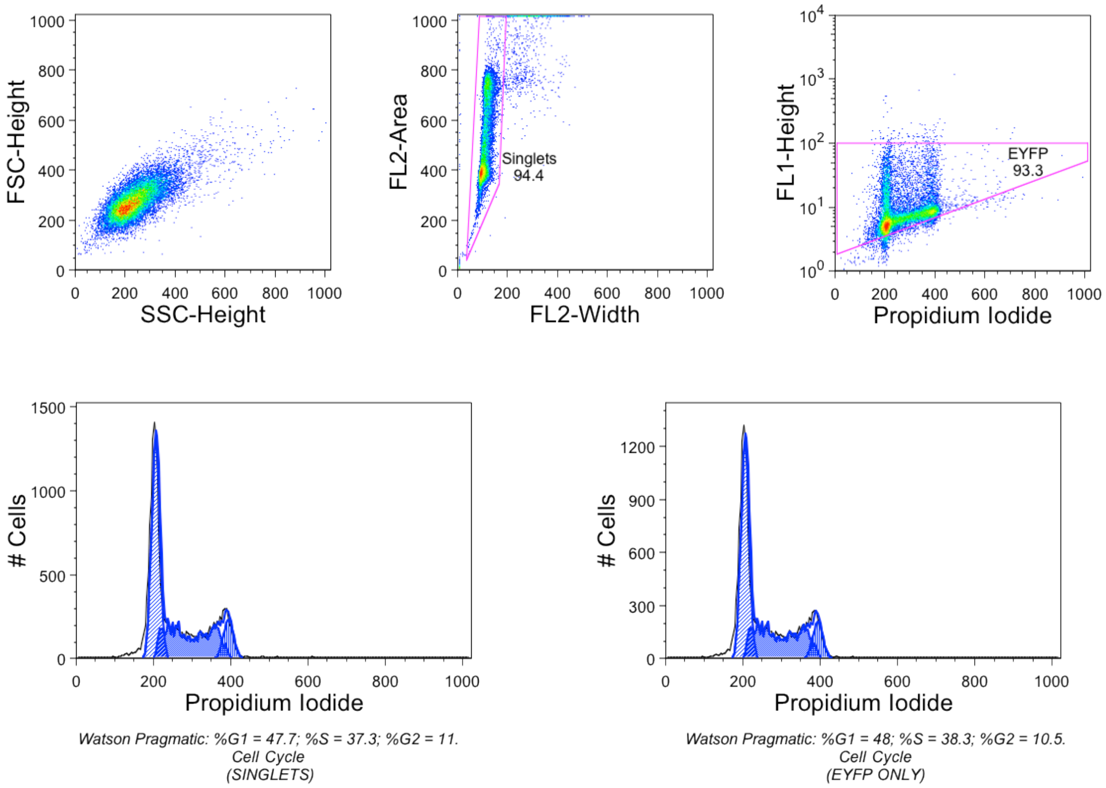

Figure 3.4.9.1 (To be continued)

C C-EYFP-NME1

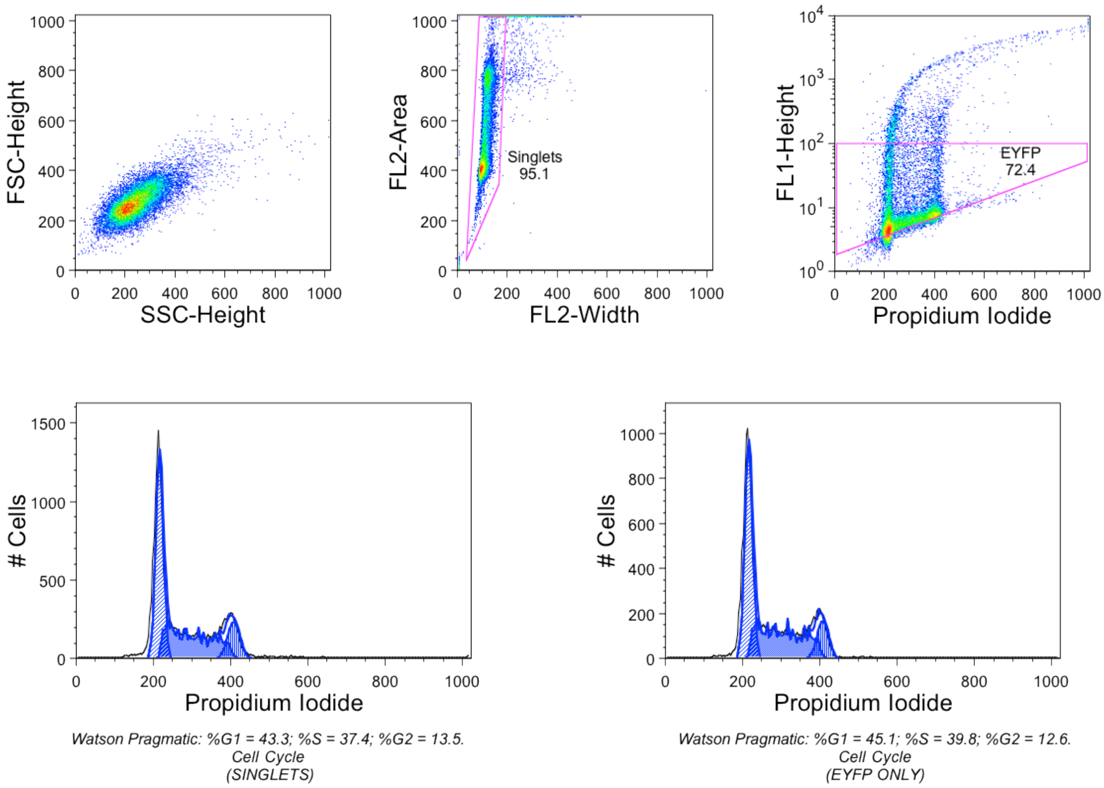

D C-EYFP-NME2

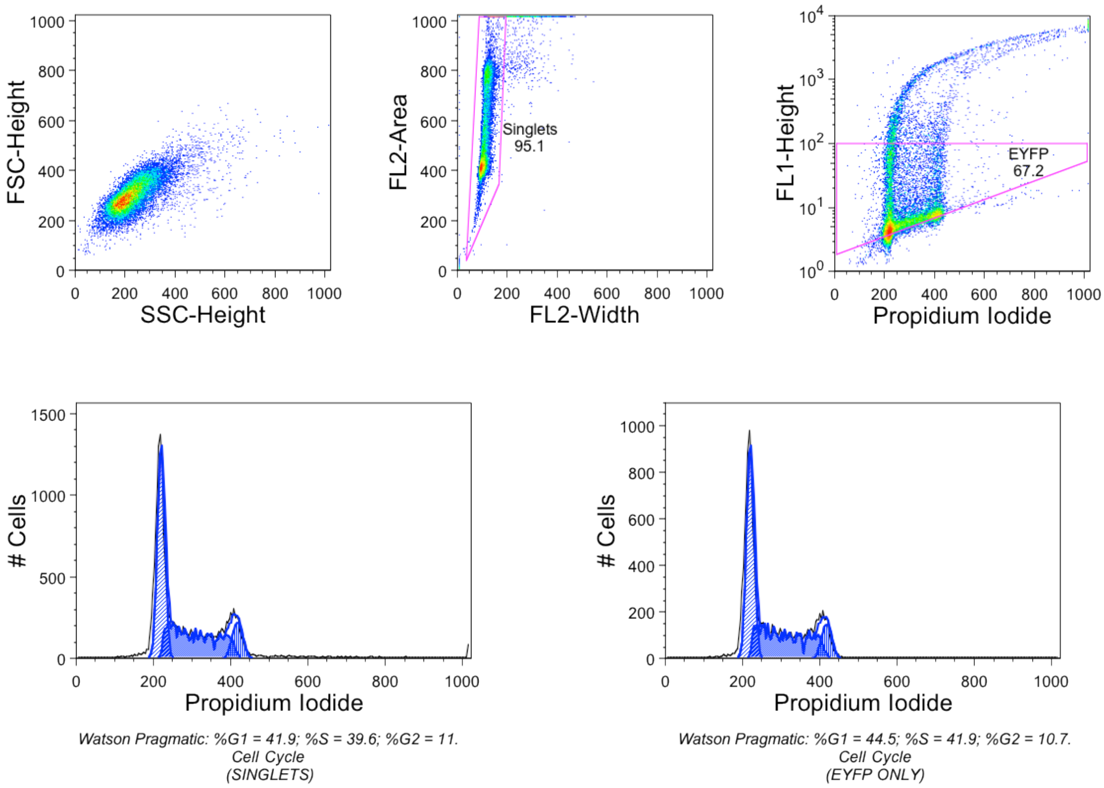

Figure 3.4.9.1 (To be continued)

E C-EYFP-NME2H118F

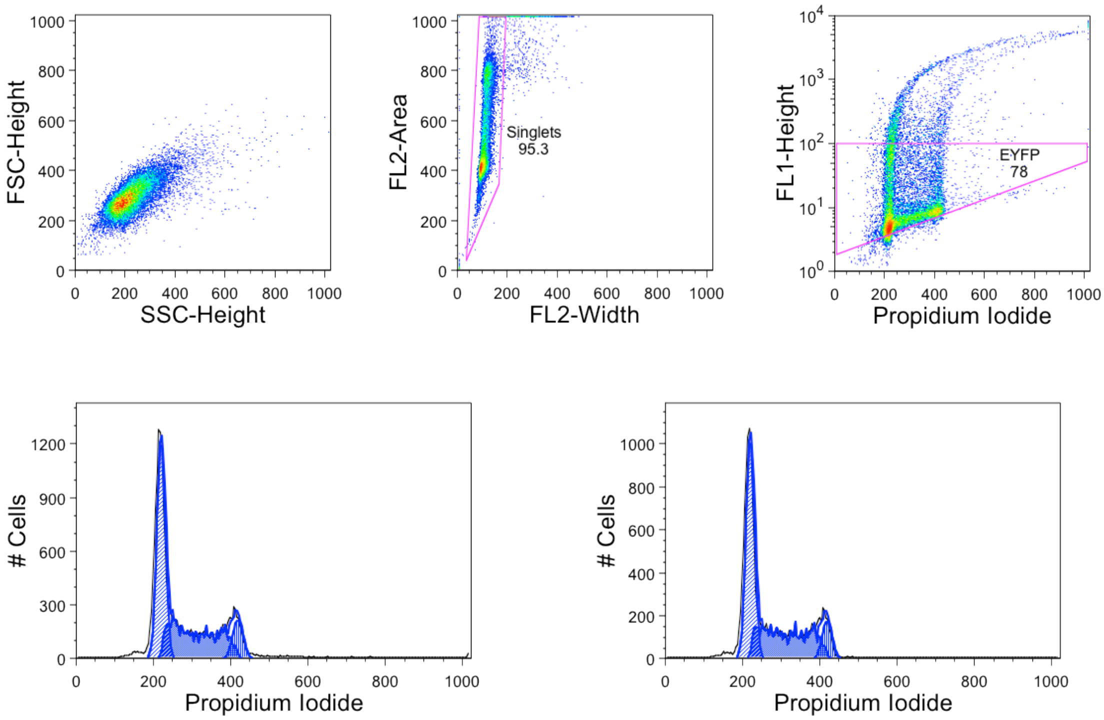

Watson Pragmatic: %G1 = 44.7; %S = 38.2; %G2 = 10.5.
Cell Cycle
(SINGLETS)

Watson Pragmatic: %G1 = 48.4; %S = 38.7; %G2 = 10.3.
Cell Cycle
(EYFP ONLY)

F C-EYFP-NM23-LV

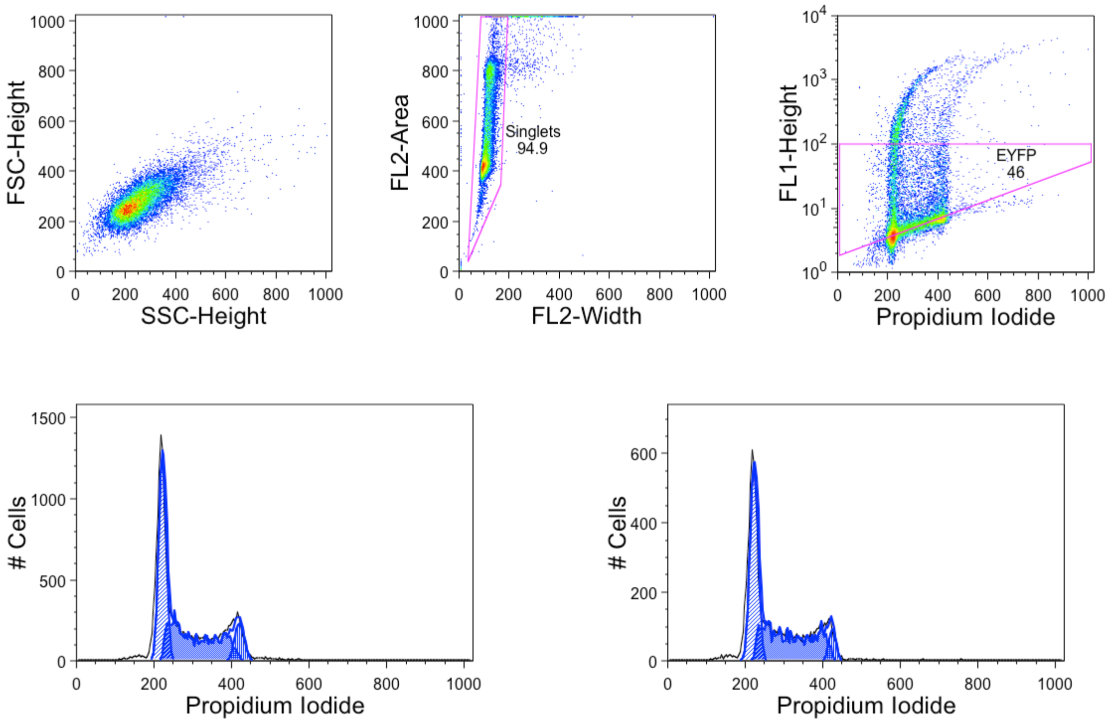

Watson Pragmatic: %G1 = 41.1; %S = 41.8; %G2 = 10.6.
Cell Cycle
(SINGLETS)

Watson Pragmatic: %G1 = 43.5; %S = 45.1; %G2 = 6.81.
Cell Cycle
(EYFP ONLY)

Figure 3.4.9.1 (To be continued)

Figure 3.4.9.1: Examining the effect NMEs on cell cycle using flow cytometry. H1299 cells were transfected with 2 μg of plasmids expressing C-YFP fusion proteins of NME1, NME2, NME2H118F and NM23-LV, in each well of a 6-well plates, using Lipofectamine 2000. Transfected cells were harvested 24h post-transfected and processed for flow cytometry analysis, as described in Materials and Methods (Section 2.17). 20,000 events were recorded for each run. Untransfected cells were used as negative control. Cell cycle analysis was performed for **A.** Untransfected, **B.** EYFP, **C.** EYFP-NME1, **D.** EYFP-NME2, **E.** EYFP-NME2H118F, and **F.** EYFP-NM23-LV transfected cells. Plots measuring the following parameters (x and y axis, respectively) were created: FSC-Area vs. SSC-Area, FL-2-Area vs. FL-2-Width, Cell Counts vs. PI, FL-1-Height (EYFP Log) vs. PI, Cell Counts vs. PI Area (of singlets gate and only EYFP positive gate). FL-2-Area vs. FL-2-Width is used to avoid doublets and clumped cells (Singlets gate). FL-1-Height (EYFP Log) vs. PI serves to select only EYFP positive cells, with gating threshold determined by running the untransfected control. Cell cycle analysis was performed using EYFP positive only cells using FlowJo Analysis Software, according to the Watson Pragmatic mathematical model to define the G1, S, and G2 phases of the cell cycle [401].

Table 3.4.9.1: Summary of cell cycle analysis for EYFP positive cells. Cell cycle analysis was performed using EYFP positive only cells, which was gated using a threshold set on untransfected cells. Cell cycle was analysed using FlowJo Analysis Software according to the Watson Pragmatic mathematical model to define the G1, S, and G2 phases of the cell cycle [401]. Note that not 100% of EYFP positive cells fit in the cell cycle analysis, as shown the Total (%) column.

Sample	EYFP positive (%)	G1 (%)	S (%)	G2 (%)	Total (%)
Untransfected	0.5	N/A	N/A	N/A	N/A
EYFP	93.3	48.0	38.5	10.4	96.9
NME1	72.4	45.3	39.4	12.6	97.3
NME2	67.2	44.6	41.6	10.7	96.9
NME2H118F	78.0	48.4	38.8	10.2	97.4
NM23-LV	46.0	43.4	45.2	6.79	95.39

Chapter 4

Discussion

4. Discussion

4.1 Interplay between MDM2 and NME2

The global aim of work presented in this thesis was to investigate the mechanism of MDM2 in promoting increased cell motility and invasiveness in RCC cells. Our results showed that when the Boyden chamber motility assay was used, cells expressing high levels of MDM2 via transient transfection were observed to display an increase in cell motility that is independent of MDM2 RING-finger (Section 3.2.3.2). This result is consistent with the published results of Polański and colleagues who demonstrated that MDM2 promotes cell motility and invasiveness in a RING-finger-independent manner [384]. Although we could detect a change in motility consistent with the published results using Boyden chamber motility assay, one possibility as to why no difference in motility could be detected using the live cell imaging system lies in the fact that live cell imaging system is based on cell migration on a solid surface in a two-dimensional manner, which may under-represent the true cell movement in a physiological system. On the other hand, Boyden chamber motility assay assesses the ability of cells to travel in three-dimension, first moving towards and then squeezing through the 8-μm pores, which may better resemble cell migration in a real tissue environment.

In order to examine the effects of NME2 on cell motility, Boyden chamber motility assays were performed using stable clones expressing shRNA NME2 to "knockdown" NME2 expression in H1299 and Clone 9 cells (H1299 overexpressing MDM2) (lines generated by Dr Maria Maguire). Down-regulation of NME2 in both HNME2:Cl.2 and Cl.7 cells resulted in significantly higher motility compared to H1299 and Scrambled controls (Figure 3.2.4.1C). Since cell motility is closely related to metastasis, this result suggests NME2 may act as a tumour suppressor by suppressing cell motility. Clone 9 cells and its derivatives NME2 knockdown cells were also more motile compared to their parental H1299. This is consistent with published findings that overexpression of MDM2 promotes cell motility [103, 384]. However, knockdown of NME2 in Clone 9 cells did not further increase cell motility compared to Clone 9, which might suggest that NME2 may not be able to exert its motility suppressive effect in cells already harbouring high levels of MDM2. Alternatively, it could be that Clone 9 and its

NME2 knockdown derivatives have reached their maximum attainable motility due to high MDM2 expression, and therefore the motility suppressive effect from NME2 is insufficient to reduce motility due to the presence of high levels of MDM2.

Since NDPK activity is responsible for the synthesis of nucleic acid precursors, it was expected that cell proliferative capacity might be affected in cells lacking NME2 expression. In addition, overexpression of NME1 has been positively correlated with proliferative activity of lymphoid cells, suggesting a role of NME1 in cell proliferation [402]. However, MTT analysis (Figure 3.2.4.1D) has shown that cell proliferation rate of all NME2 knockdown clones used in the motility assay was very similar to wild-type NME2 cells, which provides evidence that the difference in cell proliferation rate is unlikely to be responsible for the increase in motility observed in NME2 knockdown clones. Cell proliferation rate is an important consideration during motility analysis by Boyden chamber since it is the total number of cells which have migrated through the membrane which are counted and analysed, therefore if cell-lines had different proliferation rates this could over- or under- estimate the value and confound interpretation of results.

As expected, all NME2 knockdown clones have shown considerably lower NDPK activity levels (Figure 3.2.4.1B). Interestingly, NDPK activity for Clone 9 is lower compared to H1299 leading us to speculate that overexpression of MDM2 might lower cellular NDPK activity to promote cell motility. However, the same result was not observed when NDPK activity assay was repeated with additional clones that overexpress MDM2 (MDM2 Cl.1 and Cl.3) (Figure 3.2.5.1), and thus it seems that the result seen in Clone 9 cells was likely due to possible differences selected through cell cloning. This also suggests that high levels of MDM2 may not have any affect on cellular NDPK activity. Nevertheless our results show that knockdown of NME2 abrogates most of the endogenous NDPK activity and promotes increased cell motility, which leads us to speculate that the role of NME2 as a metastasis suppressor may be, at least in part, dependent on NDPK activity.

Functional redundancy between NME1 and NME2 has been described in a number of studies. As mentioned in Section 1.5.3, both *NME1* and *NME2* knockout mice are viable with only mild phenotypic differences and both strains can survive into adulthood [287, 288]. However, the combination of deleting *NME1* and *NME2* leads to lethality in mice [289], indicating that the viability of *NME1* and *NME2* knockout mice is probably due to redundancy. In addition, it has been shown that expression of both NME1 and NME2 proteins in wild-type mice is induced during liver regeneration after partial hepatectomy, in parallel with the increased hepatocyte proliferation rate [317]. However, *NME1*-null mice had no impact on liver regeneration, suggesting a compensatory mechanism by NME2 and a dispensable role of NME1 in cell proliferation [317]. Moreover, Boissan *et al.* demonstrated that the lack of an *NME1* gene in mice that develop HCC with pulmonary metastases had no influence on primary tumour formation [309]. However, there is a significant increase in NME2 protein expression in HCC tissue compared to non-tumour tissue of *NME1*$^{-/-}$ mice [309]. The increase in NME2 expression observed in *NME1* knockout when compared to *NME1* wild-type mice (p=0.034) indicates that there was a compensatory increase in NME2 protein expression in the tumour tissue in mice lacking NME1 [309]. However, our results suggest that there is a lack of compensatory effect between NME1 and NME2 in the systems we have studied. It appears that the increase in cell motility as a result of NME2 down-regulation is not compensated by motility suppressive effect of endogenous NME1 (Figure 3.2.4.1C). In addition, we have found that there was a lack of any compensatory increase of NME1 protein levels in response to down-regulation of NME2 in H1299 cells (Figure 3.2.15.1A). These observations suggest that NME1 and NME2 may have independent roles in certain biological functions that are irreplaceable by other isoforms.

The NDPK activity assay used in this study does not discriminate between NDPK activity contributed by specific isoforms of NME, but only measures the global cellular NDPK activity. Thus, we had to find a way of discriminating between the contribution of each NME1, NME2, or both, to cellular NDPK activity, whilst still using this assay. To examine the contribution of each individual NME protein towards NDPK activity, NME1 and NME2 were down-regulated, individually or in combination, in H1299 cells using siRNA. NME1 down-regulation leads to about 20% decrease in NDPK activity, whereas NME2 down-regulation leads to more than 50% decrease in activity in H1299 cells, as shown in Figure 3.2.15.1B. Interestingly, down-regulation of both NME1 and NME2 results in more than 70% decrease in cellular NDPK activity. These data suggest that although NDPK activity of NME2 represents a higher fraction of NDPK activity than NME1, it is the presence of the two NME isoforms that is responsible for the majority of the cellular NDPK activity, suggesting the importance of the oligomeric form of NME1 and NME2 [280, 290, 293]. These results are consistent with findings from other studies, for example it has been shown that NME1 silencing results in 20% and 15% reductions of the total NDPK activity in Hep2 and HCT8/S11 cells respectively [317]. Thus our results further support the notion that the NDPK intrinsic activity of NME1 only contributes to a minor proportion of the global cellular NDPK activity whereas NME2 provides considerably more and may be the single most active isoform of NME in terms of NDPK activity.

Since NME2 can exist as oligomeric protein comprised of individual active subunits, we wanted to investigate whether an NME2 kinase dead mutant competes with wild-type NME2 for limited number of cellular binding sites and exerts an allosteric, possibly dominant negative effect on the catalytic functions of wild-type NME2. We wanted to determine whether a kinase dead mutant could suppress the activity of the hexameric NDPK allosterically and if so, what would the effect of MDM2 be on cells expressing such a kinase dead form. For example, would a kinase dead NME2 mutant protect cells against the motility promoting effects of MDM2? Therefore, we examined the effect of NME2H118F kinase dead mutant on wild-type NME2 NDPK activity through co-transfection of plasmids encoding the two proteins in H1299 cells, followed by NDPK activity assay. As expected, NME2H118F failed to induce any NDPK activity due to the lack of a phospho-acceptor histidine 118 residue for the high-energy phospho-protein intermediate for the transfer of phosphate groups (Figure 3.2.7.1). NDPK activity of NME2H118F was comparable to that of EV control. Unexpectedly, co-expression of the kinase mutant and wild-type NME2 had no significant effect on NDPK activity produced by wild-type NME2. These data indicate that the kinase dead mutant NME2H118F has no effect *in trans* on cellular NDPK activity and thus it appears not to have any allosteric effect (assuming it is incorporated into hexamers). This result is surprising because independent studies using clonogenic assays have reported that the expression of an NME2H118F mutant was correlated with markedly reduced viability in human breast carcinoma and murine melanoma cells [285, 378, 403]. Assuming the expression of a kinase mutant is inhibitory for clonogen formation, it would suggest that allosteric inhibition or competitive inhibition exists. However, we observed no evidence of either, suggesting that there is no enzymatic co-operativity between these NME subunits. Intriguingly, another study by Hamby *et al.*, in which highly metastatic human melanoma cells were stably transfected with wild-type and catalytically inactive NME2H118Y, has demonstrated not only that the transfection with catalytically inactive NME2H118Y did not affect cellular viability, but also that metastatic potential of the melanoma cells was significantly reduced, as compared to transfection with wild-type NME2 [404]. The authors claimed that the metastasis suppressive effect of NME2H118Y overexpression is likely due to the ability of the catalytic inactive NME2H118Y to exert a dominant negative effect on wild-type NME2, possibly by competing with endogenous NME2 for binding sites, which implies that it is the presence of catalytically active NME2 in specific binding sites that promotes metastasis [404]. These results together with our own clearly identify conflicting indications of the impact of kinase mutations on cellular processes and on NDPK activity. Whilst it is not easy to reconcile these at this time, one possibility is that the cell type and/or cellular context may have a significant impact on the consequences of expressing NME mutants in a range of processes. Clearly, the role of NDPK activity in cellular viability and cancer metastasis requires further investigation.

Although it remains unclear whether NDPK activity plays any role in the regulation of cellular motility and tumour suppression [241, 278-280], a growing body of evidence supports the notion that NDPK activity is dispensable for NME function as a suppressor of motility/metastasis [285, 377, 378, 403, 405]. For example, it has been shown that the suppressive effect of NME1 on invasion and colonisation of human prostate carcinoma cells is not mediated by its NDPK activity [405]. Furthermore, cellular NDPK activity was not correlated to the suppression of metastatic potential in murine T1735 melanoma cells, suggesting that NDPK activity may not be required for metastasis suppression [378]. On the other hand, studies have shown that the NME1H118F mutant, that lacks the NDPK activity, exhibited compromised metastasis suppressor activity in a human melanoma cell line, suggesting that NDPK activity is required for full metastasis suppression [318].

Despite the conflicting views on the role of NDPK activity in NME-mediated metastasis suppression, it is difficult to understand how a small protein almost entirely spanned by residues that are critical for NDPK activity could suppress cellular motility as NME2 does, in an NDPK activity-independent manner. In our efforts to decipher the mechanisms of action by which MDM2 inhibits NME2 motility suppressive effect, we examined the effects of MDM2 on NME2 protein level and NDPK activity. Overall our results suggest that overexpression of MDM2 plays a role in down-regulation of NME1 and NME2 protein levels and possibly in suppression of NDPK activity. It is possible that reducing the protein levels of the non-metastatic protein NME would result in an increase in cell motility. Nevertheless, this result is in contrast to the published result by Polański *et al.* in which the authors found that ectopically expressed MDM2 has no effect upon the stability of NME2 in H1299 [183], which suggests that down-regulation of NME2 by MDM2 may not be the mechanism by which MDM2 modulates NME2 motility suppressive effect. The more apparent effect of MDM2 in down-regulating NME1, a paralogue of NME2, is not entirely surprising. NME1 shares 88% amino acid sequence similarity with NME2 and is well known for its role as a metastasis suppressor [406, 407]. Yeast two-hybrid library screening and tandem mass spectrometry analysis of MDM2 interacting proteins suggested that NME2 but not NME1 is a direct MDM2-interacting protein [183]. However, co-purification of NME1 with MDM2 in fractions from an MDM2 affinity column was also observed, suggesting that NME1 and NME2 complex with MDM2, perhaps through NME2 acting as a bridge between NME1 and MDM2 [183]. Therefore it is possible that NME2 acts as a bridge to bring MDM2 and NME1 into close proximity so that MDM2 can exert its suppressive effect on NME1 and thereby liberating the motility suppressive effect of NME1 on the cells. Nevertheless, our results have provided some potential insights into the underlying mechanism regarding how the MDM2-NME2 interaction may regulate cell motility, in which cell motility is often regarded as an underlying cause of cancer metastasis.

4.2 Sub-cellular localisation of NME proteins

It remains unclear whether the observed MDM2 suppressive effects on NME expression and NDPK activity described in Sections 3.2.10-13 were E3 ligase-dependent since our data derived from examination of RFM effects on multiple occasions were rather inconsistent. As discussed in Section 1.4.2, MDM2 is an E3 ubiquitin ligase that catalyses both the ubiquitination of its substrate proteins and also its own ubiquitination [57]. Mono-ubiquitination often leads to a change in sub-cellular localisation of target proteins, whilst poly-ubiquitination generally results in proteasomal degradation. Therefore, interaction of NME2 with MDM2 might promote the ubiquitination of NME2 or NME1 that might be present in the same complex, possibly leading to degradation and/or translocation of the NME proteins. Therefore, in addition to the observed down-regulation effect of MDM2 on NME1 and NME2 expression, it is possible that MDM2 may also have an effect on NME proteins sub-cellular localisation. Furthermore, it is possible that the suppressive effect of MDM2 is a compartmentalised effect and that it occurs, for example, in the nucleus, and that the effect could be diluted when the global NDPK activity was measured using whole cell lysate sample.

Therefore, in order to gain a better understanding of the consequences of MDM2 and NME2 interaction, we examined the cellular localisation of MDM2 and NME proteins using sub-cellular fractions of U2OS cells (prepared by Dr Carlos Rubbi). Western blot analysis of MDM2 has been performed for all fractions (cytosolic, nuclear and nucleolar) from untreated and proteasome inhibitor MG132-treated U2OS cells. Figure 3.3.1.1 shows that the main 90-kDa MDM2 band was abundant in the cytoplasmic fraction and was substantially enriched after MG132 treatment, noticeably in nucleoli. One possibility is that nucleoli may be involved in the regulation of proteasome-dependent degradation of the 90-kDa MDM2. Three different NME antibodies have been used for detection of NME proteins in fractionated U2Os samples and 17-kDa NME1 and NME2 bands were found almost exclusively in the cytoplasmic fraction (Figure 3.3.1.1), consistent with a few published reports that NME1 and NME2 are mainly localised in the cytosol [250, 270, 362]. Interestingly, treatment with proteasome inhibitor MG132 did not seem to lead to accumulation of either NME1 or NME2 proteins in the cytoplasmic fraction. This suggests that NME1 and NME2 might not be subjected to proteasomal degradation in the cytoplasm. Whilst we found the observation that MDM2 down-regulates NME1 and NME2 without targeting them for proteasomal degradation puzzling, we were also intrigued by a distinctive ~30-kDa band, found abundantly in both nucleoplasmic and, more noticeably, in nucleolar fractions (Figure 3.3.1.1). The nucleolar accumulation might reflect turnover of an ~30-kDa NME-related protein that trafficks to or through nucleoli. More interestingly, a ladder of bands was detected in the nucleolar fractions when probed with NME-specific antibodies, indicating that some post-translational modifications of some isoforms of NME proteins may occur in nucleoli. The ladder also appeared to be slightly more abundant after treatment with MG132 (Figure 3.3.1.1C and E), suggesting that the unidentified isoforms of NME could be ubiquitinated in nucleoli, possibly for protein shuttling and/or proteasomal degradation and that this might be mediated by MDM2.

4.3 NM23-LV, but not NME1 or NME2, is a substrate for MDM2-mediated ubiquitination

As described above, analysis of sub-cellular fractions from U2OS cells for MDM2 and NME suggest that NME proteins could be targets for MDM2-mediated ubiquitination. It is possible that MDM2 mono- or poly-ubiquitinates NME protein/s and that this post-translational modification then targets the NME for protein localisation or degradation, respectively. Interestingly, in a study using stable cell lines expressing 6xHis-biotin-tagged ubiquitin for purification of the ubiquitinated proteome, Meierhofer *et al.* identified NME1 as one of the potential substrate for ubiquitination in Hela cells [385]. Furthermore, mass spectrometry analyses show that both NME1 and NME2 amino acid sequences share a common peptide (VMLGETNPADS**K**PGTIR) which contains a potential ubiquitination site (K100) [385]. These data have prompted us to examine whether the NME proteins could be subjected to MDM2-mediated ubiquitination using an *in vivo* ubiquitination assay.

Although our results do not support the hypothesis that MDM2 modifies either NME1 or NME2 by ubiquitination, there are some questions that remained to be answered: (1) what is the 30-kDa band commonly detected in the nucleolar fractions when western blot of a fractionation samples was probed with three different NME antibodies (Figure 3.3.1.1C, D E)?; and (2) is it possible that there are other unknown NME isoforms that have been ubiquitinated by MDM2 as suggested by the cell fractionation data (Figure 3.3.1.1C, E) and *in vivo* ubiquitination assay (Figure 3.3.2.1.1C)? In the light of a study by Valentijn *et al.*, that identified a novel NME protein named NM23-LV as a 33-kDa product of a read-through transcript of the tandemly located *NME1* and *NME2* genes [250], we speculated that the unknown band at 30 kDa may represent NM23-LV, and that this long variant may be modified by MDM2 ubiquitination.

We therefore examined whether NM23-LV is a target for MDM2 ubiquitination using the same *in vivo* ubiquitination assay we had used previously in H1299 cells, as described in Figure 3.3.2.3.1. Interestingly, Western blot analyses of the affinity purified samples probed with an antibody that detects both NME1 and NME2 (C1C3) clearly displayed two distinctive bands, of estimated molecular weights of 36 kDa and 40 kDa, in the presence of MDM2 (Figure 3.3.2.3.1B). Considering that unmodified NM23-LV migrates at approximately 28 kDa on our western blot gels and that each ubiquitin moiety weighs approximately 8.5 kDa, it was possible that the doublet of bands were the result of mono-ubiquitinated forms of NM23-LV. If mono-ubiquitination occurred at different sites on NM23-LV this might result in the slight shift observed by Western blot and hence lead to the doublet formation. In addition, MDM2 was also shown to poly-ubiquitinate NM23-LV (Figure 3.3.2.3.1). The fact that the levels of mono- and poly-ubiquitination increased with the amount of wt MDM2 transfected strongly suggests that NM23-LV was ubiquitinated by MDM2 in a dose-dependent manner. Furthermore, NM23-LV ubiquitination was inhibited in cells transfected with RFM (Figure 3.3.2.3.1B, Lane 8), implying that ubiquitination of NM23-LV is E3 ligase-dependent.

To ensure that the results described above were not due to non-specific binding of antibody and that NM23-LV is a genuine target for MDM2-mediated ubiquitination, the experiment described in Figure 3.3.2.3.1 was repeated using HA-tagged NM23-LV plasmid. Since HA is not expressed endogenously, it provides a means of detecting the transfected epitope tagged form of NM23-LV in a highly specific manner. Our results in Figure 3.3.2.3.3 confirmed that NM23-LV is both mono- and poly-ubiquitinated by MDM2, in a RING-finger-dependent manner. Since one of the major roles for ubiquitination is to target the modified substrate for proteasomal degradation, the question arises as to whether ubiquitination of NM23-LV promotes proteasomal degradation. Treatment with proteasome inhibitor MG132 resulted in an increase in NM23-LV ubiquitination that is accompanied by stabilisation of the long variant compared to cells treated with DMSO (Figure 3.3.2.4.1), suggesting that MDM2 ubiquitinates and targets NM23-LV for proteasomal degradation.

One question that arises following these studies is how MDM2 selectively ubiquitinates NM23-LV but not NME1 or NME2, even though the long variant is identical to the amino-terminal end of NME1 and all of NME2. The answer to this is unknown but it is likely that the overall structure of NM23-LV is important, for example, perhaps exposure of the responsible lysine residue(s) for ubiquitination by MDM2 can only occur in NM23-LV or perhaps NM23-LV binds to another as of yet unidentified intermediate protein which aids MDM2-mediated ubiquitination. Little has been reported on the biological roles of NM23-LV (reviewed in Section 1.5.5), but since NM23-LV is a member of the NME family and assuming that its NME2 derived component is still functional, it is likely that the main function of NM23-LV is to act as a kinase. Therefore, we investigated whether NM23-LV functions as an NDPK in an attempt to gain a better understanding of the functional consequences of NM23-LV ubiquitination by MDM2.

4.4 NM23-LV potentially possesses NDPK activity

It is difficult to conclude whether NM23-LV possesses NDPK activity, considering that the comparatively low expression levels of transfected NM23-LV which would make detecting activity from NM23-LV difficult as it would be masked by the considerably higher abundance of endogenous NME1 and NME2 in H1299 cells (Figure 3.3.2.3.2B). Therefore it was necessary to develop an experimental system that will allow us to isolate NM23-LV from cellular NME proteins, in order to selectively measure NDPK activity contributed by NM23-LV alone. Using an immunoprecipitation approach, we first isolated HA-tagged NM23-LV and then examined whether NM23-LV possesses any NDPK activity (Figure 3.4.1.1). At the same time, since ubiquitination of a substrate by MDM2 normally involves MDM2 interacting with the substrate, we also examined the ability of MDM2 to interact with NM23-LV in the same experiment. Our results in Figure 3.4.1.1B have demonstrated that MDM2 was clearly detected in the immunoprecipitated samples upon co-transfection with HA-NM23-LV, but not in the absence of HA-NM23-LV. This indicates that MDM2 is able to form a complex with NM23-LV. Although this result does not tell us whether the interaction between MDM2 and NM23-LV is direct, it is likely that this interaction is crucial for the ability of MDM2 to ubiquitinate NM23-LV. Furthermore, our result (Figure 3.4.1.1A) has also demonstrated a dramatic MDM2 stabilisation in cells co-transfected with HA-NM23-LV and MDM2, compared to those without HA-NM23-LV, suggesting that NM23-LV can act to significantly stabilise MDM2. Reciprocally, MDM2 also has an up-regulating effect on NM23-LV levels (Figure 3.4.1.1C and E).

Immunoprecipitation of HA-NM23-LV for NDPK activity analysis demonstrated that there was a significant increase in NDPK activity in the presence of both MDM2 and HA-NM23-LV as compared to cells transfected with HA-NM23-LV alone (Figure 3.4.1.1). This suggests that MDM2 increases NDPK activity of NM23-LV, most likely by promoting NM23-LV up-regulation. Although we anticipated that isolation of NM23-LV by immunoprecipitation could eliminate the unwanted NDPK activity from endogenous NME proteins in H1299 cells, we have under-estimated the possibility that NM23-LV might interact with endogenous NME2, that has also been shown to interact with MDM2 [183]. Indeed, NME2 protein has been co-immunoprecipitated with HA-NM23-LV (Figure 3.4.1.1F and G, Lanes 3 and 4), particularly with greater abundance in the presence of MDM2 (Lane 4). Therefore, the increase in NDPK activity could be contributed by the presence of NME2 in the immunoprecipitated samples in

Figure 3.4.1.1F, Lanes 3 and 4, probably as a result of NM23-LV oligomerisation with NME2 and of the interaction between NME2 and MDM2, respectively [183].

We next examined the NDPK activity of immunoprecipitated HA-tagged NM23-LV in NME2 stable knockdown clones of the H1299 cell line (HNME2:Cl.7), to minimise possible interaction between NM23-LV and endogenous NME2 and thus to try to minimise the contribution of endogenous NDPK activity resulting from co-purification with HA-tagged NM23-LV. Our results show that NDPK activity increases with the amount of HA-NM23-LV transfected (Figure 3.4.2.1). When an equal amount of HA-NM23-LV and HA-NME2 plasmids were used for transfection, NDPK activity for cells transfected with HA-NME2 was about 3.3-fold higher than that of HA-NM23-LV transfected cells. However, densitometry analyses for the immunoprecipitated HA-tagged proteins shows that HA-NME2 expression levels were at least 6.9-fold higher than that of HA-NM23-LV (Figure 3.4.2.1). Therefore, not only may NM23-LV possess NDPK activity, but we have further estimated that if NM23-LV and NME2 were expressed at equal levels, then NM23-LV has the potential to produce NDPK activity that is at least two-fold higher than NME2. Clearly such estimates are not robust, but the point remains, that the experiments suggest that NM23-LV encodes NDPK activity. Given the low levels of co-purifying NME1 and NME2 it is unlikely that these provide the source of the NDPK activity. Therefore either the activity is derived from NM23-LV or another, co-purifying protein provides it (possibly NME3 or NME4). Further studies will be required to clarify this issue.

The occurrence of a read-through transcript connecting neighbouring genes, although rare in higher organisms, is not unprecedented, and some other examples are accompanied by functional consequences. For example, one of the functional consequences of the fusion of Kua protein with poly-ubiquitination regulator UEV (ubiquitin-conjugating enzyme variant) protein is that the domain regulating ubiquitination is redirected for localisation to cytoplasmic structures, rather than the normal UEV nuclear localisation [408]. As a result of such differences in sub-cellular localisation, nuclear UEV and cytoplasmic Kua-UEV target different substrates for poly-ubiquitination [408]. However, in the case of NM23-LV, the fused proteins originally have similar functions and also belong to the same group of the NME family of genes. It is possible that the two proteins encoded by these genes (*NME1* and *NME2*) are engaged in the same biochemical pathway, such that a requirement for functional interaction would provide driving force for their evolutionary fusion. However, as mentioned, NM23-LV lacks exon 5 of NME1 that houses H118 which is crucial for NDPK activity [250, 280], and thus it seems that the function of NDPK activity is not an obvious driver for the fusion process. Perhaps other biochemical activities such as the 3'-5' exonuclease activity or alternatively structural requirements for interactions with other proteins for functional purposes that are driving the molecular evolution process. To our knowledge, neither the 3'-5' exonuclease activity nor the ability to interact with other proteins has been documented for NM23-LV previously. Based on observations made during the course of this study (discussed in detail in Section 3.4) it is unlikely that the presence of an NM23-LV read-through transcript is a chance event with no true biological function.

The potential role of NM23-LV in supplying NDPK activity in the cells is puzzling, considering that NME1 and NME2 appears to provide sufficient supply for the cell. Since NM23-LV is a fusion product of part of NME1 and the entire NME2 protein, one could speculate that NM23-LV may negate the need for dimerisation since it is already a fusion and thus may resemble pre-formed dimers. Thus NM23-LV may provide the structural requirement for rapid assembly of the NME isoforms into oligomers, possibly for instant supply of NDPK activity. However, the NME monomers consist of four β-sheets whose surfaces are partially covered by six α-helices, and the structure of the kinase is based on folding of the β-sheets in an antiparallel orientation [284, 409]. Since the normal structure of the NME dimer consists of eight β-sheets, it is unlikely that NM23-LV, which only contains seven β-sheets due to the lack of exon 5 of its NME1 domain, is able to adapt to the antiparallel β-sheet formation in order to form a hexamer [250]. This may not be the whole story however, since our immunoprecipitation analysis has shown that NM23-LV and NME2 can co-purify as part of a complex (Figure 3.5.1.1F), suggesting the possibility of oligomerisation between NME2 and NM23-LV. However, further investigation of the direct interaction between the NM23-LV and NME1 or NME2 proteins is required to determine whether NM23-LV is structurally competent for oligomerisation and whether the potential NDPK activity detected here can be unequivocally demonstrated *in vitro*.

The NDPK activity of NM23-LV may have distinct functional consequences for the cell compared to NME1 and NME2. Intriguingly, our results suggest that MDM2 has opposing effects on NDPK activity of NM23-LV when compared to the effect on the NDPK activity of NME1. Whilst MDM2 increases NDPK activity of NM23-LV, probably through MDM2-mediated stabilisation of NM23-LV, MDM2 has a suppressive effect on NDPK activity of NME1 and possibly of NME2. This specific effect of MDM2 on NM23-LV and NME1 or NME2 may reflect differences in the biological pathways regulated by specific NME proteins. For example, the suppressive effect of MDM2 on the NDPK activity of NME1 may reduce the level of NTPs required for microtubule assembly, which is important for cell migration and differentiation [295]. On the other hand, the increased level of NDPK activity of NM23-LV may only be required for the more general role of supplying nucleotides for nucleic acid synthesis or this may have a role in providing NDPK activity to a specific sub-cellular location. Nevertheless, it is important to further confirm whether NM23-LV possesses NDPK activity before more speculations are made, for example, through NDPK activity analysis of a NM23-LV mutant that harbours H118F mutation on the NME2 part of the long variant.

4.5 NM23-LV promotes up-regulation of MDM2 and has inhibitory effects on p53 expression and transcriptional activity

Our study initially focussed on the effect of MDM2 on NM23-LV due to the ability of MDM2 to modify NM23-LV by ubiquitination. Therefore, it was surprising to discover that NM23-LV has a stabilising/upregulatory effect on MDM2 protein. It is well established that MDM2 is a negatively regulator of p53 [48, 80-83] and based on the stabilising effect NM23-LV has on MDM2, we hypothesised that NM23-LV might have a suppressive effect on p53 protein levels. Consistent with previous observations presented in this thesis (Figure 3.4.1.1A), NM23-LV and MDM2 positively regulate the steady-state levels of each other, since co-transfection of MDM2 with NM23-LV results in a marginal increase in NM23-LV levels and a substantial increase in MDM2 levels (Figure 3.4.4.1A, Lane 4). p53 protein levels decrease considerably in the presence of both NM23-LV and MDM2 (Lane 4), most likely due to the presence of a large amount of MDM2 in the cells as a result of stabilisation by NM23-LV. Interestingly, the presence of NM23-LV alone also resulted in a considerable reduction in p53 protein levels (Figure 3.4.4.1A, Lane 3). However, it is possible that the observed reduction in p53 protein levels was due to an increase in endogenous MDM2 level induced by transfected NM23-LV, even though the increase in MDM2 protein level could not be detected on Western blot (Figure 3.4.4.1A, Lanes 1 and 3).

To examine whether down-regulation of p53 by NM23-LV is independent of MDM2, the experiment described above was repeated in double null MEFs (p53$^{-/-}$, Mdm2$^{-/-}$). Although it was difficult to detect the expression of proteins produced from transfected plasmids due to the very low transfection efficiency in double null MEFs (Figure 3.4.4.1B), the expression of p53 was clearly detected in transfected cells. The effect of NM23-LV on p53 in double null MEFs recapitulated that observed in H1299 cells (Figure 3.4.4.1A). Since the presence of NM23-LV alone in the MDM2-null cells also resulted in a considerable decrease in p53 protein levels (Figure 3.4.4.1B, Lane 3), this suggests that NM23-LV has a role in p53 down-regulation that is independent of MDM2. Nonetheless, it seems likely that NM23-LV exerts a greater suppressive effect on p53 expression levels in the presence of MDM2, probably through stabilising MDM2 levels. The role of NM23-LV in p53 down-regulation then led us to examine whether NM23-LV has any effect on p53 transcriptional activity by performing luciferase reporter assays in p53-null H1299 and double null MEFs (p53$^{-/-}$, Mdm2$^{-/-}$) in which a p53 responsive element regulates luciferase expression. Hindered by the uneven *Renilla* activities we observed, most likely due to low transfection efficiency, it is difficult to determine whether NM23-LV alone is capable of suppressing p53 transcriptional activity. However, our results suggest that the presence of NM23-LV augments the suppressive effect of MDM2 on p53 transcriptional activity since NM23-LV in combination with MDM2 resulted in a greater reduction in luciferase expression then MDM2 alone (Figure 3.4.5.1). The combinatorial effect of NM23-LV and MDM2 in reducing both protein levels and p53 transcriptional activity can be explained by the stabilising effects of NM23-LV on MDM2 protein levels (Figure 3.4.4.1). Briefly, as explained in Introduction (Sections 1.4.2.1 and 1.4.4) an increase in MDM2 can lead to increased p53 poly-ubiquitination and proteasomal degradation, hence less p53 protein and subsequently less p53 activity. Conversely, what is less clear is why expression of NM23-LV alone was able to reduce protein levels of p53 independently of MDM2. Nonetheless, based on these results there appears to be a cumulative effect on p53 repression (both protein expression and transcriptional) when MDM2 and NM23-LV are co-expressed.

The role of NME proteins in regulating p53 functions has been previously described. For example, Jung *et al*. reported that NME1 and its interacting partner STRAP physically interact with p53 and induce the dissociation of MDM2 from the p53-MDM2 complex to enhance p53 stability [410]. Overexpression of NME1 and STRAP increases p53-mediated apoptosis and cell cycle arrest suggesting that NME1 and STRAP may play an important role in p53 regulation [410]. Furthermore, NME1 has also been reported to interact with the macrophage migration inhibitory factor (MIF) resulting in dissociation of MIF from MIF-p53 complexes that seems to be crucial for alleviation of MIF-mediated suppression of p53-induced apoptosis and cell cycle arrest [411]. The ability of NME1 to promote p53-mediated apoptosis and cell cycle arrest supports the function of NME1 as a tumour suppressor.

However, this seems opposite to the effect we have observed for NM23-LV on p53 expression levels and transcriptional activity since we have demonstrated that NM23-LV has the ability to down-regulate p53 and enhance MDM2-mediated p53 activity suppression. This suggests that NM23-LV may have opposing effects on p53 stability/activity compared to NME1, implying that the NME proteins may have different roles in p53-mediated biological functions. Furthermore, the opposite effects of NME1 and NM23-LV on p53 stability/activity may be due to different mechanisms employed by the NME proteins to regulate p53 stability/activity. For example, unlike NME1/STRAP, which has been demonstrated to increase p53 stability/activity by removing MDM2 from the p53-MDM2 complex [410], NM23-LV appears to exert its suppressive effect on p53 stability/activity through stabilising MDM2. This highlights the multifaceted nature of NME proteins and adds another layer of complexity to the regulation of p53 activity by NME proteins.

4.6 Functional consequences of NME proteins

Since the NME family of proteins is well known for its non-metastatic properties and the potential for cellular motility is closely related to metastasis, we wanted to examine whether NM23-LV has any effect on cellular motility. Using a Boyden chamber motility assay, our study has demonstrated that H1299 cells transfected with NM23-LV have a significantly higher motility than empty vector control ($p=0.0064$) (Figure 3.4.6.1), suggesting that NM23-LV promotes cell motility. This is not entirely surprising, since NM23-LV has been shown in our study to dramatically increase the level of MDM2 (Figure 3.4.1.1), which in turn has a role in promoting cell motility and invasiveness [103, 384]. Thus, it is possible that NM23-LV has a cell motility promoting effect that is dependent of the presence of MDM2. However, it is unclear as to whether the putative NDPK activity of NM23-LV is responsible for the motility phenotype. Both the kinase dependence and role of MDM2 could be tested in future studies, the latter using MDM2-null cells.

The discovery of NM23-LV as a highly specific ubiquitination substrate of MDM2 and the unexpected roles of NM23-LV in up-regulating MDM2 and promoting cell motility have sparked our interest in studying more functional implications of NM23-LV. In particular, we have generated constructs expressing fluorescence-labelled NME fusion proteins by fusing NME with ECFP/EYFP (Section 2.1.9.1) to study NME proteins sub-cellular distribution and their effect on cell behaviour.

To begin to study whether the functions of NME proteins can be affected by their sub-cellular distribution, H1299 cells were transfected with plasmids expressing C-EYFP labelled NME1, NME2, NMEH118F and NM23-LV, followed by live cell imaging. Our results showed that C-EYFP-tagged NME proteins were mainly found in the cytoplasm (Figure 3.4.8.1), consistent with previously published studies [250, 270]. Another common phenomenon observed was the accumulation of NME1, NME2 and NM23-LV fusion proteins at the nuclear periphery. The accumulation of the NME fusion proteins appeared to result in three different outcomes for the cell: 1) cell undergoes apoptosis; 2) accumulation of NME fusion protein disappears and the cell continues to be viable without division until the end of the course of live cell imaging; 3) accumulation of NME fusion protein disappears and cell divides into two daughter cells successfully (Figure 3.4.8.1). No accumulation of NME2H118F fusion protein, which lacks catalytic activity, was observed around the nuclear periphery that resulted in a successful mitosis (Figure 3.4.8.1D). Based on these observations, and published studies linking NME1 with cytokinesis [379], it is tempting to speculate that the accumulation of NME1 and NME2 around the nuclear periphery is generally required for mitosis and cytokinesis, perhaps to supply GTPs for the cell division process. It is also possible that NME1 and NME2 act as NDP kinases in providing local supply of nucleotides for GTPase dynamin function, as suggested in a study by Conery *et al.* in NME1 [379, 412]. In addition, Pinon *et al.* has also claimed that as well as cytosol distribution, NME1 and NME2 also partly localise to microtubules to support a role of NME in nucleotide channelling and in cell motility regulation [270]. This may explain our observation using live cell imaging (Appendix 11) which suggests that NME1 fusion proteins migrate towards the nuclear membrane in an ordered way, possibly along the microtubules. However, our result needs further verification, such as using specific marker for labelling the microtubule network.

On the other hand, it has been suggested that NME1 can translocate to the nucleus upon treatment with DNA-damaging agents, such as cisplatin and UV radiation, possibly to carry out DNA repair processes [272]. For example, it has been reported that, upon a pro-apoptotic stimulus triggered by cytotoxic T-lymphocytes, NME1 found in an ER-associated complex with other proteins is transported to the nucleus where it carries out a DNA cleavage reaction [413]. Therefore, apart from cell division purpose, the association of NME proteins with nuclei as demonstrated our live cell imaging may also appear to be required for DNA repair purposes.

It is unclear why cells transfected with C-EYFP-NM23-LV undergo cellular death (study was not supported by quantitative analysis) (Figure 3.4.8.1E). It is possible that NM23-LV may have toxic effects on cells and therefore these cells could not tolerate high levels of NM23-LV. Since our results have shown that NM23-LV fusion proteins accumulate possibly in the ER in cells that are about to undergo cellular death, it is also possible that the fusion proteins were not being processed properly in the ER. Another possibility is that NM23-LV fusion protein might be too large in size (~55 kDa) for a free diffusion through nuclear pore complexes, which typically accept proteins smaller than 40 kDa, and thus cannot enter the nucleus where ubiquitination of NM23-LV may normally occur. Perhaps it is the accumulation of NM23-LV fusion proteins, as a result of these proteins not being able to enter the nucleus, that leads to cell death. These are all just speculations since our analysis was limited by the absence of organelle markers to assist examination of the dynamic distribution of NME proteins in different sub-cellular compartments. More experimental evidence is necessary for verification and to address questions that remain unanswered, for example, where does the interaction of MDM2 and NM23-LV take place? Does ubiquitination of NM23-LV by MDM2 occurs in the nucleus or nucleolus?

Our live cell imaging results have suggested that NME proteins overexpression may play a role in causing mitotic failure, which was often accompanied by multi-nuclei formation and seems to happen after accumulation of NME proteins around the nuclear periphery. This has led us to investigate the effect of NME proteins expression on cell cycle using flow cytometry in H1299 cells (Figure 3.4.9.1). We have found that cells expressing NME1, NME2 or NM23-LV fusion proteins have a slightly lower percentage of cells in G1-phase but a higher percentage of cells in S-phase, as compared to cells that expressed EYFP only. The higher percentage of cells in S-phase is in line with the role of NDPK in DNA synthesis. Furthermore, overexpression of the NME fusion proteins seems to have no effect on the DNA ploidy, suggesting that NME proteins may not play a role in causing cytokinesis failure. Nevertheless, before confident conclusions can be made, this study needs to be repeated with higher number of replicates and with appropriate compensation to correct the emission spectral overlap between EYFP and PI to avoid sampling bias.

Chapter 5

Conclusion

5. Conclusion

In our efforts to unravel the mechanisms of action by which high levels of MDM2 promotes cell motility or metastasis, we examined how MDM2 inhibits NME2 motility suppressive effect by studying the roles of MDM2 on NME2 NDPK activity and protein levels. Overall our results suggest that overexpression of MDM2 plays a role in down-regulation of NME1 and NME2 protein levels and possibly suppression of NDPK activity. More interestingly perhaps, our current studies have identified NM23-LV as a novel and highly specific substrate for MDM2-mediated ubiquitination that is dependent on MDM2 E3 ligase activity. Furthermore, our results have also shown that NM23-LV can promote MDM2 stabilisation (Figure 3.4.1.1A), which may serve as an explanation for the observed motility promoting effects of NM23-LV. Considering the canonical tumour suppressive effect of the NME protein family, these findings have highlighted the pleiotropic effects of the NME proteins and expanded the complexity of the regulation between MDM2 and NME family members. The complicated interplay between MDM2 and NME proteins is illustrated in our model (Figure 5.1). NM23-LV-induced MDM2 overexpression may represent an alternative but functionally synonymous means of p53 inactivation. Although this does not explain the co-expression of MDM2 and p53 in RCC, our findings have undoubtedly unveiled a novel and potentially critical mechanism for MDM2 up-regulation as well as identifying a new substrate for MDM2 ubiquitination. The former observation raises the question whether NM23-LV has an inhibitory effect on MDM2 auto-ubiquitination. Perhaps NM23-LV increases MDM2 expression levels by inhibiting MDM2 auto-ubiquitination or preventing the transport of ubiquitinated MDM2 to proteasomes. This, however, requires further investigation.

Many cellular proteins are ubiquitinated at some stage in their life cycle. Whilst poly-ubiquitination has almost become a synonym for protein degradation, it is worth noting that protein ubiquitination has a plethora of signalling functions outside the proteasome pathway. There seems to be a high degree of specificity in MDM2-mediated ubiquitination of NM23-LV, since MDM2 does not seem to ubiquitinate closely related NME1 and NME2 proteins. This may highlight the stringent regulation of ubiquitination that is important for the orchestration of cellular behaviour. It is possible that MDM2 plays a dual role in regulating NM23-LV. For example, our data have suggested that MDM2 can poly-ubiquitinate NM23-LV to target it for proteasomal degradation. Perhaps MDM2-mediated mono-ubiquitination of NM23-LV plays a role in determining sub-cellular localisation, membrane trafficking or endocytosis [84, 414, 415]. Some of the key questions we need to address include: What stimulates mono- or poly-ubiquitination of NM23-LV by MDM2? Does NM23-LV ubiquitination occur in the nucleoli? What are the downstream pathways regulated by NM23-LV ubiquitination? Can the status of NM23-LV ubiquitination be reversed by DUBs as a mean of NM23-LV regulation? Perhaps most importantly, what is the function of NM23-LV? Understanding the ubiquitin signals in these pathways will be beneficial for basic biochemical research and development of therapeutics targeting the ubiquitin system. Although the present study has demonstrated that NM23-LV is a substrate for ubiquitination by MDM2 and that NM23-LV has a substantial effect on MDM2 upregulation, more physiological evidence regarding the functional consequence of these effects is required. Tissue analysis has demonstrated that NM23-LV is ubiquitously expressed at the mRNA level, with the exception of the kidney [250]. Therefore, it will be important to determine the expression or status of NM23-LV in RCC to examine whether NM23-LV plays a role in the development of the disease.

In conclusion, our studies have established a novel and apparently highly specific relationship between MDM2 and NM23-LV. This relationship not only identifies a new direction for studying the regulation of MDM2 and the possible related cancer diseases, but may also add to the functional range of the NME family. Thorough understanding of the specificity of MDM2 interaction with NM23-LV, as well as of mono- and poly-ubiquitination of NM23-LV, will help us to define the physiological functions and regulation of these proteins, which could allow development of potential therapeutic targets for RCCs and possibly other cancers.

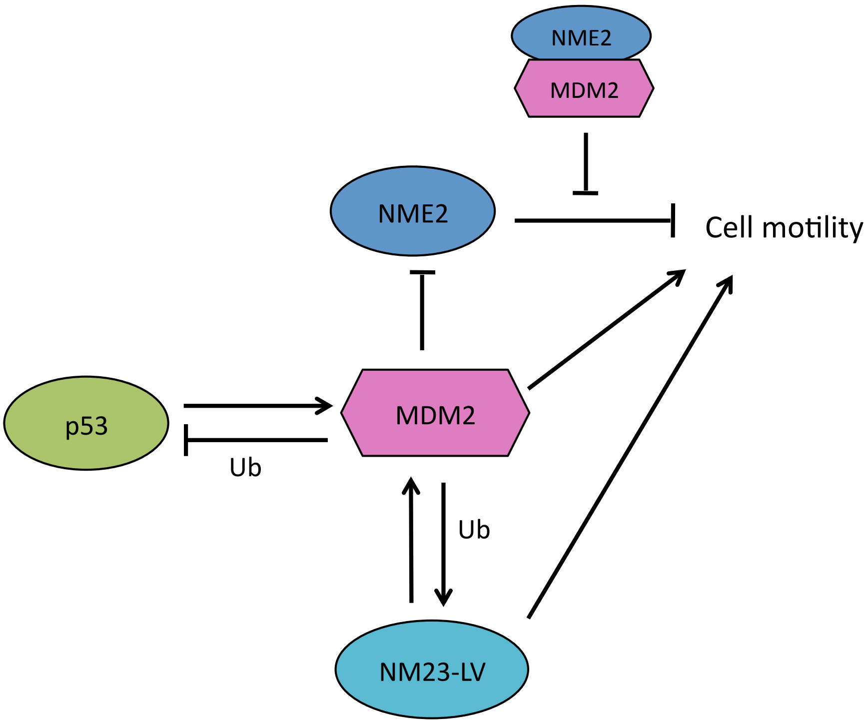

Figure 5.1: A schematic model of the interplay between p53, MDM2 and NME proteins. Ub, mono-/poly-ubiquitination.

Chapter 6

References

6. References

1. Gibbs, W.W., *Untangling the roots of cancer.* Sci Am, 2003. **289**(1): p. 56-65.
2. Hanahan, D. and R.A. Weinberg, *The hallmarks of cancer.* Cell, 2000. **100**(1): p. 57-70.
3. Luo, J., N.L. Solimini, and S.J. Elledge, *Principles of cancer therapy: oncogene and non-oncogene addiction.* Cell, 2009. **136**(5): p. 823-37.
4. Anand, P., et al., *Cancer is a preventable disease that requires major lifestyle changes.* Pharm Res, 2008. **25**(9): p. 2097-116.
5. Lengauer, C., K.W. Kinzler, and B. Vogelstein, *Genetic instabilities in human cancers.* Nature, 1998. **396**(6712): p. 643-9.
6. Sen, S., *Aneuploidy and cancer.* Curr Opin Oncol, 2000. **12**(1): p. 82-8.
7. Lee, E.Y. and W.J. Muller, *Oncogenes and tumor suppressor genes.* Cold Spring Harb Perspect Biol, 2010. **2**(10): p. a003236.
8. Negrini, S., V.G. Gorgoulis, and T.D. Halazonetis, *Genomic instability--an evolving hallmark of cancer.* Nat Rev Mol Cell Biol, 2010. **11**(3): p. 220-8.
9. Sun, W. and J. Yang, *Functional mechanisms for human tumor suppressors.* J Cancer, 2010. **1**: p. 136-40.
10. Vogelstein, B. and K.W. Kinzler, *Cancer genes and the pathways they control.* Nat Med, 2004. **10**(8): p. 789-99.
11. Hanahan, D. and R.A. Weinberg, *Hallmarks of cancer: the next generation.* Cell, 2011. **144**(5): p. 646-74.
12. Malkin, D., *Germline p53 mutations and heritable cancer.* Annu Rev Genet, 1994. **28**: p. 443-65.
13. Seizinger, B.R., et al., *Von Hippel-Lindau disease maps to the region of chromosome 3 associated with renal cell carcinoma.* Nature, 1988. **332**(6161): p. 268-9.
14. Behrendt, A., *Proteomic and Transcriptomic Investigation of the Mechanisms and Consequences of p53 Gain of Function Mutation in Laryngeal Squamous Cell Carcinoma*. 2011, University of Liverpool: Liverpool.
15. Maher, E.R., *Genomics and epigenomics of renal cell carcinoma.* Seminars in Cancer Biology, 2013. **23**: p. 10-17.
16. Baldewijns, M.M., et al., *Genetics and epigenetics of renal cell cancer.* Biochim Biophys Acta, 2008. **1785**(2): p. 133-55.
17. UK, C.R., *UK Kidney Cancer Incidence Statistics* London, United Kingdom: Cancer Research UK, 2010.
18. Lopez-Beltran, A., et al., *2009 update on the classification of renal epithelial tumors in adults.* Int J Urol, 2009. **16**(5): p. 432-43.
19. Lopez-Beltran, A., et al., *2004 WHO classification of the renal tumors of the adults.* Eur Urol, 2006. **49**(5): p. 798-805.
20. Delahunt, B. and J.N. Eble, *Papillary renal cell carcinoma: a clinicopathologic and immunohistochemical study of 105 tumors.* Mod Pathol, 1997. **10**(6): p. 537-44.
21. Pavlovich, C.P. and L.S. Schmidt, *Searching for the hereditary causes of renal-cell carcinoma.* Nat Rev Cancer, 2004. **4**(5): p. 381-93.

22. Storkel, S., et al., *Classification of renal cell carcinoma: Workgroup No. 1. Union Internationale Contre le Cancer (UICC) and the American Joint Committee on Cancer (AJCC).* Cancer, 1997. **80**(5): p. 987-9.
23. Kovacs, G., et al., *The Heidelberg classification of renal cell tumours.* J Pathol, 1997. **183**(2): p. 131-3.
24. Crotty, T.B., G.M. Farrow, and M.M. Lieber, *Chromophobe cell renal carcinoma: clinicopathological features of 50 cases.* J Urol, 1995. **154**(3): p. 964-7.
25. Axwijk, P.H., et al., *Hereditary causes of kidney tumours.* Eur J Clin Invest, 2010. **40**(5): p. 433-9.
26. Linehan, W.M., M.M. Walther, and B. Zbar, *The genetic basis of cancer of the kidney.* J Urol, 2003. **170**(6 Pt 1): p. 2163-72.
27. Bausch, B., et al., *Renal cancer in von Hippel-Lindau disease and related syndromes.* Nat Rev Nephrol, 2013. **9**(9): p. 529-38.
28. Algaba, F., et al., *Current pathology keys of renal cell carcinoma.* Eur Urol, 2011. **60**(4): p. 634-43.
29. Neumann, H.P., et al., *Prevalence, morphology and biology of renal cell carcinoma in von Hippel-Lindau disease compared to sporadic renal cell carcinoma.* J Urol, 1998. **160**(4): p. 1248-54.
30. Linehan, W.M., et al., *Genetic basis of cancer of the kidney: disease-specific approaches to therapy.* Clin Cancer Res, 2004. **10**(18 Pt 2): p. 6282S-9S.
31. Kim, W.Y. and W.G. Kaelin, *Role of VHL gene mutation in human cancer.* J Clin Oncol, 2004. **22**(24): p. 4991-5004.
32. Latif, F., et al., *Identification of the von Hippel-Lindau disease tumor suppressor gene.* Science, 1993. **260**(5112): p. 1317-20.
33. Crossey, P.A., et al., *Molecular genetic investigations of the mechanism of tumourigenesis in von Hippel-Lindau disease: analysis of allele loss in VHL tumours.* Hum Genet, 1994. **93**(1): p. 53-8.
34. Vortmeyer, A.O., et al., *Somatic point mutation of the wild-type allele detected in tumors of patients with VHL germline deletion.* Oncogene, 2002. **21**(8): p. 1167-70.
35. Hon, W.C., et al., *Structural basis for the recognition of hydroxyproline in HIF-1 alpha by pVHL.* Nature, 2002. **417**(6892): p. 975-8.
36. Stebbins, C.E., W.G. Kaelin, Jr., and N.P. Pavletich, *Structure of the VHL-ElonginC-ElonginB complex: implications for VHL tumor suppressor function.* Science, 1999. **284**(5413): p. 455-61.
37. Maxwell, P.H., et al., *The tumour suppressor protein VHL targets hypoxia-inducible factors for oxygen-dependent proteolysis.* Nature, 1999. **399**(6733): p. 271-5.
38. Pause, A., et al., *The von Hippel-Lindau tumor-suppressor gene product forms a stable complex with human CUL-2, a member of the Cdc53 family of proteins.* Proc Natl Acad Sci U S A, 1997. **94**(6): p. 2156-61.
39. Kaelin, W.G., Jr., *The von Hippel-Lindau tumor suppressor protein and clear cell renal carcinoma.* Clin Cancer Res, 2007. **13**(2 Pt 2): p. 680s-684s.
40. Cohen, H.T. and F.J. McGovern, *Renal-cell carcinoma.* N Engl J Med, 2005. **353**(23): p. 2477-90.

41. Gnarra, J.R., et al., *Molecular cloning of the von Hippel-Lindau tumor suppressor gene and its role in renal carcinoma.* Biochim Biophys Acta, 1996. **1242**(3): p. 201-10.
42. Latif, F., et al., *von Hippel-Lindau syndrome: cloning and identification of the plasma membrane Ca(++)-transporting ATPase isoform 2 gene that resides in the von Hippel-Lindau gene region.* Cancer Res, 1993. **53**(4): p. 861-7.
43. Zbar, B., R. Klausner, and W.M. Linehan, *Studying cancer families to identify kidney cancer genes.* Annu Rev Med, 2003. **54**: p. 217-33.
44. Cahilly-Snyder, L., et al., *Molecular analysis and chromosomal mapping of amplified genes isolated from a transformed mouse 3T3 cell line.* Somat Cell Mol Genet, 1987. **13**(3): p. 235-44.
45. Fakharzadeh, S.S., S.P. Trusko, and D.L. George, *Tumorigenic potential associated with enhanced expression of a gene that is amplified in a mouse tumor cell line.* Embo J, 1991. **10**(6): p. 1565-9.
46. Momand, J., et al., *The mdm-2 oncogene product forms a complex with the p53 protein and inhibits p53-mediated transactivation.* Cell, 1992. **69**(7): p. 1237-45.
47. Haupt, Y., et al., *Mdm2 promotes the rapid degradation of p53.* Nature, 1997. **387**(6630): p. 296-9.
48. Kubbutat, M.H., S.N. Jones, and K.H. Vousden, *Regulation of p53 stability by Mdm2.* Nature, 1997. **387**(6630): p. 299-303.
49. Jones, S.N., et al., *Rescue of embryonic lethality in Mdm2-deficient mice by absence of p53.* Nature, 1995. **378**(6553): p. 206-8.
50. Montes de Oca Luna, R., D.S. Wagner, and G. Lozano, *Rescue of early embryonic lethality in mdm2-deficient mice by deletion of p53.* Nature, 1995. **378**(6553): p. 203-6.
51. Shvarts, A., et al., *MDMX: a novel p53-binding protein with some functional properties of MDM2.* Embo J, 1996. **15**(19): p. 5349-57.
52. Wang, X., *p53 regulation: teamwork between RING domains of Mdm2 and MdmX.* Cell Cycle, 2011. **10**(24): p. 4225-9.
53. Parant, J., et al., *Rescue of embryonic lethality in Mdm4-null mice by loss of Trp53 suggests a nonoverlapping pathway with MDM2 to regulate p53.* Nat Genet, 2001. **29**(1): p. 92-5.
54. Shvarts, A., et al., *Isolation and identification of the human homolog of a new p53-binding protein, Mdmx.* Genomics, 1997. **43**(1): p. 34-42.
55. Shadfan, M., V. Lopez-Pajares, and Z.M. Yuan, *MDM2 and MDMX: Alone and together in regulation of p53.* Transl Cancer Res, 2012. **1**(2): p. 88-89.
56. Francoz, S., et al., *Mdm4 and Mdm2 cooperate to inhibit p53 activity in proliferating and quiescent cells in vivo.* Proc Natl Acad Sci U S A, 2006. **103**(9): p. 3232-7.
57. Iwakuma, T. and G. Lozano, *MDM2, an introduction.* Mol Cancer Res, 2003. **1**(14): p. 993-1000.
58. Chen, J., V. Marechal, and A.J. Levine, *Mapping of the p53 and mdm-2 interaction domains.* Mol Cell Biol, 1993. **13**(7): p. 4107-14.
59. Lin, J., et al., *Several hydrophobic amino acids in the p53 amino-terminal domain are required for transcriptional activation, binding to mdm-2 and the adenovirus 5 E1B 55-kD protein.* Genes Dev, 1994. **8**(10): p. 1235-46.

60. Geyer, R.K., Z.K. Yu, and C.G. Maki, *The MDM2 RING-finger domain is required to promote p53 nuclear export.* Nat Cell Biol, 2000. **2**(9): p. 569-73.
61. Lai, Z., et al., *Metal and RNA binding properties of the hdm2 RING finger domain.* Biochemistry, 1998. **37**(48): p. 7005-15.
62. Fang, S., et al., *Mdm2 is a RING finger-dependent ubiquitin protein ligase for itself and p53.* J Biol Chem, 2000. **275**(12): p. 8945-51.
63. Cyril Dominguez, Gert E. Folkers, and R. Boelens (2004) *Biological Introduction: RING domain proteins*. **3**, 338-351.
64. Yang, Y., et al., *Expression and evaluation of RING finger proteins.* Methods Enzymol, 2005. **398**: p. 103-12.
65. Lorick, K.L., et al., *RING fingers mediate ubiquitin-conjugating enzyme (E2)-dependent ubiquitination.* Proc Natl Acad Sci U S A, 1999. **96**(20): p. 11364-9.
66. Tanimura, S., et al., *MDM2 interacts with MDMX through their RING finger domains.* FEBS Lett, 1999. **447**(1): p. 5-9.
67. Linke, K., et al., *Structure of the MDM2/MDMX RING domain heterodimer reveals dimerization is required for their ubiquitylation in trans.* Cell Death Differ, 2008. **15**(5): p. 841-8.
68. Poyurovsky, M.V., et al., *Nucleotide binding by the Mdm2 RING domain facilitates Arf-independent Mdm2 nucleolar localization.* Mol Cell, 2003. **12**(4): p. 875-87.
69. Freedman, D.A. and A.J. Levine, *Nuclear export is required for degradation of endogenous p53 by MDM2 and human papillomavirus E6.* Mol Cell Biol, 1998. **18**(12): p. 7288-93.
70. Roth, J., et al., *Nucleo-cytoplasmic shuttling of the hdm2 oncoprotein regulates the levels of the p53 protein via a pathway used by the human immunodeficiency virus rev protein.* Embo J, 1998. **17**(2): p. 554-64.
71. Tasdemir, E., et al., *Regulation of autophagy by cytoplasmic p53.* Nat Cell Biol, 2008. **10**(6): p. 676-87.
72. Chipuk, J.E., et al., *PUMA couples the nuclear and cytoplasmic proapoptotic function of p53.* Science, 2005. **309**(5741): p. 1732-5.
73. Lohrum, M.A., et al., *Identification of a cryptic nucleolar-localization signal in MDM2.* Nat Cell Biol, 2000. **2**(3): p. 179-81.
74. Argentini, M., N. Barboule, and B. Wasylyk, *The contribution of the acidic domain of MDM2 to p53 and MDM2 stability.* Oncogene, 2001. **20**(11): p. 1267-75.
75. Zhu, Q., et al., *Mdm2 mutant defective in binding p300 promotes ubiquitination but not degradation of p53: evidence for the role of p300 in integrating ubiquitination and proteolysis.* J Biol Chem, 2001. **276**(32): p. 29695-701.
76. Grossman, S.R., et al., *p300/MDM2 complexes participate in MDM2-mediated p53 degradation.* Mol Cell, 1998. **2**(4): p. 405-15.
77. Lindstrom, M.S., et al., *Cancer-associated mutations in the MDM2 zinc finger domain disrupt ribosomal protein interaction and attenuate MDM2-induced p53 degradation.* Mol Cell Biol, 2007. **27**(3): p. 1056-68.
78. Schuster, K., L. Fan, and L.C. Harris, *MDM2 splice variants predominantly localize to the nucleoplasm mediated by a COOH-terminal nuclear localization signal.* Mol Cancer Res, 2007. **5**(4): p. 403-12.

79. Itahana, K., et al., *Targeted inactivation of Mdm2 RING finger E3 ubiquitin ligase activity in the mouse reveals mechanistic insights into p53 regulation.* Cancer Cell, 2007. **12**(4): p. 355-66.
80. Honda, R., H. Tanaka, and H. Yasuda, *Oncoprotein MDM2 is a ubiquitin ligase E3 for tumor suppressor p53.* FEBS Lett, 1997. **420**(1): p. 25-7.
81. Oliner, J.D., et al., *Amplification of a gene encoding a p53-associated protein in human sarcomas.* Nature, 1992. **358**(6381): p. 80-3.
82. Rodriguez, M.S., et al., *Multiple C-terminal lysine residues target p53 for ubiquitin-proteasome-mediated degradation.* Mol Cell Biol, 2000. **20**(22): p. 8458-67.
83. Nakamura, S., J.A. Roth, and T. Mukhopadhyay, *Multiple lysine mutations in the C-terminal domain of p53 interfere with MDM2-dependent protein degradation and ubiquitination.* Mol Cell Biol, 2000. **20**(24): p. 9391-8.
84. Hoeller, D., C.M. Hecker, and I. Dikic, *Ubiquitin and ubiquitin-like proteins in cancer pathogenesis.* Nat Rev Cancer, 2006. **6**(10): p. 776-88.
85. Haglund, K. and I. Dikic, *Ubiquitylation and cell signaling.* Embo J, 2005. **24**(19): p. 3353-9.
86. Hershko, A. and A. Ciechanover, *The ubiquitin system.* Annu Rev Biochem, 1998. **67**: p. 425-79.
87. Hershko, A., et al., *Components of ubiquitin-protein ligase system. Resolution, affinity purification, and role in protein breakdown.* J Biol Chem, 1983. **258**(13): p. 8206-14.
88. Rieser, E., S.M. Cordier, and H. Walczak, *Linear ubiquitination: a newly discovered regulator of cell signalling.* Trends Biochem Sci, 2013. **38**(2): p. 94-102.
89. de Bie, P. and A. Ciechanover, *Ubiquitination of E3 ligases: self-regulation of the ubiquitin system via proteolytic and non-proteolytic mechanisms.* Cell Death Differ, 2011. **18**(9): p. 1393-402.
90. Kirisako, T., et al., *A ubiquitin ligase complex assembles linear polyubiquitin chains.* Embo J, 2006. **25**(20): p. 4877-87.
91. Chau, V., et al., *A multiubiquitin chain is confined to specific lysine in a targeted short-lived protein.* Science, 1989. **243**(4898): p. 1576-83.
92. Glickman, M.H. and A. Ciechanover, *The ubiquitin-proteasome proteolytic pathway: destruction for the sake of construction.* Physiol Rev, 2002. **82**(2): p. 373-428.
93. Jacobson, A.D., et al., *The lysine 48 and lysine 63 ubiquitin conjugates are processed differently by the 26 s proteasome.* J Biol Chem, 2009. **284**(51): p. 35485-94.
94. Hoeller, D., et al., *Regulation of ubiquitin-binding proteins by monoubiquitination.* Nat Cell Biol, 2006. **8**(2): p. 163-9.
95. Stommel, J.M., et al., *A leucine-rich nuclear export signal in the p53 tetramerization domain: regulation of subcellular localization and p53 activity by NES masking.* Embo J, 1999. **18**(6): p. 1660-72.
96. Li, M., et al., *Mono- versus polyubiquitination: differential control of p53 fate by Mdm2.* Science, 2003. **302**(5652): p. 1972-5.
97. Carter, S., et al., *C-terminal modifications regulate MDM2 dissociation and nuclear export of p53.* Nat Cell Biol, 2007. **9**(4): p. 428-35.
98. Marchenko, N.D., et al., *Monoubiquitylation promotes mitochondrial p53 translocation.* Embo J, 2007. **26**(4): p. 923-34.

99. Tao, W. and A.J. Levine, *Nucleocytoplasmic shuttling of oncoprotein Hdm2 is required for Hdm2-mediated degradation of p53.* Proc Natl Acad Sci U S A, 1999. **96**(6): p. 3077-80.
100. Joseph, T.W., A. Zaika, and U.M. Moll, *Nuclear and cytoplasmic degradation of endogenous p53 and HDM2 occurs during down-regulation of the p53 response after multiple types of DNA damage.* Faseb J, 2003. **17**(12): p. 1622-30.
101. Yu, Z.K., R.K. Geyer, and C.G. Maki, *MDM2-dependent ubiquitination of nuclear and cytoplasmic P53.* Oncogene, 2000. **19**(51): p. 5892-7.
102. Boyd, M.T., N. Vlatkovic, and C.P. Rubbi, *The nucleolus directly regulates p53 export and degradation.* J Cell Biol, 2011. **194**(5): p. 689-703.
103. Yang, J.Y., et al., *MDM2 promotes cell motility and invasiveness by regulating E-cadherin degradation.* Mol Cell Biol, 2006. **26**(19): p. 7269-82.
104. Pettersson, S., et al., *Non-degradative ubiquitination of the Notch1 receptor by the E3 ligase MDM2 activates the Notch signalling pathway.* Biochem J, 2013. **450**(3): p. 523-36.
105. Yogosawa, S., et al., *Mammalian Numb is a target protein of Mdm2, ubiquitin ligase.* Biochem Biophys Res Commun, 2003. **302**(4): p. 869-72.
106. Sengupta, S. and B. Wasylyk, *Ligand-dependent interaction of the glucocorticoid receptor with p53 enhances their degradation by Hdm2.* Genes Dev, 2001. **15**(18): p. 2367-80.
107. Girnita, L., A. Girnita, and O. Larsson, *Mdm2-dependent ubiquitination and degradation of the insulin-like growth factor 1 receptor.* Proc Natl Acad Sci U S A, 2003. **100**(14): p. 8247-52.
108. Brenkman, A.B., et al., *Mdm2 induces mono-ubiquitination of FOXO4.* PLoS One, 2008. **3**(7): p. e2819.
109. Maguire, M., et al., *MDM2 regulates dihydrofolate reductase activity through monoubiquitination.* Cancer Res, 2008. **68**(9): p. 3232-42.
110. Uchida, C., et al., *Enhanced Mdm2 activity inhibits pRB function via ubiquitin-dependent degradation.* Embo J, 2005. **24**(1): p. 160-9.
111. Ranaweera, R.S. and X. Yang, *Auto-ubiquitination of Mdm2 enhances its substrate ubiquitin ligase activity.* J Biol Chem, 2013. **288**(26): p. 18939-46.
112. Stommel, J.M. and G.M. Wahl, *Accelerated MDM2 auto-degradation induced by DNA-damage kinases is required for p53 activation.* Embo J, 2004. **23**(7): p. 1547-56.
113. Honda, R. and H. Yasuda, *Activity of MDM2, a ubiquitin ligase, toward p53 or itself is dependent on the RING finger domain of the ligase.* Oncogene, 2000. **19**(11): p. 1473-6.
114. Clegg, H.V., K. Itahana, and Y. Zhang, *Unlocking the Mdm2-p53 loop: ubiquitin is the key.* Cell Cycle, 2008. **7**(3): p. 287-92.
115. Inuzuka, H., et al., *Novel insights into the molecular mechanisms governing Mdm2 ubiquitination and destruction.* Oncotarget, 2010. **1**(7): p. 685-90.
116. Kawai, H., et al., *DNA damage-induced MDMX degradation is mediated by MDM2.* J Biol Chem, 2003. **278**(46): p. 45946-53.
117. Pan, Y. and J. Chen, *MDM2 promotes ubiquitination and degradation of MDMX.* Mol Cell Biol, 2003. **23**(15): p. 5113-21.

118. Minsky, N. and M. Oren, *The RING domain of Mdm2 mediates histone ubiquitylation and transcriptional repression.* Mol Cell, 2004. **16**(4): p. 631-9.
119. Dikic, I., et al., *Targeting ubiquitin in cancers.* Eur J Cancer, 2006. **42**(18): p. 3095-102.
120. Meulmeester, E., et al., *ATM-mediated phosphorylations inhibit Mdmx/Mdm2 stabilization by HAUSP in favor of p53 activation.* Cell Cycle, 2005. **4**(9): p. 1166-70.
121. Meulmeester, E., et al., *Loss of HAUSP-mediated deubiquitination contributes to DNA damage-induced destabilization of Hdmx and Hdm2.* Mol Cell, 2005. **18**(5): p. 565-76.
122. Marchetti, A., et al., *mdm2 gene alterations and mdm2 protein expression in breast carcinomas.* J Pathol, 1995. **175**(1): p. 31-8.
123. Baunoch, D., et al., *MDM2 overexpression in benign and malignant lesions of the human breast.* Int J Oncol, 1996. **8**(5): p. 895-9.
124. Cordon-Cardo, C., et al., *Molecular abnormalities of mdm2 and p53 genes in adult soft tissue sarcomas.* Cancer Res, 1994. **54**(3): p. 794-9.
125. Deb, S.P., *Cell cycle regulatory functions of the human oncoprotein MDM2.* Mol Cancer Res, 2003. **1**(14): p. 1009-16.
126. Leach, F.S., et al., *p53 Mutation and MDM2 amplification in human soft tissue sarcomas.* Cancer Res, 1993. **53**(10 Suppl): p. 2231-4.
127. Rayburn, E., et al., *MDM2 and human malignancies: expression, clinical pathology, prognostic markers, and implications for chemotherapy.* Curr Cancer Drug Targets, 2005. **5**(1): p. 27-41.
128. Rayburn, E.R., S.J. Ezell, and R. Zhang, *Recent advances in validating MDM2 as a cancer target.* Anticancer Agents Med Chem, 2009. **9**(8): p. 882-903.
129. Chen, X., et al., *MDM2 Promotes Invasion and Metastasis in Invasive Ductal Breast Carcinoma by Inducing Matrix Metalloproteinase-9.* PLoS One, 2013. **8**(11): p. e78794.
130. Mathew, R., et al., *Alterations in p53 and pRb pathways and their prognostic significance in oesophageal cancer.* Eur J Cancer, 2002. **38**(6): p. 832-41.
131. Iwakuma, T. and N. Agarwal, *MDM2 binding protein, a novel metastasis suppressor.* Cancer Metastasis Rev, 2012. **31**(3-4): p. 633-40.
132. Gupta, G.P. and J. Massague, *Cancer metastasis: building a framework.* Cell, 2006. **127**(4): p. 679-95.
133. Zhang, L. and R.P. Hill, *Hypoxia enhances metastatic efficiency by up-regulating Mdm2 in KHT cells and increasing resistance to apoptosis.* Cancer Res, 2004. **64**(12): p. 4180-9.
134. Bertout, J.A., S.A. Patel, and M.C. Simon, *The impact of O2 availability on human cancer.* Nat Rev Cancer, 2008. **8**(12): p. 967-75.
135. Zhou, S., et al., *MDM2 Regulates Vascular Endothelial Growth Factor mRNA Stabilization in Hypoxia.* MOLECULAR AND CELLULAR BIOLOGY, 2011. **31**(24): p. 4928–4937.
136. Kannemeier, C., R. Liao, and P. Sun, *The RING finger domain of MDM2 is essential for MDM2-mediated TGF-beta resistance.* Mol Biol Cell, 2007. **18**(6): p. 2367-77.

137. Miwa, S., et al., *Mdm2-mediated pRB downregulation is involved in carcinogenesis in a p53-independent manner.* Biochem Biophys Res Commun, 2006. **340**(1): p. 54-61.
138. Haitel, A., et al., *mdm2 expression as a prognostic indicator in clear cell renal cell carcinoma: comparison with p53 overexpression and clinicopathological parameters.* Clin Cancer Res, 2000. **6**(5): p. 1840-4.
139. Noon, A.P., et al., *Combined p53 and MDM2 biomarker analysis shows a unique pattern of expression associated with poor prognosis in patients with renal cell carcinoma undergoing radical nephrectomy.* BJU Int, 2011.
140. Nenutil, R., et al., *Discriminating functional and non-functional p53 in human tumours by p53 and MDM2 immunohistochemistry.* J Pathol, 2005. **207**(3): p. 251-9.
141. Hollstein, M., et al., *p53 mutations in human cancers.* Science, 1991. **253**(5015): p. 49-53.
142. Malkin, D., et al., *Germ line p53 mutations in a familial syndrome of breast cancer, sarcomas, and other neoplasms.* Science, 1990. **250**(4985): p. 1233-8.
143. Srivastava, S., et al., *Germ-line transmission of a mutated p53 gene in a cancer-prone family with Li-Fraumeni syndrome.* Nature, 1990. **348**(6303): p. 747-9.
144. Donehower, L.A., et al., *Mice deficient for p53 are developmentally normal but susceptible to spontaneous tumours.* Nature, 1992. **356**(6366): p. 215-21.
145. Jacks, T., et al., *Tumor spectrum analysis in p53-mutant mice.* Curr Biol, 1994. **4**(1): p. 1-7.
146. Lane, D.P., *Cancer. p53, guardian of the genome.* Nature, 1992. **358**(6381): p. 15-6.
147. Alarcon-Vargas, D. and Z. Ronai, *p53-Mdm2--the affair that never ends.* Carcinogenesis, 2002. **23**(4): p. 541-7.
148. Tokino, T. and Y. Nakamura, *The role of p53-target genes in human cancer.* Crit Rev Oncol Hematol, 2000. **33**(1): p. 1-6.
149. Kastan, M.B., et al., *Participation of p53 protein in the cellular response to DNA damage.* Cancer Res, 1991. **51**(23 Pt 1): p. 6304-11.
150. Maltzman, W. and L. Czyzyk, *UV irradiation stimulates levels of p53 cellular tumor antigen in nontransformed mouse cells.* Mol Cell Biol, 1984. **4**(9): p. 1689-94.
151. Chen, J., J. Lin, and A.J. Levine, *Regulation of transcription functions of the p53 tumor suppressor by the mdm-2 oncogene.* Mol Med, 1995. **1**(2): p. 142-52.
152. Harms, K.L. and X. Chen, *The functional domains in p53 family proteins exhibit both common and distinct properties.* Cell Death Differ, 2006. **13**(6): p. 890-7.
153. Davison, T.S., et al., *Characterization of the oligomerization defects of two p53 mutants found in families with Li-Fraumeni and Li-Fraumeni-like syndrome.* Oncogene, 1998. **17**(5): p. 651-6.
154. Maki, C.G., *Oligomerization is required for p53 to be efficiently ubiquitinated by MDM2.* J Biol Chem, 1999. **274**(23): p. 16531-5.
155. Kruse, J.P. and W. Gu, *Modes of p53 regulation.* Cell, 2009. **137**(4): p. 609-22.

156. Bode, A.M. and Z. Dong, *Post-translational modification of p53 in tumorigenesis.* Nat Rev Cancer, 2004. **4**(10): p. 793-805.
157. Brooks, C.L. and W. Gu, *Ubiquitination, phosphorylation and acetylation: the molecular basis for p53 regulation.* Curr Opin Cell Biol, 2003. **15**(2): p. 164-71.
158. Oren, M., W. Maltzman, and A.J. Levine, *Post-translational regulation of the 54K cellular tumor antigen in normal and transformed cells.* Mol Cell Biol, 1981. **1**(2): p. 101-10.
159. Reich, N.C., M. Oren, and A.J. Levine, *Two distinct mechanisms regulate the levels of a cellular tumor antigen, p53.* Mol Cell Biol, 1983. **3**(12): p. 2143-50.
160. Rogel, A., et al., *p53 cellular tumor antigen: analysis of mRNA levels in normal adult tissues, embryos, and tumors.* Mol Cell Biol, 1985. **5**(10): p. 2851-5.
161. Oliner, J.D., et al., *Oncoprotein MDM2 conceals the activation domain of tumour suppressor p53.* Nature, 1993. **362**(6423): p. 857-60.
162. Xirodimas, D.P., et al., *Mdm2-mediated NEDD8 conjugation of p53 inhibits its transcriptional activity.* Cell, 2004. **118**(1): p. 83-97.
163. Wu, X., et al., *The p53-mdm-2 autoregulatory feedback loop.* Genes Dev, 1993. **7**(7A): p. 1126-32.
164. Chehab, N.H., et al., *Phosphorylation of Ser-20 mediates stabilization of human p53 in response to DNA damage.* Proc Natl Acad Sci U S A, 1999. **96**(24): p. 13777-82.
165. Hirao, A., et al., *DNA damage-induced activation of p53 by the checkpoint kinase Chk2.* Science, 2000. **287**(5459): p. 1824-7.
166. Danovi, D., et al., *Amplification of Mdmx (or Mdm4) directly contributes to tumor formation by inhibiting p53 tumor suppressor activity.* Mol Cell Biol, 2004. **24**(13): p. 5835-43.
167. Sabbatini, P. and F. McCormick, *MDMX inhibits the p300/CBP-mediated acetylation of p53.* DNA Cell Biol, 2002. **21**(7): p. 519-25.
168. Chavez-Reyes, A., et al., *Switching mechanisms of cell death in mdm2- and mdm4-null mice by deletion of p53 downstream targets.* Cancer Res, 2003. **63**(24): p. 8664-9.
169. Yin, C., et al., *Bax suppresses tumorigenesis and stimulates apoptosis in vivo.* Nature, 1997. **385**(6617): p. 637-40.
170. Lu, M.L., et al., *Impact of alterations affecting the p53 pathway in bladder cancer on clinical outcome, assessed by conventional and array-based methods.* Clin Cancer Res, 2002. **8**(1): p. 171-9.
171. Bouska, A. and C.M. Eischen, *Murine double minute 2: p53-independent roads lead to genome instability or death.* Trends Biochem Sci, 2009. **34**(6): p. 279-86.
172. Lundgren, K., et al., *Targeted expression of MDM2 uncouples S phase from mitosis and inhibits mammary gland development independent of p53.* Genes Dev, 1997. **11**(6): p. 714-25.
173. McDonnell, T.J., et al., *Loss of one but not two mdm2 null alleles alters the tumour spectrum in p53 null mice.* J Pathol, 1999. **188**(3): p. 322-8.
174. Jones, S.N., et al., *Overexpression of Mdm2 in mice reveals a p53-independent role for Mdm2 in tumorigenesis.* Proc Natl Acad Sci U S A, 1998. **95**(26): p. 15608-12.

175. Bartel, F., H. Taubert, and L.C. Harris, *Alternative and aberrant splicing of MDM2 mRNA in human cancer.* Cancer Cell, 2002. **2**(1): p. 9-15.
176. Harris, L.C., *MDM2 splice variants and their therapeutic implications.* Curr Cancer Drug Targets, 2005. **5**(1): p. 21-6.
177. Steinman, H.A., et al., *An alternative splice form of Mdm2 induces p53-independent cell growth and tumorigenesis.* J Biol Chem, 2004. **279**(6): p. 4877-86.
178. Weinberg, R.A., *The Biology of Cancer.* 2007: Garland Science.
179. Boyd, M.T., N. Vlatkovic, and D.S. Haines, *A novel cellular protein (MTBP) binds to MDM2 and induces a G1 arrest that is suppressed by MDM2.* J Biol Chem, 2000. **275**(41): p. 31883-90.
180. Kamijo, T., et al., *Functional and physical interactions of the ARF tumor suppressor with p53 and Mdm2.* Proc Natl Acad Sci U S A, 1998. **95**(14): p. 8292-7.
181. Quelle, D.E., et al., *Alternative reading frames of the INK4a tumor suppressor gene encode two unrelated proteins capable of inducing cell cycle arrest.* Cell, 1995. **83**(6): p. 993-1000.
182. Martin, K., et al., *Stimulation of E2F1/DP1 transcriptional activity by MDM2 oncoprotein.* Nature, 1995. **375**(6533): p. 691-4.
183. Polanski, R., et al., *MDM2 interacts with NME2 (non-metastatic cells 2, protein) and suppresses the ability of NME2 to negatively regulate cell motility.* Carcinogenesis, 2011. **32**(8): p. 1133-42.
184. Vlatkovic, N., et al., *MDM2 interacts with the C-terminus of the catalytic subunit of DNA polymerase epsilon.* Nucleic Acids Res, 2000. **28**(18): p. 3581-6.
185. Kostic, M., et al., *Solution structure of the Hdm2 C2H2C4 RING, a domain critical for ubiquitination of p53.* J Mol Biol, 2006. **363**(2): p. 433-50.
186. Linares, L.K., et al., *HdmX stimulates Hdm2-mediated ubiquitination and degradation of p53.* Proc Natl Acad Sci U S A, 2003. **100**(21): p. 12009-14.
187. Okamoto, K., Y. Taya, and H. Nakagama, *Mdmx enhances p53 ubiquitination by altering the substrate preference of the Mdm2 ubiquitin ligase.* FEBS Lett, 2009. **583**(17): p. 2710-4.
188. Kawai, H., et al., *RING domain-mediated interaction is a requirement for MDM2's E3 ligase activity.* Cancer Res, 2007. **67**(13): p. 6026-30.
189. Gu, J., et al., *Mutual dependence of MDM2 and MDMX in their functional inactivation of p53.* J Biol Chem, 2002. **277**(22): p. 19251-4.
190. Migliorini, D., et al., *Hdmx recruitment into the nucleus by Hdm2 is essential for its ability to regulate p53 stability and transactivation.* J Biol Chem, 2002. **277**(9): p. 7318-23.
191. Garcia, S.N. and L. Pillus, *Net results of nucleolar dynamics.* Cell, 1999. **97**(7): p. 825-8.
192. Honda, R. and H. Yasuda, *Association of p19(ARF) with Mdm2 inhibits ubiquitin ligase activity of Mdm2 for tumor suppressor p53.* Embo J, 1999. **18**(1): p. 22-7.
193. Stott, F.J., et al., *The alternative product from the human CDKN2A locus, p14(ARF), participates in a regulatory feedback loop with p53 and MDM2.* Embo J, 1998. **17**(17): p. 5001-14.

194. Tao, W. and A.J. Levine, *P19(ARF) stabilizes p53 by blocking nucleo-cytoplasmic shuttling of Mdm2.* Proc Natl Acad Sci U S A, 1999. **96**(12): p. 6937-41.
195. Weber, J.D., et al., *Nucleolar Arf sequesters Mdm2 and activates p53.* Nat Cell Biol, 1999. **1**(1): p. 20-6.
196. Sherr, C.J. and J.D. Weber, *The ARF/p53 pathway.* Curr Opin Genet Dev, 2000. **10**(1): p. 94-9.
197. Llanos, S., et al., *Stabilization of p53 by p14ARF without relocation of MDM2 to the nucleolus.* Nat Cell Biol, 2001. **3**(5): p. 445-52.
198. Korgaonkar, C., et al., *Nucleophosmin (B23) targets ARF to nucleoli and inhibits its function.* Mol Cell Biol, 2005. **25**(4): p. 1258-71.
199. Buchkovich, K., L.A. Duffy, and E. Harlow, *The retinoblastoma protein is phosphorylated during specific phases of the cell cycle.* Cell, 1989. **58**(6): p. 1097-105.
200. Weinberg, R.A., *The retinoblastoma protein and cell cycle control.* Cell, 1995. **81**(3): p. 323-30.
201. Xiao, Z.X., et al., *Interaction between the retinoblastoma protein and the oncoprotein MDM2.* Nature, 1995. **375**(6533): p. 694-8.
202. Hsieh, J.K., et al., *RB regulates the stability and the apoptotic function of p53 via MDM2.* Mol Cell, 1999. **3**(2): p. 181-93.
203. Yap, D.B., et al., *mdm2: a bridge over the two tumour suppressors, p53 and Rb.* Oncogene, 1999. **18**(53): p. 7681-9.
204. Momand, J., H.H. Wu, and G. Dasgupta, *MDM2--master regulator of the p53 tumor suppressor protein.* Gene, 2000. **242**(1-2): p. 15-29.
205. Yamasaki, L., et al., *Tumor induction and tissue atrophy in mice lacking E2F-1.* Cell, 1996. **85**(4): p. 537-48.
206. Shan, B. and W.H. Lee, *Deregulated expression of E2F-1 induces S-phase entry and leads to apoptosis.* Mol Cell Biol, 1994. **14**(12): p. 8166-73.
207. Field, S.J., et al., *E2F-1 functions in mice to promote apoptosis and suppress proliferation.* Cell, 1996. **85**(4): p. 549-61.
208. Loughran, O. and N.B. La Thangue, *Apoptotic and growth-promoting activity of E2F modulated by MDM2.* Mol Cell Biol, 2000. **20**(6): p. 2186-97.
209. Meek, D.W. and U. Knippschild, *Posttranslational modification of MDM2.* Mol Cancer Res, 2003. **1**(14): p. 1017-26.
210. Cremona, C.A. and A. Behrens, *ATM signalling and cancer.* Oncogene, 2013.
211. de Toledo, S.M., et al., *ATM complexes with HDM2 and promotes its rapid phosphorylation in a p53-independent manner in normal and tumor human cells exposed to ionizing radiation.* Oncogene, 2000. **19**(54): p. 6185-93.
212. Khosravi, R., et al., *Rapid ATM-dependent phosphorylation of MDM2 precedes p53 accumulation in response to DNA damage.* Proc Natl Acad Sci U S A, 1999. **96**(26): p. 14973-7.
213. Banin, S., et al., *Enhanced phosphorylation of p53 by ATM in response to DNA damage.* Science, 1998. **281**(5383): p. 1674-7.
214. Siliciano, J.D., et al., *DNA damage induces phosphorylation of the amino terminus of p53.* Genes Dev, 1997. **11**(24): p. 3471-81.
215. Ashcroft, M., et al., *Phosphorylation of HDM2 by Akt.* Oncogene, 2002. **21**(13): p. 1955-62.

216. Ogawara, Y., et al., *Akt enhances Mdm2-mediated ubiquitination and degradation of p53.* J Biol Chem, 2002. **277**(24): p. 21843-50.
217. Mayo, L.D. and D.B. Donner, *A phosphatidylinositol 3-kinase/Akt pathway promotes translocation of Mdm2 from the cytoplasm to the nucleus.* Proc Natl Acad Sci U S A, 2001. **98**(20): p. 11598-603.
218. Sionov, R.V., et al., *c-Abl neutralizes the inhibitory effect of Mdm2 on p53.* J Biol Chem, 1999. **274**(13): p. 8371-4.
219. Brady, M., N. Vlatkovic, and M.T. Boyd, *Regulation of p53 and MDM2 activity by MTBP.* Mol Cell Biol, 2005. **25**(2): p. 545-53.
220. Odvody, J., et al., *A deficiency in Mdm2 binding protein inhibits Myc-induced B-cell proliferation and lymphomagenesis.* Oncogene, 2010. **29**(22): p. 3287-96.
221. Vlatkovic, N., et al., *Loss of MTBP expression is associated with reduced survival in a biomarker-defined subset of patients with squamous cell carcinoma of the head and neck.* Cancer, 2011. **117**(13): p. 2939-50.
222. Iwakuma, T., et al., *Mtbp haploinsufficiency in mice increases tumor metastasis.* Oncogene, 2008. **27**(13): p. 1813-20.
223. Agarwal, N., et al., *MTBP suppresses cell migration and filopodia formation by inhibiting ACTN4.* Oncogene, 2013. **32**(4): p. 462-70.
224. Honda, K., et al., *Actinin-4, a novel actin-bundling protein associated with cell motility and cancer invasion.* J Cell Biol, 1998. **140**(6): p. 1383-93.
225. Honda, K., et al., *Actinin-4 increases cell motility and promotes lymph node metastasis of colorectal cancer.* Gastroenterology, 2005. **128**(1): p. 51-62.
226. Menez, J., et al., *Mutant alpha-actinin-4 promotes tumorigenicity and regulates cell motility of a human lung carcinoma.* Oncogene, 2004. **23**(15): p. 2630-9.
227. Gu, W. and R.G. Roeder, *Activation of p53 sequence-specific DNA binding by acetylation of the p53 C-terminal domain.* Cell, 1997. **90**(4): p. 595-606.
228. Lacombe, M.L., et al., *The human Nm23/nucleoside diphosphate kinases.* J Bioenerg Biomembr, 2000. **32**(3): p. 247-58.
229. Hama, H., et al., *Nucleoside diphosphate kinase from Escherichia coli; its overproduction and sequence comparison with eukaryotic enzymes.* Gene, 1991. **105**(1): p. 31-6.
230. Rosengard, A.M., et al., *Reduced Nm23/Awd protein in tumour metastasis and aberrant Drosophila development.* Nature, 1989. **342**(6246): p. 177-80.
231. Desvignes, T., et al., *Nme protein family evolutionary history, a vertebrate perspective.* BMC Evol Biol, 2009. **9**: p. 256.
232. Postel, E.H., et al., *Catalysis of DNA cleavage and nucleoside triphosphate synthesis by NM23-H2/NDP kinase share an active site that implies a DNA repair function.* Proc Natl Acad Sci U S A, 2000. **97**(26): p. 14194-9.
233. Venturelli, D., et al., *Overexpression of DR-nm23, a protein encoded by a member of the nm23 gene family, inhibits granulocyte differentiation and induces apoptosis in 32Dc13 myeloid cells.* Proc Natl Acad Sci U S A, 1995. **92**(16): p. 7435-9.
234. Dearolf, C.R., E. Hersperger, and A. Shearn, *Developmental consequences of awdb3, a cell-autonomous lethal mutation of Drosophila induced by hybrid dysgenesis.* Dev Biol, 1988. **129**(1): p. 159-68.

235. Okabe-Kado, J., et al., *Inhibitory action of nm23 proteins on induction of erythroid differentiation of human leukemia cells.* Biochim Biophys Acta, 1995. **1267**(2-3): p. 101-6.
236. Li, M.Q., et al., *NME1 suppression promotes growth, adhesion and implantation of endometrial stromal cells via Akt and MAPK/Erk1/2 signal pathways in the endometriotic milieu.* Hum Reprod, 2013. **28**(10): p. 2822-31.
237. Dai, Z., W. Xiao, and Y. Jin, *Inhibition of nm23-H1 gene expression in chronic myelogenous leukemia cells.* Oncol Lett, 2013. **6**(4): p. 1093-1097.
238. Marino, N., et al., *Nm23-h1 binds to gelsolin and inactivates its actin-severing capacity to promote tumor cell motility and metastasis.* Cancer Res, 2013. **73**(19): p. 5949-62.
239. Lee, M.J., et al., *Pro-oncogenic potential of NM23-H2 in hepatocellular carcinoma.* Exp Mol Med, 2012. **44**(3): p. 214-24.
240. Krebs, H.A. and R. Hems, *Some reactions of adenosine and inosine phosphates in animal tissues.* Biochim Biophys Acta, 1953. **12**(1-2): p. 172-80.
241. Berg, P. and W.K. Joklik, *Transphosphorylation between nucleoside polyphosphates.* Nature, 1953. **172**(4387): p. 1008-9.
242. Munoz-Dorado, J., M. Inouye, and S. Inouye, *Nucleoside diphosphate kinase from Myxococcus xanthus. I. Cloning and sequencing of the gene.* J Biol Chem, 1990. **265**(5): p. 2702-6.
243. Lacombe, M.L., et al., *Functional cloning of a nucleoside diphosphate kinase from Dictyostelium discoideum.* J Biol Chem, 1990. **265**(17): p. 10012-8.
244. Kimura, N., et al., *Isolation and characterization of a cDNA clone encoding rat nucleoside diphosphate kinase.* J Biol Chem, 1990. **265**(26): p. 15744-9.
245. *HUGO Gene Nomenclature Committee at the European Bioinformatics Institute*. Available from: http://www.genenames.org/.
246. Steeg, P.S., et al., *Evidence for a novel gene associated with low tumor metastatic potential.* J Natl Cancer Inst, 1988. **80**(3): p. 200-4.
247. Biggs, J., et al., *A Drosophila gene that is homologous to a mammalian gene associated with tumor metastasis codes for a nucleoside diphosphate kinase.* Cell, 1990. **63**(5): p. 933-40.
248. Timmons, L. and A. Shearn, *prune/Killer of prune: a conditional dominant lethal interaction in Drosophila.* Adv Genet, 1997. **35**: p. 207-52.
249. Boissan, M., et al., *The mammalian Nm23/NDPK family: from metastasis control to cilia movement.* Mol Cell Biochem, 2009. **329**(1-2): p. 51-62.
250. Valentijn, L.J., J. Koster, and R. Versteeg, *Read-through transcript from NM23-H1 into the neighboring NM23-H2 gene encodes a novel protein, NM23-LV.* Genomics, 2006. **87**(4): p. 483-9.
251. Prakash, T., et al., *Expression of conjoined genes: another mechanism for gene regulation in eukaryotes.* PLoS One, 2010. **5**(10): p. e13284.
252. Negroni, A., et al., *Neuroblastoma specific effects of DR-nm23 and its mutant forms on differentiation and apoptosis.* Cell Death Differ, 2000. **7**(9): p. 843-50.
253. Milon, L., et al., *The human nm23-H4 gene product is a mitochondrial nucleoside diphosphate kinase.* J Biol Chem, 2000. **275**(19): p. 14264-72.

254. Milon, L., et al., *nm23-H4, a new member of the family of human nm23/nucleoside diphosphate kinase genes localised on chromosome 16p13.* Hum Genet, 1997. **99**(4): p. 550-7.

255. Erent, M., et al., *Structural and catalytic properties and homology modelling of the human nucleoside diphosphate kinase C, product of the DRnm23 gene.* Eur J Biochem, 2001. **268**(7): p. 1972-81.

256. Biggs, J., et al., *Analysis of the lethal interaction between the prune and Killer of prune mutations of Drosophila.* Genes Dev, 1988. **2**(10): p. 1333-43.

257. Lascu, I., et al., *A Pro/Ser substitution in nucleoside diphosphate kinase of Drosophila melanogaster (mutation killer of prune) affects stability but not catalytic efficiency of the enzyme.* J Biol Chem, 1992. **267**(18): p. 12775-81.

258. Chiadmi, M., et al., *Crystal structure of the Awd nucleotide diphosphate kinase from Drosophila.* Structure, 1993. **1**(4): p. 283-93.

259. Tokarska-Schlattner, M., et al., *The nucleoside diphosphate kinase D (NM23-H4) binds the inner mitochondrial membrane with high affinity to cardiolipin and couples nucleotide transfer with respiration.* J Biol Chem, 2008. **283**(38): p. 26198-207.

260. Schlattner, U., et al., *Dual function of mitochondrial Nm23-H4 protein in phosphotransfer and intermembrane lipid transfer: a cardiolipin-dependent switch.* J Biol Chem, 2013. **288**(1): p. 111-21.

261. Munier, A., et al., *A new human nm23 homologue (nm23-H5) specifically expressed in testis germinal cells.* FEBS Lett, 1998. **434**(3): p. 289-94.

262. Munier, A., et al., *Nm23/NDP kinases in human male germ cells: role in spermiogenesis and sperm motility?* Exp Cell Res, 2003. **289**(2): p. 295-306.

263. Chapman, E.J., G. Kelly, and M.A. Knowles, *Genes involved in differentiation, stem cell renewal, and tumorigenesis are modulated in telomerase-immortalized human urothelial cells.* Mol Cancer Res, 2008. **6**(7): p. 1154-68.

264. Parris, T.Z., et al., *Clinical implications of gene dosage and gene expression patterns in diploid breast carcinoma.* Clin Cancer Res, 2010. **16**(15): p. 3860-74.

265. Mehus, J.G., P. Deloukas, and D.O. Lambeth, *NME6: a new member of the nm23/nucleoside diphosphate kinase gene family located on human chromosome 3p21.3.* Hum Genet, 1999. **104**(6): p. 454-9.

266. Tsuiki, H., et al., *A novel human nucleoside diphosphate (NDP) kinase, Nm23-H6, localizes in mitochondria and affects cytokinesis.* J Cell Biochem, 1999. **76**(2): p. 254-69.

267. Sadek, C.M., et al., *Characterization of human thioredoxin-like 2. A novel microtubule-binding thioredoxin expressed predominantly in the cilia of lung airway epithelium and spermatid manchette and axoneme.* J Biol Chem, 2003. **278**(15): p. 13133-42.

268. Schwahn, U., et al., *Positional cloning of the gene for X-linked retinitis pigmentosa 2.* Nat Genet, 1998. **19**(4): p. 327-32.

269. Yoon, J.H., et al., *The retinitis pigmentosa-mutated RP2 protein exhibits exonuclease activity and translocates to the nucleus in response to DNA damage.* Exp Cell Res, 2006. **312**(8): p. 1323-34.

270. Pinon, V.P., et al., *Cytoskeletal association of the A and B nucleoside diphosphate kinases of interphasic but not mitotic human carcinoma cell lines: specific nuclear localization of the B subunit.* Exp Cell Res, 1999. **246**(2): p. 355-67.
271. Ma, D., J.R. McCorkle, and D.M. Kaetzel, *The metastasis suppressor NM23-H1 possesses 3'-5' exonuclease activity.* J Biol Chem, 2004. **279**(17): p. 18073-84.
272. Yoon, J.H., et al., *Characterization of the 3' --> 5' exonuclease activity found in human nucleoside diphosphate kinase 1 (NDK1) and several of its homologues.* Biochemistry, 2005. **44**(48): p. 15774-86.
273. Bosnar, M.H., et al., *Subcellular localization of A and B Nm23/NDPK subunits.* Exp Cell Res, 2004. **298**(1): p. 275-84.
274. Postel, E.H., et al., *Human c-myc transcription factor PuF identified as nm23-H2 nucleoside diphosphate kinase, a candidate suppressor of tumor metastasis.* Science, 1993. **261**(5120): p. 478-80.
275. Duriez, B., et al., *A common variant in combination with a nonsense mutation in a member of the thioredoxin family causes primary ciliary dyskinesia.* Proc Natl Acad Sci U S A, 2007. **104**(9): p. 3336-41.
276. Lascu, I. and P. Gonin, *The catalytic mechanism of nucleoside diphosphate kinases.* J Bioenerg Biomembr, 2000. **32**(3): p. 237-46.
277. Morera, S., et al., *Mechanism of phosphate transfer by nucleoside diphosphate kinase: X-ray structures of the phosphohistidine intermediate of the enzymes from Drosophila and Dictyostelium.* Biochemistry, 1995. **34**(35): p. 11062-70.
278. Parks, R.E. and R.P. Agarwal, *The Enzymes (Boyer, P.D., Ed.).* Academic Press, New York, 1973. **8**: p. 307-334.
279. Agarwal, R.P., B. Robison, and R.E. Parks, Jr., *Nucleoside diphosphokinase from human erythrocytes.* Methods Enzymol, 1978. **51**: p. 376-86.
280. Gilles, A.M., et al., *Nucleoside diphosphate kinase from human erythrocytes. Structural characterization of the two polypeptide chains responsible for heterogeneity of the hexameric enzyme.* J Biol Chem, 1991. **266**(14): p. 8784-9.
281. Knowles, J.R., *Enzyme-catalyzed phosphoryl transfer reactions.* Annu Rev Biochem, 1980. **49**: p. 877-919.
282. Masoudi, N., et al., *The NM23-H1/H2 homolog NDK-1 is required for full activation of Ras signaling in C. elegans.* Development, 2013. **140**(16): p. 3486-95.
283. Hippe, H.J., et al., *Activation of heterotrimeric G proteins by a high energy phosphate transfer via nucleoside diphosphate kinase (NDPK) B and Gbeta subunits. Specific activation of Gsalpha by an NDPK B.Gbetagamma complex in H10 cells.* J Biol Chem, 2003. **278**(9): p. 7227-33.
284. Dumas, C., et al., *X-ray structure of nucleoside diphosphate kinase.* Embo J, 1992. **11**(9): p. 3203-8.
285. Baba, H., et al., *Two isotypes of murine nm23/nucleoside diphosphate kinase, nm23-M1 and nm23-M2, are involved in metastatic suppression of a murine melanoma line.* Cancer Res, 1995. **55**(9): p. 1977-81.
286. Stahl, J.A., et al., *Identification of a second human nm23 gene, nm23-H2.* Cancer Res, 1991. **51**(1): p. 445-9.

287. Arnaud-Dabernat, S., et al., *Knockout mice as model systems for studying nm23/NDP kinase gene functions. Application to the nm23-M1 gene.* J Bioenerg Biomembr, 2003. **35**(1): p. 19-30.

288. Di, L., et al., *Nucleoside diphosphate kinase B knock-out mice have impaired activation of the K+ channel KCa3.1, resulting in defective T cell activation.* J Biol Chem, 2010. **285**(50): p. 38765-71.

289. Postel, E.H., et al., *Targeted deletion of Nm23/nucleoside diphosphate kinase A and B reveals their requirement for definitive erythropoiesis in the mouse embryo.* Dev Dyn, 2009. **238**(3): p. 775-87.

290. Boissan, M. and M.L. Lacombe, *Learning about the functions of NME/NM23: lessons from knockout mice to silencing strategies.* Naunyn Schmiedebergs Arch Pharmacol, 2011. **384**(4-5): p. 421-31.

291. Presecan, E., A. Vonica, and I. Lascu, *Nucleoside diphosphate kinase from human erythrocytes: purification, molecular mass and subunit structure.* FEBS Lett, 1989. **250**(2): p. 629-32.

292. Williams, R.L., et al., *Crystal structure of Myxococcus xanthus nucleoside diphosphate kinase and its interaction with a nucleotide substrate at 2.0 A resolution.* J Mol Biol, 1993. **234**(4): p. 1230-47.

293. Schaertl, S., *Quaternary structure of human nucleoside diphosphate kinase isoforms HA and HB in solution.* FEBS Lett, 1996. **394**(3): p. 316-20.

294. Roymans, D., et al., *Nucleoside diphosphate kinase (NDPK/NM23) and the waltz with multiple partners: possible consequences in tumor metastasis.* Clin Exp Metastasis, 2002. **19**(6): p. 465-76.

295. Lombardi, D., et al., *The association of the Nm23-M1 protein and beta-tubulin correlates with cell differentiation.* Exp Cell Res, 1995. **217**(2): p. 267-71.

296. Roymans, D., et al., *Nucleoside diphosphate kinase beta (Nm23-R1/NDPKbeta) is associated with intermediate filaments and becomes upregulated upon cAMP-induced differentiation of rat C6 glioma.* Exp Cell Res, 2000. **261**(1): p. 127-38.

297. Hippe, H.J., et al., *The interaction of nucleoside diphosphate kinase B with Gbetagamma dimers controls heterotrimeric G protein function.* Proc Natl Acad Sci U S A, 2009. **106**(38): p. 16269-74.

298. Leone, A., et al., *Evidence for nm23 RNA overexpression, DNA amplification and mutation in aggressive childhood neuroblastomas.* Oncogene, 1993. **8**(4): p. 855-65.

299. Zou, M., et al., *High levels of Nm23 gene expression in advanced stage of thyroid carcinomas.* Br J Cancer, 1993. **68**(2): p. 385-8.

300. Engel, M., et al., *High levels of nm23-H1 and nm23-H2 messenger RNA in human squamous-cell lung carcinoma are associated with poor differentiation and advanced tumor stages.* Int J Cancer, 1993. **55**(3): p. 375-9.

301. Miele, M.E., et al., *Suppression of human melanoma metastasis following introduction of chromosome 6 is independent of NME1 (Nm23).* Clin Exp Metastasis, 1997. **15**(3): p. 259-65.

302. Lim, S., H.Y. Lee, and H. Lee, *Inhibition of colonization and cell-matrix adhesion after nm23-H1 transfection of human prostate carcinoma cells.* Cancer Lett, 1998. **133**(2): p. 143-9.

303. Jinka, R., et al., *Alterations in Cell-Extracellular Matrix Interactions during Progression of Cancers.* Int J Cell Biol, 2012. **2012**: p. 219196.

304. Liu, F., et al., *Transfection of the nm23-H1 gene into human hepatocarcinoma cell line inhibits the expression of sialyl Lewis X, alpha1,3 fucosyltransferase VII, and metastatic potential.* J Cancer Res Clin Oncol, 2002. **128**(4): p. 189-96.
305. Steeg, P.S., et al., *Altered expression of NM23, a gene associated with low tumor metastatic potential, during adenovirus 2 Ela inhibition of experimental metastasis.* Cancer Res, 1988. **48**(22): p. 6550-4.
306. Li, Y., et al., *[Experimental study on molecular mechanism of nm23-H1 gene transfection reversing the malignant phenotype of human high-metastatic large cell lung cancer cell line].* Zhongguo Fei Ai Za Zhi, 2006. **9**(4): p. 307-11.
307. Miyazaki, H., et al., *Overexpression of nm23-H2/NDP kinase B in a human oral squamous cell carcinoma cell line results in reduced metastasis, differentiated phenotype in the metastatic site, and growth factor-independent proliferative activity in culture.* Clin Cancer Res, 1999. **5**(12): p. 4301-7.
308. Leone, A., et al., *Reduced tumor incidence, metastatic potential, and cytokine responsiveness of nm23-transfected melanoma cells.* Cell, 1991. **65**(1): p. 25-35.
309. Boissan, M., et al., *Increased lung metastasis in transgenic NM23-Null/SV40 mice with hepatocellular carcinoma.* J Natl Cancer Inst, 2005. **97**(11): p. 836-45.
310. Thakur, R.K., et al., *Mechanisms of non-metastatic 2 (NME2)-mediated control of metastasis across tumor types.* Naunyn Schmiedebergs Arch Pharmacol, 2011. **384**(4-5): p. 397-406.
311. Fukuda, M., et al., *Decreased expression of nucleoside diphosphate kinase alpha isoform, an nm23-H2 gene homolog, is associated with metastatic potential of rat mammary-adenocarcinoma cells.* Int J Cancer, 1996. **65**(4): p. 531-7.
312. Bhujwalla, Z.M., et al., *Nm23-transfected MDA-MB-435 human breast carcinoma cells form tumors with altered phospholipid metabolism and pH: a 31P nuclear magnetic resonance study in vivo and in vitro.* Magn Reson Med, 1999. **41**(5): p. 897-903.
313. McDermott, W.G., et al., *Nm23-H1 homologs suppress tumor cell motility and anchorage independent growth.* Clin Exp Metastasis, 2008. **25**(2): p. 131-8.
314. Oda, Y., et al., *Comparison of histological changes and changes in nm23 and c-MET expression between primary and metastatic sites in osteosarcoma: a clinicopathologic and immunohistochemical study.* Hum Pathol, 2000. **31**(6): p. 709-16.
315. Niitsu, N., et al., *Serum nm23-H1 protein as a prognostic factor in aggressive non-Hodgkin lymphoma.* Blood, 2001. **97**(5): p. 1202-10.
316. Marino, N., J.C. Marshall, and P.S. Steeg, *Protein-protein interactions: a mechanism regulating the anti-metastatic properties of Nm23-H1.* Naunyn Schmiedebergs Arch Pharmacol, 2011. **384**(4-5): p. 351-62.
317. Boissan, M., et al., *Implication of metastasis suppressor NM23-H1 in maintaining adherens junctions and limiting the invasive potential of human cancer cells.* Cancer Res, 2010. **70**(19): p. 7710-22.
318. Zhang, Q., et al., *Metastasis suppressor function of NM23-H1 requires its 3'-5' exonuclease activity.* Int J Cancer, 2011. **128**(1): p. 40-50.

319. Cuello, F., et al., *Activation of heterotrimeric G proteins by a high energy phosphate transfer via nucleoside diphosphate kinase (NDPK) B and Gbeta subunits. Complex formation of NDPK B with Gbeta gamma dimers and phosphorylation of His-266 IN Gbeta.* J Biol Chem, 2003. **278**(9): p. 7220-6.
320. Wallet, V., et al., *Dictyostelium nucleoside diphosphate kinase highly homologous to Nm23 and Awd proteins involved in mammalian tumor metastasis and Drosophila development.* J Natl Cancer Inst, 1990. **82**(14): p. 1199-202.
321. Wagner, P.D. and N.D. Vu, *Phosphorylation of geranyl and farnesyl pyrophosphates by Nm23 proteins/nucleoside diphosphate kinases.* J Biol Chem, 2000. **275**(45): p. 35570-6.
322. Krishnan, K.S., et al., *Nucleoside diphosphate kinase, a source of GTP, is required for dynamin-dependent synaptic vesicle recycling.* Neuron, 2001. **30**(1): p. 197-210.
323. Dammai, V., et al., *Drosophila awd, the homolog of human nm23, regulates FGF receptor levels and functions synergistically with shi/dynamin during tracheal development.* Genes Dev, 2003. **17**(22): p. 2812-24.
324. Nallamothu, G., et al., *Awd, the homolog of metastasis suppressor gene Nm23, regulates Drosophila epithelial cell invasion.* Mol Cell Biol, 2008. **28**(6): p. 1964-73.
325. Ignesti, M., et al., *Notch signaling during development requires the function of awd, the Drosophila homolog of human metastasis suppressor gene Nm23.* BMC Biol, 2014. **12**: p. 12.
326. Boissan, M., et al., *Membrane trafficking. Nucleoside diphosphate kinases fuel dynamin superfamily proteins with GTP for membrane remodeling.* Science, 2014. **344**(6191): p. 1510-5.
327. Otero, A.S., *NM23/nucleoside diphosphate kinase and signal transduction.* J Bioenerg Biomembr, 2000. **32**(3): p. 269-75.
328. Otero, A.S., *Copurification of vimentin, energy metabolism enzymes, and a MER5 homolog with nucleoside diphosphate kinase. Identification of tissue-specific interactions.* J Biol Chem, 1997. **272**(23): p. 14690-4.
329. Mendez, M.G., S. Kojima, and R.D. Goldman, *Vimentin induces changes in cell shape, motility, and adhesion during the epithelial to mesenchymal transition.* FASEB J, 2010. **24**(6): p. 1838-51.
330. Gervasi, F., et al., *nm23 influences proliferation and differentiation of PC12 cells in response to nerve growth factor.* Cell Growth Differ, 1996. **7**(12): p. 1689-95.
331. Lakshmi, M.S., C. Parker, and G.V. Sherbet, *Metastasis associated MTS1 and NM23 genes affect tubulin polymerisation in B16 melanomas: a possible mechanism of their regulation of metastatic behaviour of tumours.* Anticancer Res, 1993. **13**(2): p. 299-303.
332. Sun, H.Q., et al., *Gelsolin, a multifunctional actin regulatory protein.* J Biol Chem, 1999. **274**(47): p. 33179-82.
333. Bierie, B. and H.L. Moses, *TGF-beta and cancer.* Cytokine Growth Factor Rev, 2006. **17**(1-2): p. 29-40.
334. Hsu, S., et al., *The role of nm23 in transforming growth factor beta 1-mediated adherence and growth arrest.* Cell Growth Differ, 1994. **5**(9): p. 909-17.

335. Matsumura, T., et al., *Regulation of transforming growth factor-beta-dependent cyclooxygenase-2 expression in fibroblasts.* J Biol Chem, 2009. **284**(51): p. 35861-71.
336. Levy, G.N., *Prostaglandin H synthases, nonsteroidal anti-inflammatory drugs, and colon cancer.* Faseb J, 1997. **11**(4): p. 234-47.
337. Herschman, H.R., *Prostaglandin synthase 2.* Biochim Biophys Acta, 1996. **1299**(1): p. 125-40.
338. Molina, M.A., et al., *Increased cyclooxygenase-2 expression in human pancreatic carcinomas and cell lines: growth inhibition by nonsteroidal anti-inflammatory drugs.* Cancer Res, 1999. **59**(17): p. 4356-62.
339. Sawaoka, H., et al., *Cyclooxygenase-2 inhibitors suppress the growth of gastric cancer xenografts via induction of apoptosis in nude mice.* Am J Physiol, 1998. **274**(6 Pt 1): p. G1061-7.
340. Peng, J.P., et al., *Overexpression of cyclooxygenase-2 in nasopharyngeal carcinoma and association with lymph node metastasis.* Oral Oncol, 2005. **41**(9): p. 903-8.
341. Kaul, R., et al., *Epstein-Barr virus protein can upregulate cyclo-oxygenase-2 expression through association with the suppressor of metastasis Nm23-H1.* J Virol, 2006. **80**(3): p. 1321-31.
342. Zhao, R., et al., *nm23-H1 is a negative regulator of TGF-beta1-dependent induction of epithelial-mesenchymal transition.* Exp Cell Res, 2013. **319**(5): p. 740-9.
343. Mosselman, S., J. Polman, and R. Dijkema, *ER beta: identification and characterization of a novel human estrogen receptor.* FEBS Lett, 1996. **392**(1): p. 49-53.
344. Kuiper, G.G., et al., *Cloning of a novel receptor expressed in rat prostate and ovary.* Proc Natl Acad Sci U S A, 1996. **93**(12): p. 5925-30.
345. Hall, J.M., J.F. Couse, and K.S. Korach, *The multifaceted mechanisms of estradiol and estrogen receptor signaling.* J Biol Chem, 2001. **276**(40): p. 36869-72.
346. Hartman, J., A. Strom, and J.A. Gustafsson, *Estrogen receptor beta in breast cancer--diagnostic and therapeutic implications.* Steroids, 2009. **74**(8): p. 635-41.
347. Rayner, K., et al., *Discovery of NM23-H2 as an estrogen receptor beta-associated protein: role in estrogen-induced gene transcription and cell migration.* J Steroid Biochem Mol Biol, 2008. **108**(1-2): p. 72-81.
348. Curtis, C.D., et al., *Interaction of the tumor metastasis suppressor nonmetastatic protein 23 homologue H1 and estrogen receptor alpha alters estrogen-responsive gene expression.* Cancer Res, 2007. **67**(21): p. 10600-7.
349. Dong, S.W., et al., *Expression patterns of ER, HER2, and NM23-H1 in breast cancer patients with different menopausal status: correlations with metastasis.* Mol Diagn Ther, 2011. **15**(4): p. 211-9.
350. Freije, J.M., et al., *Site-directed mutation of Nm23-H1. Mutations lacking motility suppressive capacity upon transfection are deficient in histidine-dependent protein phosphotransferase pathways in vitro.* J Biol Chem, 1997. **272**(9): p. 5525-32.
351. Wagner, P.D., P.S. Steeg, and N.D. Vu, *Two-component kinase-like activity of nm23 correlates with its motility-suppressing activity.* Proc Natl Acad Sci U S A, 1997. **94**(17): p. 9000-5.

352. Hartsough, M.T., et al., *Nm23-H1 metastasis suppressor phosphorylation of kinase suppressor of Ras via a histidine protein kinase pathway.* J Biol Chem, 2002. **277**(35): p. 32389-99.
353. Morrison, D.K., *KSR: a MAPK scaffold of the Ras pathway?* J Cell Sci, 2001. **114**(Pt 9): p. 1609-12.
354. Ward, Y., et al., *Signal pathways which promote invasion and metastasis: critical and distinct contributions of extracellular signal-regulated kinase and Ral-specific guanine exchange factor pathways.* Mol Cell Biol, 2001. **21**(17): p. 5958-69.
355. Steeg, P.S., *Metastasis suppressors alter the signal transduction of cancer cells.* Nat Rev Cancer, 2003. **3**(1): p. 55-63.
356. Lee, M.Y., et al., *NM23H2 inhibits EGF- and Ras-induced proliferation of NIH3T3 cells by blocking the ERK pathway.* Cancer Lett, 2009. **275**(2): p. 221-6.
357. Hall, A., *Rho GTPases and the actin cytoskeleton.* Science, 1998. **279**(5350): p. 509-14.
358. Schmidt, A. and A. Hall, *Guanine nucleotide exchange factors for Rho GTPases: turning on the switch.* Genes Dev, 2002. **16**(13): p. 1587-609.
359. Van Aelst, L. and C. D'Souza-Schorey, *Rho GTPases and signaling networks.* Genes Dev, 1997. **11**(18): p. 2295-322.
360. Iwashita, S., et al., *Lbc proto-oncogene product binds to and could be negatively regulated by metastasis suppressor nm23-H2.* Biochem Biophys Res Commun, 2004. **320**(4): p. 1063-8.
361. Otsuki, Y., et al., *Tumor metastasis suppressor nm23H1 regulates Rac1 GTPase by interaction with Tiam1.* Proc Natl Acad Sci U S A, 2001. **98**(8): p. 4385-90.
362. Fournier, H.N., et al., *Integrin cytoplasmic domain-associated protein 1alpha (ICAP-1alpha) interacts directly with the metastasis suppressor nm23-H2, and both proteins are targeted to newly formed cell adhesion sites upon integrin engagement.* J Biol Chem, 2002. **277**(23): p. 20895-902.
363. Murakami, M., et al., *The suppressor of metastasis Nm23-H1 interacts with the Cdc42 Rho family member and the pleckstrin homology domain of oncoprotein Dbl-1 to suppress cell migration.* Cancer Biol Ther, 2008. **7**(5): p. 677-88.
364. Murakami, M., et al., *Nm23-H1 modulates the activity of the guanine exchange factor Dbl-1.* Int J Cancer, 2008. **123**(3): p. 500-10.
365. Toksoz, D. and D.A. Williams, *Novel human oncogene lbc detected by transfection with distinct homology regions to signal transduction products.* Oncogene, 1994. **9**(2): p. 621-8.
366. Horak, C.E., et al., *Nm23-H1 suppresses tumor cell motility by down-regulating the lysophosphatidic acid receptor EDG2.* Cancer Res, 2007. **67**(15): p. 7238-46.
367. Zhu, J., et al., *Interaction of the Ras-related protein associated with diabetes rad and the putative tumor metastasis suppressor NM23 provides a novel mechanism of GTPase regulation.* Proc Natl Acad Sci U S A, 1999. **96**(26): p. 14911-8.
368. Tseng, Y.H., et al., *Regulation of growth and tumorigenicity of breast cancer cells by the low molecular weight GTPase Rad and nm23.* Cancer Res, 2001. **61**(5): p. 2071-9.

369. da Silva, J.S. and C.G. Dotti, *Breaking the neuronal sphere: regulation of the actin cytoskeleton in neuritogenesis.* Nat Rev Neurosci, 2002. **3**(9): p. 694-704.
370. Ji, L., M. Arcinas, and L.M. Boxer, *The transcription factor, Nm23H2, binds to and activates the translocated c-myc allele in Burkitt's lymphoma.* J Biol Chem, 1995. **270**(22): p. 13392-8.
371. Thakur, R.K., et al., *Metastases suppressor NM23-H2 interaction with G-quadruplex DNA within c-MYC promoter nuclease hypersensitive element induces c-MYC expression.* Nucleic Acids Res, 2009. **37**(1): p. 172-83.
372. Postel, E.H. and C.A. Ferrone, *Nucleoside diphosphate kinase enzyme activity of NM23-H2/PuF is not required for its DNA binding and in vitro transcriptional functions.* J Biol Chem, 1994. **269**(12): p. 8627-30.
373. Michelotti, E.F., et al., *Nm23/PuF does not directly stimulate transcription through the CT element in vivo.* J Biol Chem, 1997. **272**(36): p. 22526-30.
374. Hildebrandt, M., et al., *A human NDP-kinase B specifically binds single-stranded poly-pyrimidine sequences.* Nucleic Acids Res, 1995. **23**(19): p. 3858-64.
375. Agou, F., et al., *Single strand DNA specificity analysis of human nucleoside diphosphate kinase B.* J Biol Chem, 1999. **274**(28): p. 19630-8.
376. Shevelev, I.V. and U. Hubscher, *The 3' 5' exonucleases.* Nat Rev Mol Cell Biol, 2002. **3**(5): p. 364-76.
377. Leone, A., et al., *Transfection of human nm23-H1 into the human MDA-MB-435 breast carcinoma cell line: effects on tumor metastatic potential, colonization and enzymatic activity.* Oncogene, 1993. **8**(9): p. 2325-33.
378. MacDonald, N.J., et al., *A serine phosphorylation of Nm23, and not its nucleoside diphosphate kinase activity, correlates with suppression of tumor metastatic potential.* J Biol Chem, 1993. **268**(34): p. 25780-9.
379. Conery, A.R., S. Sever, and E. Harlow, *Nucleoside diphosphate kinase Nm23-H1 regulates chromosomal stability by activating the GTPase dynamin during cytokinesis.* Proc Natl Acad Sci U S A, 2010. **107**(35): p. 15461-6.
380. Weaver, B.A. and D.W. Cleveland, *Does aneuploidy cause cancer?* Curr Opin Cell Biol, 2006. **18**(6): p. 658-67.
381. Manchado, E., M. Guillamot, and M. Malumbres, *Killing cells by targeting mitosis.* Cell Death Differ, 2012. **19**(3): p. 369-77.
382. Nowak, M.A., et al., *The role of chromosomal instability in tumor initiation.* Proc Natl Acad Sci U S A, 2002. **99**(25): p. 16226-31.
383. Prabhu, V.V., et al., *Targeting tumor metastasis by regulating Nm23 gene expression.* Asian Pac J Cancer Prev, 2012. **13**(8): p. 3539-48.
384. Polanski, R., et al., *MDM2 promotes cell motility and invasiveness through a RING-finger independent mechanism.* FEBS Lett, 2010. **584**(22): p. 4695-702.
385. Meierhofer, D., et al., *Quantitative analysis of global ubiquitination in HeLa cells by mass spectrometry.* J Proteome Res, 2008. **7**(10): p. 4566-76.
386. Bradford, M.M., *A rapid and sensitive method for the quantitation of microgram quantities of protein utilizing the principle of protein-dye binding.* Anal Biochem, 1976. **72**: p. 248-54.
387. Lam, Y.W. and A.I. Lamond, *Isolation of nucleoli*, in *Cell Biology: A Laboratory Handbook*. 2006, Elsevier Academic Press: Amsterdam/Boston.

388. Lu, C., et al., *Increased alpha-tubulin1b expression indicates poor prognosis and resistance to chemotherapy in hepatocellular carcinoma.* Dig Dis Sci, 2013. **58**(9): p. 2713-20.
389. Liu, Y., et al., *Identification of differential expression of genes in hepatocellular carcinoma by suppression subtractive hybridization combined cDNA microarray.* Oncol Rep, 2007. **18**(4): p. 943-51.
390. Avondo, F., et al., *Fibroblasts from patients with Diamond-Blackfan anaemia show abnormal expression of genes involved in protein synthesis, amino acid metabolism and cancer.* BMC Genomics, 2009. **10**: p. 442.
391. Lee, N.V., et al., *ADAMTS1 mediates the release of antiangiogenic polypeptides from TSP1 and 2.* EMBO J, 2006. **25**(22): p. 5270-83.
392. Luque, A., D.R. Carpizo, and M.L. Iruela-Arispe, *ADAMTS1/METH1 inhibits endothelial cell proliferation by direct binding and sequestration of VEGF165.* J Biol Chem, 2003. **278**(26): p. 23656-65.
393. Esselens, C., et al., *The cleavage of semaphorin 3C induced by ADAMTS1 promotes cell migration.* J Biol Chem, 2010. **285**(4): p. 2463-73.
394. Frank, M. and R. Kemler, *Protocadherins.* Curr Opin Cell Biol, 2002. **14**(5): p. 557-62.
395. Venkov, P.V. and A.A. Hadjiolov, *Differential stability of 28s and 18s rat liver ribosomal ribonucleic acids.* Biochem J, 1969. **115**(1): p. 91-4.
396. Lascu, I., E. Presecan, and I. Proinov, *Binding of ATP to nucleoside-diphosphate kinase: a kinetic study.* FEBS Lett, 1986. **202**(2): p. 345-8.
397. Subler, M.A., D.W. Martin, and S. Deb, *Inhibition of viral and cellular promoters by human wild-type p53.* J Virol, 1992. **66**(8): p. 4757-62.
398. Pollok, B.A. and R. Heim, *Using GFP in FRET-based applications.* Trends Cell Biol, 1999. **9**(2): p. 57-60.
399. Hovmoller, S. and T. Zhou, *Why are both ends of the polypeptide chain on the outside of proteins?* Proteins, 2004. **55**(2): p. 219-22.
400. Snapp, E., *Design and Use of Fluorescent Fusion Proteins in Cell Biology.* Curr Protoc Cell Biol, 2005. **Unit–21.4**.
401. Watson, J.V., S.H. Chambers, and P.J. Smith, *A pragmatic approach to the analysis of DNA histograms with a definable G1 peak.* Cytometry, 1987. **8**(1): p. 1-8.
402. Keim, D., et al., *Proliferation-related expression of p19/nm23 nucleoside diphosphate kinase.* J Clin Invest, 1992. **89**(3): p. 919-24.
403. MacDonald, N.J., et al., *Site-directed mutagenesis of nm23-H1. Mutation of proline 96 or serine 120 abrogates its motility inhibitory activity upon transfection into human breast carcinoma cells.* J Biol Chem, 1996. **271**(41): p. 25107-16.
404. Hamby, C.V., et al., *Expression of a catalytically inactive H118Y mutant of nm23-H2 suppresses the metastatic potential of line IV Cl 1 human melanoma cells.* Int J Cancer, 2000. **88**(4): p. 547-53.
405. Lee, H.Y. and H. Lee, *Inhibitory activity of nm23-H1 on invasion and colonization of human prostate carcinoma cells is not mediated by its NDP kinase activity.* Cancer Lett, 1999. **145**(1-2): p. 93-9.
406. Palmieri, D., et al., *Translational approaches using metastasis suppressor genes.* J Bioenerg Biomembr, 2006. **38**(3-4): p. 151-61.
407. Steeg, P.S., *Perspectives on classic article: metastasis suppressor genes.* J Natl Cancer Inst, 2004. **96**(6): p. E4.

408. Thomson, T.M., et al., *Fusion of the human gene for the polyubiquitination coeffector UEV1 with Kua, a newly identified gene.* Genome Res, 2000. **10**(11): p. 1743-56.
409. Webb, P.A., et al., *The crystal structure of a human nucleoside diphosphate kinase, NM23-H2.* J Mol Biol, 1995. **251**(4): p. 574-87.
410. Jung, H., H.A. Seong, and H. Ha, *NM23-H1 tumor suppressor and its interacting partner STRAP activate p53 function.* J Biol Chem, 2007. **282**(48): p. 35293-307.
411. Jung, H., H.A. Seong, and H. Ha, *Direct interaction between NM23-H1 and macrophage migration inhibitory factor (MIF) is critical for alleviation of MIF-mediated suppression of p53 activity.* J Biol Chem, 2008. **283**(47): p. 32669-79.
412. Shpetner, H.S. and R.B. Vallee, *Dynamin is a GTPase stimulated to high levels of activity by microtubules.* Nature, 1992. **355**(6362): p. 733-5.
413. Fan, Z., et al., *Tumor suppressor NM23-H1 is a granzyme A-activated DNase during CTL-mediated apoptosis, and the nucleosome assembly protein SET is its inhibitor.* Cell, 2003. **112**(5): p. 659-72.
414. Miranda, M. and A. Sorkin, *Regulation of receptors and transporters by ubiquitination: new insights into surprisingly similar mechanisms.* Mol Interv, 2007. **7**(3): p. 157-67.
415. Ikeda, F. and I. Dikic, *Atypical ubiquitin chains: new molecular signals. 'Protein Modifications: Beyond the Usual Suspects' review series.* EMBO Rep, 2008. **9**(6): p. 536-42.

Chapter 7

Appendices

7. Appendices

Appendix 1: Conditions for amplification of NME DNA fragments by PCR. A. DNA templates and primers; **B.** PCR components and; **C.** conditions used for amplification of NME DNA fragments.

A

Template	**Forward primer**	**Reverse primer**
pCEP4-NME2	NME2-1F+ECoRI	NME2-dSTOP-R+BamHI
pCEP4-NME2	NME2-1F+ECoRI	NME2-R+BamHI
pCEP4-NME2H118F	NME2-1F+ECoRI	NME2-R+BamHI
pCEP4-NME2H118F	NME2-1F+ECoRI	NME2-dSTOP-R+BamHI
pCEP4-NME1	NME1-1F+ECoRI-S	NME1-dSTOP-R+BamHI
pCEP4-NME1	NME1-1F+ECoRI-S	NME1-R+BamHI
pcDNA3.1-NM23-LV	NME1-1F+ECoRI-S	NME2-dSTOP-R+BamHI
pcDNA3.1-NM23-LV	NME1-1F+ECoRI-S	NME2-R+BamHI

B

Components for PCR	**/ 50 µl**
5x Phusion HF Buffer	x 1
dNTPs	200 µM
F-primer	0.1 µg
R-primer	0.1 µg
Phusion DNA polymerase	1 unit
Template DNA	5 ng
Nuclease-free H_2O	To 50 µl

C

	Phusion High-Fidelity DNA polymerase	
Initial denaturisation	98°C	30 sec
15 cycles		
Denaturisation	98°C	10 sec
Anneal	60°C	30 sec
Extend	72°C	15 sec
Final extension	72°C	7 minutes
Hold	4°C	

Appendix 2: List of primers used in this study.

Name	**Sequence 5’→3’** F- forward R- reverse
ADAMTS1	F- CAGCCCACAGGAACTGGAAGCA
	R- GGCTGCCACCGAAAACAACGTG
PCDHB2	F- TAAGGCGGTCGCTCCGGGAAA
	R- TGCTCCAGCTCTGGCTCACGT
RPS24	F- GTTGGTGCTGGCAAAAAGTGAGC
	R- TCTTGCGAAAAATCCACAGTGGCC
TUBA1B	F- CCGCAGCCGCTACTTAAGAGGC
	R- AGATGCACTCACGCATAGTGGC
HPRT	F- GTGTTGGATATAAGCCAGACTTTGTT
	R- AACTCAACTTGAACTCTCATCTTAGGC
NME1-1F+EcoRI-S	F- gagaGAATTCtgGAACCATGGCCAACTGTGAGCGTACCT
NME1-dSTOP-R+BamHI	R- gagaGGATCCctTTCATAGATCCAGTTCTGAGCA
NME1-2R+BamHI	R- gagaGGATCCctCCTCCTGTCATTCATAGATCC
NME2-1F+EcoRI	F- gagaGAATTCtgCCCGGACCATGGCCAACCTGGA
NME2-dSTOP-R+BamHI	R- gagaGGATCCctTTCATAGACCCAGTCATGAGCA
NME2-2R+BamHI-S	R- gagaGGATCCTCCACCTCTTATTCATAGACCC

Appendix 3: The list of genes found to be mutually up-regulated in Clone 9 and RFM9 compared to H1299 (Batch 1) cells. Statistical analysis was performed using Student's *t*-Test. (Data analysis was performed by Dr Bryony Llyod).

Full name	Gene Symbol	Fold-Change (clone 9 vs. H1299)	p-value (clone 9 vs. H1299)	Fold-Change (RFM9 vs. H1299)	p-value (RFM9 vs. H1299)
Protocadherin beta 2	PCDHB2	6.82	7.45E-04	4.41	2.80E-03
Solute carrier family 16, member 3	SLC16A3	6.48	3.69E-05	2.28	3.11E-03
ADAM metallopeptidase with thrombospondin type 1 motif	ADAMTS1	5.70	9.29E-05	2.95	1.23E-03
Protocadherin beta 5	PCDHB5	5.56	7.76E-05	2.30	3.62E-03
G0/G1switch 2	G0S2	5.53	3.24E-03	3.09	2.07E-02
Interleukin 13 receptor, alpha 2	IL13RA2	5.38	1.39E-05	2.09	1.37E-03
Lysophosphatidylcholine acyltransferase 2	LPCAT2	4.98	1.82E-06	2.97	1.76E-05
Sestrin 3	SESN3	4.24	7.05E-04	2.20	1.32E-02
Annexin A3	ANXA3	3.85	4.91E-05	3.69	5.88E-05
Interferon, gamma-inducible protein 16	IFI16	3.71	5.51E-05	5.39	1.29E-05
Transforming growth factor, beta-induced, 68kDa	TGFBI	3.37	1.29E-02	2.78	2.60E-02
Integrin, alpha 2	ITGA2	2.98	8.37E-03	3.23	6.06E-03
RAB27B, member RAS oncogene family	RAB27B	2.89	6.24E-03	2.65	9.17E-03
MOB1, Mps One Binder kinase activator-like 2B	MOBKL2B	2.74	3.39E-04	2.41	7.08E-04
Mdm2 p53 binding protein homolog (mouse)	MDM2	2.63	2.09E-05	3.04	9.25E-06
Muscleblind-like 3 (Drosophila)	MBNL3	2.46	1.22E-05	3.50	1.73E-06
Protocadherin beta 11	PCDHB11	2.41	8.00E-03	2.16	1.41E-02
Podocalyxin-like	PODXL	2.36	6.45E-03	2.84	2.51E-03
ATP-binding cassette, sub-family D (ALD), member 2	ABCD2	2.35	2.44E-03	2.01	6.48E-03
Malic enzyme 1, NADP(+)-dependent, cytosolic	ME1	2.27	2.33E-01	2.52	1.86E-01
Interferon-induced protein with tetratricopeptide repeats	IFIT2	2.21	1.65E-03	4.55	4.83E-05
Brain expressed, X-linked 1	BEX1	2.20	1.06E-05	3.07	1.34E-06
G protein-coupled receptor associated sorting protein	GPRASP2	2.19	3.18E-03	2.70	9.47E-04
Cysteine-rich protein 2	CRIP2	2.12	2.20E-03	3.17	2.28E-04
Phosphatidylinositol glycan anchor biosynthesis, class M	PIGM	2.08	3.05E-02	-2.68	9.17E-03
Amphiphysin	AMPH	2.07	2.37E-05	2.11	2.04E-05
Zinc finger protein 418	ZNF418	-2.18	5.24E-03	-2.11	6.46E-03
Myopalladin	MYPN	-2.31	4.64E-04	2.61	2.19E-04
Adrenergic, alpha-2C-, receptor	ADRA2C	-2.37	1.39E-04	-2.63	7.36E-05
Zinc finger protein 546	ZNF546	-2.59	1.64E-02	-2.45	2.09E-02
Epithelial membrane protein 2	EMP2	-2.78	8.15E-06	2.11	5.03E-05
Melanoma antigen family B, 2	MAGEB2	-3.07	5.02E-02	21.46	5.42E-04

Appendix 4: The list of genes found to be mutually up-regulated in Clone 9 and RFM9 compared to H1299 (Batch 2) cells. Statistical analysis was performed using Student’s *t*-Test. (Data analysis was performed by Dr Bryony Llyod).

Full name	Gene Symbol	Fold-Change (RFM9 vs. H1299)	p-value (RFM9 vs. H1299)	Fold-Change (clone 9 vs. H1299)	p-value (clone 9 vs. H1299)
Tubulin, alpha 1b	TUBA1B	32.24	1.50E-05	22.29	2.87E-05
Ribosomal protein S24	RPS24	8.89	2.04E-08	8.69	2.17E-08
Thymocyte nuclear protein 1	THYN1	7.73	9.50E-06	10.33	4.37E-06
Secreted phosphoprotein 1	SPP1	6.94	2.33E-04	3.09	3.91E-03
Malic enzyme 1, NADP(+)-dependent, cytosolic	ME1	6.59	1.03E-05	5.95	1.43E-05
Carbamoyl-phosphate synthetase 1, mitochondrial	CPS1	6.29	1.16E-06	-2.69	4.29E-05
RAP1B, member of RAS oncogene family	RAP1B	5.65	7.57E-05	5.85	6.75E-05
Polo-like kinase 2 (Drosophila)	PLK2	5.62	4.94E-04	4.96	7.41E-04
Cysteine and histidine-rich domain (CHORD)-containing 1	CHORDC1	5.51	2.86E-04	6.00	2.19E-04
Coagulation factor II (thrombin) receptor-like 2	F2RL2	5.21	1.85E-03	2.68	1.97E-02
Ribosomal protein L39-like	RPL39L	4.77	1.52E-06	5.12	1.17E-06
Mediator complex subunit 27	MED27	4.55	2.02E-05	3.84	3.99E-05
Adrenomedullin	ADM	4.42	1.13E-05	5.71	4.47E-06
Ribosomal protein S29	RPS29	4.31	3.17E-07	3.67	6.38E-07
3-hydroxy-3-methylglutaryl-Coenzyme A synthase 1	HMGCS1	3.86	1.37E-03	2.61	7.31E-03
Sphingosine-1-phosphate receptor 1	S1PR1	3.81	2.33E-05	2.28	3.62E-04
Insulin-like growth factor binding protein 3	IGFBP3	3.81	7.13E-04	3.35	1.20E-03
Sema domain, immunoglobulin domain (Ig), short basic doma	SEMA3E	3.77	4.83E-05	3.05	1.29E-04
Mitochondrial ribosomal protein L33	MRPL33	3.73	1.06E-04	2.32	1.21E-03
Chromosome X open reading frame 57	CXorf57	3.71	5.17E-05	3.26	9.32E-05
Ribosomal protein S15	RPS15	3.66	1.30E-03	2.69	4.97E-03
Heterogeneous nuclear ribonucleoprotein A1	HNRNPA1	3.65	9.58E-06	4.43	4.26E-06
Ankyrin repeat domain 1 (cardiac muscle)	ANKRD1	3.63	5.61E-03	5.04	1.86E-03
Zinc finger protein 781	ZNF781	3.62	2.06E-04	4.96	5.99E-05
Chromosome 3 open reading frame 14	C3orf14	3.50	7.52E-04	4.16	3.74E-04
Eukaryotic translation initiation factor 4B	EIF4B	3.49	1.21E-03	2.56	4.94E-03
Small nuclear ribonucleoprotein polypeptide C	SNRPC	3.49	1.87E-06	2.47	1.23E-05
Lysophosphatidylcholine acyltransferase 2	LPCAT2	3.40	9.65E-06	5.69	1.22E-06
Transferrin receptor (p90, CD71)	TFRC	3.36	1.80E-04	3.18	2.34E-04
ADAM metallopeptidase with thrombospondin type 1 motif	ADAMTS1	3.34	5.85E-04	6.43	5.21E-05
Mdm2 p53 binding protein homolog (mouse)	MDM2	3.33	1.21E-06	2.88	2.58E-06
S100 calcium binding protein A11	S100A11	3.18	1.72E-03	2.56	4.77E-03
Proline rich 13	PRR13	3.17	1.51E-05	2.93	2.29E-05
Killer cell immunoglobulin-like receptor, two domains, l	KIR2DL1	3.05	3.24E-03	2.81	4.72E-03
G antigen 2A	GAGE2A	3.02	5.33E-05	2.82	7.65E-05
Cytochrome c oxidase subunit VIIb2	COX7B2	2.95	6.01E-07	3.17	4.16E-07
Diazepam binding inhibitor	DBI	2.93	3.87E-06	2.89	4.17E-06
Stromal cell-derived factor 2-like 1	SDF2L1	2.81	1.56E-04	2.63	2.25E-04
Myeloid/lymphoid or mixed-lineage leukemia	MLLT3	2.79	7.04E-06	2.47	1.47E-05
Catenin (cadherin-associated protein), alpha-like 1	CTNNAL1	2.76	4.73E-04	2.62	6.24E-04
KIT ligand	KITLG	2.70	2.13E-03	2.63	2.41E-03
7-dehydrocholesterol reductase	DHCR7	2.67	3.37E-04	2.46	5.36E-04
DBF4 homolog B (S. cerevisiae)	DBF4B	2.66	1.24E-03	2.86	8.52E-04
UDP-N-acteylglucosamine pyrophosphorylase 1	UAP1	2.65	1.25E-03	2.77	9.90E-04
Ribosomal protein L11	RPL11	2.62	4.14E-06	2.36	8.04E-06
Transforming growth factor, beta 2	TGFB2	2.61	1.27E-02	4.06	2.16E-03
ATP-binding cassette, sub-family D (ALD), member 2	ABCD2	2.60	1.39E-04	3.04	5.89E-05
NADH dehydrogenase (ubiquinone) 1 beta subcomplex, 1	NDUFB1	2.59	1.08E-06	2.94	5.10E-07
Acetyl-Coenzyme A acetyltransferase 2	ACAT2	2.58	1.09E-03	2.63	9.83E-04
Family with sequence similarity 54, member A	FAM54A	2.57	1.30E-03	3.07	5.21E-04
NADH dehydrogenase (ubiquinone) Fe-S protein 6	NDUFS6	2.51	3.78E-05	2.40	5.06E-05
NADH dehydrogenase (ubiquinone) 1 alpha subcomplex, 1	NDUFA1	2.49	3.26E-05	2.93	1.25E-05
Chromosome 18 open reading frame 55	C18orf55	2.47	3.43E-04	3.02	1.12E-04
FCF1 small subunit (SSU) processome component homolog	FCF1	2.45	2.85E-04	2.54	2.25E-04
Chromosome 11 open reading frame 48	C11orf48	2.44	2.83E-04	3.05	8.13E-05
Protocadherin beta 5	PCDHB5	2.41	2.50E-04	5.82	4.70E-06

Appendix 4 (Continued): The list of genes found to be mutually up-regulated in Clone 9 and RFM9 compared to H1299 (Batch 2) cells. Statistical analysis was performed using Student's *t*-Test. (Data analysis was performed by Dr Bryony Llyod).

Full name	Gene Symbol	Fold-Change (RFM9 vs. H1299)	p-value (RFM9 vs. H1299)	Fold-Change (clone 9 vs. H1299)	p-value (clone 9 vs. H1299)
Glutamine-fructose-6-phosphate transaminase 2	GFPT2	2.40	1.77E-04	-4.03	1.24E-05
Thyroid hormone receptor interactor 13	TRIP13	2.40	1.66E-04	2.35	1.90E-04
EMG1 nucleolar protein homolog (S. cerevisiae)	EMG1	2.33	2.36E-05	2.37	2.11E-05
Suppressor of tumorigenicity 20	ST20	2.30	7.95E-04	2.47	5.07E-04
RNA binding motif protein 24	RBM24	2.26	1.27E-04	2.84	3.12E-05
Wingless-type MMTV integration site family, member 5B	WNT5B	2.26	1.73E-04	2.42	1.09E-04
Chromosome 3 open reading frame 62	C3orf62	-2.27	7.66E-04	-2.60	3.34E-04
Chloride intracellular channel 2	CLIC2	-2.28	1.11E-04	-2.41	7.76E-05
Synaptotagmin I	SYT1	-2.29	2.25E-03	-2.27	2.36E-03
Antigen p97 (melanoma associated) identified by monoclonal	MFI2	-2.29	5.27E-04	-2.27	5.63E-04
Sushi-repeat-containing protein, X-linked	SRPX	-2.31	2.04E-05	-2.32	1.99E-05
Carboxypeptidase E	CPE	-2.31	3.23E-04	-2.61	1.55E-04
Ethanolamine kinase 2	ETNK2	-2.32	6.93E-05	-3.31	9.07E-06
Zinc finger family member 767	ZNF767	-2.32	4.46E-04	-2.64	2.07E-04
Leucine rich repeat neuronal 1	LRRN1	-2.34	1.40E-04	-4.81	4.00E-06
Zinc finger protein 643	ZNF643	-2.39	3.19E-04	-3.20	6.37E-05
Vacuolar protein sorting 13 homolog B (yeast)	VPS13B	-2.44	5.83E-05	-3.21	1.24E-05
CUB domain containing protein 1	CDCP1	-2.44	4.67E-05	-2.58	3.31E-05
Synaptonemal complex protein 2-like	SYCP2L	-2.50	1.22E-04	-2.31	1.98E-04
Adrenergic, alpha-2C-, receptor	ADRA2C	-2.52	3.16E-05	-2.27	6.25E-05
Integrin, beta 4	ITGB4	-2.52	4.86E-04	-2.64	3.75E-04
Sedoheptulokinase	SHPK	-2.53	2.63E-03	-2.49	2.85E-03
CAP-GLY domain containing linker protein 3	CLIP3	-2.53	8.47E-04	-2.53	8.57E-04
Rho GTPase activating protein 21	ARHGAP21	-2.53	1.84E-05	-2.32	3.29E-05
Stanniocalcin 1	STC1	-2.54	2.28E-03	-2.62	1.92E-03
Myotubularin related protein 11	MTMR11	-2.56	4.33E-04	-2.60	3.95E-04
Chromosome 6 open reading frame 10	C6orf10	-2.59	2.42E-04	-2.43	3.52E-04
Solute carrier family 1	SLC1A4	-2.59	5.08E-04	-3.12	1.90E-04
Golgi autoantigen, golgin subfamily a, 8B	GOLGA8B	-2.59	9.09E-03	-2.38	1.36E-02
Natriuretic peptide receptor B	NPR2	-2.60	2.65E-04	-2.33	5.16E-04
Inhibitor of DNA binding 1	ID1	-2.62	1.31E-02	-3.37	4.59E-03
Guanine nucleotide binding protein (G protein), gamma 4	GNG4	-2.62	5.31E-05	-3.36	1.41E-05
Secreted protein, acidic, cysteine-rich (osteonectin)	SPARC	-2.63	2.30E-05	-60.16	4.47E-09
Fucosidase, alpha-L- 1, tissue	FUCA1	-2.64	1.43E-03	-3.39	4.26E-04
Laminin, beta 2 (laminin S)	LAMB2	-2.66	2.05E-04	-2.98	1.10E-04
Neuropilin 1	NRP1	-2.67	1.59E-03	-3.89	2.81E-04
Ketohexokinase (fructokinase)	KHK	-2.67	2.67E-03	-2.76	2.24E-03
Dehydrogenase/reductase (SDR family) member 1	DHRS1	-2.67	2.07E-04	-3.02	1.08E-04
Chromosome 14 open reading frame 49	C14orf49	-2.67	1.25E-05	-2.30	3.29E-05
Mastermind-like 3 (Drosophila)	MAML3	-2.68	1.48E-05	-3.20	5.72E-06
Dedicator of cytokinesis 3	DOCK3	-2.70	6.60E-05	-2.26	2.00E-04
Latent transforming growth factor beta binding protein 1	LTBP1	-2.73	7.67E-04	-3.19	3.51E-04
GRAM domain containing 1B	GRAMD1B	-2.77	1.16E-04	-3.19	5.54E-05
Ventricular zone expressed PH domain homolog 1	VEPH1	-2.79	1.15E-03	-2.61	1.61E-03
Solute carrier family 6 (neurotransmitter transporter	SLC6A9	-2.80	1.07E-04	-3.79	2.46E-05
Breast carcinoma amplified sequence 3	BCAS3	-2.83	4.83E-05	-2.84	4.68E-05
ChaC, cation transport regulator homolog 1	CHAC1	-2.89	4.07E-03	-5.43	3.67E-04
Raftlin family member 2	RFTN2	-2.92	6.65E-05	-2.37	2.25E-04
Schlafen family member 5	SLFN5	-2.95	1.35E-03	-2.34	4.50E-03
Kelch-like 24 (Drosophila)	KLHL24	-2.97	3.41E-04	-2.96	3.49E-04
Septin 3	Sep-03	-3.04	1.35E-05	-2.45	4.59E-05
Chromosome 5 open reading frame 41	C5orf41	-3.04	3.87E-04	-3.14	3.30E-04
Glypican 6	GPC6	-3.05	1.11E-05	-4.33	2.25E-06
Family with sequence similarity 70, member B	FAM70B	-3.06	1.23E-05	-2.79	2.03E-05
Ras-related GTP binding B	RRAGB	-3.08	7.46E-05	-2.26	4.44E-04
Bardet-Biedl syndrome 2	BBS2	-3.09	7.77E-05	-2.57	2.10E-04
Metastasis suppressor 1	MTSS1	-3.11	1.13E-05	-2.72	2.34E-05

Appendix 4 (Continued): The list of genes found to be mutually up-regulated in Clone 9 and RFM9 compared to H1299 (Batch 2) cells. Statistical analysis was performed using Student's *t*-Test. (Data analysis was performed by Dr Bryony Llyod).

Full name	Gene Symbol	Fold-Change (RFM9 vs. H1299)	p-value (RFM9 vs. H1299)	Fold-Change (clone 9 vs. H1299)	p-value (clone 9 vs. H1299)
Glucuronidase, beta-like 2	GUSBL2	-3.12	3.24E-04	-3.71	1.48E-04
Zinc finger protein 37B (pseudogene)	ZNF37B	-3.13	1.37E-03	-2.31	6.18E-03
Neuroblastoma breakpoint family, member 11-like	RP11-94I2.2	-3.16	5.02E-04	-2.77	9.61E-04
Zinc fingers and homeoboxes 2	ZHX2	-3.17	3.72E-06	-2.46	1.61E-05
Phosphodiesterase 4B, cAMP-specific (phosphodiesterase E4	PDE4B	-3.18	1.45E-05	-6.38	9.01E-07
Testis-specific kinase 2	TESK2	-3.20	1.53E-04	-2.84	2.80E-04
Calbindin 2	CALB2	-3.24	2.54E-05	-3.60	1.56E-05
ADAM metallopeptidase with thrombospondin type 1 motif,	ADAMTS6	-3.24	1.92E-04	-4.43	5.09E-05
XK, Kell blood group complex subunit-related family, member	XKR6	-3.29	1.41E-04	-2.77	3.37E-04
1-acylglycerol-3-phosphate O-acyltransferase 3	AGPAT3	-3.34	9.57E-04	-2.53	3.57E-03
Heparan-alpha-glucosaminide N-acetyltransferase	HGSNAT	-3.35	2.58E-03	-3.71	1.71E-03
Alcohol dehydrogenase, iron containing, 1	ADHFE1	-3.36	2.97E-05	-3.89	1.53E-05
Yippee-like 2 (Drosophila)	YPEL2	-3.38	2.35E-05	-2.66	8.36E-05
Tumor protein p53 inducible nuclear protein 1	TP53INP1	-3.42	4.27E-04	-2.54	1.85E-03
Jumonji, AT rich interactive domain 2	JARID2	-3.44	6.65E-06	-3.02	1.28E-05
Potassium channel, subfamily T, member 2	KCNT2	-3.49	1.44E-05	-4.04	7.61E-06
Insulin receptor	INSR	-3.50	9.11E-06	-4.11	4.52E-06
Amylase, alpha 2B (pancreatic)	AMY2B	-3.70	4.89E-03	-5.83	1.11E-03
Solute carrier family 25, member 37	SLC25A37	-3.72	2.68E-04	-3.80	2.45E-04
Cathepsin F	CTSF	-3.82	1.54E-05	-2.63	1.01E-04
Secretogranin V (7B2 protein)	SCG5	-4.02	6.01E-06	-3.50	1.11E-05
Integrin, beta 3 (platelet glycoprotein IIIa, antigen CD61	ITGB3	-4.07	4.58E-06	-3.61	7.74E-06
F-box protein 32	FBXO32	-4.08	6.34E-06	-4.35	4.89E-06
Enkurin, TRPC channel interacting protein	ENKUR	-4.14	2.63E-04	-2.39	3.38E-03
UL16 binding protein 1	ULBP1	-4.42	6.58E-04	-3.45	1.70E-03
Transmembrane 6 superfamily member 1	TM6SF1	-4.45	2.72E-05	-3.82	5.04E-05
T-complex 11 (mouse)-like 2	TCP11L2	-4.63	1.08E-03	-7.57	2.41E-04
Protocadherin beta 13	PCDHB13	-4.69	3.61E-05	-3.46	1.25E-04
TSPY-like 5	TSPYL5	-4.80	6.33E-07	3.41	2.70E-06
Hypothetical protein LOC286161	LOC286161	-4.85	2.66E-04	-4.59	3.24E-04
Chromosome 14 open reading frame 139	C14orf139	-4.94	3.28E-05	-2.74	4.32E-04
Dpy-19-like 2 pseudogene 2 (C. elegans)	DPY19L2P2	-5.30	4.07E-04	-2.39	1.02E-02
Alanyl (membrane) aminopeptidase	ANPEP	-5.33	8.41E-05	-8.20	2.26E-05
SH3 domain and tetratricopeptide repeats 2	SH3TC2	-5.68	1.55E-06	-4.14	5.06E-06
Mucin 15, cell surface associated	MUC15	-6.18	2.01E-05	-3.39	1.96E-04
Sema domain, transmembrane domain (TM), and cytoplasmic d	SEMA6A	-6.19	4.49E-05	-5.82	5.48E-05
Deleted in malignant brain tumors 1	DMBT1	-7.17	4.06E-08	-6.16	6.56E-08
Transmembrane protein 71	TMEM71	-11.77	1.91E-07	3.08	1.93E-05

Appendix 5: Analysis of the effects of NME2, NME2 kinase dead mutant NME2H118F, MDM2 and MDM2 RING finger mutant on cell motility. Representative movies are available on the attached CD.

Appendix 6: Analysis of the effects of MDM2 overexpression on cell motility. Representative movies are available on the attached CD.

Appendix 7: Testing of the anti-NME1/2 (C1C3) antibody. Down-regulation of NME using siRNA NME1 oligo 9 and NME2 oligo 8 (40 pmol for each well of a 6-well plate, i.e. a total of 80 pmol/well). Transfected cells were harvested 48h post-transfection for western blot and probed with **A.** anti-NME1/2 (ab31019) **B.** anti-NME1/2 (C1C3) for comparison. Mock (only transfection reagent) and Scrambled siRNA serve as negative controls. Red areas indicate saturation of signal as a result of overexposure. Similar to anti-NME1/2 (ab31019), C1C3 also recognises both NME1 and NME2, except that there were fewer non-specific bands at molecular weight above 30 kDa present when blots were probed with C1C3 antibody. Therefore, we concluded that anti-NME1/2 (C1C3) is a suitable replacement antibody for ab31019.

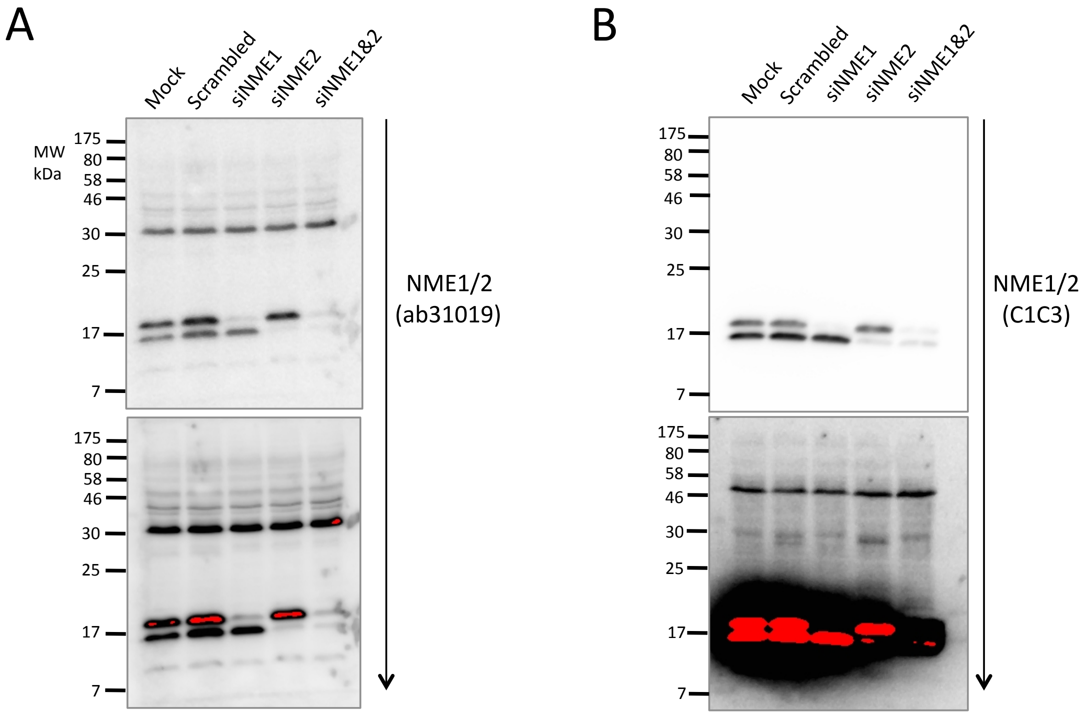

Appendix 8: Sequencing results for pcDNA3.1-NM23-LV and pcDNA3.1-HA-NM23-LV (plasmid kindly provided by Dr Linda Valentijn).

pcDNA3.1-NM23-LV

5' NM23-LV 3'

DNA sequence

CCCCGCTAGTTTACTTTAGCTTGGTACCGAGCTCGGATCCACTAGTCCAGTGTGGTGGA
ATTCGATTGCCGGAGTTCAAACCTAAGCAGCTGGAAGGAACCATGGCCAACTGTGAG
CGTACCTTCATTGCGATCAAACCAGATGGGGTCCAGCGGGGTCTTGTGGGAGAGATTA
TCAAGCGTTTTGAGCAGAAAGGATTCCGCCTTGTTGGTCTGAAATTCATGCAAGCTTC
CGAAGATCTTCTCAAGGAACACTACGTTGACCTGAAGGACCGTCCATTCTTTGCCGGC
CTGGTGAAATACATGCACTCAGGGCCGGTAGTTGCCATGGTCTGGGAGGGGCTGAATG
TGGTGAAGACGGGCCGAGTCATGCTCGGGGAGACCAACCCTGCAGACTCCAAGCCTG
GGACCATCCGTGGAGACTTCTGCATACAAGTTGGCAGGACCATGGCCAACCTGGAGC
GCACCTTCATCGCCATCAAGCCGGACGGCGTGCAGCGCGGCCTGGTGGGCGAGATCAT
CAAGCGCTTCGAGCAGAAGGGATTCCGCCTCGTGGCCATGAAGTTCCTCCGGGCCTCT
GAAGAACACCTGAAGCAGCACTACATTGACCTGAAAGACCGACCATTCTTCCCTGGGC
TGGTGAAGTACATGAACTCAGGGCCGGTTGTGGCCATGGTCTGGGAGGGGCTGAACG
TGGTGAAGACAGGCCGAGTGATGCTTGGGGAGACCAATCCAGCAGATTCAAAGCCAG
GCACCATTCGTGGGGACTTCTGCATTCAGGTTGGCAGGAACATCATTCATGGCAGTGA
TTCAGTAAAAAGTGCTGAAAAAGAAATCAGCCTATGGTTTAAGCCTGAAGAACTGGTT
GACTACAAGTCTTGTGCTCATGACTGGGTCTATGAATAAGAGGTGGACACAACAGCAG
TCTCCTTCAGCACGGCGTGGTGTGTCCCTGGACACAGCTCTTCATTCCATTGACTTAGA
GGCAACAGGATTGATCATTCTAATCACTAGTGAATTCTGCAGATATCCAGCACAGTGG
CGGCCGCTCGAGTCTAGAGGGCCCGTTTAAACCCGCTGATCAGCCTCGACTGTGCCTT
CTAGTTGCCAGCCATCTGTTGTTTGCCCCTCCCCCGTGGCTTCCTTGACCCTGGAAAGT
GGCACTCCCACTGGCCTTTCCTAATAAAATGAGGAAATTGCATCCCATTGTCTGAATA
GGTGCATTCTATCTGGGGGGGGGGGTTGGGCCA

Amino acid sequence

P L V Y F S L V P S S D P L V Q C G G I R L P E F K P K Q L E G T **Met** A N C E R T F I A I
K P D G V Q R G L V G E I I K R F E Q K G F R L V G L K F **Met** Q A S E D L L K E H Y V D
L K D R P F F A G L V K Y **Met** H S G P V V A **Met** V W E G L N V V K T G R V **Met** L G E
T N P A D S K P G T I R G D F C I Q V G R T **Met** A N L E R T F I A I K P D G V Q R G L V
G E I I K R F E Q K G F R L V A **Met** K F L R A S E E H L K Q H Y I D L K D R P F F P G L V
K Y **Met** N S G P V V A **Met** V W E G L N V V K T G R V **Met** L G E T N P A D S K P G T I R
G D F C I Q V G R N I I H G S D S V K S A E K E I S L W F K P E E L V D Y K S C A H D W
V Y E **Stop** E V D T T A V S F S T A W C V P G H S S S F H **Stop** L R G N R I D H S N H **Stop**
Stop I L Q I S S T V A A A R V **Stop** R A R L N P L I S L D C A F **Stop** L P A I C C L P L P R
G F L D P G K W H S H W P F L I K **Stop** G N C I P L S E **Stop** V H S I W G G G L G

Appendix 8 (Continued): Sequencing results for pcDNA3.1-NM23-LV and pcDNA3.1-HA-NM23-LV (plasmid kindly provided by Dr Linda Valentijn).

pcDNA3.1-HA-NM23-LV

5' HA-linker-NM23-LV 3'

DNA sequence

CCCGCTCGTTTACTTTAGCTTATGTACCCATACGATGTTCCAGATTACGCTGGATCCAT
GGCCAACTGTGAGCGTACCTTCATTGCGATCAAACCAGATGGGGTCCAGCGGGGTCTT
GTGGGAGAGATTATCAAGCGTTTTGAGCAGAAAGGATTCCGCCTTGTTGGTCTGAAAT
TCATGCAAGCTTCCGAAGATCTTCTCAAGGAACACTACGTTGACCTGAAGGACCGTCC
ATTCTTTGCCGGCCTGGTGAAATACATGCACTCAGGGCCGGTAGTTGCCATGGTCTGG
GAGGGGCTGAATGTGGTGAAGACGGGCCGAGTCATGCTCGGGGAGACCAACCCTGCA
GACTCCAAGCCTGGGACCATCCGTGGAGACTTCTGCATACAAGTTGGCAGGACCATGG
CCAACCTGGAGCGCACCTTCATCGCCATCAAGCCGGACGGCGTGCAGCGCGGCCTGGT
GGGCGAGATCATCAAGCGCTTCGAGCAGAAGGGATTCCGCCTCGTGGCCATGAAGTTC
CTCCGGGCCTCTGAAGAACACCTGAAGCAGCACTACATTGACCTGAAAGACCGACCAT
TCTTCCCTGGGCTGGTGAAGTACATGAACTCAGGGCCGGTTGTGGCCATGGTCTGGGA
GGGGCTGAACGTGGTGAAGACAGGCCGAGTGATGCTTGGGGAGACCAATCCAGCAGA
TTCAAAGCCAGGCACCATTCGTGGGGACTTCTGCATTCAGGTTGGCAGGAACATCATT
CATGGCAGTGATTCAGTAAAAAGTGCTGAAAAAGAAATCAGCCTATGGTTTAAGCCTG
AAGAACTGGTTGACTACAAGTCTTGTGCTCATGACTGGGTCTATGAATAAGAGGTGGA
CACAACAGCAGTCTCCTTCAGCACGGCGTGGTGTGTCCCTGGACACAGCTCTTCATTC
CATTGACTTAGAGGCAACAGGATTGATCATTCTAATCACTAGTGAATTCTGCAGATAT
CCAGCACAGTGGCGGCCGCTCGAGTCTAGAGGGCCCGTTTAAACCCGCTGATCAGCCT
CGACTGTGCCTTCTAGTTGCCAGCCATCTGTTGTTTGCCCCTCCCCCGTGCCTTCCTTGA
CCCTGGAAAGGTGCCACTCCCACTGGCCTTTCCTAATAAAATGAGGAAATTGCATCGC
ATTGGCTGAATAGGTGCATTCTATCTGGGGG

Amino acid sequence

P A R L L **Stop** L **Met** Y P Y D V P D Y A G S **Met** A N C E R T F I A I K P D G V Q R G L V
G E I I K R F E Q K G F R L V G L K F **Met** Q A S E D L L K E H Y V D L K D R P F F A G L
V K Y **Met** H S G P V V A **Met** V W E G L N V V K T G R V **Met** L G E T N P A D S K P G T I
R G D F C I Q V G R T **Met** A N L E R T F I A I K P D G V Q R G L V G E I I K R F E Q K G F
R L V A **Met** K F L R A S E E H L K Q H Y I D L K D R P F F P G L V K Y **Met** N S G P V V
A **Met** V W E G L N V V K T G R V **Met** L G E T N P A D S K P G T I R G D F C I Q V G R N
I I H G S D S V K S A E K E I S L W F K P E E L V D Y K S C A H D W V Y E **Stop** E V D T T
A V S F S T A W C V P G H S S S F H **Stop** L R G N R I D H S N H **Stop** **Stop** I L Q I S S T V
A A A R V **Stop** R A R L N P L I S L D C A F **Stop** L P A I C C L P L P R A F L D P G K V P L
P L A F P N K **Met** R K L H R I G **Stop** I G A F Y L G

Appendix 9: Expression of NM23-LV protein. In order to examine the expression of NM23-LV and HA-NM23-LV plasmids (provided by Dr. Linda Valentijn), H1299 cells were transfected with 4 μg of NM23-LV, HA-NM23-LV, or empty vector, as indicated, in each well of a 6-well plate using Lipofectamine 2000. Transfected cells were harvested 24h post transfection for western blot analysis using anti-NME2 (L15), anti-NME1/2 (C1C3), anti-NME1 (SC465) and anti-HA (12CA5), as indicated. White arrow (◁) indicates the position of NM23-LV; grey arrow (◀) indicates the position of NME1; black arrow (◀) indicates the position of NME2.

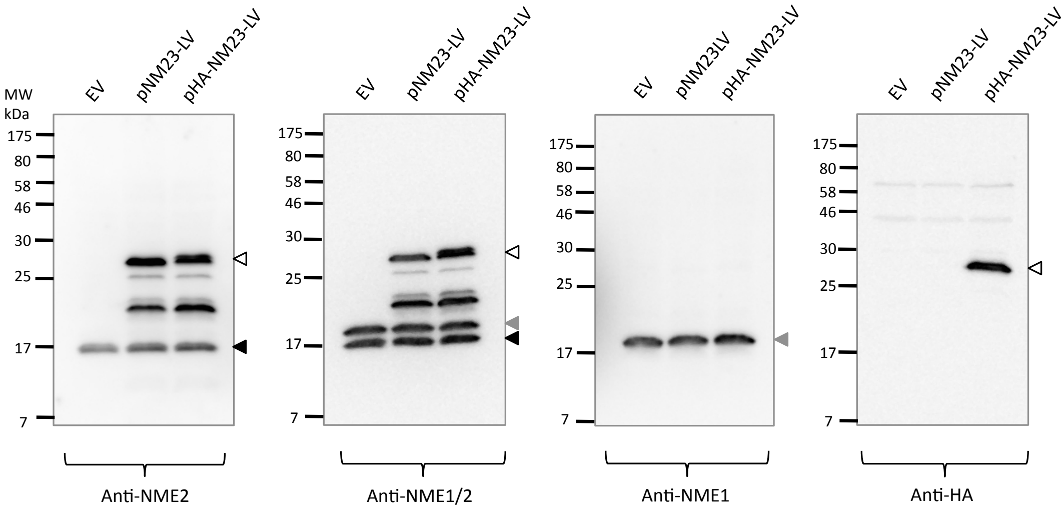

Appendix 10: Digest results for constructs expressing NME fusion proteins. Constructs that express fluorescence-labelled NME fusion proteins, NME1, NME2, NME2H118F and NM23-LV were generated by cloning these NMEs into pEYFP and pECFP vectors, resulting in both C- and N- terminally fluorescent-tagged forms of NMEs. Following NME fragments being subcloned into pEYFP and pECFP vectors at ECoRI and BamHI restriction sites, the insertions were confirmed by excising at these two restriction sites.

A **N-ECFP fusion**

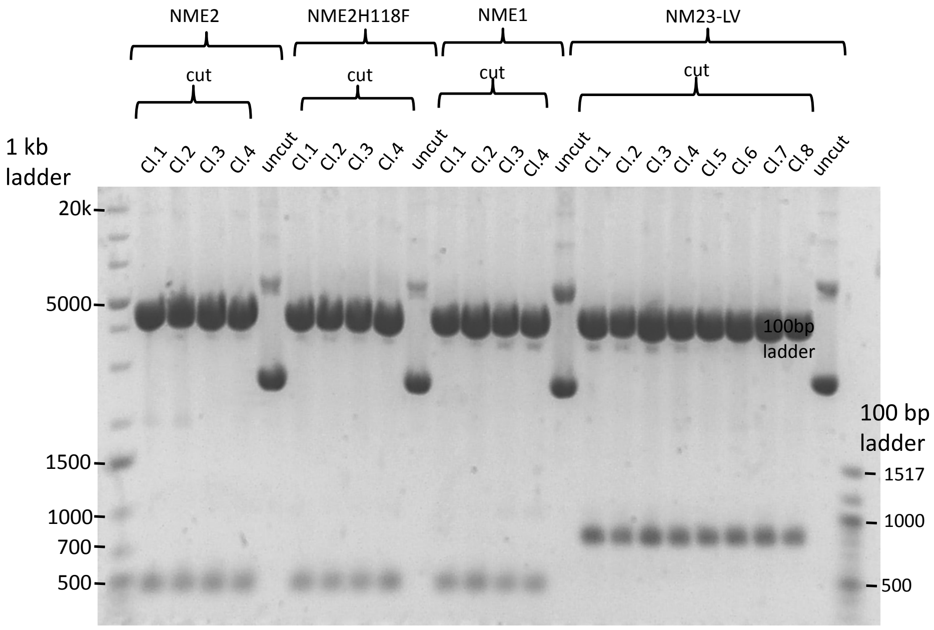

B **N-EYFP fusion**

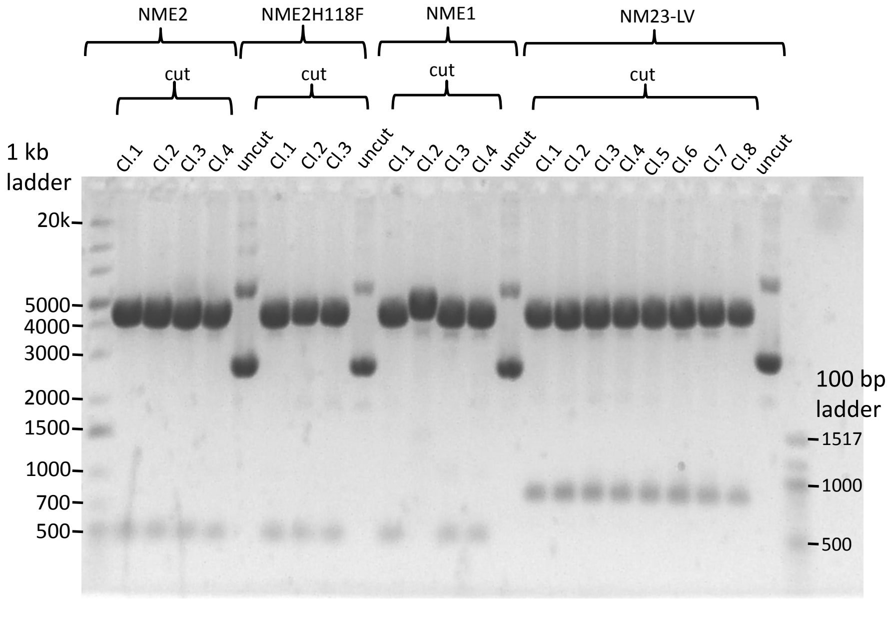

Appendix 10 (Continued): Digest results for constructs expressing NME fusion proteins.

C **C-ECFP fusion**

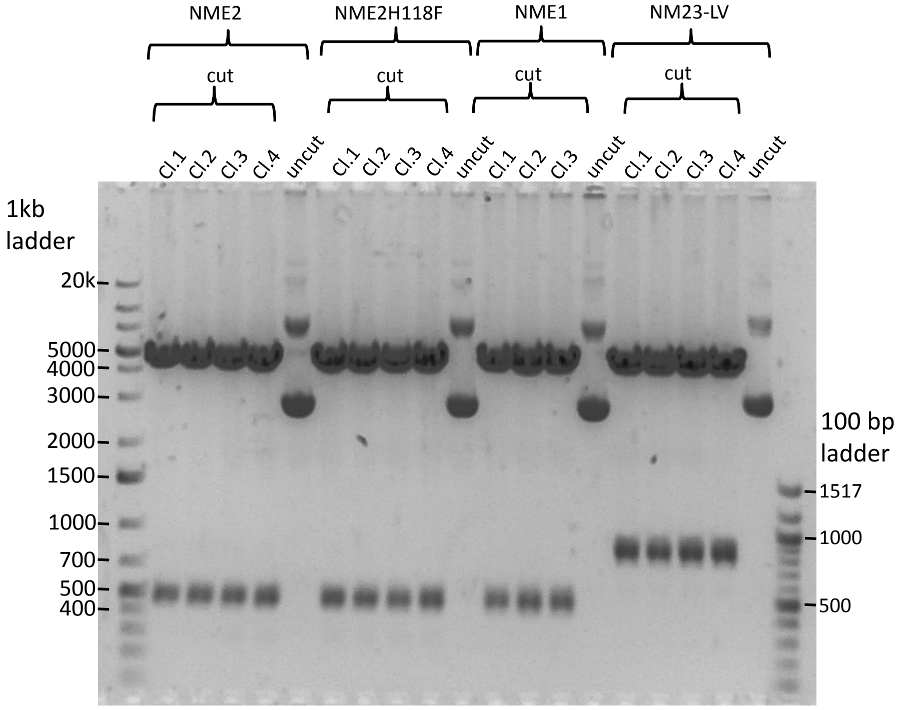

D **C-EYFP fusion**

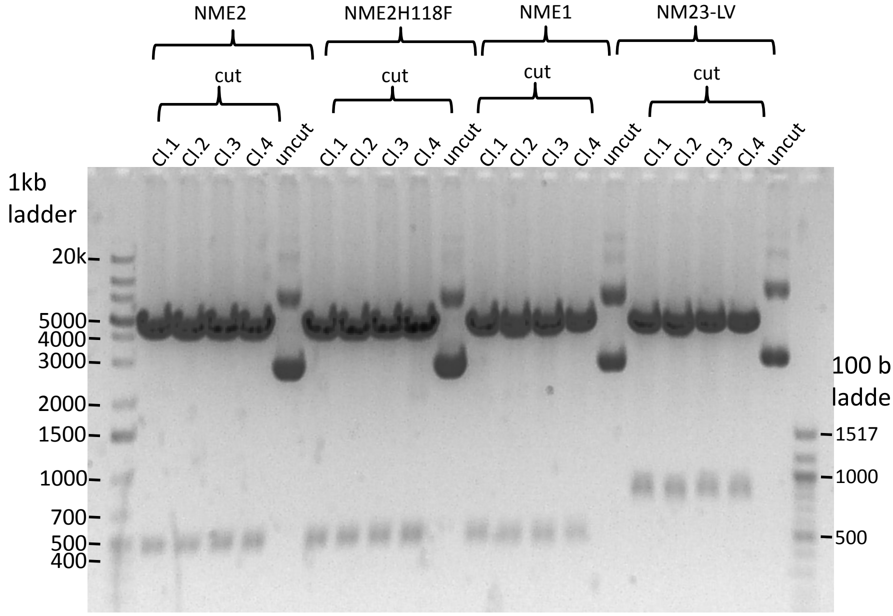

Appendix 11: Examining the cellular localisation of NME fusion proteins using live cell imaging. Representative movies are available on the attached CD. Each field is represented by two files: One for fluorescence only (F), and the other for fluorescence with phase contrast (F+PC). The fluorescence brightness for NM23-LV fusion protein was adjusted for visualisation since the level of protein expression was too low. F, fluorescence; PC, phase contrast.